HYDROELASTIC ANALYSIS OF FLOATING AND SUBMERGED FLEXIBLE STRUCTURES

Thesis
submitted in partial fulfillment of the requirements for the degree of

DOCTOR OF PHILOSOPHY

by

PRAVEEN K.M.
(AM15F06)

Under the guidance of

Dr. DEBABRATA KARMAKAR
Assistant Professor

DEPARTMENT OF APPLIED MECHANICS AND HYDRAULICS
NATIONAL INSTITUTE OF TECHNOLOGY KARNATAKA
SURATHKAL, MANGALORE - 575 025, INDIA

FEBRUARY 2020

DEDICATION

This thesis is dedicated to my loving
Father, Mother and Brother

DECLARATION

I hereby declare that the Ph.D. Thesis entitled **"HYDROELASTIC ANALYSIS OF FLOATING AND SUBMERGED FLEXIBLE STRUCTURES"** which is being submitted to **National Institute of Technology Karnataka, Surathkal,** for the partial fulfillment of the requirement for the award of degree of **Doctor of Philosophy** in the **Department of Applied mechanics and Hydraulics**, is a bonafide report of the work carried out by me. The material contained in this Ph.D Thesis has not been submitted to any university or Institution for the award of any degree.

……..

PRAVEEN K.M. (AM15F06)
Department of Applied Mechanics and Hydraulics
National Institute of Technology Karnataka, Surathkal

Place: NITK, SURATHKAL.
Date: 5th FEBRUARY 2020

CERTIFICATE

This is to certify that the Ph.D. Thesis entitled **"HYDROELASTIC ANALYSIS OF FLOATING AND SUBMERGED FLEXIBLE STRUCTURES"** submitted by **PRAVEEN K.M. (AM15F06),** as the record of the work carried out by him, is accepted as the Ph.D. Thesis submission in partial fulfillment of the requirements for the award of the degree of **Doctor of Philosophy** in the **Department of Applied Mechanics and Hydraulics, National Institute of Technology Karnataka, Surathkal**, is a bonafide work carried out by him under my supervision and guidance**.**

…….

Dr. DEBABRATA KARMAKAR

Assistant Professor
Department of Applied Mechanics and Hydraulics
National Institute of Technology Karnataka, Surathkal

…….

Chairman - DTAC

Department of Applied Mechanics and Hydraulics
National Institute of Technology Karnataka, Surathkal

ACKNOWLEDGEMENT

I take this opportunity to express my sincere gratitude and profound thanks to my guide **Dr. D. Karmakar,** Assistant Professor, Department of Applied Mechanics and Hydraulics, National Institute of Technology Karnataka, Surathkal for his advice, expert guidance, constant encouragement and reference material provided throughout my research work.

I acknowledge my sincere thanks to **Prof. Subba Rao**, Department of Applied Mechanics and Hydraulics and **Dr. A S Balu**, Department of Civil Engineering for being the members of Research Progress Assessment Committee (RPAC) and giving valuable suggestions and encouragement at various stages of this work.

I would like to express my sincere gratitude towards **Prof. G.S Dwarakish** and **Prof. Amai Mahesha**, former Heads of the Department of Applied Mechanics and Hydraulics and **Prof. Amba Shetty**, Head of the Department of Applied Mechanics and Hydraulics, National Institute of Technology Karnataka, Surathkal for providing necessary facilities and sincere co-operation throughout my stay at the NITK campus. I also extend my heartfelt gratitude to **Prof. Katta Venkataramana** and all the faulty members of the Department of Applied Mechanics and Hydraulics and also Department of Civil Engineering, NITK Surathkal.

I am very much thankful to **Prof. Carlos Guedes Soares,** President, Centre for Marine Technology and Ocean Engineering (CENTEC), IST Lisbon, Portugal for his valuable advice and suggestion during his visit to NITK Surathkal for India-Portugal Bilateral Technological Cooperation.

I would like to acknowledge Science and Engineering Research Board (SERB), Department of Science & Technology (DST), Government of India for Young Scientist research, Grant No: YSS/2014/000812 and DST for India-Portugal Bilateral Scientific Technological Cooperation Project, Grant No: DST/INT/Portugal/P-13/2017 for partial support to carry out the research work.

My special thanks to Mr. Balakrishna, Mr. B. Jagadish, Asst. Executive Engineer (Rtd.) and Mr. Seetharam, Department of Applied Mechanics and Hydraulics for their help in all the

departmental works. I would also like to thank all the non-teaching staff of the Department of Applied Mechanics and Hydraulics, National Institute of Technology Karnataka, Surathkal for their co-operation and help during the project work.

I want thank Mr. Harish Kumar for his constant support and motivation in keeping up with my research work and Mr. V. Venkateshwaralu for his valuable contribution in the preparation of my thesis. The informal support and encouragement of many friends has been indispensable. I also acknowledge the good company and help received by the research scholar of NITK, Surathkal.

I express my heartfelt gratitude to the authors of research articles which have been refereed in preparing this thesis. I also express my gratitude to the reviewers of my research articles for their invaluable suggestions in improving this work.

I am very much grateful to my father Sri. Medappa K.R. and mother Late Smt. Thilothamma K.G. who provided me the best education and encouraged me in all my endeavors. I also thank my beloved brother Mr. Puneeth K.M. for the moral support in pursuing my research work. Above all, I thank Lord, the almighty for his grace throughout the research work.

PRAVEEN K.M. (AM15F06)

Department of Applied Mechanics and Hydraulics

National Institute of Technology Karnataka, Surathkal

ABSTRACT

The present work mainly deals with a class of physical problems in the broad area of wave structure interaction related to hydroelasticity. In the present study, the major emphasis is given

- to analyse the hydroelastic behaviour of the very large floating structure based on the Timoshenko-Mindlin's plate theory in both finite and shallow water depth,

- to illustrate the significance of periodic array of articulation, change in bottom topography and wave attenuation due to the presence of vertical barriers in the hydroelastic analysis of floating structures which are of recent scientific interest in the field of Ocean and Coastal Engineering.

In the present study, the generalized expansion formulae along with the orthogonal mode-coupling relation is utilized to analyse the wave interaction with very large floating structure. The study is performed to analyse the influence of different edge support conditions on the hydroelastic behaviour of the floating elastic plate and the numerical results obtained based Timoshenko-Mindlin plate theory is compared with the Euler-Bernoulli plate theory. The gravity wave scattering by single and multiple articulated floating finite elastic plates are analyzed based on small amplitude linearized water wave theory. In the case of periodic array of multiple articulated floating elastic plates, the solution for the boundary value problem is analyzed by using both eigenfunction expansion method and wide-spacing approximation method. The transformation of gravity wave due to multiple variations in bottom topography in the presence of articulated floating elastic plate is studied by using orthogonal mode-coupling relation. Further, using shallow water approximation, the flexural gravity wave scattering due to (i) articulated floating elastic plates and (ii) abrupt changes in bottom topography are analyzed and the explicit relation for the wave scattering coefficients are obtained. Finally, surface gravity wave scattering due to the presence of vertical barriers along with the floating articulated elastic plate are analysed and the energy relation associated with transformations of gravity waves in the presence of vertical porous barrier is discussed. The numerical results for the reflection and transmission coefficients, plate deflection, strain along the floating elastic plate, bending moment and shear force are computed in different cases and analyzed.

Keywords: Orthogonal mode-coupling relation; Linearized small amplitude wave theory; Hydroelasticity; Timoshenko-Mindlin plate theory; Multiple articulation; Wide-spacing approximation.

NOMENCLATURE

ϕ_j	Velocity potential in the respective regions
m_s	Mass of the plate
L	Plate length
h_r	Water depth in reflected region
h_j	Water depth below the floating plate
h_t	Water depth in the transmitted region
d	Plate thickness
k_{jn}	Wave number in the respective regions
ρ	Density of water
ρ_p	Density of plate
E	Young modulus
ν	Poisson's ratio
G	Shear modulus of the plate
p	Pressure
μ	Transverse deformation
EI	Plate rigidity
I	Rotary inertia
S	Shear deformation
K_r	Reflection coefficient
K_t	Transmission coefficient
K_d	Dissipation coefficient
ζ_j	Surface deflection
ε	Strain in the floating plate
$M(x)$	Bending moment
$W(x)$	Shear force

ABBREVIATIONS

VLFS	-	Very Large Floating Structures
BVP	-	Boundary Value Problem
MIZ	-	Marginal Ice zones
TRAM	-	Technological Research Association of Mega float
IPCC	-	Intergovernmental Panel on Climate Change
KFSBC	-	Kinematic Free Surface Boundary Condition
DFSBC	-	Dynamic Free Surface Boundary Condition
FEM	-	Finite Element Method
BEM	-	Boundary Element Method
BIEM	-	Boundary Integral Equation Methods
HOBEM	-	Higher Order Boundary Element Method
NWT	-	Nonlinear Wave Tank
RCT	-	Residue Calculus Technique
WSA	-	Wide Spacing Approximation

LIST OF FIGURES & TABLES

Figure 1.1	Schematic diagram for wave propagation.	11
Figure 3.1	Schematic diagram for floating elastic plate**.**	62
Figure 3.2	Contour plot for the roots for the plate covered dispersion relation considering $h/L=0.15$, $E=5GPa$ and $d/L=0.02$ at (a) $k_{10}h=5$ (b) $k_{10}h=10$ (c) $k_{10}h=15$ and (d) $k_{10}h=20$.	68
Figure 3.3	Contour plot of infinite number of imaginary roots for the plate covered dispersion relation considering $h/L=0.15$, $E=5GPa$ and $d/L=0.02$ at $k_{10}h=10$**.**	68
Figure 3.4(a)	Convergence of the reflection and transmission coefficients for the number of evanescent modes, N.	76
Figure 3.4(b)	Validation of reflection coefficient along the plate length considering rotary inertia $I=0$ and shear deformation $S=0$ with Wang and Meylan (2002).	76
Figure 3.4(c)	Comparison of plate deflection with (Andrianov and Hermans, 2006) along the plate length plotted considering rotary inertia $I=0$ and shear deformation $S=0$	77
Figure 3.5	Transmission coefficient versus non-dimensional wavenumber $k_{10}h$ for different values of (a) plate thickness d/L and (b) water depth h/L.	78
Figure 3.6	(a) Reflection and (b) transmission coefficient versus non-dimensional wavenumber $k_{10}h$ for different support conditions in finite water depth at $d/L=0.02$ and $h/L=0.15$	79
Figure 3.7	(a) Plate deflection and (b) wave induced strain along the plate length x/L for different edge support conditions in finite water depth at $k_{10}h=5$**,** $d/L=0.02$ and $h/L=0.15$	80
Figure 3.8	(a) Bending moment and (b) shear force resultants along the plate length x/L for different edge support conditions in finite water depth at $k_{10}h=5$, $d/L=0.02$ and $h/L=0.15$.	81
Figure 3.9	(a) Reflection and (b) transmission coefficient versus non-dimensional wavenumber $k_{10}h$ is plotted considering $E=5GPa$, and $h/L=0.15$, $d/L=0.02$.	82

Figure 3.10	(a) Plate deflection, (b) wave induced strain, (c) bending moment and (d) shear force along the plate length plotted considering $k_{10}h = 5$, $E = 5GPa$, and $h/L = 0.15$, $d/L = 0.02$.	83
Figure 3.11	(a) Reflection and (b) transmission coefficient versus non-dimensional wavenumber $k_{10}h$ is plotted considering $E = 5GPa$, and $h/L = 0.15$, $d/L = 0.02$.	84
Figure 3.12	(a) Plate deflection, (b) wave induced strain, (c) bending moment and (d) shear force along the plate length plotted considering $k_{10}h = 3$, $E = 5GPa$, and $h/L = 0.15$, $d/L = 0.02$.	85
Figure 3.13	Wave reflection and transmission coefficient versus non-dimensional wavenumber $k_{10}h$ for different support conditions in shallow water depth at $d/L = 0.02$ and $h/L = 0.10$.	86
Figure 3.14	Plate deflection and wave induced strain along the plate length x/L for different edge support conditions in shallow water depth at $k_{10}h = 10$ $d/L = 0.02$ and $h/L = 0.10$.	87
Figure 3.15	(a) Bending moment and (b) shear force resultants along the plate length x/L for different edge support conditions in shallow water depth at $k_{10}h = 10$ $d/L = 0.02$ and $h/L = 0.10$.	88
Figure 3.16	(a) Reflection and (b) transmission coefficient versus $k_{10}h$ considering $d/L = 0.25$ and $h/L = 1.0$.	89
Figure 3.17	(a) Plate deflection (b) wave induced strain along the plate length for Timoshenko-Mindlin's and Kirchhoff's plate theory considering $E = 5GPa$, $k_{10}h = 20$, $d/L = 0.05$ and $h/L = 0.20$.	89
Figure 3.18	(a) Bending moment and (b) shear force along the plate length for Timoshenko-Mindlin and Kirchhoff's plate theory considering $E = 5GPa$, $k_{10}h = 20$, $d/L = 0.05$ and $h/L = 0.20$.	90
Figure 3.19	Comparison of (a) reflection and (b) transmission coefficient versus non-dimensional wavenumber for finite water depth and shallow water approximations varying d/L.	91
Figure 4.1(a)	Schematic diagram of multiple articulations in floating elastic plate.	97
Figure 4.1(b)	Wave scattering patterns in wide-spacing approximation	108
Figure 4.2	Non-dimensional bending moment along the plate length using Timoshenko-Mindlin plate theory, Euler- Bernoulli theory and Gao et. al. (2011).	111

Figure 4.3	(a) K_r and (b) K_t versus non-dimensional wavenumber using direct eigenfunction expansion method and WSA method for two articulated floating plate considering $h/L=0.04$ and $d/L=0.0047$.	113
Figure 4.4	(a) K_r and (b) K_t versus non-dimensional wavenumber for different articulations considering $h/L=0.083$, $d/L=0.0083$, $k_{33}=10^5\,\text{Nm}^{-1}$ and $k_{55}=10^5\,\text{Nm/rad}$.	114
Figure 4.5	(a) K_r and (b) K_t versus non-dimensional wavenumber $k_{10}h$ varying k_{33} and k_{55} in the case of three articulation considering $h/L=0.083$ and $d/L=0.0083$.	115
Figure 4.6	(a) K_r and (b) K_t versus non-dimensional wavenumber $k_{10}h$ for varying plate thickness d/L in the case of three articulations considering $h/L=0.125$, $k_{33}=10^5\,\text{Nm}^{-1}$ and $k_{55}=10^5\,\text{Nm/rad}$.	115
Figure 4.7	(a) K_r and (b) K_t versus non-dimensional wavenumber $k_{10}h$ for varying water depth h/L in the case of three articulations considering $h/L=0.125$, $k_{33}=10^5\,\text{Nm}^{-1}$ and $k_{55}=10^5\,\text{Nm/rad}$.	116
Figure 4.8	Plate deflection along the length of the plate varying (a) non-dimensional plate thickness d/L and (b) non-dimensional water depth h/L in the case of three articulation considering $k_{33}=10^5\,\text{Nm}^{-1}$, $k_{55}=10^5\,\text{Nm/rad}$ and $k_{10}h=4$.	117
Figure 4.9	Strain along the length of the plate varying (a) non-dimensional plate thickness d/L and (b) non-dimensional water depth h/L in the case of three articulation considering $k_{33}=10^5\,\text{Nm}^{-1}$, $k_{55}=10^5\,\text{Nm/rad}$ and $k_{10}h=4$.	117
Figure 4.10	Bending moment along the length of the plate varying (a) non-dimensional plate thickness d/L and (b) non-dimensional water depth h/L in the case of three articulation for $k_{33}=10^5\,\text{Nm}^{-1}$, $k_{33}=10^5\,\text{Nm}^{-1}$ and $k_{10}h=4$.	118
Figure 4.11	Shear force along the length of the plate varying (a) non-dimensional plate thickness d/L and (b) non-dimensional water depth h/L in the case of three articulation considering $k_{33}=10^5\,\text{Nm}^{-1}$, $k_{55}=10^5\,\text{Nm/rad}$. and $k_{10}h=4$.	119

Figure 4.12	(a) Reflection and (b) transmission coefficient versus non-dimensional wavenumber for different number of articulations considering $h/L=0.083$, $d/L=0.083$, $k_{33}=10^5\,\text{Nm}^{-1}$ and $k_{55}=10^5\,\text{Nm/rad}$.	120
Figure 4.13	(a) Plate deflection and (b) strain along the plate length for different number of articulations considering $k_{10}h=5$, $h/L=0.167$, $d/L=0.0167$, $k_{33}=10^5\,\text{Nm}^{-1}$ and $k_{55}=10^5\,\text{Nm/rad}$.	121
Figure 4.14	(a) Bending moment and (b) shear force resultants along the plate length for different number of articulations in the floating elastic plate at $k_{10}h=5$, $h/L=0.167$, $d/L=0.0167$, $k_{33}=10^5\,\text{Nm}^{-1}$ and $k_{55}=10^5\,\text{Nm/rad}$.	122
Figure 5.1	Schematic diagram for floating elastic platform over varying bottom topography	126
Figure 5.2	Schematic diagram for different types of sea bottom profile (a) Step-type, (b) Sloping, (c) Hump and (d) Double hump.	128
Figure 5.3	(a) K_r and (b) K_t versus $k_{10}h_r$ for varying water depth h_1/h_r in the case of single step bottom profile considering $h_t/h_r=1.0$.	141
Figure 5.4	(a) K_r and (b) K_t versus $k_{10}h_r$ for varying water depth h_1/h_r and h_t/h_r in the case of stepped sloping bottom profile.	141
Figure 5.5	(a) Deflection ζ_j/I_0 and (b) stain ε along the plate length x/L for varying water depth h_1/h_r in the case of single step bottom profile considering $k_{10}h_r=3$ and $h_t/h_r=1.0$.	143
Figure 5.6	(a) Deflection ζ_j/I_0 and (b) stain ε along the plate length x/L for varying water depth h_1/h_r and h_t/h_r in the case of stepped sloping bottom profile considering $k_{10}h_r=3$.	144
Figure 5.7	(a) Bending moment and (b) shear force along the plate length x/L for varying water depth h_1/h_r in the case of single step bottom profile considering $k_{10}h_r=3$ and $h_t/h_r=1.0$.	145
Figure 5.8	(a) Bending moment and (b) shear force along the plate length x/L for varying water depth h_1/h_r and h_t/h_r in the case of stepped sloping bottom profile considering $k_{10}h_r=3$.	146

Figure 5.9	(a) K_r and (b) K_t versus $k_{10}h_r$ varying water depth h_1/h_r and h_2/h_r in the case of two-stepped hump type bottom profile considering $h_t/h_r=1.0$.	147
Figure 5.10	(a) K_r and (b) K_t versus $k_{10}h_r$ varying water depth h_1/h_r h_2/h_r and h_t/h_r in the case of stepped sloping bottom profile.	148
Figure 5.11	(a) Deflection ζ_j/I_0 and (b) stain along the plate length x/L for varying water depth h_1/h_r and h_2/h_r in the case of two step bottom profile considering $k_{10}h_r=3$ and $h_t/h_r=1.0$.	149
Figure 5.12	Deflection ζ_j/I_0 and (b) stain ε along the plate length x/L for varying water depth h_1/h_r, h_2/h_r and h_t/h_r in the case of three stepped bottom profile considering $k_{10}h_r=3$.	150
Figure 5.13	(a) K_r and (b) K_t versus $k_{10}h_r$ for varying water depth h_1/h_r, h_2/h_r and h_3/h_r in the case of three step hump type bottom profile considering $h_t/h_r=1.0$.	152
Figure 5.14	(a) K_r and (b) K_t versus $k_{10}h_r$ for varying water depth h_1/h_r, h_2/h_r and h_3/h_r in the case of three stepped sloping type bottom profile considering $h_t/h_r=1.0$.	153
Figure 5.15	(a) Deflection ζ_j/I_0 and (b) stain ε along the plate length x/L for varying water depth h_1/h_r, h_2/h_r and h_3/h_r in the case of three step hump type sea bottom profile considering $k_{10}h_r=3$ and $h_t/h_r=1.0$.	154
Figure 5.16	(a) Deflection ζ_j/I_0 and (b) stain ε along the plate length x/L for varying water depth h_1/h_r, h_2/h_r and h_3/h_r in the case of three stepped sloping sea bottom profile considering $k_{10}h_r=3$ and $h_t/h_r=1.0$.	154
Figure 5.17	(a) K_r and (b) K_t versus $k_{10}h_r$ for varying number of steps along the plate covered region.	156
Figure 5.18	(a) Deflection ζ_j/I_0 and (b) stain along the plate length x/L for varying number of steps considering $k_{10}h_r=3$.	157

Figure 6.1(a)	Schematic diagram for articulated floating elastic plate with bottom standing barrier.	162
Figure 6.1(b)	Schematic diagram for articulated floating elastic plate with surface piercing barrier.	164
Figure 6.2	(a) Reflection, (b) transmission and (c) dissipation coefficient versus non-dimensional wavenumber for varying porosity effect parameter G_0 considering $h_1/h=0.5$ and $L_1/L=0.1$.	175
Figure 6.3	(a) Reflection, (b) transmission and (c) dissipation coefficient versus non-dimensional wavenumber for varying barrier heights considering $G_0=0.5+0.5i$, and $L_1/L=0.1$.	176
Figure 6.4	(a) Reflection, (b) transmission and (c) dissipation coefficient versus non-dimensional wavenumber for varying spacing between the barrier considering $G_0=0.5+0.5i$, and $h_1/h=0.5$.	177
Figure 6.5	(a) Plate deflection (b) wave induced strain (c) bending moment and (d) shear force resultants along the plate length x/L for different porosity of the bottom standing barrier considering $k_{10}h=2$, $h_1/h=0.5$ and $L_1/L=0.1$.	178
Figure 6.6	(a) Plate deflection (b) wave induced strain (c) bending moment and (d) shear force resultants along the plate length x/L for varying barrier heights considering $k_{10}h=2$, $G_0=0.5+0.5i$, and $L_1/L=0.1$.	179
Figure 6.7	(a) Plate deflection (b) wave induced strain (c) bending moment and (d) shear force resultants along the plate length x/L for finite spacing L_1/L considering $k_{10}h=2$, $G_0=0.5+0.5i$, and $h_1/h=0.5$	180
Figure 6.8	(a) Reflection, (b) transmission and (c) dissipation coefficient versus non-dimensional wavenumber for varying porosity of vertical barrier considering $h_1/h=0.5$ and $L_1/L=0.1$.	181
Figure 6.9	(a) Reflection, (b) transmission and (c) dissipation coefficient versus non-dimensional wavenumber for varying barrier heights considering $G_0=0.5+0.5i$, and $L_1/L=0.1$.	182
Figure 6.10	(a) Reflection, (b) transmission and (c) dissipation coefficient versus non-dimensional wavenumber for varying spacing between the barrier and floating elastic plate considering $G_0=0.5+0.5i$, and $h_1/h=0.5$.	183

Figure 6.11 (a) Plate deflection (b) wave induced strain (c) bending moment and (d) shear force resultants along the plate length x/L for varying porosity considering $k_{10}h = 2,\ h_1/h = 0.5$ and $L_1/L = 0.1$. 184

Figure 6.12 (a) plate deflection (b) wave induced strain (c) bending moment and (d) shear force resultants along the plate length x/L for varying heights of the surface piercing barrier considering $k_{10}h = 2,$ $G_0 = 0.5 + 0.5i,$ and $L_1/L = 0.1.$ 185

Figure 6.13 (a) Plate deflection (b) wave induced strain (a) bending moment and (b) shear force resultants along the plate length x/L for finite spacing L_1/L considering $k_{10}h = 2,\ G_0 = 0.5 + 0.5i$ and $h_1/h = 0.5$ 186

Figure 6.14 (a) Reflection, (b) transmission and (c) dissipation coefficient versus non-dimensional wavenumber for varying k_{33} and k_{55} considering $G_0 = 0.5 + 0.5i,\ L_1/L = 0.1$ and $h_1/h = 0.5$ in the case of bottom standing porous barrier. 188

Figure 6.15 (a) Reflection, (b) transmission and (c) dissipation coefficient versus non-dimensional wavenumber for varying k_{33} and k_{55} considering $G_0 = 0.5 + 0.5i,\ L_1/L = 0.1$ and $h_1/h = 0.5$ in the case of surface piercing porous barrier. 189

Figure 6.16 (a) Plate deflection (b) wave induced strain (c) bending moment and (d) shear force resultants along the plate length x/L for varying k_{33} and k_{55} considering $k_{10}h = 2,\ G_0 = 0.5 + 0.5i,$ $L_1/L = 0.1$ and $h_1/h = 0.5$ in the case of bottom standing barrier. 190

Figure 6.17 (a) Plate deflection (b) wave induced strain (c) bending moment and (d) shear force resultants along the plate length x/L for varying k_{33} and k_{55} considering $k_{10}h = 2,\ G_0 = 0.5 + 0.5i,$ $L_1/L = 0.1$ and $h_1/h = 0.5$ the case of surface piercing barrier. 191

Figure 6.18 (a) Reflection, (b) transmission and (c) dissipation coefficient versus non-dimensional wavenumber for different support condition considering $G_0 = 0.5 + 0.5i,\ L_1/L = 0.1$ and $h_1/h = 0.5$ in the case of bottom standing barrier. 192

Figure 6.19 (a) Reflection, (b) transmission and (c) dissipation coefficient versus non-dimensional wavenumber for different support conditions considering $G_0 = 0.5 + 0.5i,\ L_1/L = 0.1$ and $h_1/h = 0.5$ in the case of surface piercing barrier**.** 193

Figure 6.20	(a) Plate deflection (b) wave induced strain (c) bending moment and (d) shear force resultants along the articulated plate length x/L for different edge support conditions considering $k_{10}h=2$, $G_0=0.5+0.5i$, $L_1/L=0.1$ and $h_1/h=0.5$ in the case of bottom standing barrier.	194
Figure 6.21	(a) Plate deflection (b) wave induced strain (c) bending moment and (d) shear force resultants along the articulated plate length x/L for different edge support conditions considering $k_{10}h=2$, $G_0=0.5+0.5i$, $L_1/L=0.1$ and $h_1/h=0.5$ in the case of surface piercing barrier.	195
Table 4.1	List of physical constants and variable values/range	98
Table 4.2	Typical nature of k_{33} and k_{55} (Praveen et al., 2018)	99
Table 4.3	Convergence of evanescent modes.	111

TABLE OF CONTENTS

DECLARATION

CERTIFICATE

ACKNOWLEDGEMENT…….. i

ABSTRACT ……..…….. iii

NOMENCLATURE ……... v

ABBREVIATION …….…….… vii

LIST OF FIGURES & TABLES ……... xi

TABLE OF CONTENTS…… xvii

CHAPTER 1

GENERAL INTRODUCTION…… 1

1.1 PREAMBLE…….…….……... 1

1.1.1 Wave Interaction with Floating Structures…… 3

1.1.2 Wave Scattering Due to Articulated Elastic Plate…….…… 3

1.1.3 Wave Transformation Due to Change in Topography…….. 4

1.1.4 Wave Interaction with Submerged Structures…….……. 4

1.2 MOTIVATION……. 5

1.3 AIM AND OBJECTIVES……. 6

1.3.1 Objectives of the Research Study…….…….…… 6

1.3.2 Scope of Work…….…….. 7

1.4 BRIEF OVERVIEW OF THE THESIS…….…….…….. 7

1.5 FUNDAMENTALS OF WAVES AND FLEXIBLE STRUCTURE …….. 11

1.5.1 Basic Equations of Water waves……..…….. 11

1.5.2 Basic Structure equations…….…….…… 16

1.5.3 Coupled boundary conditions ……... 18

1.5.4 Shallow water approximations ……. 23

1.6 EXPANSION FORMULA FOR WAVE STRUCTURE INTERACTION 24

1.6.1 Havelock's expansion formulae …….. 25

1.6.2 Gravity wave in the presence of surface tension (Rhodes-Robinson, 1971) ……... 27

1.6.3 Flexural gravity wavemaker problems (Sahoo et al., 2001) ……..… 28

1.6.4 Modified expansion formulae (Manam et al., 2006) …..……. 31

1.6.5 Generalized Expansion Formulae (Karmakar et al., 2007) …….. 33

1.7 CLOSURE……...…..…… 36

CHAPTER 2

LITERATURE REVIEW…….…… 37

2.1 GENERAL INTRODUCTION ……...……. 37

2.2 WAVE INTERACTION WITH FLOATING STRUCTURES …….. 37

2.2.1 Wave interaction with floating ice-sheets……. 39

2.2.2 Hydroelasticity based on different plate theories…….. 42

2.2.3 Hydroelastic behaviour of VLFS with different support condition.. 48

2.2.4 Wave scattering due to articulated floating elastic plate……... 51

2.2.5 Wave transformation due to bottom topography ……..…… 52

2.2.6 Wave attenuation due to submerged structures…..... 56

2.3 CRITICAL REVIEW…….…..…….. 58

2.4 CLOSURE……...……. 59

CHAPTER 3

WAVE INTERACTION WITH FLOATING PLATE……..……. 61

3.1 GENERAL INTRODUCTION …….……..…….. 61

3.2 MATHEMATICAL FORMULATION…….…….……. 61

3.2.1 Edge-support condition of the elastic plate…….……...……... 64

3.3 METHOD OF SOLUTION…….…….…… 66

3.3.1 Finite water depth…….……. 66

3.3.2 Shallow water approximation …….……. 73

3.4 NUMERICAL RESULTS AND DISCUSSIONS…….……... 75

3.4.1 Finite water depth…….……. 77

3.4.2 Comparative study based on plate theories…….…….. 82

3.4.3 Shallow water approximation…… 85

3.4.4 Comparative study based on Kirchhoff's and Timoshenko-Mindlin theory…….…… 88

3.4.5 Comparative study for finite and shallow water depth ……. 91

3.5 CONCLUSIONS…….…….. 92

CHAPTER 4

WAVE SCATTERING DUE TO ARTICULATED ELASTIC PLATE……. 95

4.1 GENERAL INTRODUCTION …….……... 95

4.2 MATHEMATICAL FORMULATION…….……... 96

4.3 METHOD OF SOLUTION……... 100

4.3.1 Direct Eigenfunction Expansion Method…….……. 100

4.4 NUMERICAL RESULTS AND DISCUSSIONS…….……... 110

4.4.1 Finite water depth ……. 112

4.4.2 Shallow water approximation…….……... 119

4.5 CONCLUSIONS……...…….……... 123

CHAPTER 5

WAVE TRANSFORMATION DUE TO CHANGES IN TOPOGRAPHY… 125

5.1 GENERAL INTRODUCTION …….……. 125

5.2 MATHEMATICAL FORMULATION……...……. 125

5.2.1 Different types of sea bottom profile…….……... 128

5.3 METHOD OF SOLUTION……... 129

5.3.1 Single step bottom topography…….……. 129

5.3.2 Multiple step bottom topography…….…….…… 134

5.4 NUMERICAL RESULTS AND DISCUSSIONS…….……... 140

5.4.1 Single step bottom topography…….…… 140

5.4.2 Two step bottom topography…… 146

5.4.3 Three step bottom topography…….. 151

5.4.4 Comparative study for different number of steps ……. 155

5.5 CONCLUSIONS……... 157

CHAPTER 6

WAVE ATTENUATION DUE TO SUBMERGED STRUCTURES……... 161

6.1 GENERAL INTRODUCTION …….……... 161

6.2 MATHEMATICAL FORMULATION…...……. 161

6.3 METHOD OF SOLUTION…….…….…… 166

6.4 NUMERICAL RESULTS AND DISCUSSIONS…….…….. 173

6.4.1 Bottom standing vertical porous barrier ……...…… 174

6.4.2 Surface piercing vertical porous barrier ……...…… 180

6.4.3 Effect of articulation on floating plate…….. 187

6.4.4 Effect of different support conditions……..... 192

6.4.5 Conclusions…….…….. 196

CHAPTER 7

CONCLUSIONS AND FUTURE WORK…….…… 199

7.1 SUMMARY OF THE RESEARCH WORK ...…… 199

7.2 SIGNIFICANT CONTRIBUTION OF THE THESIS……. 201

7.3 FUTURE SCOPE OF RESEARCH……....…….. 205

REFERENCES…….…… 205

AUTHOR'S RESUME

CHAPTER 1

GENERAL INTRODUCTION

1.1 PREAMBLE

The present era of innovation and technology has led to rapid industrialization and urbanization with increasing demand for land and energy. The recent developments in the construction of very large floating structures have made an attempt to provide a solution to the problem of land and energy shortage which includes exploration of ocean-related to coastal and offshore structures. These floating structures are mainly used to build infrastructures such as floating airports, floating ports, storage facilities (for oil & natural gas), military and emergency base, offshore renewable energy plants and recreation parks. Such huge floating structures are categorized as very large floating structures (VLFS). These types of ocean structures are unique in nature primarily because of their unprecedented length, displacement and associated hydroelastic response, analysis and design. These structures lie on the sea level like a giant plate floating on an inviscid fluid foundation and are suitable for use in calm waters, often inside a lagoon and near the shoreline. These floating structures act as an alternative to the traditional land reclamation processes and can be used for ocean space utilization for human activities like floating airports, storage facilities, military purposes, industrial space etc. Further, the majority of the world population is located along the coastal areas, out of which most cities are densely populated. The effect of global warming with a rise in global temperature has set an alarming situation of sea-level rise over these places. Natural disasters such as hurricanes, tsunamis are constant threats to these coastal cities. Land reclamation from the sea has raised serious concerns over damage to marine ecosystems. So, the construction of the very large floating structures (VLFS) is expected to have minimal impact on the marine ecosystem, water quality and natural current flows.

A similar branch of study is related to the polar region, when ocean waves penetrate into the ice fields to generate flexural gravity waves and the floating ice-sheet is modelled as an elastic plate. These waves weaken and rupture continuously to sea-ice

forming cracks and fissures, which under the action of wind and current may contribute to the demise of the ice-sheet. As a result, more open water regions are created which allow more wave to penetrate into the marginal ice zones (MIZs) in both polar regions. In both cases, because of the large structural size, the hydroelastic responses are more important than their rigid body motions. The main advantages of hydroelasticity theory compared to rigid body analysis are physically more accurate idealization of the fluid-structure interaction system and consequently, more rigorous analysis by which dynamic responses, such as the stresses and bending moments, in the waves can be obtained. This interdisciplinary branch of hydroelasticity embodies the basic equations of fluid mechanics, structural mechanics, concepts on wave propagation and the critically important role of some special type of boundary conditions. The complexities with this class of problems over the gravity wave problems are the conditions at the fluid-structure interface which are of higher order than the governing equations and most of the existing theories developed for the gravity wave problems have to be generalized to incorporate the elastic effects. It is assumed that the deformation gradients experienced by these floating structures due to waves are of sufficiently small amplitude and thus linear wave theory and small amplitude structural response are employed for various aspects of the hydroelastic analysis in the literature. However, for more accurate analysis, non-linear effects are to be considered taken into account to analyse the effect of irregular waves on which the literature is very scanty and the analysis is quite complex.

The study of very large floating structures (VLFS) is gaining momentum to develop infrastructure facilities along the coastal and offshore regions. These floating structures create less conflicts with the marine environment and coastal hazards due to very less physical interaction with the sea bottom. These structures being huge in dimensions, hydroelastic analysis becomes dominant as compared to rigid body motions. These kinds of structures are usually constructed in modules at yards and joined on-site along the connecting joints. These articulated joints are also modelled to reduce the hydroelastic responses of the structures. These structures have a heavy risk of getting damaged due to constant interaction of ocean waves. In order to reduce the impact of ocean waves on to the structures, vertical barriers are placed in front of the VLFS. These vertical barriers are either bottom standing or surface piercing structures depending on the mode of operation and requirement to interact with the incoming ocean waves.

These vertical barriers are also designed for varying porosity in the structure to attenuate and dissipate the wave energy. The study in the consideration of vertical barrier to attenuate the wave energy in front of the large floating structures is very limited.

1.1.1 Wave interaction with floating structures

Very large floating structures are very large in length and width as compared to depth. These structures are usually built near the shore to construct important infrastructure facilities. The wavelength of ocean waves is too short as compared with the huge size of the structure to induce the rigid body motions. These structures are considered to be flexible as compared to other offshore structures and hence the study of hydroelastic behaviour is important. In decades to come, there is going to be a rise in the scarcity of land and this scarcity is leading to the construction of offshore floating structures. In recent years, the hydroelastic performance of the floating structure is given more attention due to the increased design and analysis of multi-use combined platform for the development of infrastructure in the ocean environment. These large floating structures are constructed for building infrastructures like floating airports, mobile offshore bases, floating cities, floating storage device and recreational parks. There is already significant research available for such kind of very large floating structures and some of the existing large floating structures vary from 100 m to 1000 m's in length.

1.1.2 Wave scattering due to the articulated elastic plate

The VLFS to be operational, it has to be designed to take very minimal deflections even under extreme environment conditions. In order to overcome these problems, these large structures are fabricated in modules onshore. The large floating structures are constructed by articulating the small units using vertical liner spring and flexural rotational springs. The articulated joints are considered to restrain for linear and/or rotational motions. Most of the studies consider the structure to be thin for the hydroelastic analysis of VLFS based on Kirchhoff thin plate theory, but these structures have a considerable thickness and hence Timoshenko-Mindlin's plate theory is more realistic for the analysis as formulated by Mindlin (1951). The studies on the effect of articulation are of practical importance to predict the strength and stability of the structure.

1.1.3 Wave transformation due to change in topography

The VLFS is usually constructed near shore and hence the effect of sea bottom profile becomes significant. Sea bottom is not flat throughout, there is various kind of undulations which give rise to wave refraction, shoaling and wave breaking. The topographic variation is very common in most of the ocean-wave propagation problems. Even for the simplest of such problems, like wave scattering by a sudden change in bottom topography, one has to take recourse to approximate solutions. The study on the change in bottom topography provides an insight into the effect of sea bed profile over the wave interaction with floating thick elastic plate.

1.1.4 Wave interaction with submerged structures

Submerged structures are usually not as large as compared to VLFS. These structures are usually built to support the infrastructures such as floating airports, mobile offshore bases, energy plants, recreational parks maybe offshore or near to coastal structures. With the rise in the developments along the coastal and offshore regions, there is a need for submerged structures such as submerged breakwaters, large submerged pontoons supporting floating structures, submerged storage tanks, submerged rail/road tunnels and anti-motion devices. These structures do not cause hindrance to the scenic beauty but reduce the wave effect on coastal and offshore structures.

The studies performed on the wave structure interaction problem in the present thesis consist of both wave and structural part. The wave part is analyzed based on the assumption of the linearized theory of water waves whereas the structures are considered as floating elastic plate, which is modelled using Timoshenko-Mindlin equation. In the study of the wave-structure interaction problem, the physical modelling leads to a class of boundary value problems (BVPs) associated with Laplace equation satisfying certain higher-order boundary conditions. In the present thesis, the wave structure interaction problems analysed are based on the scattering theory of wave motion with emphasis on surface gravity wave and their mutual interactions. In the analysis of the wave scattering problem, the incoming wave is considered as normalized incident waves, the wave that is reflected back is known as “reflected wave” and the wave which is transmitted, is known as “transmitted wave”. The non-dimensional constant such as reflection and transmission coefficients (K_r, K_t) are obtained using

the amplitude of incident, reflected and transmitted wave. The analysis and computation of the reflection and transmission coefficients are important in the analysis of the wave structure interaction problems. The knowledge of reflection and transmission coefficients reveals important information about the amount of wave energy reflected and/or transmitted by the structure. In the present thesis, the emphasis is given to perform hydroelastic analysis of the floating structures along with determination and analyse reflection and transmission coefficient, deflection of the floating elastic plate, strain along the floating elastic plate, bending moment and shear force on the floating elastic plate.

1.2 MOTIVATION

The floating and submerged structures are more advantageous as compared to permanent structures fixed to the sea bottom, extending from shore into open water or onshore structures, over traditional land reclamation in creating land from the sea. The advantage of the design and construction of VLFS are as follows:

- The VLFS are environmentally friendly as they do not damage the marine ecosystem or silt-up deep harbours or disrupt the ocean currents.
- The floating structures are easy to construct, since much of the construction is completed onshore and the installation is rapid and can be easily relocated, removed, or expanded.
- The VLFS is immune to seismic shock since VLFSs are inherently base-isolated.
- The VLFS is cost-effective when the water depth is large or sea bed is soft. They do not suffer from the differential settlement as in reclaimed soil consolidation.
- There is no problem with rising sea level due to global warming and their location in coastal waters provide a scenic body of water all around making them suitable for development associated with leisure and water sport activities.
- The position of VLFS with respect to the water surface is constant and thus facilitate small boats and ship to come alongside when used as piers and berths.

The VLFS is designed for maximum wave height as well as for extreme conditions, but these structures are suitable for the use in calm waters associated with naturally sheltered coastal formations. So, the use of submerged breakwaters, anti-motion devices, anchor or mooring systems is required for the stability of the structures.

1.3 AIM AND OBJECTIVES

The proposed work is focused on the study of the hydroelastic behaviour of large floating flexible structures based on Timoshenko-Mindlin plate theory. The significance and importance of rotary inertia and shear deformation in analysing the hydroelastic behaviour large floating structures are studied. This work aims at studying the influence of different types of edge support conditions, the effect of articulation, variation in bottom topography and the presence of submerged vertical barriers on the hydroelastic behaviour of the large floating elastic plate.

1.3.1 Objectives of the research study

The primary objective of this research is to investigate the hydroelastic behaviour due to the wave interaction with floating and submerged flexible structures based on Timoshenko Mindlin plate theory. In order to achieve the proposed work, the objective of the present study is

- To formulate and analyse the hydroelastic behaviour of large floating elastic plate based on Timoshenko-Mindlin plate theory and compare the results with Kirchhoff thin plate theory at finite and shallow water depth.
- To study the influence of different edge support conditions on the hydroelastic behavior of the floating elastic plate in finite and shallow water depth.
- To understand the significance of articulations in analysing the hydroelastic behaviour of the large floating elastic plate. Further to study the application of wide spacing approximation in reducing the complexity due to the periodic array of multiple articulations in the floating elastic plate.
- To study the significance of different types of bottom topography on the wave interacting with a large floating elastic plate over varying sea bed profile.
- To study the wave attenuation due to the interaction of waves with submerged vertical porous barriers in front of the large floating structures. Further, the effect of articulation and different support conditions are studied.

1.3.2 Scope of work

The scope of research work includes normalized values and realistic assumptions in the analysis of the wave structure interaction. In the present study, a very large floating flexible structure with varying length and infinite width along the lateral direction is considered. The plate thickness is varied along with the finite water depth and shallow water approximation is considered in the analysis. The types of edge boundary conditions considered for the analysis include free-free edge, simply supported edge, fixed edge and moored edge conditions. The bottom topography is considered to be flat and varied stepped for hump or sloping type sea bottom profile. The variation in rotational and linear spring stiffness is considered for the analysis of connected joints in the articulated floating elastic plate. Further, the analysis is performed considering the submerged bottom standing or surface piercing vertical porous barriers in front of the large floating elastic plate.

1.4 BRIEF OVERVIEW OF THE THESIS

The content of the thesis is organised consisting of seven Chapters depending on the physical problem investigated and the solution approach considered in the problem formulation. The detail description of the Chapters are as follows:

In Chapter 1, the introduction and the motivation behind the present work is discussed along with the detail fundamental theory of wave and floating structure is presented. The boundary conditions associated with the wave structure interaction problems considering Timoshenko-Mindlin plate theory in finite and shallow water depths is presented and the development of the expansion formula is discussed in detail. The basic objective of this Chapter is to make the thesis self-contained.

In Chapter 2, the detail review of literature relevant to the wave interaction with floating elastic plates, periodic arrays of articulated floating thick plates, wave transformation due to change in bottom topography and wave attenuation due to the presence of vertical barriers is discussed thoroughly. Further, the research gap based on the literature review is discussed followed by a brief introduction to the research work pursued in this thesis.

In Chapter 3, the hydroelastic response of very large floating structures (VLFS) under the action of ocean waves is analysed considering the small-amplitude wave theory.

The numerical study is performed to analyse the wave reflection and transmission characteristics of the floating plate under the influence of different support conditions using eigenfunction expansion method along with the orthogonal mode coupling relation in the case of finite water depth. The hydroelastic behaviour in terms of reflection and transmission coefficient, plate deflection, plate induced strain, bending moment and shear force of the floating thick elastic plate with support conditions is analysed and compared for finite and shallow water depth.

In Chapter 4, the periodic array of multiple articulated floating elastic plate acted upon by ocean waves is analysed. The floating elastic plate is placed periodically and is interconnected with vertical linear and flexural rotational springs which act as an articulated joint. The interconnected joints are considered to be flexible, with variable translation and rotational stiffness. Further, the wide-spacing approximation method is employed to analyse the hydroelastic behaviour of the multiple articulated floating elastic plate. The results obtained using the eigenfunction expansion method is compared with the results based on wide-spacing approximation at finite water depth and validated with the results available in the literature.

In Chapter 5, the propagation of gravity waves along the finite floating elastic plate over varying sea bottom profile is studied considering the abrupt change in the bottom profile such as (a) step-type, (b) sloping bottom, (c) hump and (d) double hump below the plate covered region. Detail comparison of the numerical results is performed for different step bottom topography on the hydroelastic characteristics of a floating elastic platform. The study provides an insight into the effect of ocean bottom profile on the wave propagation due to the presence of large floating elastic plate at finite water depth.

In Chapter 6, the attenuation of the incident wave interacting with very large floating structures (VLFS) in the presence of vertical barriers is analysed considering small-amplitude wave theory. The mitigation in the hydroelastic response due to the wave interaction with articulated floating elastic plate in the case of bottom standing and surface piercing vertical barrier is performed using eigenfunction expansion method along with the orthogonal mode coupling relation The influence of different edge support conditions in combination of articulation in mitigating the hydroelastic behaviour of floating elastic plate is discussed in detail. The study provides an understanding of articulation in combination with the different types of support and vertical porous barriers in mitigating the structural response.

Finally, Chapter 7 summarizes the work done in the thesis followed by the future scope of research. The major contributions made in the thesis are also highlighted in this Chapter. The following manuscripts are written during the preparation of the present thesis and the details of their publication status in various Journals, Book Chapters and Conference proceedings are given below.

List of publication in Journals:

1. Praveen, K.M., Karmakar, D. & Guedes Soares, C. (2020), "Wave interaction with floating elastic plate based on Timoshenko-Mindlin plate theory." *Journal of Offshore Mechanics and Arctic Engineering (ASME),* vol 142(1), pp. 011601-1-15.
2. Praveen, K.M., Karmakar, D. & C. Guedes Soares (2019), "Hydroelastic analysis of periodic arrays of multiple articulated floating elastic." *Ships and Offshore Structures,* DOI: 10.1080/17445302.2019.1615167, (In Press).
3. Praveen, K.M., Karmakar, D. & Guedes Soares, C. (2019), "Influence of support conditions on the hydroelastic behaviour of floating thick elastic plate." *Journal of Marine Science and Applications,* vol. 18(3), pp. 295-313.
4. Praveen, K.M., Karmakar, D. & Guedes Soares, C. (2018), "Hydroelastic analysis of articulated floating elastic plate based on Timoshenko–Mindlin plate theory." *Ships and Offshore Structures,* 13(S1), pp. 287-301.
5. Praveen, K.M., Venkateswarlu, V. & Karmakar, D. (2020). "Wave transformation due to finite floating elastic plate with abrupt change in bottom topography." (Submitted).
6. Praveen, K.M., Venkateswarlu, V. & Karmakar, D. (2020). "Hydroelastic response of floating elastic plate in the presence of vertical porous barriers." (Submitted).

List of publication in Book Chapters:

7. Praveen, K.M., Karmakar, D., & Nasar, T. (2016), "Hydroelastic analysis of floating elastic thick plate in shallow water depth." *Perspectives in Science*, Vol *8,* pp 770-772. (*International Conference on Recent Trends in Engineering and Materials Science* (ICEMS-2016), 17th -19th March 2016, Jaipur National University, Jaipur).

8. Praveen, K.M., Karmakar, D. (2019), "Wave Transformation Due to Floating Elastic Thick Plate over Changing Bottom Topography." *Lecture Notes in Civil Engineering, book series*, vol 23, pp 417-430, Springer, Singapore (*4th International Conference in Ocean Engineering* (ICOE 2018), 18th - 21st February 2018, IIT Madras, Chennai, India).

9. Praveen, K.M. and Karmakar, D. (2019). "Wave transformation due to floating elastic thick plate over multiple stepped bottom topography." *IOP: Journal of Physics Conference Series*, vol. 1276(1), pp. 012-18, IOP Publishing. (*International Conference on Recent Advances in Fluid and Thermal Sciences* (iCRAFT 2018), 5th – 8th December 2018, BITS Pilani, Dubai Campus, Dubai, UAE.)

List of publication in Conference Proceedings:

10. Praveen K.M. and Karmakar, D. (2016). "Hydroelastic analysis of floating elastic plate in finite water depth based on Timoshenko-Mindlin Theory." *21st Conference on Hydraulics, Water resources & Environmental Engineering* (HYDRO 2016), 8th - 10th December 2016, Central Water & Power Research Station, Pune, India.

11. Praveen, K.M., Karmakar, D & Guedes Soares, C. (2018), "Hydroelastic analysis of articulated floating elastic plate based on Timoshenko–Mindlin plate theory." *2nd International Conference on Ships and Offshore Structures* (ICSOS 2017), 11th - 13th September 2017, Shenzhen, China.

12. Praveen K.M. and Karmakar, D. (2018). "Wave interaction with multiple articulated floating elastic plates based on Timoshenko Mindlin Plate Theory." *6th Indian National Conference on Coastal, Harbour and Ocean Engineering* (INCHOE 2018), 26th – 28th September 2018, CWPRS, Pune, India.

13. Praveen K M, Venkateswarlu, V and Karmakar, D. (2019). "Wave attenuation due to the presence of submerged barrier along with floating VLFS." *24th Conference on Hydraulics, Water Resources & Environmental Engineering* (HYDRO 2019), 18th – 20th December 2019, Osmania University, Hyderabad, India.

1.5 FUNDAMENTALS OF WAVES AND FLEXIBLE STRUCTURE

In order to analyze the fluid-structure interaction problem, certain physical assumptions are made to formulate the mathematical model of the physical problem. In this Section, the basic equation for the water wave theory and the basic equations for the flexible floating structure along with the boundary conditions related to the present research work is discussed in brief. Further, the details on the development of the expansion formulae for the wave structure interaction problem is described and discussed.

1.5.1 Basic equations of water wave

In the present section, the fluid is considered to be irrotational motion, inviscid and incompressible which is bounded above the free surface and is under the action of gravity and constant atmospheric pressure. The monochromatic wave is assumed to act along the positive *x*-axis. A 2D Cartesian coordinate system is considered which has a longitudinal *x*-axis and the y-axis is vertically downwards positive. The fluid is bounded below by the smooth rigid bottom surface of uniform depth h in the case of finite and shallow water depth and the fluid is of infinite horizontal extent in both the cases. The fluid occupies the infinite strip $-\infty < x, z < \infty$, $0 < y < h$ in both the cases of fluid of finite and shallow depth. The instantaneous upper fluid surface is defined by the wave profile $y = \zeta(x, z, t)$ where $\zeta(x, z, t)$ is the free surface elevation at the time t (see Figure 1.1).

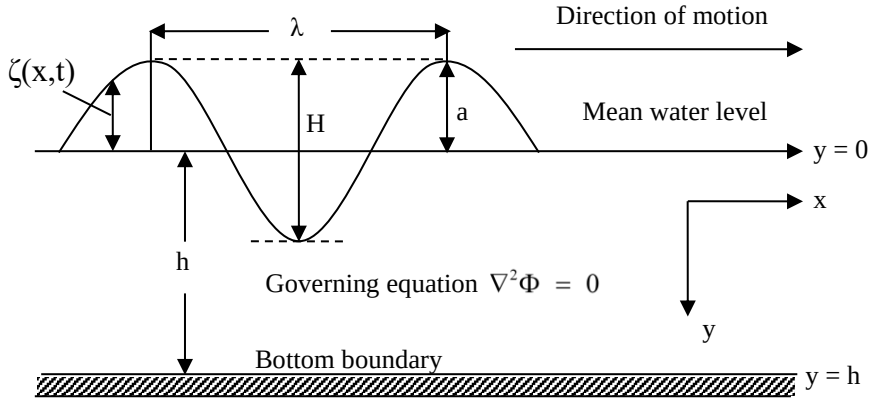

Figure 1.1: Schematic diagram for wave propagation.

Under the assumption of the fluid to be irrotational motion, inviscid and incompressible as mentioned above, we have the existence of a velocity potential $\Phi(x, y, t)$ which satisfies the Laplace equation given by

$$\frac{\partial^2 \Phi_j}{\partial x^2} + \frac{\partial^2 \Phi_j}{\partial y^2} = 0 \text{ at } -\infty < x < \infty, 0 < y < h. \tag{1.1}$$

In the wave structure interaction problems, the governing equation is the two/three-dimensional Laplace equation as mentioned above. Next, we will discuss the various types of boundary conditions which arise in the wave structure interaction problems.

1.5.1.1 Kinematic free surface boundary condition (KFSBC)

Let us consider $F(x, y, z, t) = 0$ to be the surface that constitutes a fixed or moving boundary. Then, the kinematic boundary condition is derived based on the assumption that there is no gap across the surface/interface, which yields

$$\frac{DF}{Dt} = 0, \tag{1.2}$$

where D/Dt represents the material derivative, which is a combination of time and space derivatives and is given by

$$\frac{D}{Dt} \equiv \partial_t + u\partial_x + v\partial_y + w\partial_z, \tag{1.3}$$

where u, v and w being the x, y and z components of the fluid velocity V. In the context of water waves, we have two surfaces namely (i) the bottom surface and (ii) the free surface. In general, the bottom boundary surface is described as $y = h(x, z, t)$, where the origin is at the mean free surface $y = 0$ and $h(x, z, t)$ represents the water depth. In the context of the present work, the bottom surface is assumed to be impermeable and is given by $F(x, y, z, t) = y - h(x, z, t)$. Thus, a similar assumption that there is no gap between the bottom surface and the fluid at $y = h(x, z, t)$ yields

$$\left\{\partial_t + u\partial_x + w\partial_z\right\} h - v = 0. \tag{1.4}$$

On the other hand, in the case of water of finite depth, i.e., for $y = h$, the bottom boundary condition is given by

$$\frac{\partial \Phi}{\partial y} = 0 \text{ at } y = h. \tag{1.5}$$

In a similar manner, the free surface of a wave can be described as $F(x, y, z, t) = y - \zeta(x, z, t)$, where $\zeta(x, z, t)$ is the vertical displacement of the free

surface about the horizontal plane $y = 0$ (referred to as the mean free surface). Thus, from the condition (1.2), the kinematic condition on the free surface becomes

$$\zeta_t + \Phi_x \zeta_x + \Phi_z \zeta_z = \Phi_y \text{ on } y = \zeta(x, z, t). \tag{1.6}$$

Next, using the Taylor series expansion, we expand the terms present in the Equation (1.6) with respect to the mean free surface $y = 0$, which yield

$$\left(\Phi_y - \zeta_t - \Phi_x \zeta_x - \Phi_z \zeta_z\right)\Big|_{y=0} + \zeta \partial_y \left(\Phi_y - \zeta_t - \Phi_x \zeta_x - \Phi_z \zeta_z\right)\Big|_{y=0} + \ldots = 0. \tag{1.7}$$

Under the assumptions of the linearized theory of water waves, the velocity of the water particles, the free surface elevation $\zeta(x, z, t)$ and their derivatives are small quantities, which yield that the product and square terms of ζ and Φ are very small. Hence, neglecting the product, square and higher powers of the dependent variables ζ and Φ, the linearized kinematic condition on the mean free surface $y = 0$ is obtained as

$$\zeta_t = \Phi_y \text{ on } y = 0. \tag{1.8}$$

1.5.1.2 Dynamic free surface boundary condition (DFSBC)

A fixed surface like rigid bottom topography can support the pressure variation, whereas the free surface like the air-water interface can not support the variations in pressure. Thus, a second boundary condition is required to describe the pressure distribution on the free surface boundary, which is called the dynamic free surface boundary condition. The dynamic free surface boundary condition is derived under the assumption that on the free surface $y = \zeta(x, z, t)$, the hydrodynamic pressure is the same as the atmospheric pressure. Thus, from Bernoulli's equation, we have

$$\Phi_t + \frac{1}{2}\left\{\Phi_x^2 + \Phi_y^2 + \Phi_z^2\right\} - gy = \frac{P}{\rho}, \text{ on } y = \zeta(x, z, t), \tag{1.9}$$

where P is the atmospheric pressure, which is assumed to be constant and is taken as $P = 0$ without loss of generality. It may be noted that in the dynamic condition on the free surface, the effect of surface tension is neglected. Proceeding in a similar manner as in Equation (1.6), the Taylor series expansion of the terms present in Equation (1.8) with respect to the mean free surface $y = 0$ yields

$$\left[\Phi_t + \frac{1}{2}\left\{\Phi_x^2 + \Phi_y^2 + \Phi_z^2\right\} - gy\right]\Big|_{y=0} + \zeta\partial_y\left[\Phi_t + \frac{1}{2}\left\{\Phi_x^2 + \Phi_y^2 + \Phi_z^2\right\} - gy\right]\Big|_{y=0} + \ldots = 0. \quad (1.10)$$

Proceeding with similar assumption as in case of the kinematic condition (1.6), here also we neglect the product, square and higher powers of the dependent variables ζ and Φ, to obtain the linearized dynamic free surface condition on the mean free surface $y = 0$ as given by

$$\Phi_t = g\zeta \text{ on } y = 0. \quad (1.11)$$

It may be noted that these linearized forms in Equations (1.7) and (1.9) can also be obtained by using a perturbation series expansion for ζ and Φ, as in Stoker (1957). Eliminating ζ from the Equations (1.7) and (1.9), we arrive at the boundary condition on the mean free surface as given by

$$\Phi_{tt} = g\Phi_y \text{ on } y = 0. \quad (1.12)$$

Once, Φ is obtained, $\zeta(x,z,t)$ can be computed from any one of the Equations (1.7) and (1.9). Assuming that the fluid motion is simple harmonic in time with angular frequency ω, the velocity potential $\Phi(x,y,z,t)$ and the surface elevation $\zeta(x,z,t)$ can be written in the form $\Phi(x,y,z,t) = \mathrm{Re}\left\{\phi(x,y,z)e^{-i\omega t}\right\}$ and $\zeta(x,z,t) = \mathrm{Re}\left\{\eta(x,z)e^{-i\omega t}\right\}$ Thus, the spatial velocity potential $\phi(x,y,z)$ satisfies the Laplace Equation (1.1) and the bottom boundary condition (1.5). However, the linearized free surface boundary condition (1.10) yields

$$\phi_y + K\phi = 0 \text{ at } y = 0, \quad (1.13)$$

where $K = \omega^2/g$. The condition (1.11) represents the free surface condition in the absence of surface tension in the linearized theory of surface water waves of homogeneous density having a free surface.

1.5.1.3 Velocity potential, surface elevation and dispersion relation

In the case of obliquely incident surface waves, the water surface profile associated with a monochromatic progressive wave is in general given by

$$\zeta(x,z,t) = \frac{H}{2}\cos\left\{\left(k_x\right)x + \left(k_z\right)z - \omega t\right\}, \quad (1.14)$$

where H is water depth, $k = (= 2\pi / \lambda)$ is wavenumber, λ is wavelength, $\omega (= 2\pi / \mathrm{T})$ is angular frequency, T is wave period, $k_x = k\cos\theta$ and $k_z = k\sin\theta$ with θ being the angle made by the wave with the positive $x-$ axis. The corresponding velocity potential $\Phi(x, y, z, t)$ satisfying the governing Equation (1.1) along with the bottom boundary condition (1.5a) and the linearized free surface condition (1.11) is expressed as

$$\Phi(x, y, z, t) = \frac{H}{2}\frac{g}{\omega}\frac{\cosh k(h-y)}{\cosh kh}\sin\left\{(k_x)x + (k_z)z - \omega t\right\}, \tag{1.15}$$

where k and ω are related by the dispersion relation given by

$$\omega^2 = gk\tanh kh \tag{1.16}$$

Now we make a note on wave classification which is based on relative water depth h/λ. The waves are called shallow-water waves or long waves if $h/\lambda < 1/20$. In case $h/\lambda > 1/2$, the waves are called deep water waves. In the intermediate range $1/20 < h/\lambda < 1/2$, the waves are termed as the intermediate depth waves. The dispersion relation for shallow water reduces to $\omega^2 = gk^2h$ and in case of deep water waves, it is given by $\omega^2 = gk$.

1.5.1.4 Far-field boundary condition

In the case of a BVP defined in an infinite/semi-infinite domain, the uniqueness of the solution demands the behaviour of the function at the far-field. In case of water wave problems, often the fluid domains are either the half/quarter-planes or infinite/semi-infinite strips depending on whether the problem is considered in the water of infinite or finite depths. Without going into theoretical details, we will prescribe the far-field boundary conditions in the case of plane progressive waves as given by

$$\Phi(x, y, z, t) \sim \left\{Ae^{i(k_x x + k_z z - \omega t)} + Be^{-i(k_x x + k_z z + \omega t)}\right\}\frac{\cosh k(h-y)}{\cosh kh}, \quad x, z \to \pm\infty, \tag{1.17}$$

in the case of finite water depth and for the case of shallow water depth is given by

$$\Phi(x, y, z, t) \sim \left\{Ae^{i(k_x x + k_z z - \omega t)} + Be^{-i(k_x x + k_z z + \omega t)}\right\}, \; x, z \to \pm\dot{\infty}. \tag{1.18}$$

In the above conditions, A and B are constants associated with the wave amplitudes at the far-field and depend upon the physical nature of the problem.

1.5.2 Basic structure equations

In this subsection, the plate equations and boundary conditions associated with the floating elastic plate are discussed. The derivation of the Timoshenko-Mindlin plate theory is explained in detail.

1.5.2.1 Timoshenko-Mindlin plate theory

Timoshenko presented a method to account for rotary inertia and shear deformation for beam given by Timoshenko beam theory. The Timoshenko beam theory was extended by Mindlin (1951) know as Timoshenko-Mindlin plate theory applicable to thick plates. The Timoshenko-Mindlin theory is an extension of Kirchhoff-Love plate theory and it takes into account the shear deformations through the thickness of a plate. Main reason to the use of the Timoshenko beam theory is to take into account the shear deformation and rotational bending effects. Because of this it is applicable for thick beams, sandwich composite beams, or beams subject to high-frequency excitation when the wavelength approaches the thickness of the beam. This theory is special for the thick plates in which the normal to the mid plate surface remains straight but not necessarily perpendicular to the mid plate surface. Normally, this Mindlin plate theory is used to calculate the deformations and stresses in a plate whose thickness is of the order of one tenth the planar dimensions or higher. Taking into account the added mechanisms of deformation effectively lowers the stiffness of the beam and this can result into a larger deflection under a static load and lower predicted eigen frequencies for a given set of boundary conditions. This effect is more noticeable for higher frequencies as the wavelength becomes shorter (i.e. in principle comparable to the height of the beam or shorter). Thus, the distance between opposing shear forces decreases.

Equilibrium approach is considered which utilizes the strain displacement relations, stress resultants to derive the Timoshenko-Mindlin plate theory (Rao, 2007). Using the stress-strain relations and strain-displacement relations, the force and moment resultants per unit length for the Timoshenko-Mindlin plate are given by

$$Q_x = \mu G d\left(\delta_x + \frac{\partial \zeta}{\partial x}\right),\ Q_y = \mu G d\left(\delta_y + \frac{\partial \zeta}{\partial y}\right)\Bigg\} \quad \text{Shear force,} \tag{1.19}$$

$$M_x = EI\left(\frac{\partial \delta_x}{\partial x} + \nu\frac{\partial \delta_y}{\partial y}\right),\ M_y = EI\left(\frac{\partial \delta_y}{\partial y} + \nu\frac{\partial \delta_x}{\partial x}\right)\Bigg\} \quad \text{Bending moment,} \tag{1.20}$$

$$M_{xy} = M_{yx} = \frac{EI(1-\nu)}{2}\left(\frac{\partial \delta_x}{\partial y} + \frac{\partial \delta_y}{\partial x}\right)\Bigg\} \quad \text{Twisting moment,} \tag{1.21}$$

where δ_x denotes the rotation in the $x-z$ plane, δ_y is denotes the rotation in the $y-z$ plane and ζ denotes the plate deflection. The equilibrium equations for the Mindlin plate by considering the effect of rotary inertia is given as

Vertical force equilibrium in the z-direction:

$$\frac{\partial Q_x}{\partial x} + \frac{\partial Q_y}{\partial y} + P = \rho_p d \frac{\partial^2 \zeta}{\partial t^2}. \tag{1.22}$$

Moment equilibrium about the x-axis:

$$-Q_y + \frac{\partial M_y}{\partial y} + \frac{\partial M_{xy}}{\partial x} = \frac{\rho_p d^3}{12}\frac{\partial^2 \delta_y}{\partial t^2}. \tag{1.23}$$

Moment equilibrium about the y-axis:

$$-Q_x + \frac{\partial M_x}{\partial x} + \frac{\partial M_{xy}}{\partial y} = \frac{\rho_p d^3}{12}\frac{\partial^2 \delta_x}{\partial t^2}. \tag{1.24}$$

Substituting force and moment resultants into the above equations, the equation of motion in terms of displacement unknowns $\zeta(x,z,t)$, δ_x and δ_y is given by

$$\mu G d\left(\nabla^2 \zeta + \Omega\right) + P = \rho_p d \partial_t^2 \zeta, \tag{1.25}$$

$$\frac{EI}{2}\left[(1-\nu)\nabla^2 \delta_x + (1+\nu)\partial_x \Omega\right] - \mu G d\left(\delta_x + \frac{\partial \zeta}{\partial x}\right) = \frac{\rho d^3}{12}\partial_t^2 \delta_x, \tag{1.26}$$

$$\frac{EI}{2}\left[(1-\nu)\nabla^2 \delta_y + (1+\nu)\partial_y \Omega\right] - \mu G d\left(\delta_y + \frac{\partial \zeta}{\partial y}\right) = \frac{\rho_p d^3}{12}\partial_t^2 \delta_y, \tag{1.27}$$

where $\Omega = \frac{\partial \delta_x}{\partial x} + \frac{\partial \delta_y}{\partial y}$. Combining Eqs. (1.26) and (1.27) and rewriting, we get

$$EI\nabla^2 \Omega - \mu G d\Omega - \mu G d\nabla^2 \zeta = \frac{\rho_p d^3}{12}\partial_t^2 \Omega. \tag{1.28}$$

Combining Eqs. (1.25) and (1.28) and rewriting, we obtain the Timoshenko-Mindlin thick plate equation

$$\left(\nabla^2 - \frac{\rho_p}{\mu G}\partial_t^2\right)\left(EI\nabla^2 - \frac{\rho_p d^3}{12}\partial_t^2\right)\zeta + \rho_p d\partial_t^2\zeta = -\left(1 - \frac{EI}{\mu G d}\nabla^2 + \frac{\rho_p d^2}{12\mu G}\partial_t^2\right)P, \quad (1.30)$$

where $EI = Ed^3/12(1-\nu^2)$ is the plate rigidity and $G = E/2(1+\mu)$ is the shear modulus of the plate, $\mu = \frac{\pi^2}{12}$ is the transverse shear coefficient, E is Young's modulus, ν is the Poisson's ratio, $m_s = \rho_p d$ is the mass per unit area, ρ_p is the density of plate, g is the acceleration due to gravity and d is the plate thickness. If the shear modulus of the beam material approaches infinity and the beam becomes rigid in shear and if rotational inertia effects are neglected, Timoshenko beam theory converges towards ordinary beam theory. Additionally, for the case for small deflections of a beam that are subjected to lateral loads only, the Timoshenko beam theory will reduce to the Euler-Bernoulli beam theory. The Kirchhoff-Love theory or simply Kirchhoff's thin plate theory is applicable to thinner plates.

1.5.2.1 Kirchhoff's plate theory

Kirchhoff's thin plate theory assumes the plate thickness to be small and neglects the effect of rotary inertia and shear deformation. If effects of rotary inertia, I_R and shear deformation, S are neglected, then the terms involving $I_R = d^2/12$ and $S = EI/\mu Gd$ will be zero. Thus, the above equation (1.30) reduces to the Kirchhoff's thin plate equation given by

$$EI\nabla^4\zeta + \rho_p d\partial_t^2\zeta = p. \quad (1.31)$$

1.5.3 Coupled boundary conditions

In the wave structure interaction problems, the fluid and structure parts are analysed separately and are coupled at the end to obtain required physical quantities. In the present Subsection, the boundary conditions at the interface of the structure and the fluid are coupled and are presented in terms of the velocity potential. As a result, the whole physical problem is easily expressed as a boundary value problem associated with the Laplace equation satisfying the higher-order boundary in terms of the velocity potential $\Phi(x, y, z, t)$. Assuming the fluid characteristics as presented in Section 1.5.1, the fluid pressure P_s is obtained from the linearized Bernoulli's equation given by

$$P_s = -\rho\Phi_t + \rho g\zeta, \quad \text{on } y = 0, \tag{1.32}$$

where ρ is the density of the water and g is the acceleration due to gravity. The linearized kinematic condition is given by

$$\zeta_t = \Phi_y \text{ on } y = 0 \tag{1.33}$$

Timoshenko- Mindlin thick plate equation in terms of the plate deflection $\zeta(x,z,t)$ in two-dimension is given by

$$\left\{\left(EI\nabla^2 - m_s I_R \partial_t^2\right)\left(\nabla^2 - \frac{m_s S}{EI}\partial_t^2\right)\zeta + m_s\zeta_{tt}\right\} = -\left\{1 - S\nabla^2 + \frac{m_s I_R S}{EI}\partial_t^2\right\}P(x,z,t), \tag{1.34}$$

where $P(x,z,t)$ is the external pressure due to the fluid and is given by (1.32). Combining the kinematic and dynamic boundary conditions (1.32), (1.33) and (1.34), the boundary condition on the plate covered mean free surface $y = 0$ is obtained as

$$\begin{aligned}\left\{\left(EI\nabla^2 - m_s I_R \partial_t^2\right)\left(\nabla^2 - \frac{m_s S}{EI}\partial_t^2\right) + m_s\partial_t^2\right\}\Phi_y + \rho g\left\{1 - S\nabla^2 + \frac{m_s I_R S}{EI}\partial_t^2\right\}\Phi_y \\ = \rho\left\{1 - S\nabla^2 + \frac{m_s I_R S}{EI}\partial_t^2\right\}\Phi_{tt}.\end{aligned} \tag{1.35}$$

In the case of time-harmonic motions with angular frequency ω, the plate covered free surface condition (1.35) will reduce to the form as given by

$$\left(\alpha_0 + \alpha_1\nabla^2 + \alpha_2\nabla^4\right)\phi_y + \left(\beta_0 - \beta_1\nabla^2\right)\phi = 0 \text{ on } y = 0. \tag{1.36}$$

Since ϕ satisfies the Laplace equation, the above equation is often rewritten in the following form

$$\left(\alpha_0 - \alpha_1\partial_y^2 + \alpha_2\partial_y^4\right)\phi_y + \left(\beta_0 - \beta_1\partial_y^2\right)\phi = 0 \text{ on } y = 0, \tag{1.37}$$

where $\alpha_0 = \left\{1 - m_s\omega^2\left(\frac{I_R S}{EI}\right)\right\}$, $\alpha_1 = \left\{\frac{m_s\omega^2 I_R}{\left(\rho g - m_s\omega^2\right)} - S\right\}$, $\alpha_2 = \frac{EI}{\left(\rho g - m_s\omega^2\right)}$,

$\beta_0 = \frac{\rho_p\omega^2}{\left(\rho g - m_s\omega^2\right)}\left(1 - m_s\omega^2\frac{I_R S}{EI}\right)$, $\beta_1 = -\frac{\rho_p\omega^2 S}{\left(\rho g - m_s\omega^2\right)}$ and $I_R = d^2/12$.

It may be noted that in the case of $L/d < 10$, where L is the characteristic length of the elastic plate, shear deformation and rotary inertia play important roles. In such a situation, one has to use the Timoshenko-Mindlin thick plate model to describe the dynamic behaviour of the floating elastic plate. On the other hand, if $L/d > 10$, then shear deformation and rotary inertia can be neglected and in such a situation, the thick plate equation reduces to thin plate equation in one-dimension, based on Kirchhoff thin plate equation, and is given by

$$\left(\alpha_2 \partial_y^4 + 1\right)\phi_y + \beta_0 \phi = 0. \tag{1.38}$$

It can be easily observed that if $EI = 0$ and $\rho_p = 0$, Equation (1.38) reduces to the linearized capillary gravity wave mean free surface boundary condition.

1.5.3.1 Edge conditions

The wave interaction with the floating elastic plate is based on the edge conditions at the plate edges. The floating elastic plate is considered to satisfy one of the following edge support conditions (Timoshenko and Krieger (1959), Rao (2007)). Three types of edge conditions i.e. free – free edge support, simply supported edge and fixed edge along with the articulation conditions at the connecting joints are considered in the analysis.

Case 1: Freely floating elastic plate

The freely floating elastic plate represents zero bending moment and zero shear force at the plate edge. In the case of finite water depth, the bending moment and shear force at the plate edge $x = 0, -a$ satisfies the relation given by

$$\partial_y^3 \phi_j\left(x, y\right) = 0 \text{ and } \partial_{xy^3}^4 \phi_j\left(x, y\right) = \wp \partial_{xy}^2 \phi_j\left(x, y\right) \text{ for } x = 0, -a \text{ at } y = 0, \tag{1.39}$$

where $\wp = \left\{ \dfrac{m\omega^2 (S + I)}{EI} \right\}$, j represents the respective domain in considerations.

Case 2: Simply supported floating elastic plate

In this case the simply supported edge, the edge condition represents the bending moment and deflection to vanish at the edges or at the supports for finite water depth.

The plate edge is considered to be having zero deflection/displacement and zero bending moment at $x = 0, -a$ satisfying the relation

$$\partial_y \phi_j (x, y) = 0 \text{ and } \partial_y^3 \phi_j (x, y) = 0 \text{ for } x = 0, -a \text{ at } y = 0. \tag{1.40}$$

Case 3: Fixed edge floating elastic plate

In the case of fixed edge condition, the deflection and slope vanish at the edge. So, for finite water depth, we consider zero slopes and zero deflection/displacement at the plate edge $x = 0, -a$ which satisfies the relation

$$\partial_y \phi_j (x, y) = 0 \text{ and } \partial_{xy}^2 \phi_j (x, y) = 0 \text{ for } x = 0, -a \text{ at } y = 0. \tag{1.41}$$

Case 4: Articulation conditions

In the case of articulation in the floating elastic plate, the connecting joints are exhibited as connection with vertical linear and/or flexural rotational springs with stiffness k_{33} and k_{55} respectively. The bending moment and shear force acting at the articulated edges are formulated based on the nature of k_{33} and k_{55} given by the relation (Xia et al., 2000, Chung and Fox, 2005)

$$EI\partial_y^3 \phi_j (x+, 0) = -k_{55} \left\{ \partial_{xy}^2 \phi_j (x+, 0) - \partial_{xy}^2 \phi_{(j+1)} (x-, 0) \right\}, \tag{1.42a}$$

$$EI\partial_y^3 \phi_{(j+1)} (x-, 0) = -k_{55} \left\{ \partial_{xy}^2 \phi_j (x+, 0) - \partial_{xy}^2 \phi_{(j+1)} (x-, 0) \right\}, \tag{1.42b}$$

$$EI\left[\partial_{xy^3}^4 \phi_j (x+, 0) - \wp \partial_{xy}^2 \phi_j (x+, 0) \right] = k_{33} \left\{ \partial_y \phi_j (x+, 0) - \partial_y \phi_{(j+1)} (x-, 0) \right\}, \tag{1.42c}$$

$$EI\left[\partial_{xy^3}^4 \phi_{(j+1)} (x-, 0) - \wp \partial_{xy}^2 \phi_{(j+1)} (x-, 0) \right] = k_{33} \left\{ \partial_y \phi_j (x+, 0) - \partial_y \phi_{(j+1)} (x-, 0) \right\}. \tag{1.42d}$$

Depending upon the nature of the vertical linear spring and/or a flexural rotational spring, the shear force and the bending moment at the articulated joints are formulated. The values of k_{33} and k_{55} tends to zero for the case of free edge condition. If either of the spring stiffness k_{33} or k_{55} tends to zero, then the connection illustrates a hinge connector or a slider connection. For a rigid connection, the stiffness values tend to infinity i.e. $k_{33} \to \infty$ and $k_{55} \to \infty$ as explained in as in Table 4.2.

Case 5: Continuity equations

The continuity of velocity and pressure across the interfaces using the conservation of mass in the fluid domains is given by

$$\phi_{jx}(x,y)=\phi_{(j+1)x}(x,y) \text{ and } \phi_j(x,y)=\phi_{(j+1)}(x,y), x=-a \text{ and } x=0,\ 0<y<h. \quad (1.43)$$

In order to formulate the boundary value problem for varying bottom topography, the continuity equation (Karmakar et al., 2010) for deflection, slope, bending moment and shear force at the step interfaces is given by

$$\partial_y\phi_j(x,y)=\partial_y\phi_{(j+1)}(x,y), \quad (1.44a)$$

$$\partial^2_{xy}\phi_j(x,y)=\partial^2_{xy}\phi_{(j+1)}(x,y), \quad (1.44b)$$

$$\partial^3_y\phi_j(x,y)=\partial^3_y\phi_{(j+1)}(x,y), \quad (1.44c)$$

$$\left(\partial^4_{xy^3}-\wp\partial^2_{xy}\right)\phi_j(x,y)=\left(\partial^4_{xy^3}-\wp\partial^2_{xy}\right)\phi_{(j+1)}(x,y). \quad (1.44d)$$

1.5.3.2 Boundary condition at the vertical barrier

Due to the presence of a vertical porous barrier in front of the floating elastic plate, the boundary condition considering Darcy's law is given by

$$\partial\phi_{jx}=-ik_{10}G_0(\phi_2-\phi_1),\ j=1,2, \quad (1.45)$$

where $G_0=G_r+iG_i$ is the complex porous parameter with the real part G_r represents the resistance effect of the porous material against the seepage flow while the imaginary part G_i denotes the inertia effect of the fluid inside the porous material. The complex effect porous parameter is defined by Yu and Chwang (1994) as given by

$$G_0=\frac{\varepsilon\left(f+iS_i\right)}{k_{10}d\left(f^2+S_i^{\,2}\right)}, \quad (1.46)$$

where ε is the porosity constant, f is the resistance force coefficient, S_i is the inertial force coefficient, d is the thickness of the porous medium and k_{10} is the wavenumber of the incident wave. The boundary conditions at the porous vertical barrier is derived by combining the boundary condition at the vertical porous barrier as in Eq. (1.45) and the continuity equation for velocity at $x=0$ (Yu and Chwang, 1994).

$$-ik_{10}G_0(\phi_{j+1}-\phi_j)=\begin{cases}0, & \text{for open gap,}\\ \dfrac{\partial\phi_j}{\partial x}, & \text{for vertical barrier.}\end{cases} \tag{1.47}$$

1.5.4 Shallow water approximation

In this section, we are considering the surface gravity waves that get influenced by the by water depth. This implies that the depth of water is equal to or less than the half of wavelength. These types of waves are called long waves. In the case of long waves, the horizontal component of the fluid velocity is much larger compared to the vertical components. In a fluid domain of finite depth which is infinitely large in both x and z directions with q being the fluid particle velocity with components (u,v,w) and y being considered vertically downward positive, the equation of motion for the linearized long waves takes the form

$$u_t-g\zeta_x=0,\quad w_t-g\zeta_z=0. \tag{1.48}$$

Further, the equation of continuity for the two-dimensional long wave is given by

$$\zeta_t-\partial_x(hu)-\partial_z(hw)=0, \tag{1.49}$$

which can be rewritten as

$$\zeta_t=h\nabla_{xz}^2\Phi, \tag{1.50}$$

where $u=\Phi_x$, $v=\Phi_y$, $w=\Phi_z$ and h is the water depth.

From Equations (1.49) and (1.50), the two-dimensional long wave having a free surface is obtained as

$$\zeta_{tt}=gh\{\zeta_{xx}+\zeta_{zz}\}. \tag{1.51}$$

The Timoshenko- Mindlin thick plate equation in terms of the plate deflection $\zeta(x,z,t)$ in two-dimension is given by

$$\left\{\left(EI\nabla^2-m_sI_R\partial_t^2\right)\left(\nabla^2-\frac{m_sS}{EI}\partial_t^2\right)\zeta+m_s\zeta_{tt}\right\}=-\left\{1-S\nabla^2+\frac{m_sI_RS}{EI}\partial_t^2\right\}P(x,z,t), \tag{1.52}$$

where EI is the flexural rigidity of the plate, $P(x,z,t)$ is the external pressure due to the fluid and in the present case it is the hydrodynamic pressure. Equating the hydrodynamic pressure with the external pressure on the plate, we obtain

$$\left(EI\nabla^2 - m_s I_R \partial_t^2\right)\left(\nabla^2 - \frac{m_s S}{EI}\partial_t^2\right)\zeta + m_s\zeta_{tt} + \rho g\zeta = \left\{1 - S\nabla^2 + \frac{m_s I_R S}{EI}\partial_t^2\right\}\rho\Phi_t. \quad (1.53a)$$

Differentiating eq. (1.50) with respect to t and then in eq. (1.53) for ζ at uniform water depth h, we obtain the plate covered long wave equation in terms of Φ as

$$h\left\{\left(EI\partial_x^2 - m_s I_R\partial_t^2\right)\left(\partial_x^2 - \frac{m_s S}{EI}\partial_t^2\right) + m_s + \rho g\right\}\partial_x^2\Phi = \left\{1 - S\partial_x^2 + \frac{m_s I_R S}{EI}\partial_t^2\right\}\rho\Phi_t^2. \quad (1.53b)$$

Further, assuming the velocity potential to be in simple harmonic in time with wave frequency ω, the velocity potential is expressed as $\Phi(x,t) = \mathrm{Re}\left\{\phi(x)e^{-i\omega t}\right\}$, where Re denotes the real part and $\phi(x)$ denotes spatial velocity potential. Eliminating Φ from eq. (1.53b) and rearranging, we get the long wave equation of motion in the plate covered region based on the Timoshenko-Mindlin plate equation as

$$\begin{aligned} h\left\{\frac{EI}{\left(\rho g - m_s\omega^2\right)}\partial_x^4 + \left(\frac{m_s\omega^2 I_R}{\left(\rho g - m_s\omega^2\right)} - S\right)\partial_x^2 + \left(1 - \frac{m_s\omega^2 I_R S}{EI}\right)\right\}\partial_x^2\phi \\ + \frac{\rho\omega^2}{\left(\rho g - m_s\omega^2\right)}\left\{1 - \frac{m_s\omega^2 I_R S}{EI} - S\partial_x^2\right\}\phi = 0. \end{aligned} \quad (1.54)$$

In particular, for $I_R = 0$ and $S = 0$, the above equation reduces to the long-wave equation for floating elastic plate based on Kirchhoff's theory. Further, for $EI = 0$ and $m_s = 0$, the above equation reduces to the two-dimensional long wave equation. It may be noted that although the derivation of the long-wave equation for floating elastic plate is based on Timoshenko-Mindlin/Kirchhoff's theory, the open water surface longwave equation is derived as a particular case.

1.6 EXPANSION FORMULAE FOR WAVE STRUCTURE INTERACTION

The wave interaction with very large floating elastic plate comes under a class of hydroelasticity problems associated with flexural gravity waves. These flexural gravity waves are defined by boundary value problems based on the Laplace equation for higher-order boundary conditions. Since the present study is concerned with the problems of hydroelasticity, so the mathematical formulation is based on the assumption of linearized hydroelasticity theory. In this section, the development of the expansion formula is explained in detail.

1.6.1 Havelock's expansion formulae

The solution procedure for the classical wavemaker problem involving free surface water wave motion was developed using the eigenfunction expansion method by Havelock (1929). The boundary value problem is based on the linearized wave theory for a water wave motions with free surface generated by a vertical plane wavemaker in the two-dimensional coordinate system. The spatial velocity potential $\phi(x, y)$ satisfies the two-dimensional Laplace equation

$$\frac{\partial^2 \phi}{\partial x^2} + \frac{\partial^2 \phi}{\partial y^2} = 0. \tag{1.55}$$

On the free surface boundary at $y = 0$, the velocity potential $\phi(x, y)$ satisfies the boundary condition of the following form

$$\mathcal{L}\left(\frac{\partial}{\partial x}\right)\frac{\partial \phi}{\partial y} + \mathcal{M}\left(\frac{\partial}{\partial x}\right)\phi = 0, \tag{1.56}$$

where $\mathcal{L}\left(\frac{\partial}{\partial x}\right) = 1$, and $\mathcal{M}\left(\frac{\partial}{\partial x}\right) = K$, $K = \omega^2 / g$ is a constant.

The mean free surface satisfies the combined linearised kinematic and dynamic boundary condition, bottom boundary condition are same as defined earlier. Using the method of separation of variables, the velocity potential is obtained as

$$\phi = A_0 \frac{\cosh k(h-y)}{\cosh kh} e^{ikx} \quad \text{for finite water depth,} \tag{1.57}$$

where A_0 is the wave amplitude and k is the wavenumber which is related with the frequency ω given by the dispersion relation

$$K = k \tanh kh \quad \text{for finite water depth,} \tag{1.58}$$

where $K = \omega^2 / g$, Equation (1.58) has only one positive real root k_0 and an infinite number of purely imaginary roots of the form $k_n = i\kappa_n$, $n = 1, 2, ...$ where κ_n satisfy

$$K = \kappa_n \tan \kappa_n h \tag{1.59}$$

By ordering k_n such that $k_1 < k_2 < ...$ it can be graphically seen that $(n-1/2)\pi < k_n h < n\pi,$ and $k_n h \to n\pi$ as $n \to \infty$.

The two-dimensional spatial velocity potential $\phi(x, y)$ is expanded in the form

$$\phi(x,y)=\begin{cases} A_0^{\pm}e^{\pm ik_0x}f_0(y)+\sum_{n=1}^{\infty}A_ne^{-\kappa_n x}f_n(y), & \text{for } x>0, \\ B_0^{\pm}e^{\pm ik_0x}f_0(y)+\sum_{n=1}^{\infty}B_ne^{+\kappa_n x}f_n(y), & \text{for } x<0, \end{cases} \tag{1.60}$$

$$f_n(y)=\frac{\cos k_n(h-y)}{\cos k_n h} \text{ for } n\geq 0, \tag{1.61}$$

with $A_0^{\pm}, B_0^{\pm}$ are the unknown constants associated with the amplitudes of the plane progressive waves and $A_n, B_n, \text{n}=1,2,...$ are the unknown constants associated with the evanescent modes, which decay as $x\to\pm\infty$. It can be easily verified that these set of eigenfunctions are orthogonal in the range $[0,h]$ with respect to the inner product as given by

$$\langle f_m(y), f_n(y)\rangle=\int_0^h f_m(y)\,f_n(y)dy, \tag{1.62}$$

and satisfy the orthogonality relation

$$\langle f_m(y), f_n(y)\rangle=\begin{cases} 0 & \text{for } m\neq n, \\ N_n & \text{for } m=n, \end{cases} \tag{1.63}$$

where $N_n=\dfrac{2k_nh+\sin 2k_nh}{4k_n\cos^2 k_nh}$ for $n\geq 0$.

The nature of the constants depend on the physical problem at hand and the appropriate sign will depend on the direction of the wave propagation. The decaying modes are included in the expansion to describe the fluid motion local to any body non-uniform in the vertical coordinate in the fluid domain and decay exponentially away from the body. If there is no body to interact with an incident wave, these evanescent modes will not be present in the expansion and the potential will be described only by the propagating modes.

The expansion formulae for $\phi(x, y)$ as given in the above relation Equation (1.60) is known as the Havelock's expansion formulae. This formula is used to obtain expansion formulae associated with the BVPs in infinite and semi-infinite strip type domains apart from circular/rectangular/ square type domain. In the context of water wave problems,

it is used to solve a class of problems in finite water depth. One of the basic advantages associated with these expansion formulae is that the eigenfunctions are orthogonal which often reduces the BVPs into a diagonally dominant linear system of equations. As a result, the method becomes computationally efficient to solve the associated physical problem. However, Havelock's expansion fails when the BVP involves a higher-order condition.

1.6.2 Gravity wave in the presence of surface tension (Rhodes-Robinson, 1971)

The wavemaker problem was investigated by Rhodes-Robinson (1971) taking into account the effect of surface tension which gives a third-order boundary condition. Green's function approach was adopted to derive the expansion theorem for the potential functions in the finite water depth. Rhodes-Robinson (1979a,b) proposed orthogonal relations to study the wave interaction with rigid structures in the presence of surface tension. The fluid in the finite water depth is assumed to occupy the region $x > 0,\ 0 < y < h.$ The velocity potential $\phi(x, y)$ satisfies the Laplace equation given by

$$\frac{\partial^2 \phi}{\partial x^2} + \frac{\partial^2 \phi}{\partial y^2} = 0 \quad \text{at } x > 0,\ 0 < y < h. \tag{1.64}$$

On the free surface boundary at $y = 0, x > 0$, the velocity potential $\phi(x, y)$ satisfies the boundary condition with the surface tension of the following form

$$\mathcal{L}\left(\frac{\partial}{\partial x}\right)\frac{\partial \phi}{\partial y} + \mathcal{M}\left(\frac{\partial}{\partial x}\right)\phi = 0, \tag{1.65}$$

where $\mathcal{L}\left(\frac{\partial}{\partial x}\right) = \left(1 + M\frac{\partial^2}{\partial x^2}\right)$ and $\mathcal{M}\left(\frac{\partial}{\partial x}\right) = K.$

The boundary condition at the free surface due to the presence of surface tension is rewritten as

$$K\phi + \phi_y + M\phi_{yyy} = 0, y = 0 \tag{1.66}$$

where $K = \sigma^2/g$ and $M = T/\rho g$, T is the surface tension, ρ the density and g the acceleration of gravity. It may be noted that for $M = 0,$ the relation (1.56) reduces to plane wavemaker problem. The wavemaker at $x = 0, 0 < y < h$ satisfies the condition given by

$$\phi_x = U(y) \text{ at } x = 0, \quad 0 < y < h, \tag{1.67}$$

where $U(y)$ is complex-valued and suitably limited. The bottom boundary condition is given by

$$\frac{\partial \phi}{\partial y} = 0 \text{ on } y = h \text{ for finite water depth.} \tag{1.68}$$

The condition for outgoing waves at infinity is of the form

$$\phi(x, y) \sim \left\{ \text{multiple of } \cosh k_0(h-y) e^{ik_0 x} \text{ as } x \to \infty, \right. \tag{1.69}$$

where κ_0 is the wavenumber with surface tension and satisfies the relation

$$k_0(1 + Mk_0^2)\sinh k_0 h - K \cosh k_0 h = 0, \tag{1.70}$$

and $\kappa_n(1 - M\kappa_n^2)\sin \kappa_n h + K \cos \kappa_n h = 0$ for $\kappa_n = ik_n$ for $n = 1, 2, \ldots.$ are infinite series on the imaginary axis. The wave-maker solution for finite depth in the presence of surface tension is obtained as

$$\begin{aligned} \phi(x, y) = 4\pi i \frac{A_0 \cosh k_0 h \cosh k_0 (h-y) e^{i\kappa_0 x}}{(2k_0 h)(1 + Mk_0^2) + (1 + 3Mk_0^2)\sinh(2k_0 h)} \\ + 4\pi \sum_{n=1}^{\infty} \frac{A_n \cos \kappa_n h \cosh \kappa_n (h-y) e^{-\kappa_n x}}{(2\kappa_n h)(1 - M\kappa_n^2) + (1 - 3M\kappa_n^2)\sin(2\kappa_n h)}, \end{aligned} \tag{1.71}$$

where $A_0 = \dfrac{1 - Mk_0^2}{\pi \cosh k_0 h} \displaystyle\int_0^h U(y) \cosh k_0 (h-y) dy + M\lambda$ and

$A_n = -\dfrac{1 - M\kappa_n^2}{\pi \cosh \kappa_n h} \displaystyle\int_0^h U(y) \cos \kappa_n (h-y) dy + M\lambda,$ for $\text{n} = 1, 2, \ldots.,$ which depend on normal velocity $U(y)$. This has been derived for $x \geq 0$, $0 \leq y \leq h$.

1.6.3 Flexural gravity wavemaker problems (Sahoo et al., 2001)

In the present subsection, the expansion formulae are derived based on orthogonal mode-coupling relations in the case of semi-infinite strips as well as quarter-plane problems. In the case of finite depth, an equivalent form of the orthogonal relation of Lawrie & Abrahams (1999) is obtained for the semi-infinite strip. This form of the expansion formula provided the motivation behind the theoretical development of a new orthogonal mode coupling relation.

It is considered that, a semi-infinite elastic plate of thickness floats on the surface $-\infty < x < 0,\ y = 0$ of a fluid domain $-\infty < x < \infty, 0 < y < h$ in a two-dimensional Cartesian coordinate system. The fluid is assumed to be inviscid and incompressible, and the flow is irrotational and simple harmonic in time with the angular frequency which ensures the existence of a velocity potential $\Phi(x, y, t)$ of the form $\Phi(x, y, t) = \mathrm{Re}\{\phi(x, y)\} e^{-i\omega t}$. The spatial velocity potential $\phi(x, y)$ satisfies the Laplace's equation given by

$$\frac{\partial^2 \phi}{\partial x^2} + \frac{\partial^2 \phi}{\partial y^2} = 0,\ -\infty < x < \infty, 0 < y < h. \tag{1.72}$$

On the structural boundary at $y = 0,$ the velocity potential $\phi(x, y)$ satisfies the boundary condition of the following form

$$\mathcal{L}\left(\frac{\partial}{\partial x}\right)\phi_y + \mathcal{M}\left(\frac{\partial}{\partial x}\right)\phi = 0, \tag{1.73}$$

where $\mathcal{L}\left(\frac{\partial}{\partial x}\right) = \left(\alpha_0 + \alpha_1 \frac{\partial^2}{\partial x^2} + \alpha_2 \frac{\partial^4}{\partial x^4}\right)$ and $\mathcal{M}\left(\frac{\partial}{\partial x}\right) = \beta_0$, $\alpha_0, \alpha_1, \alpha_2$ and β_0 are the constants. The rigid bottom boundary condition is given by

$$\frac{\partial \phi}{\partial y} = 0 \text{ on } y = h\ ,\ -\infty < x < \infty, \text{for finite water depth.} \tag{1.74}$$

Under the assumption of a linearized theory of surface waves, the free surface condition in the absence of surface tension in the open water region is given by

$$\frac{\partial \phi}{\partial y} + K_1 \phi = 0 \text{ at } y = 0,\ 0 < x < \infty, \tag{1.75}$$

where $K_1 = \omega^2 / g.$ The fluid domain is divided into two regions such as the upstream open region $0 < y < h$ and the plate-covered region $0 < y < h.$ The spatial velocity potentials in the corresponding regions are expressed as

$$\begin{aligned} \phi_1 &= \left(I_0 e^{-ik_0 x} + R_0 e^{ik_0 x}\right)\psi_0 + \sum_{m=1}^{\infty} R_m e^{-k_m x}\psi_m, && \text{for } x > 0, \\ \phi_2 &= T_0 e^{-ip_0 x} f_0 + \sum_{n=I}^{IV} T_n e^{p_n x} f_n + + \sum_{n=1}^{\infty} T_n e^{p_n x} f_n, && \text{for } x < 0, \end{aligned} \tag{1.76}$$

where

$$\psi_m = \begin{cases} \dfrac{\cosh k_0(h+y)}{\cosh k_0 h}, (m=0), \\ \dfrac{\cos k_m(h+y)}{\cos k_m h}, \ (m=1,2,3...,) \end{cases}, \quad f_n = \begin{cases} \dfrac{\cosh p_0(h+y)}{\cosh p_0 h}, (n=0), \\ \dfrac{\cos p_n(h+y)}{\cos p_n h}, \ (n=I,II,III,IV,1,2,3...,) \end{cases},$$

where $I_0 = -\dfrac{igH_0}{2\omega}$ with H_0 being the incident wave height.

The constants satisfy the dispersion relations

$$\omega^2 = gk_0 \tanh k_0 h = -gk_n \tan k_n h, \ (\mathrm{n}=1,2,3...), \tag{1.77}$$

with $(\mathrm{n}-1)\pi / h < k_n < n\pi / h, \ \text{for} \ (\mathrm{n}=1,2,3...)$.

The eigenfunctions $\psi_m (m=1,2,3...)$ are orthogonal and complete in the usual sense. On the other hand, p_n's satisfy the dispersion relations

$$K = p_0(1+Lp_0^4)\tanh p_0 h, \tag{1.78a}$$

$$K = -p_n(1+Lp_n^4)\tan p_n h, \qquad (n=I,II,III,IV,1,2,3...) \tag{1.78b}$$

with $L = EI/(\rho g - m_s\omega^2)$ and $K = \rho\omega^2/(\rho g - m_s\omega^2)$.

It should be noted that p_I and p_{II} are complex conjugates with positive real parts, p_{III} and p_{IV} are complex conjugates with negative real parts, p_n's are positive and real $(\mathrm{n}-1)\pi / h < p_n < n\pi / h, \ (\mathrm{n}=1,2,3...)$ and R_n, T_n, $(n=0,I,II,III,IV,1,2,3...)$ are unknown constants to be determined to obtain the velocity potentials. The assumption that the velocity potentials are bounded at infinity suggests that $T_{III} = T_{IV} = 0$.

The inner products are defined as

$$\langle f_m, f_n \rangle = \begin{cases} \int_0^h f_m(y) f_n(y) dy + \dfrac{L}{K}\left\{ \dfrac{\partial f_m}{\partial y}\dfrac{\partial^3 f_n}{\partial y^3} + \dfrac{\partial^3 f_m}{\partial y^3}\dfrac{\partial f_n}{\partial y} \right\}_{y=0}, & m=n, \\ 0 & m \neq n, \end{cases} \tag{1.79}$$

for $m = n = 0, I, II, III, IV, 1, 2, 3.....$

$$\langle f_0, f_0 \rangle = \frac{2p_0h(1+Lp_0^4)+(1+5Lp_0^4)\sinh 2p_0h}{4p_0(1+Lp_0^4)},$$

$$\langle f_n, f_n \rangle = \frac{2p_nh(1+Lp_n^4)+(1+5Lp_n^4)\sinh 2p_nh}{4p_n(1+Lp_n^4)}, \quad (n = I, II, III, IV, 1, 2, 3...),$$

which suggests that the set of functions are orthogonal with respect to the inner product as defined by the above relation. However, the eigenfunctions in the plate covered region are not standard ones as the operator involved is not self-adjoint.

1.6.4 Modified expansion formulae (Manam et al., 2006)

In the present section, expansion formulae are derived based on orthogonal mode-coupling relations in the case of semi-infinite strips as well as quarter-plane problems. In the case of finite depth, an equivalent form of the orthogonal relation of Lawrie and Abrahams (1999) is obtained for the semi-infinite strip. The form of the expansion formula provides the motivation behind the theoretical development of a new orthogonal mode coupling relation. The spatial velocity potential $\phi(x, y)$ satisfies the Laplace's equation given by

$$\frac{\partial^2\phi}{\partial x^2}+\frac{\partial^2\phi}{\partial y^2}=0 \quad \text{at} \quad 0<x<\infty,\ 0<y<h. \tag{1.80}$$

On the structural boundary at $y = 0$, the velocity potential $\phi(x, y)$ satisfies the boundary condition of the following form:

$$\mathcal{L}\left(\frac{\partial}{\partial x}\right)\frac{\partial\phi}{\partial y}+\mathcal{M}\left(\frac{\partial}{\partial x}\right)\phi=0, \tag{1.81}$$

where $\mathcal{L}$ and $\mathcal{M}$ are the linear differential operators of the forms $\mathcal{L}\left(\frac{\partial}{\partial x}\right)=\sum_{k=0}^{k_0}\alpha_k\frac{\partial^{2k}}{\partial x^{2k}}$ and $\mathcal{M}\left(\frac{\partial}{\partial x}\right)=\beta_0$, α_k and β_0 assumed to be known constants.

Finally, the far-field radiation condition is of the form

$$\phi(x, y) \sim \left\{\text{multiple of } \frac{\cosh p_0(h-y)}{\cosh p_0h}e^{ip_0x}, \right. \tag{1.82}$$

where p_0 satisfy the relation

$$\beta_0 = \left\{ p_0 \left[\sum_{m=0}^{k_0} (-1)^m \alpha_m p_0^{2m} \right] \tanh\, p_0 h, \right. \tag{1.83}$$

In the context of wave propagation problems, the above equation is referred to as the dispersion relation. The rigid bottom boundary condition is given by

$$\frac{\partial \phi}{\partial y} = 0 \text{ on } y = h \text{ for finite water depth.} \tag{1.84}$$

The BVP satisfying equation along with the boundary conditions and the radiation condition is not of standard Sturm–Liouville type and the eigenfunctions involved are not orthogonal in the usual sense. The more general expansion formulae based on the eigenfunctions are developed along with appropriate mode-coupling relations in the case of finite water depth. In the case of fluid of finite depth using the eigenfunction expansion method, the velocity potential $\phi(x, y)$ satisfying the governing equation, the boundary conditions and the radiation condition can be expanded in the generalized form as

$$\phi(x, y) = A_0(x) I_0(y) + \sum_{n=I}^{2k_0} A_n(x) I_n(y) + \sum_{n=1}^{\infty} A_n(x) I_n(y), \tag{1.85}$$

where the unknown functions $A_n(x)$ are of the form

$$A_n(x) = \begin{cases} A_n e^{ip_n x}, & n = 0, I, II, ..., 2k_0, \\ A_n e^{-p_n x}, & n = 1, 2, 3, ... \end{cases} \tag{1.86}$$

and the eigenfunctions $I_n(y)$ are of the form as given by

$$I_n(y) = \begin{cases} \dfrac{\cosh p_n (h - y)}{\cosh p_n h}, & n = 0, I, II, ..., 2k_0, \\ \dfrac{\cos p_n (h - y)}{\cos p_n h}, & n = 1, 2, 3..., \end{cases} \tag{1.87}$$

with p_n satisfying the relations

$$\beta_0 = \begin{cases} p_n \left[\sum_{m=0}^{k_0} (-1)^m \alpha_m p_n^{2m} \right] \tanh\, p_n h, n = 0, I, II, ..., 2k_0, \\ -p_n \left[\sum_{m=0}^{k_0} \alpha_m p_n^{2m} \right] \tan\, p_n h, \qquad n = 1, 2, 3..., \end{cases} \tag{1.88}$$

The eigenfunctions $I_n(y)$ are not orthogonal in the usual sense. In this context, the relevant form of the orthogonal relation satisfied by $I_n(y)$ which was given by Lawrie and Abrahams (1999) for the two-dimensional problem with a rigid bottom boundary and give an equivalent form of the orthogonal relation, which is referred to as mode-coupling relation is presented.

The equivalent form of the orthogonal relation in the form of mode-coupling relation is given by

$$\left\langle I_m(y), I_n(y) \right\rangle = \int_0^h I_m(y) I_n(y) dy + \sum_{j=1}^{k_0} (-1)^j \frac{\alpha_j}{d_0} \sum_{k=1}^{j} I_m^{2k-1}(0) I_n^{2j-(2k-1)}(0), \qquad (1.89)$$

which satisfies

$$\left\langle I_m, I_n \right\rangle = \begin{cases} \dfrac{\left(\sum_{k=0}^{k_0} \alpha_k (-1)^k p_n^{2k} \right) 2p_n h + \left(\sum_{k=0}^{k_0} (2k+1) \alpha_k (-1)^k p_n^{2k} \right) \sinh 2p_n h}{4p_n \left(\sum_{k=0}^{k_0} \alpha_k (-1)^k p_n^{2k} \right) \cosh^2 p_n h}, \\ \qquad\qquad m = n = 1, I, ..., 2k_0 \\ \dfrac{\left(\sum_{k=0}^{k_0} \alpha_k p_n^{2k} \right) 2p_n h + \left(\sum_{k=0}^{k_0} (2k+1) \alpha_k p_n^{2k} \right) \sin 2p_n h}{4p_n \left(\sum_{k=0}^{k_0} \alpha_k p_n^{2k} \right) \cos^2 p_n h}, m = n = 1, 2, ... \end{cases} \qquad (1.90)$$

In this case, the expansion formulae are modified considering the higher-order in the linear differential operator $\mathcal{L}\left(\frac{\partial}{\partial x}\right) = \sum_{k=0}^{k_0} \alpha_k \frac{\partial^{2k}}{\partial x^{2k}}$ and constant value in the linear differential operator $\mathcal{M}\left(\frac{\partial}{\partial x}\right) = \beta_0$.

1.6.5 Generalized Expansion Formulae (Karmakar et al., 2007)

The generalised expansion formulae for wave structure interaction problems with applications in hydroelasticity is developed by Karmakar et al. (2007). The Fourier transform and Fourier series is used to obtain the solution for the BVPs in semi-infinite domains and in semi-infinite strips. The Fourier integral transform is applied to derive the expansion formula for the velocity potentials in a semi-infinite strip for a class of

BVPs arising in the broad area of fluid-structure interaction having higher-order boundary condition in one of the boundaries. These expansion formulae can be easily extended to half-plane or infinite strip by using the geometrical symmetry of the problem under study. The fluid is assumed to occupy the region $0 < x < \infty, 0 < y < h.$

The spatial velocity potential $\phi(x, y)$ satisfies the Laplace's equation given by

$$\frac{\partial^2 \phi}{\partial x^2} + \frac{\partial^2 \phi}{\partial y^2} = 0. \tag{1.91}$$

On the structural boundary at $y = 0$, the velocity potential $\phi(x, y)$ satisfies the boundary condition of the following form

$$\mathcal{L}\left(\frac{\partial}{\partial x}\right)\phi_y + \mathcal{M}\left(\frac{\partial}{\partial x}\right)\phi = 0, \tag{1.92}$$

where $\mathcal{L}$ and $\mathcal{M}$ are the linear differential operators of the forms $\mathcal{L}\left(\frac{\partial}{\partial x}\right) = \sum_{n=0}^{n_0} \alpha_n \partial_x^{2n}$, $\mathcal{M}\left(\frac{\partial}{\partial x}\right) = \sum_{n=0}^{m_0} \beta_n \partial_x^{2n}$ with α_n's and β_n's are assumed to be known constants, $n_0, m_0 \in N$ and $m_0 \le n_0$. Further, assuming the existence of a wave-like solution, the far-field radiation condition is of the form

$$\phi(x, y) \sim \left\{ \text{multiple of } \frac{\cosh k_0(h-y)}{\cosh k_0 h} e^{ik_0 x}, \right. \tag{1.93}$$

where k_0 is assumed to be real and positive for the realistic physical problem and satisfices the relation in k as given by

$$Q(k; m_0) = P(k; n_0) \tanh kh, \tag{1.94}$$

$P(k; n_0) = \sum_{n=0}^{n_0} (-1)^n \alpha_n k^{2n+1}$ and $Q(k; m_0) = \sum_{n=0}^{m_0} (-1)^n \beta_n k^{2n}$ being the characteristic polynomials associated with the differential operators $\mathcal{L}(\partial_x)\phi_y$ and $\mathcal{M}(\partial_x)$, respectively. In the context of wave propagation problems, the above equation is referred to as the dispersion relation.

Finally, the bottom boundary condition is given by

$$\frac{\partial \phi}{\partial y} = 0 \quad \text{on} \quad y = h. \tag{1.95}$$

The velocity potential $\phi(x, y)$ is assumed satisfies one of the following two boundary conditions on the vertical boundary at $x = 0$, which are given by

$$\phi(x, y) = U(y) \text{ and } \phi_x(x, y) = V(y). \tag{1.96}$$

The general form of the velocity potential $\phi(x, y)$ satisfying the governing Equation (1.91) along with the boundary conditions is given by

$$\phi(x, y) = \sum_{n=0,I}^{2n_0} A_n f_n(y) e^{ik_n x} + \sum_{n=1}^{\infty} A_n f_n(y) e^{-k_n x}, \tag{1.97}$$

where

$$A_n = \frac{1}{C_n} \int_0^h f_n(t) u(t) dt + \frac{1}{C_n Q(k_n; m_0)} \left[\left\{ \sum_{j=1}^{n_0} (-1)^{(j+1)} \alpha_j \sum_{k=1}^{j} k_n^{2(j-k)} u^{2k-1}(0) \right\} k_n + \left\{ \sum_{j=1}^{m_0} (-1)^{(j+1)} \beta_j \sum_{k=1}^{j} k_n^{2(j-k)} u^{2k-2}(0) \right\} k_n \right] \tanh k_n h$$

and $C_n = \frac{h}{2\cosh^2 k_n h} + \frac{1}{2P(k_n; n_0)} \left\{ P'(k_n; n_0) \tanh k_n h - Q'(k_n; m_0) \right\}$.

with $f_n(y) = \cosh k_0 (h - y) / \cosh k_0 h$ and $k_n = ik_n$ for $n = 1, 2, ...$

Further, the expansion formula is based on the assumptions that Equation (1.94) has one positive real root at $k = k_0, 2n_0$ number of complex roots $k = k_n$ of the form $\pm\alpha \pm i\beta$ for $n = I, II, ...2n_0$ and infinitely many imaginary roots of the form $k_n = ik_n$ for $n = 1, 2, ...$ The mode coupling relation developed by Manam et al. (2006) is generalised and presented as a generalized mode coupling relation.

The eigenfunctions $f_n(y)$ in the case of finite water depth associated with general higher-order boundary condition satisfy the orthogonal mode-coupling relation as given by

$$\langle f_m, f_n \rangle = \begin{cases} \frac{h}{2\cosh^2 k_n h} + \frac{1}{2P(k_n; n_0)} \left\{ P'(k_n; n_0) \tanh k_n h - Q'(k_n; m_0) \right\} & \text{for } m = n, \\ 0 & \text{for } m \neq n. \end{cases} \tag{1.98}$$

$$\left\langle f_m, f_n \right\rangle = \int_0^h f_m(y) f_n(y) dy + \sum_{j=1}^{n_0} (-1)^j \frac{\alpha_j}{Q(k_n; m_0)} \sum_{k=1}^{j} f_m^{2k-1}(0) f_n^{2j-(2k-1)}(0) + \sum_{j=1}^{m_0} (-1)^{j+1} \frac{\beta_j k_n}{P(k_n; n_0)} \sum_{k=1}^{j} f_m^{2k-2}(0) f_n^{2j-2k}(0). \quad (1.99)$$

1.7 CLOSURE

In this chapter, the importance of the hydroelastic analysis of the flexible floating structure is discussed in detail. The basic theory of water waves along with the flexible floating structure based on Kirchhoff's thin plate theory and Timoshenko-Mindlin plate theory is presented. Further, the edge conditions associated with the plate theories for both finite and shallow water depth is discussed. In addition, the development of the expansion formula for the wave structure interaction problem using the Fourier transform technique by various researchers is explained.

CHAPTER 2

LITERATURE REVIEW

2.1 GENERAL INTRODUCTION

This chapter presents the review of literature related to the hydroelastic analysis of a floating elastic plate under the action of ocean waves. The review includes literature on wave interaction with floating structures considering different types of edge support condition, different articulations, change in the seabed profile and the presence of submerged structures at finite water depth and shallow water approximations. A remarkable study based on numerous theories is discussed for the hydroelastic analysis of floating structures both analytically and numerically. Various studies carried out to understand the hydroelastic behaviour of floating structures and also on the propagation of flexural gravity waves over sea-ice is discussed. The study is concentrated on floating structures, different methods employed, wave loading and responses of VLFS. The recent progress and future studies on the research of hydroelastic responses are also summarised and gives an idea about the scope of work.

2.2 WAVE INTERACTION WITH FLOATING STRUCTURES

In the past few decades, Very Large Floating Structures (VLFS) has gained significant interest in the area of research and development for future infrastructures. The studies on the design and development of VLFS started at the beginning of the 18^{th} century for various humanitarian activities and military operations. In 1894, a 124m long floating wooden railroad bridge (now abandoned) was constructed over Mississippi River in Wisconsin. In 1943, the US navy constructed a pontoon type floating airfield which consisted of the flight deck and parking area. A floating bridge to Mercer Island across lake Washington in 1940 was renamed Lacey V Murrow floating bridge and a second parallel floating bridge was opened in 1989, named as Homer M Hadley floating bridge. In 1975, the Okinawa International Ocean Exhibition, Japan was held on Aquapolis, constructed as a large semi-submersible unit of a floating city. Two floating oil storage bases were constructed at the Kamigoto island of Nagasaki in 1988 and Shirashima

island offshore Fukuoka city in 1996. The Technological Research Association of Mega float (TRAM) project was founded in 1995 and research activities on mega float construction continued till 2001 in Tokyo Bay, Japan. A significant floating bridge was finished in 2002 in Osaka, Japan to solve the problem of maintaining a wide shipping channel. The floating pre-stressed concrete pier was constructed at Ujina Port, Hiroshima, Japan and a floating terminal dock at Valdez, Alaska. The floating rescue emergency bases were constructed at Tokyo and Osaka bay and floating heliport at Vancouver, Canada. In 2013, Japan has built a 70 MW floating solar plant in the Kagoshima prefecture of the southern part of Japan. The Kagoshima Nanatsujima Mega Solar Power Plant is the largest solar power plant in Japan and it can generate enough electricity to power approximately 22,000 average households.

In literature, substantial research has been carried out on very large floating structures and some of the prominent works in the field of hydroelastic analysis for large floating structures are consolidated and presented by Kashiwagi (2000). The review on the recent progress and future studies on the research of hydroelastic responses of the large floating structure is discussed and the study is mainly divided into pontoon type and columns supported type structures using frequency-domain and time-domain analysis. Watanabe et al. (2004) presented the basic assumptions, equations and boundary conditions for preliminary hydroelastic analysis of floating structures. The review reported the development of more refined work on pontoon-type VLFS. Ohmatsu (2005) presented an overview of wave loading and responses of VLFS. The detailed outline is proposed on the development of various methods for the hydroelastic response and qualitative risk analysis of mooring system. Chen et al. (2006b) reviewed the hydroelastic theories for the global response on marine structures with special focus on VLFS. Squire (2007) presented a review paper on ocean waves and sea-ice. The study performed on the semi-infinite or infinite ice-sheet and the accumulation of independent flexible floating bodies is presented and discussed. Karmakar et al. (2011) reviewed the existing hydroelasticity theories to analyse different types of floating and submerged structures relevant to the field of Marine Technology and Arctic Engineering. The theoretical progress made in the application of hydroelasticity for the analysis of Very Large Floating Structures (VLFS) and large floating ice-fields is presented. A brief discussion on wave interaction with flexible breakwaters, an

overview of ship hydroelasticity and recent developments on wave propagation over a flexible bottom are analysed.

In the study of the very large floating structure, Wang and Tay (2011) summarized two decades of work on the applications, research and development of VLFS. The study includes the recent innovative methods to minimize the hydroelastic motion, and to improve the mooring system with the structural integrity of the VLFS. Pardo et al. (2015) reviewed the application of VLFS for both coastal and offshore structures. The study categorized the advantages and disadvantages of different types of VLFS. An overview for various models, depths and proximity of the structures around the coast is studied and a brief comparison between VLFS and other types of floating structures is presented. Recently, Dai et al. (2018) reviewed the developments on floating breakwaters and the review includes the recent progress and future studies on the hydroelastic behaviour and wave loading of VLFS, and outlined the development of various methods to calculate the hydroelastic response at different conditions. The analysis is performed for the hydroelastic theories for the global response on marine structures and the study demonstrated the pontoon type and columns supported type structures based on frequency-domain and time-domain analysis. In addition, the application of VLFS is discussed and categorised the advantages and disadvantages of different types of VLFS in comparison to other types of floating structures. The study also includes various models, depths and proximity of the structures around the coast.

2.2.1 Wave interaction with floating ice-sheets

A significant amount of progress on wave-ice interaction is made in the literature using the floating elastic plate model which finds its application in the field of cold region science and technology as the large sheets of ice that covers a vast area of the ocean surface in the Arctic and Antarctic regions. In Polar and sub-polar Regions, waves travel from open-ocean onto ice-covered seas generating flexural waves. The waves travel over ice sheets have considerable surface elevation to induce stress in the ice sheets. These flexural waves are found to cause fractures and cracks in the ice sheets. Thus, the study of wave-ice interaction is an important subject of research. Press and Ewing (1951) derived equations for the propagation of elastic waves in floating ice sheet with emphasis on phase velocity for very large and small wavelengths. The

thickness and mechanical strength of the ice for position fixing and long-range signalling are determined and analysed. Bates and Shapiro (1980) developed a model for the floating ice sheet with compressive stress based on the thin elastic plate to find the impulse response of the system. It is observed that the floating membrane gravity waves exist at all frequencies below the flexural gravity wave band and an elastic plate supported on an elastic foundation was apt for these long-period waves. The study concluded that elastic energy stored in the compressed ice is sufficient to produce measurable long-period waves in floating ice.

Squire and Dixon (2001) considered the effect of long ice coupled waves acting on an iceberg that is trapped in ice sheets of infinite extent in deep waters. The analysis considers the ice coupled waves to be generally of longer periods and the numerical method based on Green's function is formulated approximating iceberg to follow thin elastic plate theory. A fully three-dimensional model for the motion and bending of a solitary ice floe due to wave forcing is presented by Meylan (2002). The ice floe is modelled as a thin plate and its motion is expanded in the thin plate modes of vibration. The scattered energy is calculated and it is shown that the scattering is strongly dependent on ice floe stiffness. Further, it is observed that there exists a critical value of stiffness, below which the scattered energy is not a significant function of ice floe geometry, and above which the average scattering is a significant function of ice floe geometry. Peter and Meylan (2004) extended the works on finite-depth interaction theory to the infinite water depth and structure of arbitrary geometry.

The calculations for the structure of arbitrary geometry developed by Goo and Yoshida (1990) is extended to infinite depth, and the diffraction transfer matrix is calculated for rotating bodies. The developed interaction theory is applied to the wave forcing on multiple ice floes and a method to solve the full diffraction problem is presented. The convergence studies are performed comparing the interaction method with the full diffraction calculations and the finite and infinite depth interaction methods. A new coupled-mode system of horizontal equations for the hydroelastic analysis of large floating bodies or ice sheets of finite thickness, lying over variable bathymetry regions is presented by Athanassoulis and Belibassakis (2009) and the study extended the existing third-order plate theories to plates and beams of general shape. The variational principle is used with the one-field functional of the elastodynamics in the plate region,

and a pressure functional in the water region. The scattering of linear, coupled, hydroelastic waves propagating through an inhomogeneous sea ice environment is determined consisting of ice sheets of variable thickness and a non-mildly-sloped interface. Squire (2011) examined the current and emergent advances on the topic of hydroelasticity theory and response of sea ice under the action of ocean surface waves and swell. Kohout et al. (2011) derived a relation for the wave attenuation due to drag from the bottom roughness of ice floes. It is observed that the combined scatter and drag (CSD) model improved the rate of decay of the attenuation coefficient with the increasing period, but simultaneously weakened the representation of the attenuation at the rollover.

The behaviour of flexural gravity waves propagating over a semi-infinite floating ice sheet under the assumptions of small amplitude linear wave theory is studied by Bhattacharjee and Guedes Soares, (2012). The higher-order mode-coupling relations are applied to determine the unknown coefficients present in the Fourier expansion formula of the potential functions and modelled ice-sheet as a thin semi-infinite elastic beam. Three different edge conditions are considered at the finite edge of the floating ice-sheet and also the effects of different edge conditions, the thickness of the ice-sheet and the water depth on the surface strain, the shear force along the ice-sheet, the horizontal force on the vertical wall, and the flexural gravity wave profile are analysed. Bennetts and Squire (2012) modelled the exponential attenuation of ocean surface waves in ice-covered regions of the polar sea considering thin elastic plate. The study showed the attenuation produced by long floes obtained from the scattering properties of a single ice edge and wave interaction theory in ice-covered regions requires evanescent and damped-propagating motions to be included when scattering sources are relatively nearby. Williams et al. (2013a) developed a theoretical model for wave-ice interaction in the marginal ice zone (MIZ) based on floe size distribution. The attenuation of ocean surface waves by sea-ice and the concomitant breaking of the ice into smaller floes by the waves is calculated and discussed. Williams et al. (2013b) developed a numerical scheme to simulate the wave energy lost during ice breakage. The one-dimensional transects of the ocean surface are considered to test the sensitivities of the wave ice interaction using idealized ice thickness and concentration profiles.

Papathanasiou et al. (2014) presented a higher-order finite-element method (FEM) for the numerical simulation of the transient response of thin floating bodies in shallow water wave conditions. The hydroelastic initial-boundary value problem, in an inhomogeneous environment, characterized by bathymetry and plate thickness variation is analysed for two configurations: (i) a freely floating strip modelling an ice floe or a very large floating structure and (ii) a semi-fixed floating beam representing an ice shelf or shore fast ice, both under long-wave forcing. Papathanasiou et al. (2015) analysed the transient hydroelastic response of an ice shelf under long-wave excitation by means of the finite element method. Study presented a simple model for the simulation of the generated kinematic and stress fields in an ice shelf, when the latter interacts with a tsunami wave. Gerostathis et al. (2016) developed a coupled-mode model to study the hydroelastic behaviour of 3D large floating bodies of finite extent and shallow draft or ice sheets of small thickness, lying over variable bathymetry regions. Bai et al. (2017) investigated the response of ice floes in regular waves. The results of the numerical investigation from HydroSTAR and OpenFOAM are compared with the experimental data.

2.2.2 Hydroelasticity based on different plate theories

The study on the hydroelastic analysis of VLFS is mainly based on two plate theories: (a) Euler-Bernoulli beam theory and (b) Timoshenko-Mindlin thick plate theory. Mostly, the researchers studied the hydroelastic behaviour of large floating structure based on the Euler-Bernoulli beam theory. The Euler-Bernoulli beam theory neglects the effect of rotary inertia and shear deformation, but the large floating structures being large along the length and width also has considerable depth. So, the consideration of the effect of rotary inertia and shear deformation becomes inevitable for the hydroelastic analysis of floating structures using Timoshenko-Mindlin plate theory. The literature based on the Timoshenko-Mindlin plate theory considering the presence of rotary inertia and transverse shear deformation is very limited. Further, few researchers analysed the hydroelastic behaviour of ice sheets based on Timoshenko-Mindlin thick plate theory interacting with ocean waves. All the above studies as presented in the subsection reported that, the sea-ice or floating platform is either infinite or semi-infinite in length.

2.2.2.1 Euler-Bernoulli beam theory

A significant study on the hydroelastic analysis of the VLFS is performed considering Euler-Bernoulli beam theory. The study mainly considers the thickness of the structure to be thin and the assumption seems to be more realistic while analysing the very large floating structures where the horizontal dimensions are much larger than the vertical dimension. Some of the earliest work in the analysis of VLFS is proposed by Stoker (1958) for two-dimensional analysis of a floating elastic body. Meylan and Squire (1994) developed a linearized, model based on Euler-Bernoulli thin plate theory for an ice floe and a pair of adjacent ice floes of finite length under the action of ocean waves at infinite and finite water depths. Meylan and Squire (1996) presented a new model to study the behaviour of a solitary, circular, flexible ice-floe under the action of long-crested sea waves. The vibration of a circular thin plate is considered to be governed by the Euler-Bernoulli beam equation with free edge conditions. The comparison of the result is performed with two independent methods: an eigenfunction expansion method for the thin circular plate, and Green's function approach for the ice-floe. The model is used to investigate the strain field generated in the ice-floe, surge response, and the energy initiated in the water encircling due to the ice-floe. Sim and Choi (1998) analysed the hydroelastic behaviour of large floating structures under the action of oblique waves. Namba and Ohkusu (1999) presented a new mathematical model to analyse the bending vibration of a very thin elastic plate floating on waves. An oblique incident wave is considered in the analysis to interact with an infinitely long rectangular plate. The kinematic condition underneath the plate is imposed on the level of calm water surface. The plate is treated to be a part of the water surface and the fluid flow, and the deflection is determined.

Taylor and Ohkusu (2000) used Green's function theory for the hydroelastic analysis of beams and thin plates based on Euler-Bernoulli beam theory. The alternative forms are developed for the free-free beam, in terms of the sinusoidal eigenmodes of a pinned-pinned beam and the rigid body modes. The direct formulation applying the Stokes transformation and an energy approach is used to obtain the Green function for the beam. Meylan (2001) derived a variational equation on the thin-plate equation of motion by including the wave forcing using the free surface Green function. The study is extended for the case of variable plate properties and to multiple floating plates.

Khabakhpasheva and Korobkin (2001, 2002a) described two approaches to reduce elastic deflection of floating plates with a 2D linear theory based on Euler homogenous beam model. The first approach is based on the concept of vibration absorber. The second approach considered the floating beam to be connected to the sea bottom with a spring and the rigidity of the spring is adjusted in such a way that the beam deflection due to incident waves is reduced. They modelled the beam to be (i) homogenous, (ii) cracked, (iii) compound with an elastic connection between the parts of the beam and (iv) elastically connected to the sea bottom.

Takagi (2002) applied ray theory to study the hydroelastic behaviour of VLFS based on thin elastic plate theory. The wave amplitude is suddenly changed along the ray that passed through a corner and the parabolic approximation is applied as a smoothing function to overcome the difficulty at the corners. A small variation is applied for the incident angle from the head sea to represent the hydroelastic response. The approximation study gave an idea of the complexity involved with the corner effect on the analysis. Khabakhpasheva and Korobkin (2002) introduced an inverse method for solving the hydroelastic problem of floating plate based on Euler beam equation. The hydrodynamic pressures under the floating plate are evaluated for the liquid boundary and plate deflection is identified, and hence the distribution of the external loads along the plate is constructed. Chen et al. (2003) developed a numerical method for analysing the hydroelastic characteristics of a VLFS in multidirectional monochromatic incident waves taking into account the effect of the membrane forces. A pontoon type VLFS is considered as a thin plate undergoing large vertical deflections. Von Karman plate theory is used with the mode expansion method in the frequency domain to obtain the membrane forces. Chung and Linton (2003) derived a new mathematical model based on thin elastic plate coupled with an inviscid, incompressible fluid for computing the coefficients of the modal expansion of the velocity potential using Residue Calculus Technique (RCT). A new direct method was proposed by Ohkusu and Namba (2004) considering the draft of the plate to be asymptotically zero and the plate bottom surface to be located at the water surface. Thin plate theory is used to analyse the fluid-structure interaction in shallow water depth with incident waves along the length of the structure.

The influence of flexural gravity waves on various irregularities in the ice field is investigated by Williams and Squire (2004). A uniform Euler-Bernoulli plate is

considered for the theoretical model and the Green's function approach is used for the solution required in finite water depth. Finally, the investigation is carried out to select the type of irregularities which caused the observed low pass filter response. Andrianov and Hermans (2003, 2006) performed the hydroelastic analysis of VLFS considering the structure to be pontoon/mat type and modelled as a thin elastic isotropic plate. An integro-differential formulation with Green's theorem is used to obtain velocity potentials and the plate deflection. The influence of water depth is compared for incompressible fluid at infinite, finite and shallow water depths. A geometrical-optics approach and Lindstedt method were used by Andrianov and Hermans (2006) to determine the reduced wavenumbers, amplitudes, deflection of zero draft order. Andrianov (2005) presented the motion of a floating structure and its response to surface water waves based on thin-plate theory. An analytical solution and numerical results are derived for various shapes and dimensions of the floating plate. New approaches for the hydroelastic analysis of the VLFS is proposed based on a general integro-differential equation method.

A semi-analytic method to solve the free-surface wave interaction with a plate of finite thickness is developed by Hermans (2003a, 2003b, 2004, 2007). An integro-differential equation is formulated considering plate behaviour in terms of thin plate theory and water pressure at the plate applied at finite depth. Xu and Lu (2011) developed an analytical method to analyse the floating plate of arbitrary geometry for the hydroelastic analysis based on thin-plate theory. Vertical and angular eigenfunction methods were formulated at three cases of edge boundary conditions. Brocklehurst et al. (2012) modelled the ice sheet as a thin elastic plate based on Euler-Bernoulli thin-plate theory involving fourth-order derivatives of the plate deflection in space. The linear diffraction of hydroelastic waves is studied considering vertical cylinder and the behaviour of the forces under variation of parameters and the strain distribution in the ice sheet is investigated. Wang and Cheng (2013) studied the nonlinear hydroelastic waves under an ice-sheet lying over an incompressible inviscid fluid of finite uniform depth based on Homotopy Analysis Method (HAM). The effects of the water depth are studied and two important physical parameters including Young's modulus and the thickness of the ice sheet on the wave energy and its elevation. Wang and Lu (2013) investigated a train of nonlinear hydroelastic progressive waves travelling in a thin finite elastic plate in

deep water. They demonstrated that the stiffness, thickness, density of plate and the amplitude of the incident wave have major effects on the hydroelastic response of an ice-sheet or a VLFS. Papathanasiou and Belibassakis (2014) presented three hydroelastic interaction models for wave interaction with floating bodies of large dimensions. They represented the water-wave potential with an enhanced mode expansion with unknown modal amplitudes in the free surface and structure deflection on the horizontal plane. Kara (2015) modelled three-dimensional transient wave-body interaction by the use of Boundary Integral Equation Methods (BIEM) and Neumann–Kelvin linearization for the hydrodynamic part. The Euler–Bernoulli beam equation is used with analytically defined mode shapes for the structural part for the time domain prediction of the hydroelasticity of the floating bodies. Lu et al. (2016) introduced a new method based on multi-body hydrodynamics and Euler–Bernoulli beam assumption to study hydroelastic behaviours of very large floating structures. The numerical results are compared with experimental results and numerically calculated data by three-dimensional hydroelasticity theory. Liao and Ma (2016) presented the vibration characteristics of an elastic thin plate placed at the bottom of a three-dimensional rectangular container filled with compressible inviscid fluid.

2.2.2.2 Timoshenko-Mindlin theory

The analysis to understand the hydroelastic characteristics performed using the Euler-Bernoulli beam theory does not consider the significance of rotary inertia and shear deformation of an elastic plate. However, the elastic plate has a substantial thickness, hence the inclusion of the rotary inertia and shear deformation is important in analysing the hydroelastic characteristics for VLFS (Mindlin, 1951). Thus, Timoshenko-Mindlin plate theory which consists of the terms related to rotary inertia and shear deformation for a plate needs to be considered to analyse the hydroelastic characteristics of a VLFS. The study considering Timoshenko-Mindlin plate theory was introduced by Fox and Squire (1991) for the flexural gravity wave propagation over the ice-shelf. Fox and Squire (1991) performed the coupling of a long period surface gravity ocean waves with massive ice shelf considering the wave-induced strain on the ice shelf. Meylan and Squire (1996) developed a theoretical model to study the flexure for a circular disk acted upon by long-crested wave and the study reveals that the long-crested wave is not affected due to the deformation of thin ice floe but the bending induced in the ice floe

affects the wave motion in the free surface. Barrett and Squire (1996) studied the ice coupled waves travelling in an ice plate with abrupt changes in the plate properties. Two cases of plate discontinuity with the plate being either joined or crack is analysed. The flexural gravity wave propagation over the ice-covered region is performed by Keller (1998) in water of finite depth and the study is conducted for waves of any wavelength which is simplified for short and long waves. The reflection and transmission of surface gravity waves are presented by Balmforth and Craster (1999) for the ice sheets under the action of waves. The Fourier transforms and Wiener-Hopf technique is used in the simplification of the wave scattering problem. The wave interaction with a cracked floating ice sheet is analysed by Karmakar and Sahoo (2006) using the Fourier transform approach considering Timoshenko-Mindlin plate theory. Further, a detailed study on the hydroelastic characteristics of VLFS is analysed by Karmakar et al. (2009) considering the Fourier transform approach for the infinite and semi-infinite elastic plate.

The study based on the Timoshenko-Mindlin plate theory considering the presence of rotary inertia and transverse shear deformation is very limited. Recently, the hydroelastic response was analysed for a pontoon-type VLFS connected with a flexible line connection by Gao et al. (2011) based on Mindlin plate theory. The solution procedure involved modal expansion method for the formulation of the physical problem and the solution is obtained using the BEM approach. The study was also extended for the ocean wave-ice interaction. A study on the reduction of the hydroelastic behaviour of VLFS was presented by Tay and Wang (2012) by altering the geometry of the structure considering the Mindlin plate theory. The floating structure was considered to be located in a channel to account for the head sea interaction of ocean waves. The study showed a reduction in the hydroelastic characteristics of floating structures by altering the geometry of the structure. Papaioannou et al. (2013) developed a method for hydroelastic analysis of VLFS subject to a directional wave spectrum. The analysis is carried out in the frequency domain by application of the modal expansion method. A BEM-FEM model is used to discretize the fluid-structure interaction based on Mindlin plate theory. The derived linear system allows for the application of linear random vibration theory for the evaluation of response spectra.

The hydroelastic characteristics of a VLFS connected by a flexible line along with gill cells at their bottom surface are examined by Gao et al. (2013) under the action of gravity wave. A substantial reduction in the hydroelastic characteristics was presented by suitably placing the flexible line and distributing gill cells. A nonlinear theory is developed by Ertekin and Xia (2014) to analyse the hydroelastic characteristics of large floating structures under the action of cnoidal waves. The boundary value problem is developed based on the Green-Naghdi theory in the open water region. Agarwal and Nair (2014) analysed the structural response of a floating airport subjected to landing/taking off of an aeroplane by using a Fourier Transformation in space in wavenumber domain rather than using the wave propagation method to reduce the analysis to a substructure. Ertekin and Xia (2014) developed a nonlinear theory to predict the hydroelastic response of a VLFS in the presence of cnoidal waves and compared the predictions with the linear theory. Papathanasiou and Belibassakis (2014) presented three hydroelastic interaction models with application to the problem of water wave interaction with VLFS. The dispersion characteristics of the hydroelastic models are studied based on standard beam theories. A brief discussion on the variational formulation of the derived equations and their finite element approximation is also studied. Zhao et al. (2015) analysed the relationships between the amplitude distribution of the deflection and bending moments for 2D compound floating plates and the stiffness of the connection under the action of different periods of incident waves on a fluid of finite depth is studied using Wiener-Hopf technique and the Mindlin plate theory. Liao and Ma (2016) presented a mathematical derivation of the vibration characteristics of an elastic thin plate placed at the bottom of a three-dimensional rectangular container filled with compressible inviscid fluid. Recently, Praveen et al. (2016, 2018) discussed the hydroelastic characteristics of the floating elastic plate in the case of shallow water approximations and the effect of interconnected joints in the plate is analysed considering Timoshenko-Mindlin's theory. A significant variation is observed on the hydroelastic behaviour as compared to Euler-Bernoulli beam theory.

2.2.3 Hydroelastic behaviour of VLFS with different support condition

In order to study the influence of edge support conditions, various researchers have attempted to consider different edge support conditions based on the requirement of the structure. In most of the study on the hydroelastic behaviour of VLFS, considers the

structure to be freely floating based on the free edge boundary condition. The wave interaction with large floating structures induces vertical and horizontal motions and a mooring system is necessary to restraint the floating structure from wave-induced motion. In practical, the VLFS's are anchored to the seabed with a mooring system or supported at the edges by different edge conditions such as simply supported or fixed edge support. Onsite, the edges of these large floating structures are secured on to the seabed with a mooring line based on different edge conditions such as simply supported or fixed edge support. The consideration of edge support condition for the large floating structure is based on the functionality of the structure. Most of the studies consider a freely floating structure based on the free edge boundary condition. On the other hand, few researchers have considered different types of edge support conditions in the study of hydroelastic behaviour of VLFS. Teng et al. (2001) used a modified eigenfunction expansion method to analyse the reflection and transmission of ocean waves at a semi-infinite thin elastic plate. The study is extended for the cases of simply supported and built-in edges and it was demonstrated that the modified error function method satisfies well for the energy conservation relation at all three cases of edge conditions. Sahoo et al. (2001) developed the orthogonal-mode coupling model based on the eigenfunction expansion approach to study the scattering of waves due to a floating semi-infinite elastic plate in the case of finite water depth. The influence of different edge conditions is investigated for the case of free-free, simply supported and a built-in edge. The study summarized that the built-in edge condition induces the maximum wave reflection and the minimum wave transmission.

The hydroelastic behaviour of a semi-infinite horizontal elastic plate floating on a homogenous fluid of finite depth is analysed by Xu and Lu (2009) using the eigenfunction expansion method. The study concluded that the plate thickness and the density of the plate do not influence the wave reflection and transmission characteristics. Kohout and Meylan (2009) studied the wave scattering by multiple floating elastic plates with spring connectors or hinges at the plate edges. The behaviour of the plate is observed depends strongly on the boundary conditions at the plate edges. Gao et al. (2011) analysed the hydroelastic response of pontoon-type, very large floating structures (VLFS) with a flexible line connection based on Mindlin plate theory. The modal expansion method is adopted in the frequency domain with a

combined BEM-FEM method. Karmakar and Guedes Soares (2012) analysed the wave scattering by a finite floating elastic plate connected with mooring lines at its corners in the presence of lateral pressure load. The hydroelastic behaviour of the floating elastic plate is investigated by analyzing the effect of the stiffness of the mooring lines on the reflection and transmission characteristics of the gravity waves. Loukogeorgaki et al. (2014) implemented a 3D experimental and numerical investigation for the performance of a pontoon-type floating structure. The pontoon-type floating structure configuration is considered consisting of modules connected with hinge-type connectors and moored with chains. The study focused on the analysis of the wave characteristics effect on mooring lines tension and the hydroelastic response of the pontoon-type floating structure.

The hydroelastic behaviour of an elastic floating plate connected to the sea bed using a time-domain approach is examined by Karperaki et al. (2016). The elastic plate is modelled based on Euler-Bernoulli theory in shallow water depth and the study mainly concentrates on the multiple elastic connectors joined by simple spring-dashpot systems along with the structure. Wang et al. (2016) developed a finite element model to analyse the hydroelastic response of a horizontal elastic plate. The threshold values of the forward speed and compressive force for the beam is calculated for various length and different edge boundary conditions. The deflection in the middle points of the plate with three different boundary conditions is compared with available experimental and numerical results and the study suggests that the deflection in the beam are affected largely due to the beam length and boundary conditions. The oblique scattering of waves by a semi-infinite floating elastic plate over a stepped topography was studied by Guo et al. (2016). The influence of three different types of edge conditions are examined and that the edge conditions have a considerable effect on the plate deflection and moment. Loukogeorgaki et al. (2017) conducted 3D experiments to investigate the hydroelastic and the structural response of a pontoon-type modular floating breakwater moored with chains modules, under the action of perpendicular and oblique regular waves. The oblique wave interaction with a floating flexible porous plate is studied by Koley et al. (2018) in both the cases of finite and infinite water depths. The effects of three types of plate edge conditions namely free-free, fixed and simply supported is analysed and the study suggested that the strain is lower in case of a plate having free edges compared with fixed and simply-supported edges.

2.2.4 Wave scattering due to the articulated floating elastic plate

The studies on the effect of articulation are of practical importance to predict the strength and stability of the structure. The VLFS that are constructed in the open ocean is very long and wide, the draft is assumed to be small and the structure behaves like an elastic plate consisting of several modules. These large floating structures are usually fabricated in modules at shipyards and assembled together with connecting joints on-site using welding. The effect of articulated joints in floating elastic plates has been of research interest in the reduction of hydroelastic responses. The studies on the effect of articulation are of practical importance to predict the strength and stability of the structure. The interaction of waves with articulated floating elastic plate considering a 2D articulated plate with connectors based on Euler-Bernoulli's beam theory is investigated by Xia et al. (2000). The study suggests that the hydroelastic characteristics depend on the connector stiffness and frequency of the incoming wave and extended the study for hydroelastic behaviour of the multi-module articulated plate.

The hydroelastic behaviour of compound floating elastic plate anchored to sea bottom was analyzed by Khabakhpasheva and Korobkin (2002) based on coupled hydrodynamics and structural dynamics. The study suggests that, a rigid plate of smaller length in the front of the structure and a spring connecting the floating beam to the sea bottom with suitable spring rigidity can reduce the vibration of the floating structure. Karmakar and Sahoo (2005) presented the wave scattering for an articulated floating elastic plate at infinite water depth considering Euler-Bernoulli beam theory. The analysis of the hydroelastic behaviour of floating elastic plate of different spring stiffness is studied and the analysis suggests that the articulated joints behave as a continuous plate for higher values of spring stiffness. The wave propagation across the transition between two semi-infinite floating elastic plates considering the vertical and rotational springs is performed by Chung and Fox (2005) using the Wiener-Hopf technique. The wave propagation is observed dependent on the transition condition and the large fluctuation in the wave reflection due to a small change in the transition condition. Sturova (2009) proposed a method to analyze the linear unsteady behaviour of the floating hinged homogeneous elastic beam in shallow water. The beam behaviour for different hinged positions and actions of the medium is presented and analyzed. Karmakar et al. (2009) discussed the flexural gravity wave scattering by multiple

articulated floating elastic plate using the wide-spacing approximation and also direct method considering Euler-Bernoulli beam theory to analyze the effect of stiffness connectors on the wave propagation. The Bragg's resonance in the periodic articulated floating plates is observed due to the periodic structures and it was suggested that a limiting value for both the stiffness constants exits, beyond which the articulated plate behaves as a continuous plate.

The hydroelastic response of the flexible floating interconnected structure using translation and rotational stiffness based on general hydroelasticity theory is performed by Fu et al. (2007) taking into account hinged rigid modes. The effect of the connector is studied and it was found that the stiffness of the connectors and the modules are important for the determination of the hydroelastic response of the structure. Riyansyah et al. (2010) studied the minimum hydroelastic response on the floating body considering the mechanical semi-rigid connection of two floating beams using boundary element method for the fluid domain and finite element method for the structural domain. The study suggests that the presence of the rotational stiffness affects the compliance of the floating beam system and can improve the design of the floating beam system. Gao et al. (2013) investigated the hydroelastic response of a long rectangular VLFS under the action of the wave. The effect of flexible line connector and gill cells on the hydroelastic behaviour of VLFS is analyzed and it was observed that the presence of flexible line connector and appropriate distribution of gill cells in the VLFS were found to significantly reduce the hydroelastic response and stress resultants. The hydroelastic behaviour of compound hinged floating plates using the Wiener-Hopf technique is presented by Zhao et al. (2015) for different periods of incident waves to understand the influence of the hinge connection in the floating body. The study suggests that the vibration of the plate and the amplitude of the dynamic stress can be reduced by selecting proper spring stiffness and hinged position.

2.2.5 Wave transformation due to bottom topography

The floating structures are usually construed near shore and hence the effect of sea bottom profile becomes significant. Sea bottom is not flat throughout, there is various kind of undulations which give rise to wave refraction, shoaling and wave breaking. The wave transformation due to floating thick elastic plate over multiple stepped bottom topography has been of research interest due to the effect of sea bed unevenness

in the hydroelastic responses. Newman (1965) presented a theoretical and experimental results wave reflection and transmission over a step type bottom topography with finite and infinite depths. It is concluded that the wave frequency plays an important role in the shallow water domain for relatively long waves.

The wave scattering due to a rectangular obstacle in a finite depth channel is analysed by Mei et al. (1969). The variational formulation for the numerical computations is employed and the scattering properties for bottom and surface obstacles of various proportions are presented including thin barriers and surface docks. The results are compared with existing experimental and theoretical data. A new approach was adopted by Evans and Linton (1994) to solve the wave scattering due to varying bottom topography using 2D linear water wave theory. The varying bottom topography is modelled as a uniform strip to be considered in the variable free surface boundary condition. Grue (1992) studied the incoming deep water wave propagating over a slight submerged circular cylinder or a rectangular shelf experimentally and theoretically in the wave channel. The theoretical model accounted for the nonlinearity by using the Boussinesq equations in the shallow water depth over the obstacle in combination with linearized potential theory at deep water. The wave underwent a strong deformation at the obstacle for a finite wave amplitude. O'Hare and Davies (1992) presented a new model for wave propagation over a region of arbitrary bottom topography. The smoothly varying sea bed profile is divided into a series of horizontal shelves separated by abrupt steps. A transfer matrix is used to relate the wave fields on either side of each step and a rotation matrix is defined for the wave propagation along the shelf between the adjacent steps. The model is observed to perform well for a rapidly varying bottom topography.

Further, in O'Hare and Davies (1993) the successive application matrix model is compared with the extended mild slope equation derived by Kirby (1986). The two models are applied for the two types of bottom topography as given by the existing laboratory data for the wave reflection over a sinusoidal bed and doubly-sinusoidal beds. The models are observed to provide reasonably good results and the matrix model can be applied for rectangular shape and smoothly varying bottom topography. A consistent coupled-mode theory is employed by Athanassoulis and Belibassakis (1999) to analyse the wave propagation over variable bottom topography. The additional mode

is introduced to describe the influence of the bottom slope and modelled all the wave phenomena such as refraction, reflection, diffraction, which serves as a useful tool in the analysis. Athanassoulis and Belibassakis (1999) employed a consistent coupled-mode theory and extension of the theory by Belibassakis and Athanassoulis (2005, 2013) is used to analyse the wave propagation over variable seabed profile. Further, the extension of a consistent coupled-mode theory was applied by Belibassakis and Athanassoulis (2004) to analyse the hydroelastic behaviour of large floating bodies with a shallow draught and ice sheets of small and uniform thickness over variable bottom topography.

The hydroelastic behaviour of large floating structures or ice-sheets is analysed by Athanassoulis and Belibassakis (2009) for finite thickness over a sea bed of varying bathymetry. A coupled-mode system is presented using the variational principle along with the plate covered region and pressure functional for the open water region. Three models based on the importance of rotary inertia and/or shear deformation is presented by Papathanasiou and Belibassakis (2014) in analysing the hydroelastic characteristics of VLFS with varying thickness. A coupled-mode system is proposed considering a consistent local mode expansion and solved using FEM solvers based on the variational formulation. The hydroelastic behaviour of a VLFS over varying sea bottom topography is considered by Kyoung et al. (2005) for four different cases. The FEM based on the variational formulation is used to calculate the sea-bottom effects in the fluid domain and Kirchhoff's plate theory is used to model the pontoon type floating structure. The mode superposition method is adopted to calculate the hydroelastic behaviour of the floating structure. The wave scattering due to a semi-infinite floating membrane is analysed by Karmakar and Sahoo (2008) for a changing bottom topography. The steps are considered to be a finite and infinite step in the analysis of reflection, transmission and deflection of a floating membrane. Further, due to significant changes in the amplitude and length of the membrane gravity waves, it is suggested that the membrane can be used as an effective breakwater. The oblique flexural gravity wave scattering by multiple stepped bottom topography in finite water depth and shallow water approximations is analysed by Karmakar et al. (2010) acted upon by obliquely incident waves. The wide spacing approximation is employed to analyse the wave scattering from multiple steps and submerged blocks using the results

of a single step. The energy relation for oblique flexural gravity wave scattering is derived due to a change in bottom topography using the argument of wave energy flux.

The diffraction pattern due to the obliquely incident wave onto a floating structure with a wall is analysed by Bhattacharjee and Soares (2011) over step type bottom topography in finite water depth and shallow water approximations. The eigenfunction expansion method is used to obtain the solution of the problem under the potential flow approach. The interaction of the oblique incident wave with a moored floating membrane is analysed by Karmakar and Soares (2012) for both the cases of finite water depth and shallow water approximation with changes in bottom topography. The energy relation for the oblique gravity wave in the presence of floating membrane due to an abrupt change in bottom topography is derived for various cases using the law of conservation of energy flux and alternately by the direct application of Green's second identity. The edges of the membrane are considered to be moored on to the ocean bottom with various values of spring stiffness. The extension of the coupled-mode model is considered by Belibassakis et al. (2013) in the hydroelastic analysis of the shallow draft, 3D large floating bodies or ice sheets with small thickness over variable bottom topography. Dhillon et al. (2013) investigated the oblique wave scattering from a semi-infinite rigid dock over a varying bottom topography. They employed a simplified perturbation analysis with appropriate use of Green's integral theorem to solve the boundary value problem. The study concludes that the sinusoidal bottom topography does not affect the incident wave for certain frequencies. Further, Bragg's resonance is observed for all the cases. Dhillon et al. (2016) analysed wave scattering due to a floating rigid dock with finite width over a step type bottom topography with abrupt changes in water depth. The eigenfunction expansion method is considered along with matching conditions to solve the problem in both the cases of bottom profile with incoming waves from lower and higher water depth.

The scattering of waves using a porous barrier near a rigid wall along a stepped type bottom topography is studied by Behera et al. (2015) under the action of oblique waves. The eigenfunction expansion method is used along with multi-mode approximation and the modified mild-slope equation is used to take into consideration the variations in bottom topography. The efficiency of a dual-chamber oscillating water column is analysed by Rezanejad et al. (2015) for step type bottom topography based on the

matched eigenfunction expansion and the boundary integral equation method (BIEM). The wave diffraction due to undulating bed along with different kinds of thin vertical barriers was examined by Choudhary and Martha (2016). The perturbation analysis and Green's function technique is used to obtain the solution for the wave structure interaction. The coupled-mode model is extended by Gerostathis et al. (2016) to analyse the hydroelastic behaviour of 3D large floating bodies of shallow draft lying over variable bathymetry regions. They assumed a general bathymetry characterized by a continuous depth function combining two regions of constant or maybe even with varying depth. The scattering of waves due to the semi-infinite elastic plate over a step type bottom topography is analysed by Guo et al. (2016) acted upon by obliquely incident waves. An analytical method using matched eigenfunction expansions method is developed based on potential theory and the plate was modelled considering Euler-Bernoulli beam theory. The effects of the wave incident angle, the plate draft, the plate edge conditions and the sea-bottom topography is analysed for various hydrodynamic quantities. Cheng et al. (2017) established a time-domain fully nonlinear NWT using HOBEM to analyse the hydroelastic behaviour of floating elastic plate over variable bottom topography. The analysis is carried out for various shapes and arrangements of the trapezoid-shaped bottom topography. They concluded that the plate surface nonlinearity increased for the propagation of wave over an uneven sea-bottom. Belibassakis et al. (2017) extended the coupled-mode model applied to the hydroelastic analysis of three-dimensional large floating bodies of shallow draft or ice sheets of small thickness, lying over variable bathymetry regions. The problem is formulated based on linearized water-wave and thin elastic-plate theory for the ice sheets. They used a complete, local, hydroelastic-mode series expansion of the wave field, enhanced by an appropriate sloping-bottom mode to treat the wavefield beneath the elastic floating plate, down to the sloping bottom boundary.

2.2.6 Wave attenuation due to submerged structures

The ocean wave interaction with large floating elastic plate produces hydroelastic response which could damage the structure. Hence, a proper mitigation method needs to be employed to reduce the wave interaction with the structure. The hydroelastic response due to the wave interaction with a pontoon-type VLFS along with a breakwater is presented by Ohmatsu (2000). The gap between the breakwater and the

floating structure determines the resonance phenomena based on the wavelength. The results are validated with the numerical and experimental results, further stating that the response decreased for low values of the reflection coefficient. The wave-induced response due to the interaction with the floating elastic plate with an attached submerged plate at the fore-end was analysed by Watanabe et al. (2003). The significant reduction in the response is achieved due to the attachment of the submerged plate. Wave interaction with multiple moored surface-piercing membrane acting as breakwaters was analysed by Karmakar et al. (2013). The BVP is solved using the eigenfunction expansion method along with least square approximation method. The gap between the vertical floating breakwaters was observed to attenuate the wave height. Cheng et al. (2014) analysed the hydroelastic response of the pontoon-type VLFS edged with the perforated, non-perforated plates and combination of both, which acts as an anti-motion device using both numerical and experimental methods. A higher wave energy dissipation and added damping are observed for a perforated-impermeable-plate combination attached to the fore-end and back-end of the VLFS.

The wave trapping by a porous barrier near a rigid wall with a step-type bottom bed was studied by Behera et al. (2015). The varying distance between the porous barrier and rigid wall showed full reflection for different values of wavenumber. Karmakar and Guedes Soares (2013, 2015) analysed the wave interaction with multiple bottom-standing flexible porous breakwaters acted upon by oblique waves. The wave attenuation based on varying porosity, barrier depth, and the gap between the barriers is analysed to understand its effectiveness as a breakwater. The ocean wave trapping due to the porous barriers near a wall was studied by Kaligatla et al. (2017). A considerable reduction in wave reflection is observed due to the presence of dual porous barriers. The study suggests that on properly placing the dual porous barriers in front of the rigid wall could be efficient in wave trapping with negligible wave force on the rigid walls.

The wave scattering due to a submerged permeable vertical flexible membrane barrier was investigated by Koley and Sahoo (2017) for obliquely incident waves considering a bottom-standing, surface-piercing and complete membrane barrier. The solution for BVP was obtained analytically by using the eigenfunction expansion method and numerically using coupled BEM-FEM method. The study is extended for a vertical

flexible porous plate (Koley et al., 2015) using Green's function technique converting the BVP into a system of Fredholm integral equation. Recently, Singla et al. (2018) studied the effect of three different configurations of the vertical barrier in mitigating the hydroelastic behaviour of the large floating structures. The study concluded that the responses of the structure can be reduced by suitably selecting the configurations for the porous barriers in front of the very large floating structure. The previous study suggests that very limited studies were performed considering a vertical barrier to attenuate the wave energy in front of the large floating structures and further studies are required to be initiated to understand the effect of barriers in reducing the incident wave height.

2.3 CRITICAL REVIEW

In the past few decades, the research interest was to understand the behaviour of VLFS in ocean waves using Euler-Bernoulli beam theory. The elastic body motion is considered in comparison to the rigid body motions for the wave interaction with VLFS. The review of the literature shows that most of the floating structures are located in shallow water depths, whereas the studies are also performed for the floating structures in finite and infinite water depths. In the literature, the change in the bottom topography, multiple articulations of the elastic plate and different support conditions are analysed using different numerical approach. The literature indicates that, the study of the floating elastic plate using Timoshenko-Mindlin plate theory is limited and no significant research is performed considering the effect of rotary inertia and transverse shear deformation of the elastic plate. Further, the studies using the change in bottom topography is beneficial in the proper design of the floating structure. Most of the researcher conducted studies on the submerged structures such as submerged breakwaters, large submerged pontoons supporting floating structures, submerged storage tanks and anti-motion devices. The study on the submerged structures along with the VLFS based on Timoshenko-Mindlin plate theory is limited and no significant development on the floating and submerged structure are performed. The study on the wave interaction with floating structures based on Timoshenko-Mindlin theory and submerged structure will provide an effective analysis of the effect of rotary inertia and transverse shear deformation of the elastic plate.

2.4 CLOSURE

In this Chapter, the wave interaction with floating and submerged structure and the hydroelastic behaviour of the floating structure are presented and discussed in detail. The detailed review of literature is presented for the fluid-structure interaction considering different types of theories at various water depths. The comprehensive study for the fluid-structure interaction is carried out and is grouped under various categories. The study performed based on Euler-Bernoulli beam theory and Timoshenko-Mindlin plate theory is grouped and discussed in detail. The numerical techniques adopted in the analysis of floating structure such as eigenfunction expansion method, Fourier analysis, Wiener-Hopf technique, partitioned approach, mild slope approach, approximate analysis, finite element method and boundary element method are presented and discussed in detail.

CHAPTER 3

WAVE INTERACTION WITH FLOATING PLATE

3.1 GENERAL INTRODUCTION

In this chapter, the hydroelastic response of very large floating structures (VLFS) under the action of ocean waves is analysed considering the small-amplitude wave theory. The very large floating structure is modelled as a floating thick elastic plate based on Timoshenko-Mindlin plate theory and the analysis for the hydroelastic response is performed considering different edge boundary conditions. The numerical study is performed to analyse the wave reflection and transmission characteristics of the floating plate under the influence of different support conditions using eigenfunction expansion method along with the orthogonal mode-coupling relation in the case of finite water depth. Further, the analysis is extended for shallow water depth and the continuity of energy and mass flux is applied along the edges of the plate to obtain the solution for the problem. The hydroelastic behaviour in terms of reflection and transmission coefficient, plate deflection, strain, bending moment and shear force of the floating thick elastic plate with support conditions is analysed and compared for finite and shallow water depth. The study reveals an interesting aspect in the analysis of the floating elastic plate with support condition due to the presence of the rotary inertia and transverse shear deformation. Further, the study is extended for shallow water approximation and the results are compared for both Timoshenko-Mindlin plate theory and Kirchhoff's plate theory.

3.2 MATHEMATICAL FORMULATION

The wave interaction with the finite floating elastic plate with different edge support conditions is analysed based on Timoshenko-Mindlin plate theory under the assumption of linearized wave theory. A two-dimensional coordinate system is considered for the wave-interaction with the floating plate as shown in Figure 3.1. The wave is incident normally along the positive *x*-axis horizontally and the y-axis is considered positive vertically downward. The thick elastic plate is considered to be floating at the free

surface of the fluid $I_2 = -a < x < 0, y = 0$ and termed as plate covered region 2. The open water surface divided into upstream open water domain $I_1 = 0 < x < \infty, 0 < y < h$ as region 1 and downstream open water domain $I_3 = -\infty < x < 0, 0 < y < h$ as region 3. The plate width is considered to be extended infinitely in the lateral direction and the two edges of the floating thick elastic plate at $x = 0$ and $x = -a$ are considered to satisfy edge support boundary conditions.

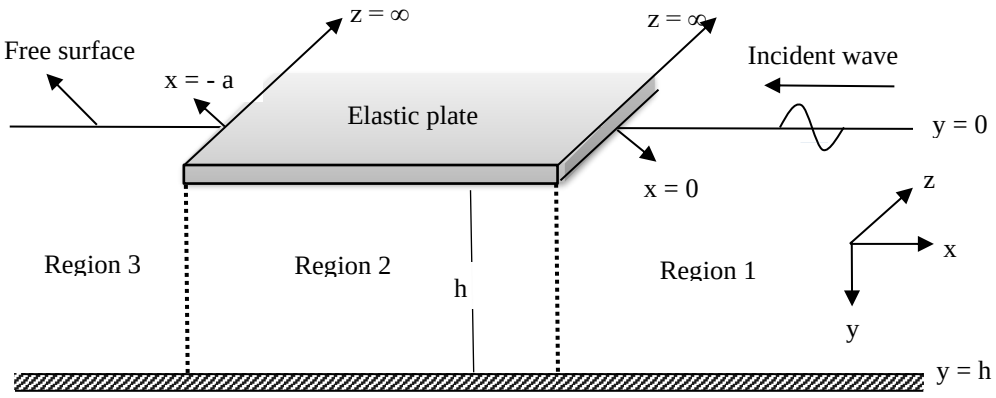

Figure 3.1: Schematic diagram for the floating elastic plate

Under the assumption of the linearized wave theory the velocity potential, Φ satisfies the Laplace's equation given by

$$\nabla^2 \Phi_j = 0 \text{ at } -\infty < x < \infty, 0 < y < h. \tag{3.1}$$

The linearized kinematic boundary condition at the mean free surface is of the form

$$\zeta_{jt} = \Phi_{jy}, \text{ at } y = 0. \tag{3.2}$$

The dynamic free surface boundary condition is given by

$$\rho \Phi_{jt} - \rho g \zeta_j = p_{\text{atm}} \quad \text{at} \quad y = 0, \tag{3.3}$$

where p_{atm} is the atmospheric pressure. The bottom boundary condition is given by

$$\Phi_{jy} = 0, \text{ at } y = h. \tag{3.4}$$

In the plate covered region $j = 2$, it is assumed that the plate satisfies the Timoshenko-Mindlin theory (Fox and Squire, 1991) which includes the effect of rotary inertia and transverse shear deformation of the form

$$\left(\partial_x^2-\frac{\rho_p}{\mu Gd}\partial_t^2\right)\left(EI\partial_x^2-\frac{\rho_p d^3}{12}\partial_t^2\right)\zeta_j+\rho_p d\partial_t^2\zeta_j=-\left(1-\frac{EI}{\mu Gd}\partial_x^2+\frac{\rho_p d^2}{12\mu G}\partial_t^2\right)p, \quad (3.5)$$

where d is the plate thickness, ρ_p is the plate density, $EI=Ed^3/12(1-\nu^2)$ is the plate rigidity, E is the Young's Modulus, ν is the Poisson's ratio, $G=E/2(1+\mu)$ is the shear modulus of the plate, and $\mu=\frac{\pi^2}{12}$ is the transverse shear coefficient of the plate.

Assuming that the wave elevation and the plate deflection are simple harmonic motion in time with the frequency ω, the velocity potential $\Phi_j(x,y,t)$ and the surface deflection $\zeta_j(x,t)$ can be written as $\Phi_j(x,y,t)=\mathrm{Re}\{\phi_j(x,y)\}e^{-i\omega t}$ and $\zeta_j(x,t)=\mathrm{Re}\{\zeta_j(x)\}e^{-i\omega t}$ where Re denotes the real part. In the open water region, the linearized free surface boundary condition is given by

$$\phi_{jy}(x,y)-\kappa\phi_j(x,y)=0, \text{ for } x>0 \text{ and } x<-a \quad (3.6)$$

where $\kappa=\omega^2/g$. The plate covered boundary condition in the region $j=2$ is obtained by combining the linearised kinematic condition at the surface, Bernoulli's equation and Timoshenko-Mindlin equation as

$$\begin{aligned}&\left\{\frac{EI}{\left(\rho g-m_s\omega^2\right)}\partial_x^4+\left(\frac{m_s\omega^2 I}{\left(\rho g-m_s\omega^2\right)}-S\right)\partial_x^2+\left(1-\frac{m_s\omega^2 IS}{EI}\right)\right\}\phi_{jy}(x,y)\\&\quad+\frac{\rho\omega^2}{\left(\rho g-m_s\omega^2\right)}\left\{1-\frac{m_s\omega^2 IS}{EI}-S\partial_x^2\right\}\phi_j(x,y)=0, \text{for } -a<x<0\end{aligned} \quad (3.7)$$

where ρ is the density of water, g is the acceleration due to gravity, $m_s=\rho_p d$ is the mass per unit area, ρ_p is the density of plate, d is the plate thickness, $I=d^2/12$ is the rotary inertia, and $S=EI/\mu Gd$ is the shear deformation.

The continuity of velocity and pressure at the interface $x=0$ and $x=-a$ for $j=1,2$, $0<y<h$ is given by

$$\phi_{jx}(x,y)=\phi_{(j+1)x}(x,y) \text{ and } \phi_j(x,y)=\phi_{(j+1)}(x,y). \quad (3.8)$$

The far-field radiation condition is given by

$$\phi_j(x) = \begin{cases} \left(e^{-ik_{10}x} + R_0 e^{ik_{10}x}\right) f_{10}(y) & \text{as} \quad x \to \infty, \\ \left(T_0 e^{-ik_{30}x}\right) f_{30}(y) & \text{as} \quad x \to -\infty, \end{cases} \tag{3.9}$$

with R_0 and T_0 are the complex amplitudes of the reflected and transmitted waves. The eigenfunctions for $j = 1,3$ are of the form $f_{j0}(y) = \cosh k_{j0}(h-y) / \cosh k_{j0}h$ and k_{j0} for $j = 1,3$ are the positive real roots satisfies the dispersion relation in the case of finite water depth given by

$$k_{j0} \tanh k_{j0}h - \omega^2 / g = 0. \tag{3.10}$$

3.2.1 Edge-support condition of the elastic plate

The type of supports at the edge forms a boundary condition at the plate edges. In the wave interaction with the floating elastic plate, different support conditions are considered in the study for the hydroelastic performance of the elastic plate under the action of ocean waves. The support conditions are based on the vertical shear forces, bending and twisting moments acting on the plate edges. These conditions represent the slope, deflection, bending moment and generalized shear force at the edges of the elastic plate. The consideration of the edge boundary condition in the hydroelastic analysis of large floating structures helps in the analysis and design of the VLFS.

The major application of free-free edge boundary condition is in the study of the ocean wave interaction with the sea ice. The study mainly includes the wave attenuation due to the presence of sea ice and the breaking of the ice sheets due to incident ocean waves (Williams et. al., 2013). However, most of the manmade large floating structures such as floating runways, floating oil storage base, offshore renewable energy plants etc. needs to be anchored at the edges by cables, ropes or piles to ensure safety and stability of structures. The floating oil storage base requires the structure to be stable under the action of ocean waves, which requires strong edge support to restrain the heave motion of the structure. Hence, the consideration of support conditions such as simply supported or fixed edge support condition becomes significant in the analysis. The floating elastic plate is considered to satisfy one of the following edge support conditions (Timoshenko and Krieger, 1959; Rao. 2007).

3.2.1.1 Freely floating elastic plate

The freely floating elastic plate represents zero bending moment and zero shear force at the plate edge or at the supports for finite water depth. In the case of finite water depth, the shear force and bending moment at the plate edge $x = 0, -a$ for $j = 2$ satisfies the relation given by

$$\partial_y^3 \phi_j(x, y) = 0 \text{ and } \partial_{xy^3}^4 \phi_j(x, y) = \wp \partial_{xy}^2 \phi_j(x, y) \text{ for } x = 0, -a \text{ at } y = 0. \quad (3.11)$$

In the case of shallow water approximation, the zero bending moment and zero shear force at the plate edge $x = 0, -a$ satisfies the relation given by

$$\partial_x^4 \phi_j(x) = 0 \text{ and } \partial_x^5 \phi_j(x) = \wp \partial_x^3 \phi_j(x) \text{ for } x = 0, -a, \quad (3.12)$$

where $\wp = \left\{ \frac{m\omega^2 (S + I)}{EI} \right\}$.

3.2.1.2 Simply supported floating elastic plate

In this case the simply supported edge, the edge condition represents the bending moment and deflection to vanish at the edges or at the supports for finite water depth. The plate edge is considered to be having zero deflection/displacement and zero bending moment at $x = 0, -a$ for $j = 2$ satisfying the relation

$$\partial_y \phi_j(x, y) = 0 \text{ and } \partial_y^3 \phi_j(x, y) = 0 \text{ for } x = 0, -a \text{ at } y = 0. \quad (3.13)$$

In the case of shallow water approximation, the zero deflection/displacement and zero bending moment at the plate edge $x = 0, -a$ for $j = 2$ satisfies the relation

$$\partial_x^2 \phi_j(x) = 0 \text{ and } \partial_x^4 \phi_j(x) = 0 \text{ for } x = 0, -a. \quad (3.14)$$

3.2.1.3 Fixed Edge Floating Elastic Plate

In the case of fixed edge condition, the deflection and slope vanish at the edge or at the supports for finite water depth. So, for finite water depth, we consider zero slope and zero deflection/displacement at the plate edge $x = 0, -a$ for $j = 2$ which satisfies the relation

$$\partial_y \phi_j(x, y) = 0 \text{ and } \partial_{xy}^2 \phi_j(x, y) = 0 \text{ for } x = 0, -a \text{ at } y = 0. \quad (3.15)$$

In the case of shallow water approximation, we consider zero slope and zero deflection/ displacement at the plate edge $x = 0, -a$ for $j = 2$ which satisfies the relation

$$\partial_x^2 \phi_j(x) = 0 \text{ and } \partial_x^3 \phi_j(x) = 0 \text{ for } x = 0, -a. \tag{3.16}$$

In the next section, the solution procedure of the wave interaction with the finite floating elastic plate is presented and discussed in detail.

3.3 METHOD OF SOLUTION

The solution procedure for the wave interaction with finite floating elastic plate based on Timoshenko-Mindlin plate theory is analysed for both finite water depth and shallow water approximation.

3.3.1 Finite water depth

The boundary value problem for the scattering of the wave by a finite floating elastic plate with different edge boundary condition is formulated in the case of finite water depth. The velocity potentials $\phi_j(x, y)$ for $j = 1, 2, 3$ satisfying the governing Equation (3.1) along with the boundary condition (3.4), (3.6), (3.7) and (3.9) are of the form

$$\begin{aligned}
\phi_1(x, y) &= \left(I_0 e^{-ik_{10}x} + R_0 e^{ik_{10}x}\right) f_{10}(y) + \sum_{n=1}^{\infty} R_n e^{-\kappa_{1n}x} f_{1n}(y) && \text{for } x > 0 \\
\phi_2(x, y) &= \sum_{n=0,I}^{II} \left(A_n e^{-ik_{2n}x} + B_n e^{ik_{2n}x}\right) f_{2n}(y) + \sum_{n=1}^{\infty} \left(A_n e^{\kappa_{2n}x} + B_n e^{-\kappa_{2n}x}\right) f_{2n}(y) && \\
& && \text{for } -a < x < 0 \\
\phi_3(x, y) &= T_0 e^{-ik_{30}x} f_{30}(y) + \sum_{n=1}^{\infty} T_n e^{\kappa_{3n}x} f_{3n}(y) && \text{for } x < -a
\end{aligned} \tag{3.17}$$

where $R_n, T_n, n = 0, 1, 2...,$ and $A_n, B_n, n = 0, I, II, 1, 2...$ are the unknown constants to be determined. The eigenfunctions $f_{jn}(y)$'s for $j = 2$ is given by

$$f_{jn}(y) = \frac{\cosh k_{jn}(h - y)}{\cosh k_{jn} h} \text{ for } n = 0, I, II \text{ and } f_{jn}(y) = \frac{\cos \kappa_{jn}(h - y)}{\cos \kappa_{jn} h} \text{ for } n = 1, 2,.. \tag{3.18a}$$

and the eigenfunctions $f_{jn}(y)$'s for $j = 1, 3$ are of the form

$$f_{jn}(y) = \frac{\cosh k_{jn}(h - y)}{\cosh k_{jn} h} \text{ for } n = 0 \text{ and } f_{jn}(y) = \frac{\cos \kappa_{jn}(h - y)}{\cos \kappa_{jn} h} \text{ for } n = 1, 2,... \tag{3.18b}$$

where k_{jn} for $j=1,3$ and $n=2$ are the eigenvalues satisfy the dispersion relation in the open water region given by

$$k_{j0}\tanh k_{j0}h-\omega^2/g=0, \tag{3.19}$$

with $k_{jn}=i\kappa_{jn}$ for $n=1,2...$ and the dispersion relation has one real root k_{j0} and an infinite number of purely imaginary roots κ_{jn} for $n=1,2...$ In the plate covered region the k_{jn} for $j=2$ satisfies the dispersion relation given by

$$\left(\alpha_0-\alpha_1k_{jn}^2+\alpha_2k_{jn}^4\right)k_{jn}\tanh k_{jn}h-\left(\beta_0-\beta_1k_{jn}^2\right)=0, \tag{3.20}$$

where $\alpha_0=\left\{1-m_s\omega^2\left(\frac{IS}{EI}\right)\right\}$, $\alpha_1=\left\{\frac{m_s\omega^2 I}{\left(\rho g-m_s\omega^2\right)}-S\right\}$, $\alpha_2=\frac{EI}{\left(\rho g-m_s\omega^2\right)}$,

$\beta_0=\frac{\rho\omega^2}{\left(\rho g-m_s\omega^2\right)}\left(1-m_s\omega^2\frac{IS}{EI}\right)$, $\beta_1=-\frac{\rho\omega^2 S}{\left(\rho g-m_s\omega^2\right)}$, $I=d^2/12$ is the rotary inertia, $EI=Ed^3/12(1-\nu^2)$ is the plate rigidity, $S=EI/\mu Gd$ is the shear deformation of the plate, $G=E/2(1+\mu)$ is the shear modulus of elastic material, $\mu=\pi^2/12$ is the transverse shear coefficient, E is Young's modulus, ν is the Poisson's ratio, m_s is the mass of the plate.

The dispersion relation as in Equation (3.20) has two real root k_{j0} and four complex roots k_{jn}, $n=I,II,III,IV$ of the form $\pm\alpha\pm i\beta$. In addition, there are infinite numbers of purely imaginary roots κ_{jn} for $n=1,2....$

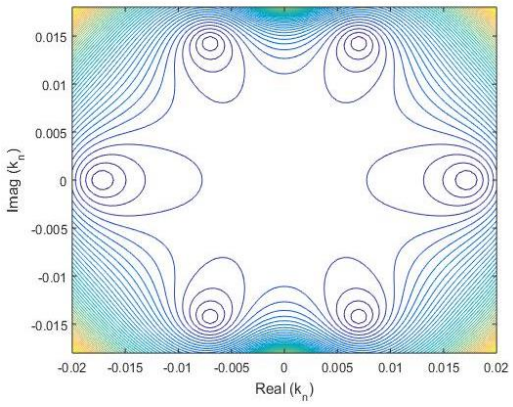

(a)

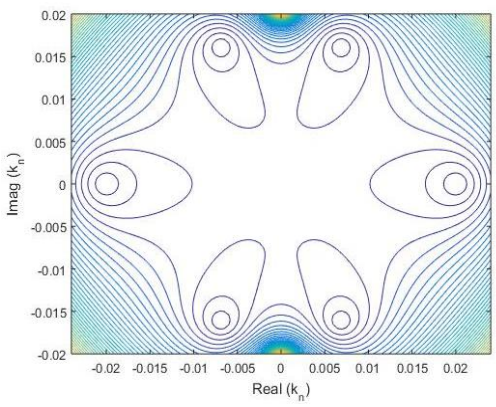

(b)

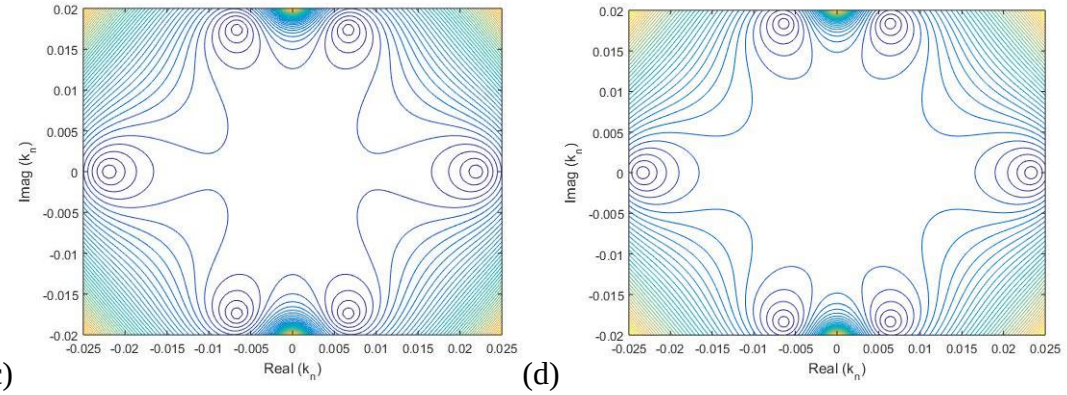

(c) (d)

Figure 3.2: Contour plot for the roots for the plate covered dispersion relation considering $h/L=0.15,\ E=5GPa$ and $d/L=0.02$ at (a) $k_{10}h=5$ (b) $k_{10}h=10$ (c) $k_{10}h=15$ and (d) $k_{10}h=20$.

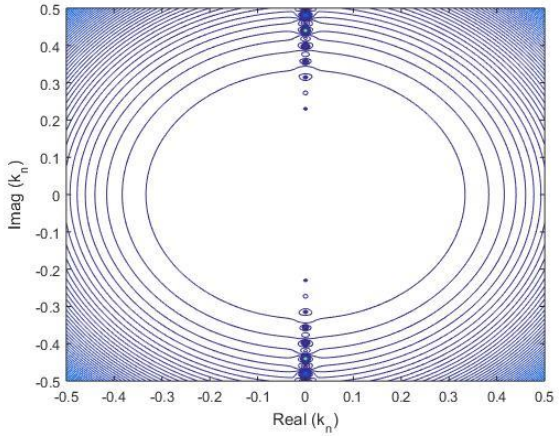

Figure 3.3: Contour plot of infinite number of imaginary roots for the plate covered dispersion relation considering $h/L=0.15,\ E=5GPa$ and $d/L=0.02$ at $k_{10}h=10.$

In order to visualize the variation of the roots of the plate covered dispersion relation, the contour plots are presented in Figure 3.2(a-d) and Figure 3.3 which demonstrate the existence of two real and four complex conjugate roots along with infinitely many imaginary roots for the plate covered region. The occurrences of the infinitely many imaginary roots show the existence of evanescent modes (Manam et al., 2005). The roots of the dispersion relation are determined using the Newton–Raphson method and the contour plots helps to identify the initial guess. It may be noted that the eigenfunctions $f_{jn}(y)$'s in the open water and plate covered region satisfy the orthogonality relation as given by

$$\left\langle f_{jm}, f_{jn} \right\rangle_{j=1,3} = \begin{cases} 0 & \text{for } m \neq n, \\ C_n' & \text{for } m = n, \end{cases} \text{ and } \left\langle f_{jm}, f_{jn} \right\rangle_{j=2} = \begin{cases} 0 & \text{for } m \neq n, \\ C_n'' & \text{for } m = n, \end{cases} \tag{3.21}$$

with respect to the orthogonal mode-coupling relation defined by

$$\left\langle f_{jm}, f_{jn} \right\rangle_{j=1,3} = \int_0^h f_{jm}(y) f_{jn}(y) dy, \tag{3.22}$$

$$\begin{aligned} \left\langle f_{jm}, f_{jn} \right\rangle_{j=2} = & \int_0^h f_{jm}(y) f_{jn}(y) dy - \frac{\alpha_1}{Q\left(k_{jn}\right)} \left\{ f'_{jm}(0) f'_{jn}(0) \right\} \\ & + \frac{\alpha_2}{Q\left(k_{jn}\right)} \left\{ f'''_{jm}(0) f'_{jn}(0) + f'_{jm}(0) f'''_{jn}(0) \right\} + \frac{\beta_1}{P\left(k_{jn}\right)} f_{jm}(0) f_{jn}(0), \end{aligned} \tag{3.23}$$

where $C'_n = \dfrac{2k_{jn}h + \sinh 2k_{jn}h}{4k_{jn}\cosh^2 k_{jn}h}$ for $j = 1,3,\ m = n = 0,$

$$C''_n = \frac{(\alpha_0 - \alpha_1 k_{jn}^2 + \alpha_2 k_{jn}^4) 2k_{jn}h + (\alpha_0 - 3\alpha_1 k_{jn}^2 + 5\alpha_2 k_{jn}^4) \sinh 2k_{jn}h + (4\beta_1 k_{jn} \cosh^2 k_{jn}h)}{(4k_{jn}\cosh^2 k_{jn}h)(\alpha_0 - \alpha_1 k_{jn}^2 + \alpha_2 k_{jn}^4)}$$

for $j = 2,\ m = n = 0, I, II,$

with $P\left(k_{2n}\right) = \left(\alpha_0 - \alpha_1 k_{2n}^2 + \alpha_2 k_{2n}^4\right)$ and $Q\left(k_{2n}\right) = \left(\beta_0 - \beta_1 k_{2n}^2\right).$

The constant term C_n', C_n'', $P\left(k_{jn}\right)$ and $Q\left(k_{jn}\right)$ for $n = 1, 2, \ldots$ are obtained by substituting $k_{jn} = i\kappa_{jn}$ for $n = 1,2,3$. In order to determine the unknown coefficients, the mode-coupling relation is applied to the velocity potential along with the respective eigenfunction and the edge conditions to obtain the system of linear equation.

Applying the mode-coupling relation as in Equation (3.23) on the velocity potential $\phi_2(x,y)$ at $x = 0, -a$ along with the eigenfunction $f_{2m}(y)$ to obtain the equations given by

$$\begin{aligned} \left\langle \phi_2(0,y), f_{2m}(y) \right\rangle = & \int_0^h \phi_2(0,y) f_{2m}(y) dy - \frac{\alpha_1}{Q\left(k_{2n}\right)} \left\{ \phi_{2y}(0,y) f'_{2m}(0) \right\} \\ & + \frac{\alpha_2}{Q\left(k_{2n}\right)} \left\{ \phi_{2yyy}(0,0) f'_{2m}(0) + \phi_{2y}(0,0) f'''_{2m}(0) \right\} + \frac{\beta_1}{P\left(k_{2n}\right)} \phi_2(0,0) f_{2m}(0), \end{aligned} \tag{3.24a}$$

$$\begin{aligned} \left\langle \phi_2(-a,y), f_{2m}(y) \right\rangle = & \int_0^h \phi_2(-a,y) f_{2m}(y) dy - \frac{\alpha_1}{Q\left(k_{2n}\right)} \left\{ \phi_{2y}(-a,y) f'_{2m}(0) \right\} \\ & + \frac{\alpha_2}{Q\left(k_{2n}\right)} \left\{ \phi_{2yyy}(-a,0) f'_{2m}(0) + \phi_{2y}(-a,0) f'''_{2m}(0) \right\} + \frac{\beta_1}{P\left(k_{2n}\right)} \phi_2(-a,0) f_{2m}(0), \end{aligned} \tag{3.24b}$$

for $m = 0, I, II, 1, 2, \ldots$

Again applying the mode-coupling relation as in Equation (3.23) on the velocity potential $\phi_{2x}(x,y)$ at $x=0,-a$ along with the eigenfunction $f_{2m}(y)$ to obtain the equations given by

$$\begin{aligned}\left\langle \phi_{2x}(0,y),\, f_{2m}(y)\right\rangle &= \int_0^h \phi_{2x}(0,y)\, f_{2m}(y)dy - \frac{\alpha_1}{Q(k_{2n})}\left\{\phi_{2xy}(0,y)\, f'_{2m}(0)\right\} + \\ &\frac{\alpha_2}{Q(k_{2n})}\left\{\phi_{2xyyy}(0,0)\, f'_{2m}(0) + \phi_{2xy}(0,0)\, f'''_{2m}(0)\right\} + \frac{\beta_1}{P(k_{2n})}\phi_{2x}(0,0)\, f_{2m}(0),\end{aligned} \tag{3.25a}$$

$$\begin{aligned}\left\langle \phi_{2x}(-a,y),\, f_{2m}(y)\right\rangle &= \int_0^h \phi_{2x}(-a,y)\, f_{2m}(y)dy - \frac{\alpha_1}{Q(k_{2n})}\left\{\phi_{2xy}(-a,y)\, f'_{2m}(0)\right\} \\ &+ \frac{\alpha_2}{Q(k_{2n})}\left\{\phi_{2xyyy}(-a,0)\, f'_{2m}(0) + \phi_{2xy}(-a,0)\, f'''_{2m}(0)\right\} + \frac{\beta_1}{P(k_{2n})}\phi_{2x}(-a,0)\, f_{2m}(0),\end{aligned} \tag{3.25b}$$

for $m=0,I,II,1,2,...$ The linear system of equation in Equations. (3.24a,b) and (3.25a,b) is reformulated using the orthogonal property of the eigenfunction $f_{2m}(y)$ as in Equation (3.21) along with continuity of pressure and velocity across the vertical interface $x=0,-a$ and $0<y<h$ as in Equation (3.8). Further, the equations are simplified using the suitable edge boundary conditions to obtain a linear system of algebraic equations. The modified system of equation using the edge support condition is described in detail in the next subsection.

3.3.1.1 Free-free edge support condition

In the case of free-free edge condition, the bending moment and shear force terms vanish and the system of equations is simplified as

$$\begin{aligned}&R_0\int_0^h f_{10}(y)\, f_{2m}(y)dy + \sum_{n=1}^{N+2} R_n \int_0^h f_{1n}(y)\, f_{2m}(y)dy \\ &+\left\{\sum_{n=0,I}^{II}(A_n+B_n)+\sum_{n=1}^{N}(A_n+B_n)\right\}\left[\frac{\alpha_2}{Q(k_{2n})}\, f'_{2n}(0)\, f'''_{2m}(0) - \frac{\alpha_1}{Q(k_{2n})}\, f'_{2n}(0)\, f'_{2m}(0)\right. \\ &\left.+\frac{\beta_1}{P(k_{2n})}\, f_{2n}(0)\, f_{2m}(0) - \delta_{mn}\left\langle f_{2n}, f_{2m}\right\rangle\right] = -I_0\int_0^h f_{10}(y)\, f_{2m}(y)\, dy,\end{aligned} \tag{3.26a}$$

$$\begin{aligned}&T_0 e^{ik_{30}a}\int_0^h f_{30}(y)\, f_{2m}(y)dy + \sum_{n=1}^{N+2} T_n e^{-\kappa_{3n}a}\int_0^h f_{3n}(y)\, f_{2m}(y)dy + \sum_{n=0,I,II}^{N}\left(A_n e^{-ik_{2n}a} + B_n e^{ik_{2n}a}\right) \\ &\left[\frac{\alpha_2}{Q(k_{2n})}\, f'_{2n}(0)\, f'''_{2m}(0) - \frac{\alpha_1}{Q(k_{2n})}\, f'_{2n}(0)\, f'_{2m}(0) + \frac{\beta_1}{P(k_{2n})}\, f_{2n}(0)\, f_{2m}(0) - \delta_{mn}\left\langle f_{2n}, f_{2m}\right\rangle\right] = 0,\end{aligned} \tag{3.26b}$$

$$ik_{10}R_0\int_0^h f_{10}(y)\,f_{2m}(y)dy-\kappa_{1n}\sum_{n=1}^{N+2}R_n\int_0^h f_{1n}(y)\,f_{2m}(y)dy+\left\{ik_{2n}\sum_{n=0,I}^{II}(A_n-B_n)-\right.$$

$$\left.-\kappa_{2n}\sum_{n=1}^{N}(A_n-B_n)\right\}\left[\frac{\alpha_2}{Q(k_{2n})}\left\{\wp f'_{2n}(0)\,f'_{2m}(0)+f'_{2n}(0)\,f'''_{2m}(0)\right\}-\frac{\alpha_1}{Q(k_{2n})}f'_{2n}(0)\,f'_{2m}(0)\right. \quad (3.26c)$$

$$\left.+\frac{\beta_1}{P(k_{2n})}f_{2n}(0)\,f_{2m}(0)-\delta_{mn}\left\langle f_{2n},f_{2m}\right\rangle\right]=-ik_{10}I_0\int_0^h f_{10}(y)\,f_{2m}(y)\,dy,$$

$$-ik_{30}T_0e^{ik_{30}a}\int_0^h f_{30}(y)\,f_{2m}(y)dy+\kappa_{3n}\sum_{n=1}^{N+2}T_ne^{-\kappa_{3n}a}\int_0^h f_{3n}(y)\,f_{2m}(y)dy+\left\{ik_{2n}\sum_{n=0,I}^{II}(A_ne^{-ik_{2n}a}-B_ne^{ik_{2n}a})\right.$$

$$\left.-\kappa_{2n}\sum_{n=1}^{N}(A_ne^{\kappa_{2n}a}-B_ne^{-\kappa_{2n}a})\right\}\left[\frac{\alpha_2}{Q(k_{2n})}\left\{\wp f'_{2n}(0)\,f'_{2m}(0)+f'_{2n}(0)\,f'''_{2m}(0)\right\}\right.$$

$$\left.-\frac{\alpha_1}{Q(k_{2n})}f'_{2n}(0)\,f'_{2m}(0)+\frac{\beta_1}{P(k_{2n})}f_{2n}(0)\,f_{2m}(0)-\delta_{mn}\left\langle f_{2n},f_{2m}\right\rangle\right]=0, \quad (3.26d)$$

for $m=0,I,II,1,2,...$

3.3.1.2 Simply supported edge condition

In the case of simply support edge condition, the bending moment and deflection terms vanish and the system of equation is simplified as

$$R_0\int_0^h f_{10}(y)\,f_{2m}(y)dy+\sum_{n=1}^{N+2}R_n\int_0^h f_{1n}(y)\,f_{2m}(y)dy+\left\{\sum_{n=0,I}^{II}(A_n+B_n)+\sum_{n=1}^{N}(A_n+B_n)\right\}$$

$$\left[\frac{\beta_1}{P(k_{2n})}f_{2n}(0)\,f_{2m}(0)-\delta_{mn}\left\langle f_{2n},f_{2m}\right\rangle\right]=-I_0\int_0^h f_{10}(y)\,f_{2m}(y)\,dy, \quad (3.27a)$$

$$T_0e^{ik_{30}a}\int_0^h f_{30}(y)\,f_{2m}(y)dy+\sum_{n=1}^{N+2}T_ne^{-\kappa_{3n}a}\int_0^h f_{3n}(y)\,f_{2m}(y)dy$$

$$+\sum_{n=0,I,II}^{N}\left(A_ne^{-ik_{2n}a}+B_ne^{ik_{2n}a}\right)\left[\frac{\beta_1}{P(k_{2n})}f_{2n}(0)\,f_{2m}(0)-\delta_{mn}\left\langle f_{2n},f_{2m}\right\rangle\right]=0, \quad (3.27b)$$

$$ik_{10}R_0\int_0^h f_{10}(y)\,f_{2m}(y)dy-\kappa_{1n}\sum_{n=1}^{N+2}R_n\int_0^h f_{1n}(y)\,f_{2m}(y)dy+\left\{ik_{2n}\sum_{n=0,I}^{II}(A_n-B_n)-\right.$$

$$\left.\kappa_{2n}\sum_{n=1}^{N}(A_n-B_n)\right\}\left[\frac{\alpha_2}{Q(k_{2n})}\left\{f'''_{2n}(0)\,f'_{2m}(0)+f'_{2n}(0)\,f'''_{2m}(0)\right\}-\frac{\alpha_1}{Q(k_{2n})}f'_{2n}(0)\,f'_{2m}(0)\right. \quad (3.27c)$$

$$\left.+\frac{\beta_1}{P(k_{2n})}f_{2n}(0)\,f_{2m}(0)-\delta_{mn}\left\langle f_{2n},f_{2m}\right\rangle\right]=-ik_{10}I_0\int_0^h f_{10}(y)\,f_{2m}(y)\,dy,$$

$$-ik_{30}T_0e^{ik_{30}a}\int_0^h f_{30}(y)\,f_{2m}(y)dy+\kappa_{3n}\sum_{n=1}^{N+2}T_ne^{-\kappa_{3n}a}\int_0^h f_{3n}(y)\,f_{2m}(y)dy+\left\{ik_{2n}\sum_{n=0,I}^{II}(A_ne^{-ik_{2n}a}-B_ne^{ik_{2n}a})\right.$$
$$\left.-\kappa_{2n}\sum_{n=1}^{N}(A_ne^{\kappa_{2n}a}-B_ne^{-\kappa_{2n}a})\right\}\left[\frac{\alpha_2}{Q(k_{2n})}\left\{f_{2n}'''(0)\,f_{2m}'(0)+f_{2n}'(0)\,f_{2m}'''(0)\right\}\right.$$
$$\left.-\frac{\alpha_1}{Q(k_{2n})}f_{2n}'(0)\,f_{2m}'(0)+\frac{\beta_1}{P(k_{2n})}f_{2n}(0)\,f_{2m}(0)-\delta_{mn}\left\langle f_{2n},f_{2m}\right\rangle\right]=0, \tag{3.27d}$$

for $m=0,I,II,1,2,...$

3.3.1.3 Fixed edge/ built-in edge support condition

In the case of fixed edge condition, the deflection and slope terms vanish and the system of equation is simplified as

$$R_0\int_0^h f_{10}(y)\,f_{2m}(y)dy+\sum_{n=1}^{N+2}R_n\int_0^h f_{1n}(y)\,f_{2m}(y)dy+\left\{\sum_{n=0,I}^{II}(A_n+B_n)+\sum_{n=1}^{N}(A_n+B_n)\right\}\times$$
$$\left[\frac{\alpha_2}{Q(k_{2n})}f_{2n}'''(0)\,f_{2m}'(0)+\frac{\beta_1}{P(k_{2n})}f_{2n}(0)\,f_{2m}(0)-\delta_{mn}\left\langle f_{2n},f_{2m}\right\rangle\right]=-I_0\int_0^h f_{10}(y)\,f_{2m}(y)\,dy, \tag{3.28a}$$

$$T_0e^{ik_{30}a}\int_0^h f_{30}(y)\,f_{2m}(y)dy+\sum_{n=1}^{N+2}T_ne^{-\kappa_{3n}a}\int_0^h f_{3n}(y)\,f_{2m}(y)dy+\sum_{n=0,I,II}^{N}\left(A_ne^{-ik_{2n}a}+B_ne^{ik_{2n}a}\right)\times$$
$$\left[\frac{\alpha_2}{Q(k_{2n})}f_{2n}'''(0)\,f_{2m}'(0)+\frac{\beta_1}{P(k_{2n})}f_{2n}(0)\,f_{2m}(0)-\delta_{mn}\left\langle f_{2n},f_{2m}\right\rangle\right]=0, \tag{3.28b}$$

$$ik_{10}R_0\int_0^h f_{10}(y)\,f_{2m}(y)dy-\kappa_{1n}\sum_{n=1}^{N+2}R_n\int_0^h f_{1n}(y)\,f_{2m}(y)dy+\left\{ik_{2n}\sum_{n=0,I}^{II}(A_n-B_n)-\kappa_{2n}\sum_{n=1}^{N}(A_n-B_n)\right\}\times$$
$$\left[\frac{\alpha_2}{Q(k_{2n})}f_{2n}'''(0)\,f_{2m}'(0)+\frac{\beta_1}{P(k_{2n})}f_{2n}(0)\,f_{2m}(0)-\delta_{mn}\left\langle f_{2n},f_{2m}\right\rangle\right]=-ik_{10}I_0\int_0^h f_{10}(y)\,f_{2m}(y)\,dy, \tag{3.28c}$$

$$-ik_{30}T_0e^{ik_{30}a}\int_0^h f_{30}(y)\,f_{2m}(y)dy+\kappa_{3n}\sum_{n=1}^{N+2}T_ne^{-\kappa_{3n}a}\int_0^h f_{3n}(y)\,f_{2m}(y)dy+\left\{ik_{2n}\sum_{n=0,I}^{II}(A_ne^{-ik_{2n}a}-B_ne^{ik_{2n}a})\right.$$
$$\left.-\kappa_{2n}\sum_{n=1}^{N}(A_ne^{\kappa_{2n}a}-B_ne^{-\kappa_{2n}a})\right\}\left[\frac{\alpha_2}{Q(k_{2n})}f_{2n}'''(0)\,f_{2m}'(0)+\frac{\beta_1}{P(k_{2n})}f_{2n}(0)\,f_{2m}(0)-\delta_{mn}\left\langle f_{2n},f_{2m}\right\rangle\right]=0, \tag{3.28d}$$

For $m=0,I,II,1,2,...$ Using the edge conditions, the linear equations as in sections 3.1.1-3.1.3 for different edge conditions are truncated up to a finite number of M terms

in order to solve the system of $(4M+12)$ equations. The velocity potentials for each of the three regions as in Equation (3.17) consists of $(4M+12)$ unknown coefficients such as $R_n, T_n,\ n=0,1,2,...M, M+1, M+2,\ A_n, B_n, n=0, I, II, 1, 2, ..., M.$ On solving the system of the algebraic equation the full solution is obtained in terms of the potential functions with the reflection and transmission coefficients are obtained as

$$K_r = |R_0| \text{ and } K_t = \left| \frac{k_{30} \tanh k_{30} h}{k_{10} \tanh k_{10} h} T_0 \right|. \tag{3.29}$$

The reflection and transmission coefficients are observed to satisfy the energy balance relation $K_r^2 + K_t^2 = 1.$

3.3.2 Shallow water approximation

In the present section, the wave scattering due to the finite floating thick elastic plate with different support condition is analysed based on shallow water approximation. The geometry of the physical problem is considered the same as discussed in Section 2 but the wave motion is based on linearized long wave theory. Integrating the equation of continuity for fluids over the water depth, the relation between velocity potential and elevation for long waves is derived as

$$\zeta_{jt} = h\partial_x^2 \Phi_j \quad \text{for} \quad j = 1, 2, 3. \tag{3.30}$$

The long wave equation of motion in the fluid domain for $j = 1, 3$ is given by

$$\Phi_{jt} - g\zeta_j = 0, \text{ for } x > 0 \text{ and } x < -a. \tag{3.31}$$

Considering the wave elevation and deflection in the plate to be in simple harmonic in time with wave frequency ω, the velocity potential is expressed as, $\Phi_j(x,t) = \mathrm{Re}\{\phi_j(x)\} e^{-i\omega t}$ and the elastic plate deflection is expressed as $\zeta_j(x,t) = \mathrm{Re}\{\zeta_j(x)\} e^{-i\omega t}$, where Re denotes the real part. Combining the long-wave equation of continuity as in Equation (3.30) and the long-wave equation of motion in the fluid domain given by Equation (3.31), the linearized long-wave equation in the fluid domain is derived as

$$h\partial_x^2 \phi_j - \kappa \phi_j = 0, \text{ for } x > 0 \text{ and } x < -a. \tag{3.32}$$

The long wave equation of motion in the plate covered region is obtained by combining the equation of motion for fluid and the Timoshenko-Mindlin plate equation given by

$$h\left\{\frac{EI}{\left(\rho g-m_s\omega^2\right)}\partial_x^4+\left(\frac{m_s\omega^2 I}{\left(\rho g-m_s\omega^2\right)}-S\right)\partial_x^2+\left(1-\frac{m_s\omega^2 IS}{EI}\right)\right\}\partial_x^2\phi_2 + \frac{\rho\omega^2}{\left(\rho g-m_s\omega^2\right)}\left\{1-\frac{m_s\omega^2 IS}{EI}-S\partial_x^2\right\}\phi_2=0, \quad \text{for} \quad -a<x<0, \tag{3.33}$$

where ρ is the density of water, m_s is the mass of the plate, ν is the Poisson's ratio, $EI=Ed^3/12(1-\nu^2)$ is the flexural rigidity, E is Young's modulus, $G=E/2(1+\mu)$ is the shear modulus and μ is the transverse shear coefficient of the thick plate. The continuity of energy and mass flux at the interface $x=0,-a$ for $j=1,2$ is given by

$$\phi_{jx}\left(x\right)=\phi_{(j+1)x}\left(x\right) \text{ and } \phi_j\left(x\right)=\phi_{(j+1)}\left(x\right) \text{ at } x=-a \text{ and } x=0. \tag{3.34}$$

Further, the floating elastic plate is considered to satisfy the edge support conditions as described in section 3.2.1 for the case of shallow water depth. The far-field radiation condition in terms of velocity potential is given by

$$\phi_j\left(x\right)=\begin{cases}e^{-ik_{10}x}+R_0e^{ik_{10}x} & \text{as} \quad x\to\infty,\\ T_0e^{-ik_{30}x} & \text{as} \quad x\to-\infty,\end{cases} \tag{3.35}$$

where R_0 and T_0 are the complex co-efficient of reflection and transmission and k_{j0} at $j=1,3$ are the roots of dispersion relation in shallow water

$$k_{j0}^2-\left(\frac{\omega^2}{gh}\right)=0. \tag{3.36}$$

In order to analyse the wave scattering by a floating elastic plate based on shallow water approximation, the fluid domain is divided into three sub-domains as in Figure 1. The velocity potentials $\phi_j\left(x\right)$ for $j=1,2,3$ at the free surface and the plate covered regions are of the form

$$\phi_j\left(x\right)=\begin{cases}\left(I_0e^{-ik_{10}x}+R_0e^{ik_{10}x}\right) & \text{for} \quad x>0,\\ A_0e^{-ik_{20}x}+\overline{A}_0e^{ik_{20}x}\sum\limits_{n=I,II}^{IV}A_ne^{-ik_{2n}x} & \text{for} \quad -a<x<0,\\ T_0e^{-ik_{30}x} & \text{for} \quad x<-a,\end{cases} \tag{3.37}$$

where $R_0, T_0 A_n, n = 0, I, .., IV$ and $\bar{A}_0$ are the unknown constants to be determined with k_{jn} at $j = 2$ and $n = 0, I, II, III, IV$ are eigenvalues satisfy the dispersion relation

$$h\left[\frac{EI}{\left(\rho g - m_s\omega^2\right)}k_n^6 + \left(\frac{m_s\omega^2 I}{\left(\rho g - m_s\omega^2\right)} - S\right)k_n^4 + \left\{\left(1 - \frac{m_s\omega^2 IS}{EI}\right) - \frac{\rho\omega^2 S}{h\left(\rho g - m_s\omega^2\right)}\right\}k_n^2\right]$$
$$- \frac{\rho\omega^2}{\left(\rho g - m_s\omega^2\right)}\left\{1 - \frac{m_s\omega^2 IS}{EI}\right\} = 0, \quad \text{for} \quad -a < x < 0. \tag{3.38}$$

On the application of the continuity equations as in Equation (3.35) and edge boundary conditions as in section 3 for the case of shallow water depth, a system of eight linear algebraic equations are obtained having the unknown constants R_0, T_0 $A_n, n = 0, I, .., IV$. The unknown constants associated with the amplitude of the waves are determined by solving the system of algebraic equations. Once the unknowns R_0 and T_0 are obtained, the reflection and transmission coefficient is derived from the relation

$$K_r = |R_0| \quad \text{and} \quad K_t = \left|\left(\frac{k_{30}^2}{k_{10}^2}\right)T_0\right|. \tag{3.39}$$

The reflection and transmission coefficients obtained for the shallow water approximation satisfy the energy balance relation $K_r^2 + K_t^2 = 1$.

3.4 NUMERICAL RESULTS AND DISCUSSIONS

The hydroelastic behaviour of the floating elastic plate under the action of the incident wave is analysed based on Timoshenko-Mindlin theory in finite and shallow water depth. The study is performed to analyze the reflection coefficient K_r, transmission coefficient K_t, plate deflection ζ_j, bending moment $M(x)$, shear force $W(x)$ and strain on the plate ε for different support conditions. Three different cases of edge support condition i.e. free-free edge, simply supported edge and fixed edge conditions are considered and compared in the present study. The numerical computations are carried out for different water depth h/L and plate thickness d/L considering Young's Modulus $E = 5\text{GPa}$, $\rho_p / \rho_w = 0.9$, $\nu = 0.3$ and $g = 9.8\text{ms}^{-2}$. The numerical

parameters such as plate length $L = 100\text{m}$ and non-dimensional wave number $k_{10}h = 5$ for finite water depth and $k_{10}h = 10$ for shallow water depth are considered to be fixed unless otherwise mentioned. The accuracy of the computed numerical results are checked with the energy relation which satisfies the energy balance relation $K_r^2 + K_t^2 = 1.$

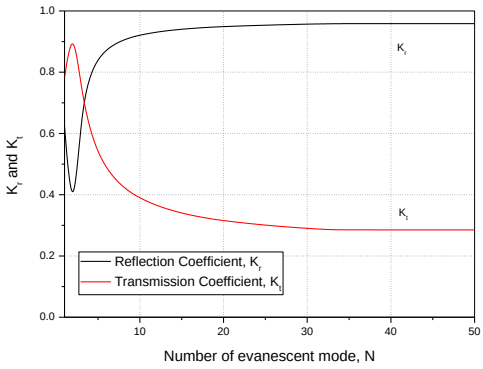

Figure 3.4(a): Convergence of the reflection and transmission coefficients for the number of evanescent modes, N.

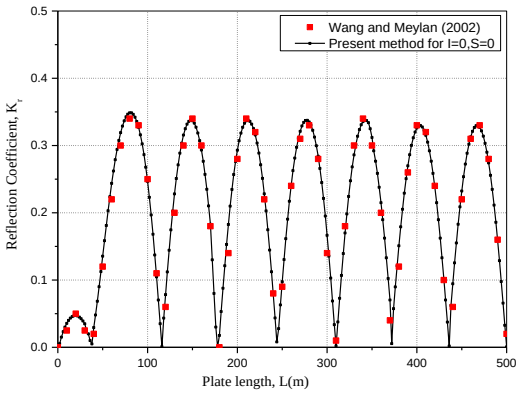

Figure 3.4(b): Validation of reflection coefficient along the plate length considering rotary inertia $I = 0$ and shear deformation $S = 0$ with Wang and Meylan (2002).

The convergence of K_r and K_t for an increasing number of the evanescent modes are presented in Figure 3.4(a). The convergence of K_r and K_t is observed for an evanescent wave mode of $N \geq 35$. In Figure 3.4(b), the numerical result is presented considering negligible rotary inertia and shear deformation and is validated with Wang and Meylan (2002) keeping the parameters the same as in the literature. The plate equation as in Equation (3.7) for negligible rotary inertia and shear deformation results

in the Euler-Bernoulli equation. The numerical results obtained in Figure 3.4(b) is observed to agree well with Wang and Meylan (2002).

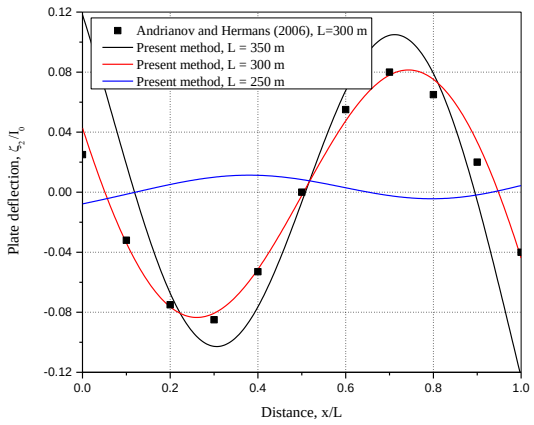

Figure 3.4(c): Comparison of plate deflection with (Andrianov and Hermans, 2006a) along the plate length plotted considering rotary inertia $I = 0$ and shear deformation $S = 0$.

The plate deflection versus the non-dimensional plate length is validated with the results obtained by (Andrianov and Hermans, 2006a) as shown in Figure 3.4(c) considering the plate length $L = 300m$, plate thickness $d = 2m$ and wavelength, $\lambda = 60m$. The analysis of floating elastic plate is based on Kirchhoff thin plate theory by (Andrianov and Hermans, 2006a), and the present method is based on Timoshenko–Mindlin theory with negligible rotary inertia and transverse shear deformation in finite water depth. The results obtained using both the methods are observed to agree well considering the plate length $L = 300m$. In the case of rigid body analysis, the plate deflection is not significant as compared to hydroelastic analysis of floating plate. But, in this case it is observed that, the increase in the plate length increases the deflection suggesting the importance of hydroelstic behaviour for larger plate lengths.

3.4.1 Finite water depth

In this section, the wave scattering due to floating thick elastic plate in finite water depth is analysed considering different edge support conditions. The hydroelastic behaviour of the floating plate is studied by analysing the reflection and transmission coefficients, surface deflection, strain in the elastic plate, bending moment and shear force of the plate.

3.4.1.1 Reflection and Transmission Coefficient

The wave reflection and transmission coefficient for the floating elastic plate in relation (3.29) is having the wave number in the incident and transmitted region the same. So, the reflection and transmission coefficient reduces to

$$K_r = |R_0| \quad \text{and} \quad K_t = |T_0|. \tag{3.40}$$

In Fig. 3.5(a,b), the K_t is plotted versus $k_{10}h$ for varying non-dimensional plate thickness d/L and non-dimensional water depth h/L. The transmission coefficient K_t is almost unity for lesser values of $k_{10}h$. The transmission coefficient equals to unity signifies the complete transmission of waves due to the resonance phenomena. It may be noted that for the least value of $k_{10}h$, the wavelength for the incident wave and wave period is high. This shows that in the case of large wavelength and wave period all the waves gets transmitted below the plate. In Fig. 3.5(a), the unity in the values of K_t is also observed for certain values of $k_{10}h$ and with the surge in the plate thickness d/L a reduction in the unity for K_t is observed due to increase in plate rigidity. The observed bumps for the case of low plate thickness might be due to the plate excitation for higher frequency. The forward shift in the K_t within $0.1 < k_{10}h < 10$ for lower values of $k_{10}h$ is due to higher values of wavelengths. The surge in the plate thickness d/L has caused the unity in the transmission coefficient to take place for higher values of wavelength.

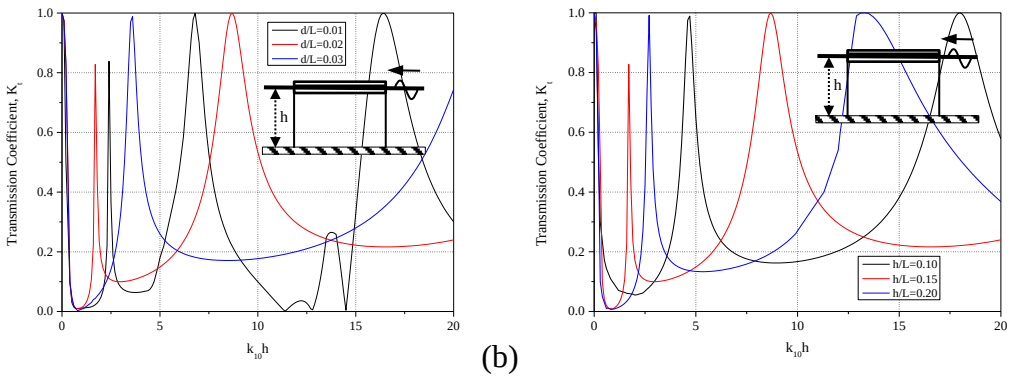

(a) (b)

Figure 3.5: Transmission coefficient versus non-dimensional wavenumber for different values of (a) plate thickness d/L at $h/L = 0.15$, (b) water depth h/L at $d/L = 0.02$.

Further, Fig. 3.5(b) demonstrate that with the surge in the values of h/L, the unity in the values of K_t increases and is observed to shift towards higher values of $k_{10}h$. The

study reveals that, with the surge in the water depth, majority of waves gets transmitted for smaller wavelengths at certain values of $k_{10}h$. An opposite pattern in the wave reflection is witnessed and found to follow the energy balance relation $K_r^2 + K_t^2 = 1$.

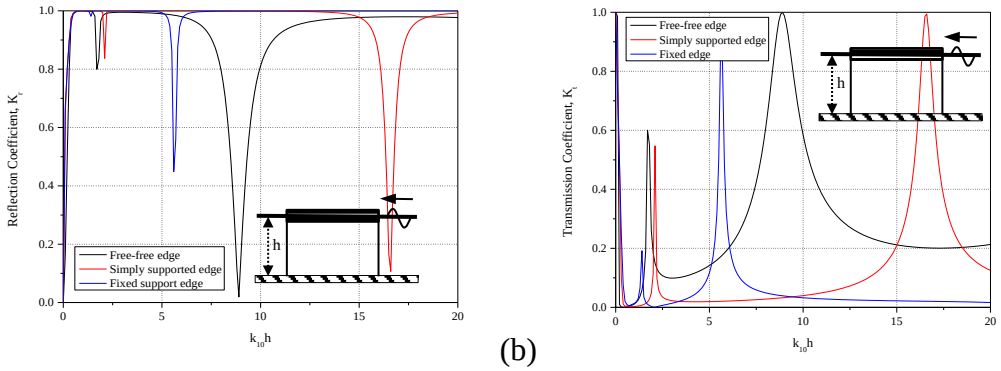

(a) (b)

Figure 3.6: (a) Reflection and (b) transmission coefficient versus non-dimensional wavenumber $k_{10}h$ for different support conditions in finite water depth at $d/L = 0.02$ and $h/L = 0.15$.

In Figure 3.6(a,b), the reflection and transmission coefficients are plotted versus non-dimensional wavenumber $k_{10}h$ for different support condition considering $d/L = 0.02$ and $h/L = 0.15$. The zeros in the reflection coefficient at certain values of $k_{10}h$ indicate the complete transmission of waves and may be termed as local minima. Initially for $0 < k_{10}h < 0.1$, the wave reflection is minimum and the wave transmission is maximum for all the support conditions. The fixed edge support shows higher wave reflection for as compared to the free-free edge and simply supported edge condition. The wave reflection coefficient approaches to one with the increase in $k_{10}h$ which suggests that for the wave with smaller wavelength, the wave reflection is higher. The forward shift in the zeros in the wave reflection and transmission coefficient is noted for different support conditions. The transmission coefficient approaching one indicates complete wave transmission for that particular $k_{10}h$. In the case of simply supported edge condition the zeros in reflection coefficient or full-wave transmission are observed for $5 < k_{10}h < 5.5$ and $16 < k_{10}h < 17$, whereas in the case of free-free edge condition, the full-wave transmission is observed for $8 < k_{10}h < 9$. The study shows that the optimum values of reflection and transmission are higher for simply supported edge condition.

3.4.1.2 Plate deflection and wave-induced strain

The plate deflection and wave-induced strain in the floating elastic plate are given by the relation

$$\zeta_j = \frac{i}{\omega}\phi_{jy} \quad \text{on} \quad y = 0, \quad j = 2. \tag{3.41}$$

$$\varepsilon = \frac{d}{2}\partial_x^2\zeta_2 = \frac{id}{2\omega}\partial_{x^2y}^3\phi_2 \quad \text{at} \quad y = 0. \tag{3.42}$$

In Figure 3.7(a), the surface deflection along the length of the plate for different support conditions are presented. The plate deflection is found to be least for simply supported edge and highest for free-free edge support condition. The lower value to plate deflection for simply support edge condition and fixed edge condition as compared to free-free edge condition is due to the effect of restraints at the edge. Further at the incident edge, $x/L = 0$, the plate deflection is observed to be zero for the case of simply supported and fixed edge condition whereas, the plate deflection is zero at the centre of plate for the case of free-free edge condition.

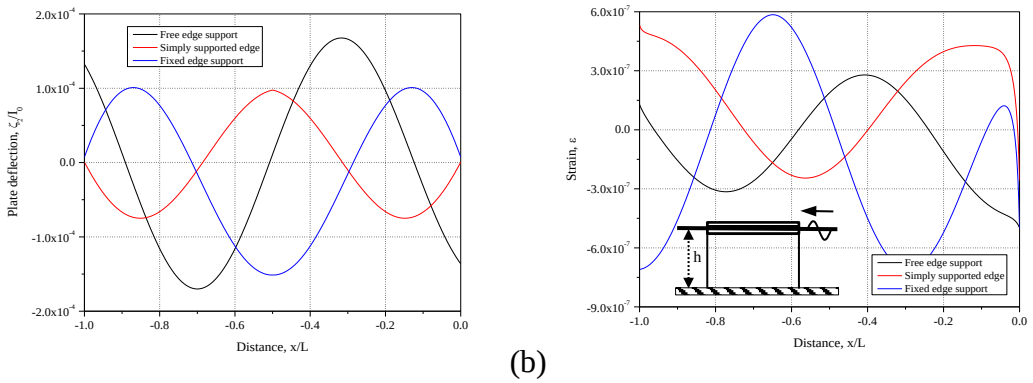

(a) (b)

Figure 3.7: (a) Plate deflection and (b) wave-induced strain along the plate length x/L for different edge support conditions in finite water depth at $k_{10}h = 5$, $d/L = 0.02$ and $h/L = 0.15$.

On the other hand, in Figure 3.7(b), the strain induced in the floating elastic plate due to the action of ocean waves are analyzed for different support conditions. The wave-induced strain is found to be least for simply supported edge and highest for fixed edge support condition. The strain along the floating elastic plate is higher for the free-free-edge condition at the incident edge $x/L = 0$, whereas the strain in the transmitted edge $x/L = -1$, is higher for fixed edge condition. Further, for the case of fixed edge support,

it is observed that the wave-induced strain is reduced at the centre of the floating elastic plate due to higher rigidity at the edges of the structure.

3.4.1.3 Bending moment and shear force

The bending moment and shear force of the floating elastic plate due to the interaction of wave are given by the relation

$$M(x) = EI\partial_y^3\phi_2 \quad \text{on} \quad y = 0. \tag{3.43}$$

$$W(x) = EI\left\{\partial_{xy^3}^4\phi_2 - \wp\partial_{xy}^2\phi_2\right\} \quad \text{on} \quad y = 0. \tag{3.44}$$

In Figure 3.8(a), the bending moment resultants due to the wave interaction with the floating elastic plate are plotted along the plate length for different support conditions. The bending moment resultant is observed to be least for the floating structure with a simply supported edge and highest for free-free edge support condition. On the other hand, the bending moment is observed to increase at the centre of the structure for the case of free-free edge support which may be due to the change in the phase of the incident, reflected and transmitted waves propagating below the floating elastic plate.

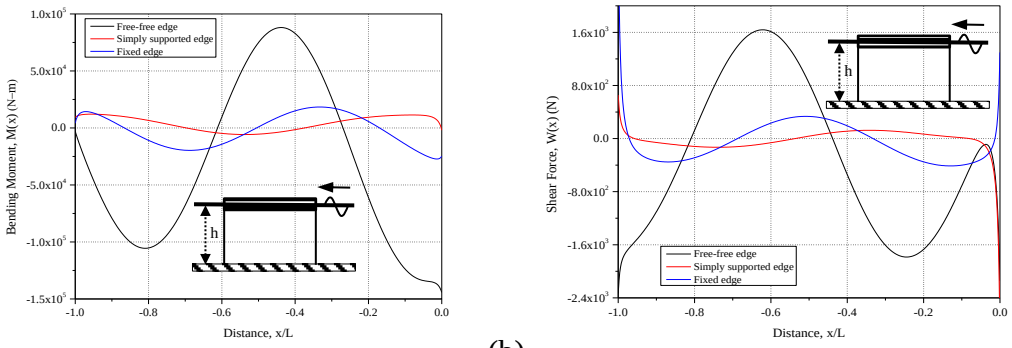

(a) (b)

Figure 3.8: (a) Bending moment and (b) shear force resultants along the plate length x/L for different edge support conditions in finite water depth at $k_{10}h = 5$, $d/L = 0.02$ and $h/L = 0.15$.

The shear force resultants (Figure 3.8b) due to the wave interaction with the floating elastic plate are plotted along the plate length for different support conditions. The shear force resultant is observed to be least for floating structure with a simply supported edge and highest for free-free edge support condition as observed similar in the case of bending moment along the plate length. The shear force and bending moment for the simply supported edge and fixed edge condition is minimum at the incident edge

$x/L=0$ and at the transmitted edge $x/L=-1$. Further, at the centre of the plate the shear force is higher for the free-free edge condition as compared to simply supported and fixed edge condition.

3.4.2 Comparative study based on plate theories

The comparison of the thin and thick elastic plate based on Timoshenko-Mindlin plate theory and Kirchhoff's plate theory for the simply supported edge condition and fixed edge condition is presented. The detailed comparison of the thin and thick plate is performed on analysing hydroelastic characteristics of the floating elastic plate.

3.4.2.1 Simply supported edge condition

The wave reflection and transmission coefficients (Figure 3.9a, b) based on Kirchhoff's plate theory are compared with Timoshenko-Mindlin plate theory varying non-dimensional wave number in the case of simply supported edge condition. The values K_r and K_t for both the plate theories are the same for $0<k_{10}h<2.5$, but with the increase in the non-dimensional wave number the deviation in the K_r and K_t are noted. The wave transmission is observed more for thin plate theory for higher values of non-dimensional wave number. This suggests that for lower wavelength the wave transmission is more in the case of thin plate theory. Timoshenko Mindlin plate theory shows higher resistance to wave transformation, whereas the complete transmission peaks are observed to be similar for both the theories. The comparison using both plate theories suggests that the presence of rotary inertia and shear deformation is significant in the wave transformation and hydroelastic behaviour of the floating elastic plate.

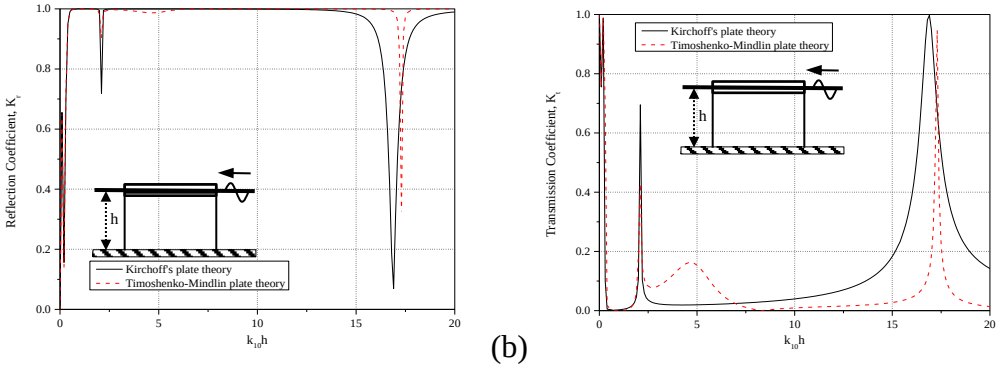

(a) (b)

Figure 3.9: (a) Reflection and (b) transmission coefficient versus non-dimensional wavenumber $k_{10}h$ are plotted considering $E=5\text{GPa}$ and $h/L=0.15,\ d/L=0.02$.

In Figure 3.10(a-d), the plate deflection, wave-induced strain, bending moment and shear force of a floating elastic plate are compared based on Timoshenko-Mindlin's plate theory and Kirchhoff's plate theory for the simply supported edge condition. The variation it the plate deflection (Figure 3.10a) using both the plate theory is minimal but the deflection is higher at the plate centre and at the incident edge $x/L=0$ of the plate. A significant variation in the strain in the floating elastic plate (Figure 3.10b) using both Kirchhoff's plate theory and Timoshenko-Mindlin plate theory is noted. The strain in the floating elastic plate is higher for the Timoshenko-Mindlin plate theory. The bending moment and shear force (Figure 3.10c,d) are higher for Kirchhoff's plate theory as compared to Timoshenko-Mindlin plate theory. Thus, the study shows that due to the presence of rotary inertia and shear deformation, a significant reduction in bending moment and shear force with a slight reduction in plate deflection and increase in wave-induced strain is obtained as compared to Kirchhoff's thin plate theory.

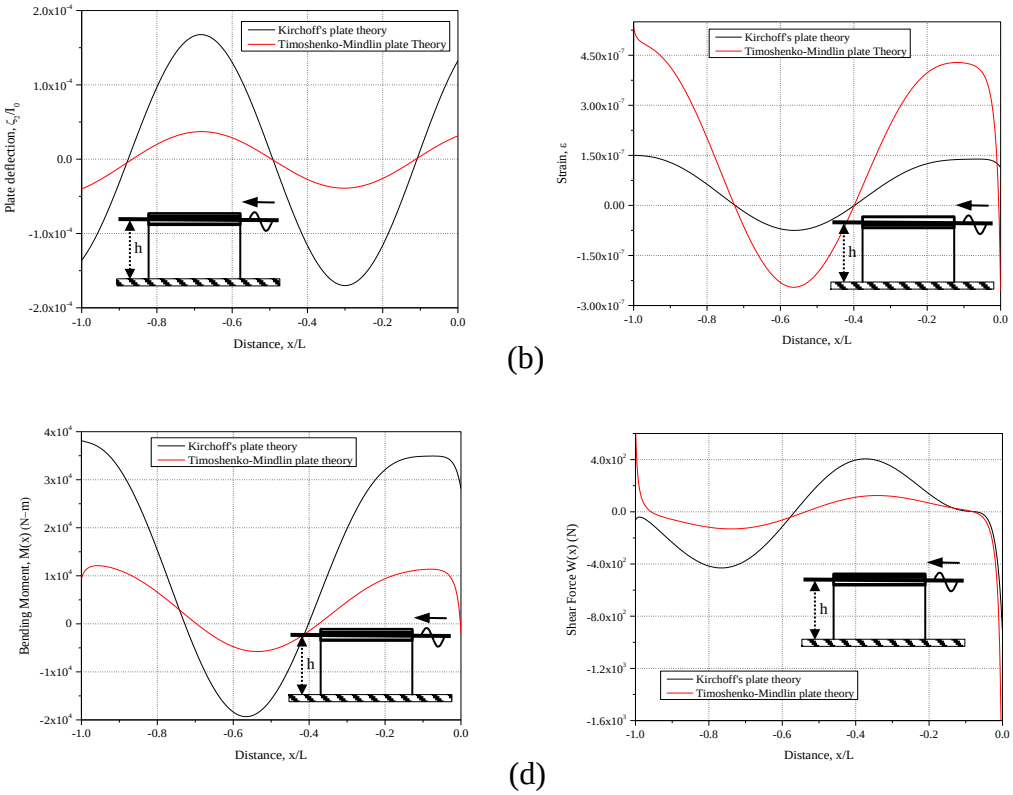

Figure 3.10: (a) Plate deflection, (b) wave-induced strain, (c) bending moment and (d) shear force along the plate length plotted considering $k_{10}h=5$, $E=5\text{GPa}$ and $h/L=0.15$, $d/L=0.02$.

3.4.2.2 Fixed edge support condition

The wave reflection and transmission coefficients based on Kirchhoff's thin plate theory is compared with Timoshenko Mindlin plate theory versus non-dimensional wave number for the fixe edge condition in Figure 3.11(a,b). The variation in the K_r and K_t is significant for $2.5 < k_{10}h < 7.5$ and with the increase in the non-dimensional wave number the variation is minimal. The wave reflection and transmission characteristics using Timoshenko Mindlin plate theory are higher whereas the complete transmission of waves is observed to be same within $5 < k_{10}h < 5.5$ for both the plate theories. The variation of K_r and K_t using both the theories suggests that the presence of rotary inertia and shear deformation plays a significant role in the wave transformation and hydroelastic behaviour of fixed edge supported elastic plate.

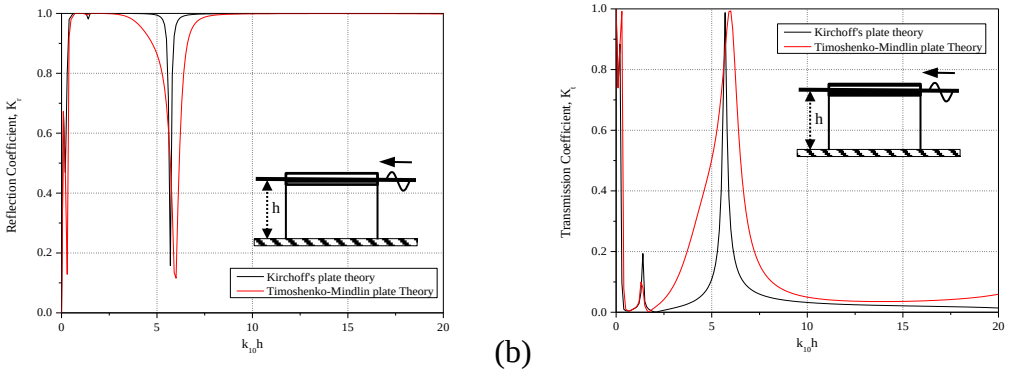

(a) (b)

Figure 3.11: (a) Reflection and (b) transmission coefficient versus non-dimensional wavenumber $k_{10}h$ are plotted considering $E = 5\text{GPa}$ and $h/L = 0.15,\ d/L = 0.02$.

The hydroelastic behaviour in terms of plate deflection, wave-induced strain, bending moment and shear force of a floating elastic plate with fixed edge support are compared based on Timoshenko-Mindlin plate theory and Kirchhoff's plate theory in Figure 3.12(a-d). The variation in plate deflection (Figure 3.12a) is significant as compared using both Timoshenko-Mindlin plate theory and Kirchhoff's plate theory. The plate deflection near to the incident edge $x/L = 0$ is higher for the Kirchhoff's plate theory whereas at the central plate section the plate deflection using Timoshenko-Mindlin plate theory is slightly more as compared to Kirchhoff's plate theory. The strain (Figure 3.12b) in the floating elastic plate is higher for Timoshenko-Mindlin plate theory and the reduction in the bending moment and shear force (Figure 3.12c,d) is observed for

Timoshenko-Mindlin plate theory. Thus, the presence of rotary inertia and shear deformation shows reduction in plate deflection, wave-induced strain, bending moment and shear force at the incident edge of the floating plate, whereas an increase in hydroelastic behaviour is observed at the transmitted edge.

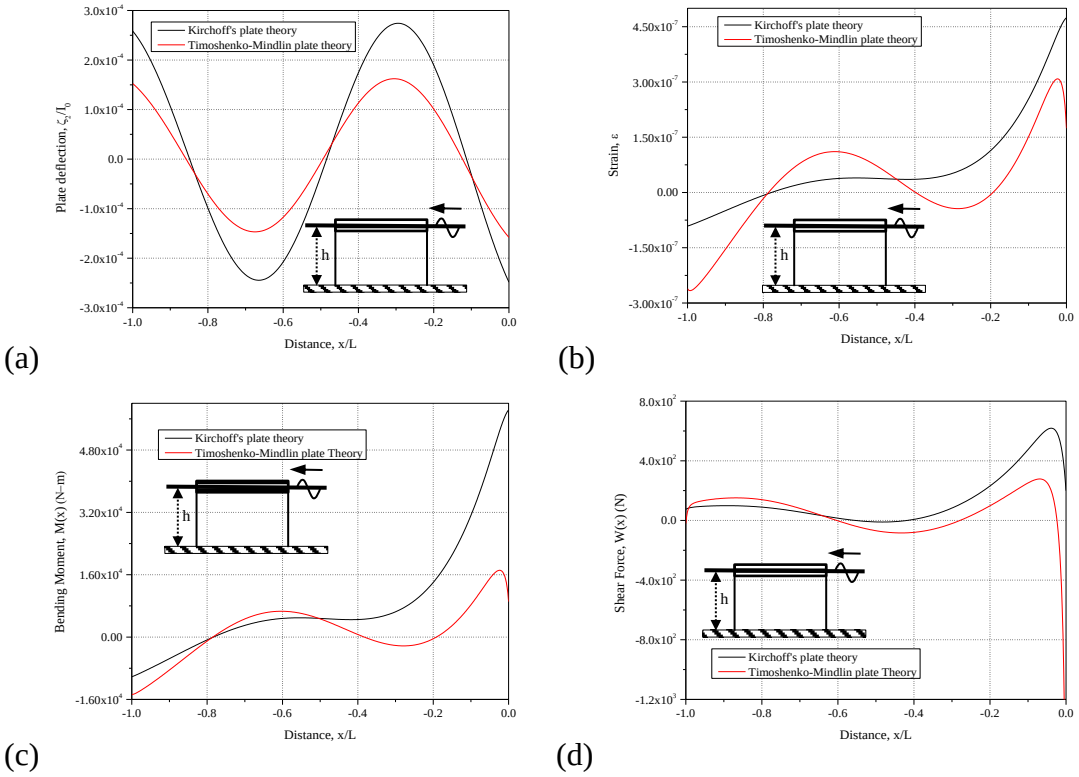

Figure 3.12: (a) Plate deflection, (b) wave-induced strain, (c) bending moment and (d) shear force along the plate length plotted considering $k_{10}h = 5$, $E = 5\text{GPa}$ and $h/L = 0.15$, $d/L = 0.02$.

3.4.3 Shallow water approximation

In this section, the wave interaction with a floating elastic plate is analyzed based on shallow water approximation. The hydroelastic behaviour of the floating elastic plate in shallow water depth analyzed and compared with the different cases of edge support conditions.

3.4.3.1 Reflection and transmission coefficient

The reflection and transmission coefficients for the floating elastic plate based on shallow water approximation are same as described in Equation (3.40). In Figure 3.13(a,b), the reflection and transmission coefficients versus the non-dimensional wave

number are plotted for different cases of edge support conditions. It is observed that the zeros in the wave reflection is least for free-free edge support condition and higher for fixed edge support condition. At very low values of non-dimensional wave number, the variation in reflection and transmission coefficient is observed to be more as compared to higher values of $k_{10}h$. Further, the higher transmission of waves is observed at very low frequencies for free-free edge support condition due to zero restraints at the edges. The simply supported edge is observed to transmit a higher number of waves as compared to fixed support edge but lesser than free-free support condition due to the constraint in deflection at the edges.

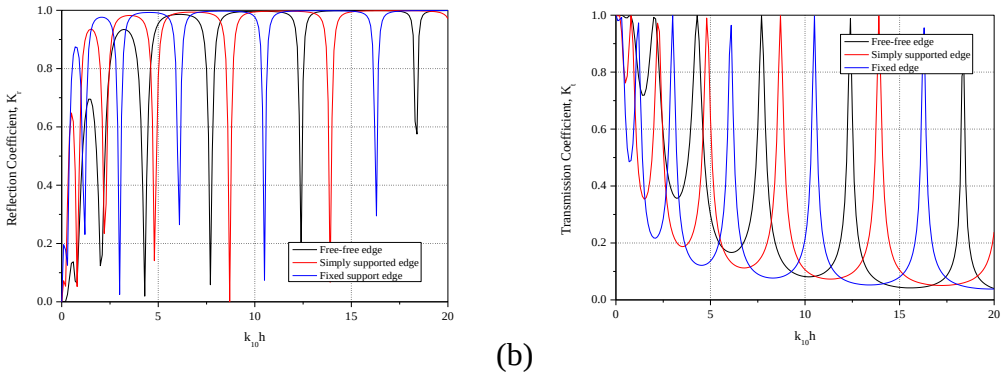

(a) (b)

Figure 3.13: Wave (a) reflection and (b) transmission coefficient versus non-dimensional wavenumber $k_{10}h$ for different support conditions in shallow water depth at $h/L = 0.10$ and $d/L = 0.02$.

3.4.3.2 Plate deflection and wave-induced strain

The plate deflection and wave-induced strain of the elastic plate in shallow water depth are given by the relation

$$\zeta_j = \frac{ih}{\omega}\partial_x^2\phi_j \quad \text{for } j = 2. \tag{3.45}$$

$$\varepsilon = \frac{d}{2}\partial_x^2\zeta_2 = \frac{idh}{2\omega}\partial_x^4\phi_2. \tag{3.46}$$

The plate deflection along the length of the plate at different edge support conditions are presented in Figure 3.14(a). The plate deflection is observed to be zero at the edges of the plate for the case of simply supported and fixed edge support conditions, which is due to restraints at the edges. The plate deflection is observed to be higher at the edges of the plate for free-free edge boundary condition due to zero restraints at the edges. Due to the zero deflection at the plate edge for the simply supported edge and fixed

edge condition, the deflection is observed to be lesser for simply supported edge and fixed edge condition as compared to free-free edge support. In Figure 3.14(b), the strain induced in the plate due to the action of ocean waves is plotted for different support edge conditions. It is observed that the wave-induced strain is highest at the plate edges for fixed edge support condition and zero for the cases of free-free edge and simply supported edge condition which is mainly due to restraints in the plate for the corresponding edge conditions. A lower strain is observed for the free-free edge and simply supported edge due to the non-zero slope condition. An increase in wave-induced strain is observed at the centre of the structure for the case of fixed edge condition due to zero slope condition.

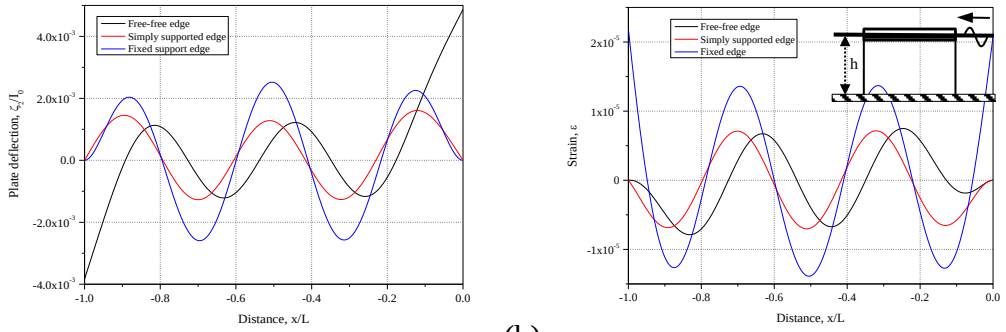

(a) (b)

Figure 3.14: Plate deflection and strain along the plate length x/L for different support conditions in shallow water depth at $k_{10}h=10,\ h/L=0.10$ and $d/L=0.02$.

3.4.3.3 Bending moment and shear force

The bending moment and shear force of the floating elastic plates is given by

$$M(x)=EI\partial_x^4\phi_2. \tag{3.47}$$

$$W(x)=EI\left\{\partial_x^5\phi_2-\wp\partial_x^3\phi_2\right\}. \tag{3.48}$$

In Figure 3.15(a), the bending moment on the plate due to incident waves is plotted along the length of the plate for different edge support conditions. At the edges of the plate, the bending moment is observed to be zero for the case of a free-free edge and simply supported edge due to zero moment condition. On the other hand, a maximum bending moment is observed at the edges and at the centre of the structure due to the edge restraints in the case of fixed edge support condition. The shear force on the plate due to incident waves is plotted along the length of the plate in Figure 3.15(b) for different edge support conditions. At the plate edges, zero shear force is observed for

the case of a free-free edge condition but for the case of fixed edge support, a maximum shear force is observed at the edges and zero at the centre of the structure due to edge constraints.

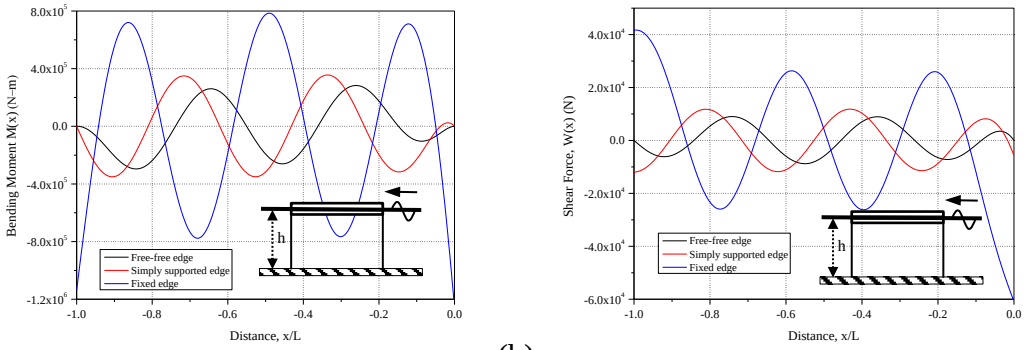

(a) (b)

Figure 3.15: (a) Bending moment and (b) shear force resultants along the plate length x/L for different support conditions in shallow water depth at $k_{10}h=10,\ h/L=0.10$ and $d/L=0.02$.

3.4.4 Comparative study based on Kirchhoff's and Timoshenko-Mindlin theory

The hydroelastic behaviour of the finite floating plate is compared and analysed based on both Timoshenko-Mindlin's plate theory and Kirchhoff's plate theory in finite water depth. The wave reflection and transmission coefficients, plate deflection and wave-induced strain along with bending moment and shear force along the plate are presented and compared.

3.4.4.1 Reflection and transmission coefficient

In Figure 3.16(a,b), the reflection and transmission coefficient based on Kirchhoff's plate theory and Timoshenko-Mindlin plate theory is analyzed. The deviation in the K_r and K_t is observed at $0.01<k_{10}h<6.0$ but at high values of $k_{10}h$ the K_r and K_t are almost same for both the plate theories. The variation of K_r and K_t within $0.01<k_{10}h<6.0$ suggests a significant variation in the values of K_r and K_t for the waves with higher wavelength. The variation in the K_r and K_t for $0.01<k_{10}h<6.0$ in the presence of rotary inertia and shear deformation shows a substantial effect on the hydroelastic characteristics of the floating elastic plate acted upon by ocean waves. The wave reflection tends towards unity for $k_{10}h>4.0$ which suggest that additional waves get reflected for waves of shorter wavelength. It is observed that the reflected waves are

higher for a thick plate theory up to certain wavenumber and it reduces thereafter, signifying the effect of variation in wavenumber. The comparative study based on Timoshenko-Mindlin plate theory and Kirchhoff's plate theory illustrates the importance of rotary inertia and shear deformation in the hydroelastic analysis of the floating structures.

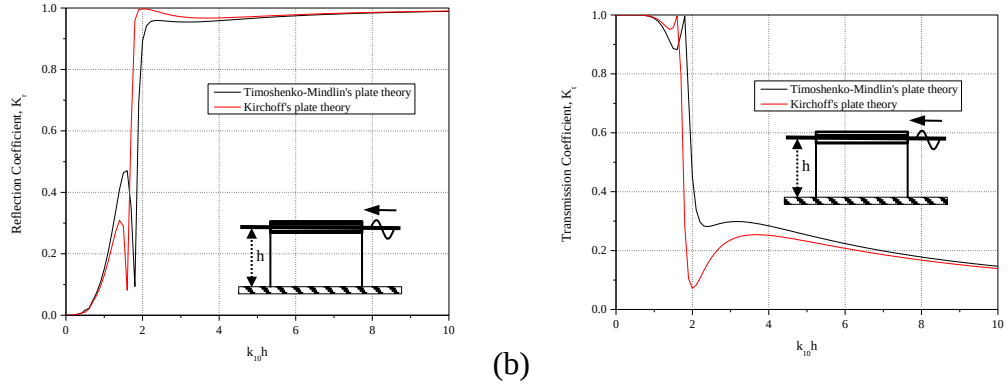

(a) (b)

Figure 3.16: (a) Reflection and (b) transmission coefficients versus non-dimensional wavenumber $k_{10}h$ considering $d/L=0.25$ and $h/L=1.0$.

3.4.4.2 Surface deflection and wave-induced strain

In Figure 3.17(a,b), the normalized deflection and wave-induced strain along the length of the plate for Timoshenko-Mindlin and Kirchhoff's plate theory are compared. In order to analyze the hydroelastic analysis for shorter wavelength, the deflection and wave-induced strain along the plate length is compared for high values of $k_{10}h$. The plate deflection is observed to reduce for the case of Timoshenko-Mindlin plate theory as compared with the Kirchhoff's plate theory.

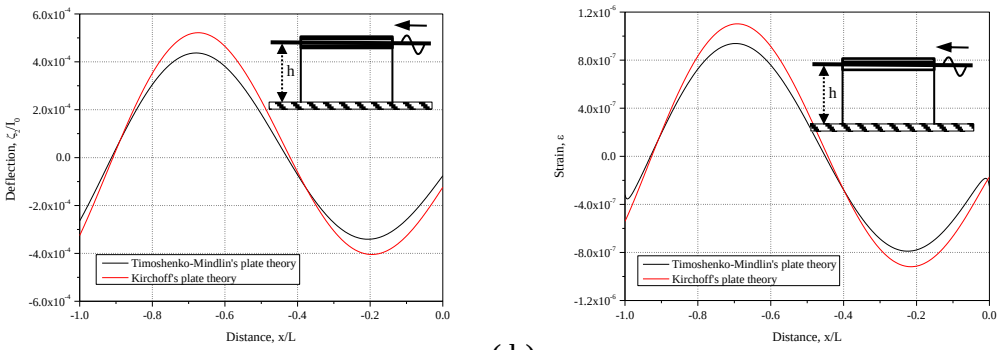

(a) (b)

Figure 3.17: (a) Plate deflection (b) wave-induced strain along the plate length for Timoshenko-Mindlin's and Kirchhoff's plate theory considering $E=5GPa$, $k_{10}h=20$, $d/L=0.05$ and $h/L=0.20$.

The variation in the deflection using both the theories is around 15%. The normalized plate deflection is within $6.0\times10^{-4} < \zeta_2(x)/I_0 < -4.0\times10^{-4}$ and the plate deflection at the plate edges is reduced for Timoshenko-Mindlin plate theory as compared with the Kirchhoff's plate theory. The reduction is due to the consideration of rotary inertia and shear deformation in the analysis. Further, Figure 3.17(b) compares the strain-induced along the length of the plate considering Timoshenko-Mindlin and Kirchhoff's plate theory. The wave-induced strain in the floating plate is reduced by around 16% for Timoshenko-Mindlin plate theory. The strain in the elastic plate is within $-8\times10^{-7} < \varepsilon < 1.2\times10^{-6}$ but the absence of rotary inertia and shear deformation shows an increase in the strain for Kirchhoff's plate theory. Thus, the variation in the deflection and strain is observed for waves of shorter wavelength.

3.4.4.3 Bending moment and shear force

In Figure 3.18(a,b), the non-dimensional bending moment $M(x)$ and shear force $W(x)$ and along the non-dimensional plate length are studied considering Timoshenko-Mindlin and Kirchhoff's plate theory. The bending moment (Figure 3.18a) is observed high for Timoshenko-Mindlin plate theory as compared to Kirchhoff's plate theory. The bending moment based on Timoshenko-Mindlin plate theory is within $-4.0\times10^5 < M(x) < 4.0\times10^5$ but for Kirchhoff's plate theory the bending moment lies within $-2\times10^5 < M(x) < 2\times10^5$. The presence of rotary inertia and transverse shear deformation shows an increase in $M(x)$ for Timoshenko-Mindlin plate theory.

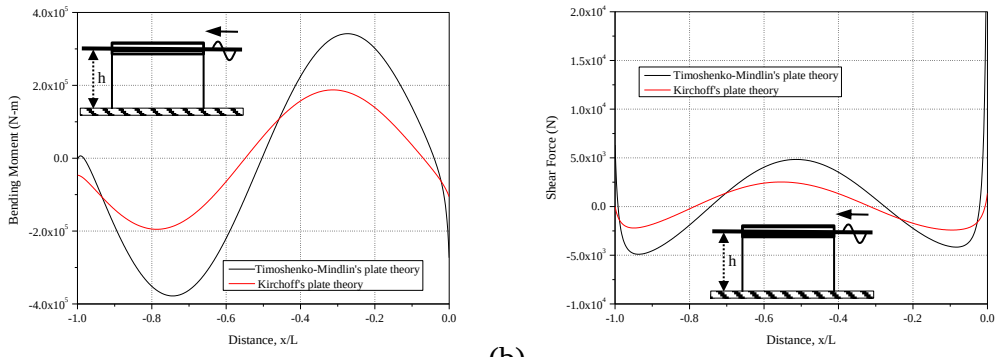

(a) (b)

Figure 3.18: (a) Bending moment and (b) shear force along the plate length for Timoshenko-Mindlin and Kirchhoff's plate theory considering $E = 5GPa$, $k_{10}h = 20$, $d/L = 0.05$ and $h/L = 0.20$.

Further, the increase in the shear force (Figure 3.18b) for Timoshenko-Mindlin plate theory is also noted on comparing with Kirchhoff's plate theory. The increase in the shear force for Timoshenko-Mindlin plate theory is around 40%. The shear force lies within $-5.0\times10^{3} < W(x) < 5.0\times10^{3}$ for Kirchhoff's plate theory. The rotary inertia and transverse shear deformation in Timoshenko-Mindlin plate theory show an increase in the shear force to be within $-2.5\times10^{3} < W(x) < 2.5\times10^{3}$. Hence, the consideration of rotary inertia and transverse shear deformation is observed to show a substantial effect on the variation of bending moment and shear force along the floating elastic plates.

3.4.3 Comparative study for finite and shallow water depth

In Figure 3.19(a,b), the reflection and transmission coefficient K_r and K_t versus non-dimensional wavenumber for the case of finite water depth is compared for shallow water approximations. The numerical computation is carried out considering non-dimensional water depth $h/L = 0.1$ for different values of non-dimensional d/L.

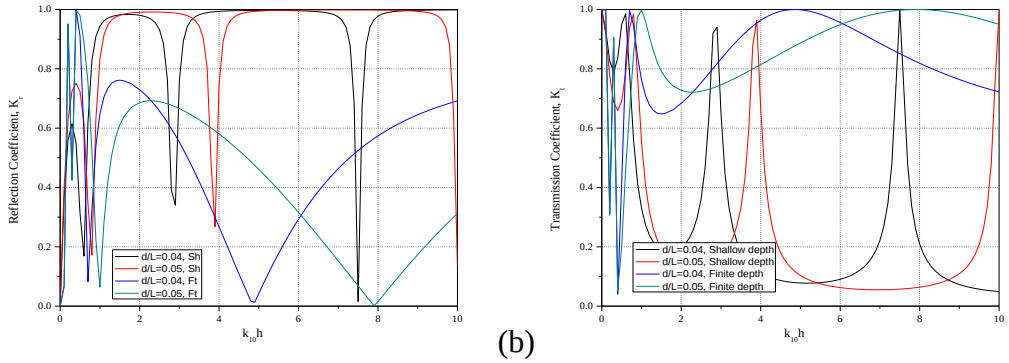

(a) (b)

Figure 3.19: Comparison of (a) reflection and (b) transmission coefficient versus non-dimensional wavenumber for finite water depth and shallow water approximations varying d/L.

The K_r and K_t at finite water depth shows varying behaviour as compared to shallow water approximations. At low non-dimensional wavenumber $0.01 < k_{10}h < 1.0$, similar patterns in the K_r and K_t are observed for finite and shallow water depths. However, at higher non-dimensional wavenumber $k_{10}h$, a higher variation in the K_r and K_t is observed at both the water depths. The variation in K_r and K_t is mainly due to the consideration of evanescent wave modes in the finite water depth. The surge in plate thickness shows a reduction in the completely transmitted waves at both the water

depths. In the case of shallow water approximations, the surge in plate thickness shows a slight increase in reflected waves at lower non-dimensional wavenumber $0.01 < k_{10}h < 1.0,$ and decreases at higher non-dimensional wavenumber. Further, the surge in plate thickness shows a reduction in reflected waves at all the wavenumber for finite water depth due to the surge in the rigidity of the plate as the values of d / L are increased.

3.5 CONCLUSIONS

The influence of edge support conditions on the hydroelastic behaviour of floating elastic plate based on Timoshenko-Mindlin plate theory is analyzed. The study of normally incident wave on floating elastic plate is performed for finite and shallow water depths. The numerical study is performed based on the eigenfunction expansion method. The wave reflection and transmission coefficients are computed and observed to satisfy the energy balance relation for both the cases of water depths. The hydroelastic characteristics of floating elastic plate are compared for different support conditions. In addition, a brief comparison of the numerical results for simply supported edge condition and fixed edge condition for both Kirchhoff's plate theory and Timoshenko-Mindlin plate theory is discussed in detail. The results demonstrating the effects of wave directionality on the application of the present model will be presented in future work. The following conclusions drawn from the present study are as follows:

- The high variations in reflection and transmission behavior are observed for higher values of non-dimensional wave numbers for different support conditions in the case of finite and shallow water depth.
- The free-free edge support condition shows higher transmission of waves whereas, lower wave transmission for fixed edge support is observed at finite and shallow water depth.
- The hydroelastic behavior is found to be higher for free-free edge support conditions and least for fixed edge due to restraints from the boundary conditions in the case of finite water depth. On the other hand, the bending moment and shear force resultants are found to be highest for fixed edge support and least for simply supported edge condition in the case of shallow water depth.

- The bending moment is observed to increase at the centre of the structure for the case of free-free edge support at finite water depth which may be due to the change in the phase of the incoming and outgoing wave propagating below the floating elastic plate.
- The comparison of the floating elastic plate for different edge conditions using both Kirchhoff's plate theory and Timoshenko-Mindlin plate theory suggests that the presence of rotary inertia and shear deformation is significant in the hydroelastic behaviour of the floating elastic plate.
- At shallow water depth, the plate deflection is observed to be zero for the case of simply supported and fixed edge support conditions. Further, wave-induced strain is found to be zero for the free-free edge and simply supported edge condition.
- The bending moment and shear force resultants are zero for free-free edge and simply supported edge due to the restraints at the edges in shallow water depth.

CHAPTER 4

WAVE SCATTERING DUE TO ARTICULATED FLOATING ELASTIC PLATE

4.1 GENERAL INTRODUCTION

In the previous chapter, the hydroelastic analysis of large floating elastic plate is studied based on Timoshenko-Mindlin's plate theory in finite water depth and shallow water approximations. The significance and importance of rotary inertia and shear deformation in the hydroelastic analysis of VLFS are presented. Further, the influence of support conditions on the hydroelastic behaviour of floating thick elastic plate is also presented.

In this chapter, the wave interaction with articulated floating elastic plate is analyzed based on Timoshenko-Mindlin's plate theory in finite water depth and shallow water approximations. The wave scattering from a single articulated floating elastic plate based on Timoshenko-Mindlin's thick plate theory is analyzed. The eigenfunction expansion method along with orthogonal mode coupling relation is utilized in the formulation of the boundary value problem at finite water depth. Further, the wave scattering from a periodic array of multiple articulated floating elastic plates is analyzed based on Timoshenko-Mindlin's equation in finite water depth and shallow water approximations. Two methods are used to analyze the multiple articulated floating elastic plates in finite water depth. Firstly, the direct method of solution used for the single articulated floating elastic plate based on the eigenfunction expansion method along with mode coupling relation is extended for multiple articulations in the floating elastic plate. In order to simplify the complexity of BVP with the increasing number of articulations, the wide spacing approximations method is used to analyze the periodic array of floating elastic plate with connecting joints based on the wave scattering behaviour of the single articulated floating elastic plate. On the other hand, for the case of shallow water approximations, the continuity of energy and mass flux along with boundary conditions are used to obtain the unknowns in the velocity potential. The connecting joints are modelled as a connector with linear spring and/or rotational spring

stiffness. The effect of the articulated joint is analyzed by varying the spring stiffness for different cases of articulated joints having hinged connection, semi-rigid connection, and rigid connection. The numerical computation is performed to analyze the wave reflection and transmission behaviour due to wave interaction with a single and multiple articulated floating elastic plate in finite water depth and shallow water approximations. The hydroelastic characteristics of single and multiple articulated floating thick elastic plate acted upon by ocean wave are studied by considering the vertical deflection, wave induced strain, bending moment and shear force for the plate. The significance of connectors with linear and/or rotational spring stiffness in analyzing the hydroelastic behaviour of articulated floating plates is also studied. Further, the application of wide-spacing approximation method in the hydroelastic analysis of a periodic array of multiple articulated floating elastic plate is presented.

4.2 MATHEMATICAL FORMULATION

The wave scattering due to periodic arrays of multiple articulated floating thick elastic plate is formulated considering linearized wave theory. The monochromatic wave is assumed to be incident along the positive $x-$ axis. A two-dimensional floating elastic plate is modelled with $x-$ axis along the plate length and the $y-$ axis across the vertically downward direction as shown in Figure 1. The fluid is considered to be extended infinitely along the horizontal plane $-\infty < x < \infty$ at the water depth $0 < y < h$. A periodic array of multiple plates interconnected at N articulated joints by vertical linear and flexural rotational springs occupy the region $-a_{N+2} < x < -a_1$ and the free surface exists in the regions $-\infty < x < -a_{N+2}$ and $-a_1 < x < \infty$. The fluid domain is divided into $(N+3)$ regions along the vertical interfaces having N articulations at the interconnected edge of the $(N+1)$ floating elastic plate at $x = -a_j, y = 0,$ $j = 2,3,...,(N+1)$ as shown in the Figure 4.1(a). The fluid domain is divided into upstream open water region at $I_1 \equiv (-a_1 < x < \infty)$ with $0 < y < h$, the multiple articulated plates covered region $I_j \equiv (-a_j < x < -a_{j-1})$ with $0 < y < h$ for $j = 2,3,...,(N+2)$ and downstream open water region $I_{N+3} \equiv (-\infty < x < -a_{N+2})$ with $0 < y < h$. The plate edges at $x = -a_1$ and $x = -a_{N+2}$ satisfies the free edge support condition.

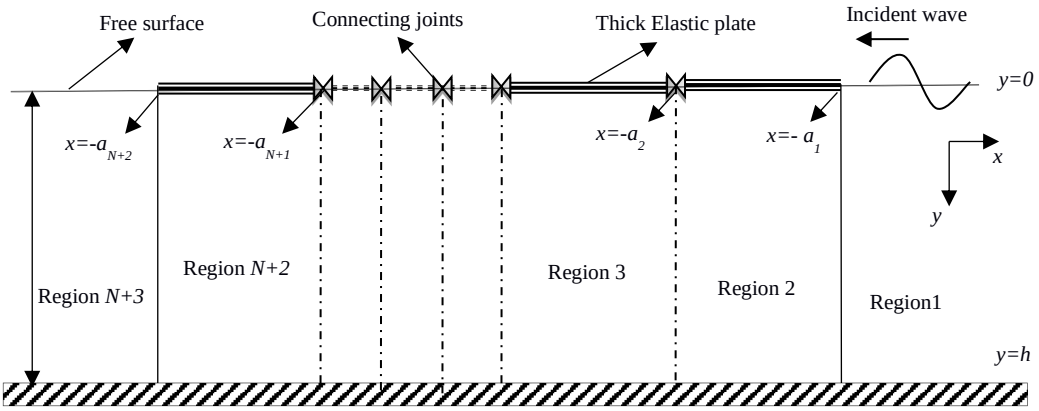

Figure 4.1(a): Schematic diagram of multiple articulations in floating elastic plate.

The spatial velocity potential, ϕ_j, $j=1,2,....(N+3)$ in the fluid domain, satisfies the Laplace's equation given by

$$\nabla^2\phi_j(x,y)=0 \quad \text{on} \quad -\infty<x<\infty, \quad 0<y<h. \tag{4.1}$$

The linearized plate covered boundary condition on the free surface is obtained by combining the linearized kinematic condition and dynamic condition with Timoshenko-Mindlin equation for $j=2,3,...,(N+2)$ is of the form

$$\begin{aligned}&\left\{\frac{EI}{\left(\rho g-m_s\omega^2\right)}\partial_x^4+\left(\frac{m_s\omega^2 I}{\left(\rho g-m_s\omega^2\right)}-S\right)\partial_x^2+\left(1-\frac{m_s\omega^2 IS}{EI}\right)\right\}\partial_y\phi_j\\&+\frac{\rho\omega^2}{\left(\rho g-m_s\omega^2\right)}\left\{1-\frac{m_s\omega^2 IS}{EI}-S\partial_x^2\right\}\phi_j=0 \quad \text{for} \quad -a_{N+2}<x<-a_1,\end{aligned} \tag{4.2}$$

where, $EI=Ed^3/12(1-\nu^2)$ is the plate rigidity, E is the Young's Modulus, $G=E/2(1+\mu)$ is the shear modulus of the plate, μ is the transverse shear coefficient, $I=d^2/12$ is the rotary inertia and $S=EI/\mu Gd$ is the shear deformation.

The typical values of physical constants and variables that are used for the wave scattering problem (Balmforth and Craster, 1999, Watanabe et al, 2004, Karmakar and Sahoo, 2005, Suzuki 2005) are listed in Table 4.1. In the fluid domain $j=1,(N+3)$ the linearized free surface boundary condition is obtained as

$$\partial_y\phi_j-\left(\omega^2/g\right)\phi_j=0, \quad \text{for } x>-a_1 \text{ and } x<-a_{N+2},\ j=1,(N+3). \tag{4.3}$$

Table 4.1: List of physical constants and variable values/range

Physical Constants/ Variables	**Typical value/range**
E	$5*10^9$ Pa - $10*10^9$ Pa
ν	0.3
ρ_w	1025 kg /m^3
ρ_p	922.5 kg /m^3
ω	0.1-10 rad/ sec
h	10 m – 500 m
d	0.5 – 200 m
L	100 – 1500 m

The continuity of pressure and velocity at the edges $x=-a_j$ of the floating elastic plate is given by

$$\phi_j=\phi_{(j+1)} \text{ and } \phi_{jx}=\phi_{(j+1)x} \text{ at } x=-a_j,\ j=1,2,...,(N+2),\ 0<y<h. \tag{4.4}$$

The edges of the periodic arrays of the articulated floating thick elastic plate $x=-a_1,-a_{N+2}$ are considered to be freely floating, so the bending moment and the shear force vanishes at the edges $x=-a_1$ and $x=-a_{N+2}$, $0<y<h$ as follows

$$\partial_y^3\phi_j(x,y)=0 \text{ and } \partial_{xy^3}^4\phi_j(x,y)=\wp\partial_{xy}^2\phi_j(x,y) \text{ at } x=-a_1 \text{ and } x=-a_{N+2},\ y=0, \tag{4.5}$$

with $\wp=m\omega^2(S+I)/EI$. The connecting joints along the multiple articulated floating elastic plate are considered to be connected with vertical linear and/or flexural rotational springs with stiffness k_{33} and k_{55} respectively. The bending moment and shear force acting at the articulated edges $j=2,3,...,(N+1)$ are formulated based on the nature of k_{33} and k_{55} given by the relation

$$EI\partial_y^3\phi_j(x+,0)=-k_{55}\left\{\partial_{xy}^2\phi_j(x+,0)-\partial_{xy}^2\phi_{(j+1)}(x-,0)\right\}, \tag{4.6a}$$

$$EI\partial_y^3\phi_{(j+1)}(x-,0)=-k_{55}\left\{\partial_{xy}^2\phi_j(x+,0)-\partial_{xy}^2\phi_{(j+1)}(x-,0)\right\}, \tag{4.6b}$$

$$EI\left[\partial_{xy^3}^4\phi_j(x+,0)-\wp\partial_{xy}^2\phi_j(x+,0)\right]=k_{33}\left\{\partial_y\phi_j(x+,0)-\partial_y\phi_{(j+1)}(x-,0)\right\}, \tag{4.6c}$$

$$EI\left[\partial^4_{xy^3}\phi_{(j+1)}(x-,0)-\wp\partial^2_{xy}\phi_{(j+1)}(x-,0)\right]=k_{33}\left\{\partial_y\phi_j(x+,0)-\partial_y\phi_{(j+1)}(x-,0)\right\}. \quad (4.6d)$$

The values of k_{33} and k_{55} tends to zero for the case of free edge condition, for hinged connector, either of the spring stiffness k_{33} or k_{55} tends to zero and for rigid connection the stiffness values tend to infinity i.e. $k_{33}\to\infty$ and $k_{55}\to\infty$ as shown in Table 4.2.

In Table 4.2, the nature of the articulation at the interconnected joints related to the stiffness of the vertical linear spring k_{33} and flexural rotational spring k_{55} is described.

Table 4.2: Typical nature of k_{33} and k_{55}

Nature of k_{33} and k_{55}	**Edge condition**
$k_{33}=0$ and $k_{55}=0$	Free edge connection
$k_{33}=0$ and $k_{55}\to\infty$	Roller/Slider connection
$k_{33}\to\infty$ and $k_{55}=0$	Hinged connection
k_{33} and k_{55} intermediate value	Semi-rigid connection
$k_{33}\to\infty$ and $k_{55}\to\infty$	Rigid connection

The far-field radiation condition is given by

$$\phi_j(x)=\begin{cases}\left(e^{-ik_{10}x}+R_{10}e^{ik_{10}x}\right)f_{10}(y) & \text{as} \quad x\to\infty,\\ \left(T_{(N+3)0}e^{-ik_{(N+3)0}x}\right)f_{(N+3)0}(y) & \text{as} \quad x\to-\infty,\end{cases} \quad (4.7)$$

with R_{10} and $T_{(N+3)0}$ are the wave amplitudes in the reflected and transmitted regions and k_{j0} for $j=1,(N+3)$ are the positive real root satisfying the free surface dispersion relation as follows

$$k_{j0}\tanh k_{j0}h-\omega^2/g=0. \quad (4.8)$$

In the next section, a detailed solution approach for the multiple articulated floating elastic plate based on the Timoshenko-Mindlin plate theory acted upon by ocean waves in finite water depth is presented.

4.3 METHOD OF SOLUTION

In this section, the solution procedure for the wave interaction with a single articulated floating elastic plate is presented for finite water depth and shallow water approximation. Further, the effect of multiple articulations in floating thick elastic plate is also analysed in finite water depth and shallow water approximation. The articulated floating elastic plate is considered to have $(N+1)$ finite elastic plate connected with N articulations. The analysis multiple articulated floating elastic plate is carried out using the eigenfunction expansion method along with the orthogonal mode-coupling relation and compared with wide-spacing approximation method in finite water depth.

4.3.1 Direct Eigenfunction Expansion Method

The periodic array of floating elastic plate interconnected at the articulated joint is analyzed using the eigenfunction expansion method along with orthogonal mode-coupling relation (Karmakar et al., 2009) is described in detail in the next sub-section.

4.3.1.1 Finite water depth

The articulated floating elastic plate is considered to be having N articulation interconnected with $(N+1)$ plates and the edges $x=-a_1$ and $x=-a_{N+2}$ is considered to be free edges. The velocity potentials $\phi_j(x,y)$ in the fluid domain for the respective regions are expressed as

$$\begin{aligned}
\phi_1(x,y) &= \left(I_{10}e^{-ik_{10}x}+R_{10}e^{ik_{10}x}\right)f_{10}(y)+\sum_{n=1}^{\infty}R_{1n}e^{-\kappa_{1n}x}f_{1n}(y), && \text{for } x>a_1,\\
\phi_j(x,y) &= \sum_{n=0,I}^{II}\left(A_{jn}e^{-ik_{jn}x}+B_{jn}e^{ik_{jn}x}\right)f_{jn}(y)+\sum_{n=1}^{\infty}\left(A_{jn}e^{\kappa_{jn}x}+B_{jn}e^{-\kappa_{jn}x}\right)f_{jn}(y), && \\
& && \text{for } -a_{N+2}<x<-a_1,\\
\phi_{N+3}(x,y) &= T_{(N+3)0}e^{-ik_{(N+3)0}x}f_{(N+3)0}(y)+\sum_{n=1}^{\infty}T_{(N+3)n}e^{\kappa_{(N+3)n}x}f_{(N+3)n}(y), && \text{for } x<-a_{N+2},
\end{aligned} \tag{4.9}$$

where $R_{1n}, T_{(N+3)n}$ at $n=0,1,2...$, A_{jn} and B_{jn} at $n=0,I,II,1,2...$, $j=2,3....,(N+2)$ are the unknown coefficients to be determined. The eigenfunction $f_{jn}(y)$'s in the respective fluid domains are given by

$$f_{jn}(y)=\frac{\cosh k_{jn}(h-y)}{\cosh k_{jn}h} \text{ for } n=0,I,II \text{ and } f_{jn}(y)=\frac{\cos k_{jn}(h-y)}{\cos k_{jn}h} \text{ for } n=1,2,...$$

(4.10)

where k_{j0} for $j=1,(N+3)$ are the eigenvalues in the open water region obtained from the dispersion relation given by

$$k_{jn}\tanh k_{jn}h-\omega^2/g=0. \tag{4.11}$$

The eigenvalues $k_{j0},\ j=1,(N+3)$ are the real root and $k_{jn}=i\kappa_{jn}$ for $n=1,2...$ are the purely imaginary roots obtained from the free surface dispersion relation as in Equation (4.11). The term k_{jn} for $j=2,3,....(N+2),\ n=0,I,II$ are the eigenvalues for the plate covered region satisfies the dispersion relation given by

$$\left(\alpha_0-\alpha_1k_{jn}^2+\alpha_2k_{jn}^4\right)k_{jn}\tanh k_{jn}h-\left(\beta_0-\beta_1k_{jn}^2\right)=0, \tag{4.12}$$

where $\alpha_0=\left\{1-m_s\omega^2\left(\frac{IS}{EI}\right)\right\}$, $\alpha_1=\left\{\frac{m_s\omega^2 I}{\left(\rho g-m_s\omega^2\right)}-S\right\}$, $\alpha_2=\frac{EI}{\left(\rho g-m_s\omega^2\right)}$,

$\beta_0=\frac{\rho\omega^2}{\left(\rho g-m_s\omega^2\right)}\left(1-m_s\omega^2\frac{IS}{EI}\right)$, $\beta_1=-\frac{\rho\omega^2 S}{\left(\rho g-m_s\omega^2\right)}$, $m_s=\rho_p d$ is the mass per unit area. The eigenvalues k_{j0} for $j=2,3,....(N+2)$ signify the real root and $k_{jn},\ j=2,3,....(N+2)$ for $n=I,II,III,IV$ are the four complex conjugate roots of the form $\pm\alpha\pm i\beta$ obtained from the plate covered dispersion relation. The eigenfunctions $f_{jn}(y)$'s in the fluid domains at $j=1,2,3,...(N+3)$ satisfy the orthogonality condition given by

$$\left\langle f_{jm},f_{jn}\right\rangle_{j=1,(N+3)}=\begin{cases}0 & \text{for } m\neq n,\\ C_n' & \text{for } m=n,\end{cases} \text{ and } \left\langle f_{jm},f_{jn}\right\rangle_{j=2,3,...(N+2)}=\begin{cases}0 & \text{for } m\neq n,\\ C_n''' & \text{for } m=n,\end{cases}$$

(4.13)

where $C_n'=\frac{2k_{jn}h+\sinh 2k_{jn}h}{4k_{jn}\cosh^2 k_{jn}h}$ and

$$C_n'''=\frac{\left(\alpha_0-\alpha_1k_{jn}^2+\alpha_2k_{jn}^4\right)2k_{jn}h+\left(\alpha_0-3\alpha_1k_{jn}^2+5\alpha_2k_{jn}^4\right)\sinh 2k_{jn}h+\left(4\beta_1k_{jn}\cosh^2 k_{jn}h\right)}{4k_{jn}\cosh^2 k_{jn}h\left(\alpha_0-\alpha_1k_{jn}^2+\alpha_2k_{jn}^4\right)},$$

$$\left\langle f_{jm}, f_{jn} \right\rangle_{j=1,(N+3)} = \int_0^h f_{jm}(y) f_{jn}(y) dy, \tag{4.14}$$

$$\left\langle f_{jm}, f_{jn} \right\rangle_{j} = \int_0^h f_{jm}(y) f_{jn}(y) dy - \frac{\alpha_1}{Q\left(k_{jn}\right)} \left\{ f'_{jm}(0) f'_{jn}(0) \right\} + \frac{\alpha_2}{Q\left(k_{jn}\right)} \left\{ f'''_{jm}(0) f'_{jn}(0) + f'_{jm}(0) f'''_{jn}(0) \right\} + \frac{\beta_1}{P\left(k_{jn}\right)} f_{jm}(0) f_{jn}(0),\ j = 2,3,...,\left(N+2\right), \tag{4.15}$$

where $P(k_{jn}) = \left(\alpha_0 - \alpha_1 k_{jn}^2 + \alpha_2 k_{jn}^4\right)$ and $Q(k_{jn}) = \left(\beta_0 - \beta_1 k_{jn}^2\right)$.

The unknown coefficients are determined by applying the mode-coupling relation on the velocity potentials $\phi_j\left(x, y\right)$ at the edges $x = -a_j,\ \ j = 2,3,...,\left(N+1\right)$ along with the respective eigenfunction $f_{jn}(y)$. The continuity of pressure and velocity is applied across the vertical boundary at $x = -a_j,\ j = 1,2,...,\left(N+2\right)$ along with the free edge support condition and articulated condition at the plate interfaces to obtain a system of linear equations.

The mode-coupling relation as in Equation (4.15) is applied on $\phi_2\left(-a_1, y\right)$ and $f_{2m}(y)$ at $x = -a_1$ to obtain

$$\left\langle \phi_2\left(-a_1, y\right), f_{2m}(y) \right\rangle = \int_0^h \phi_2\left(-a_1, y\right) f_{2m}(y) dy - \frac{\alpha_1}{Q(k_{2n})} \left\{ \phi_{2y}\left(-a_1, 0\right) f'_{2m}(0) \right\} + \frac{\alpha_2}{Q(k_{2n})} \left\{ \phi_{2yyy}\left(-a_1, 0\right) f'_{2m}(0) + \phi_{2y}\left(-a_1, 0\right) f'''_{2m}(0) \right\} + \frac{\beta_1}{P(k_{2n})} \phi_2\left(-a_1, 0\right) f_{2m}(0), \tag{4.16}$$

for $m = 0, I, II, 1, 2...$

Further, the orthogonality condition as in Equation (4.13) is applied for the eigenfunction $f_{2m}(y)$ and the expression of velocity potentials as in Equation (4.9) along with the continuity for pressure as in Equation (4.4) applied across the vertical boundary at $x = 0, 0 < y < h$ and the free edge condition considering bending moment $\partial_y^3 \phi_2\left(-a_1, 0\right) = 0$ as in Equation (4.5).

The simplified expression with unknowns $R_{1n}, n = 0,1,2,...,\ \ A_{2n}$ and B_{2n}, $n = 0, I, II, 1, 2,....$ given by

$$R_{10}e^{-ik_{10}a_1}\int_0^h f_{10}(y)\,f_{2m}(y)dy+\sum_{n=1}^{M+2}R_{1n}e^{\kappa_{1n}a_1}\int_0^h f_{1n}(y)\,f_{2m}(y)dy$$
$$+\left\{\sum_{n=0,I}^{II}(A_{2n}e^{ik_{2n}a_1}+B_{2n}e^{-ik_{2n}a_1})+\sum_{n=1}^{M}(A_{2n}e^{-\kappa_{2n}a_1}+B_{2n}e^{\kappa_{2n}a_1})\right\}\left[\frac{\alpha_2}{Q(k_{2n})}f_{2n}^{'}(0)\,f_{2m}^{'''}(0)\right.$$
$$-\frac{\alpha_1}{Q(k_{2n})}f_{2n}^{'}(0)\,f_{2m}^{'}(0)+\frac{\beta_1}{P(k_{2n})}f_{2n}(0)\,f_{2m}(0)$$
$$\left.-\delta_{mn}\left\langle f_{2n},f_{2m}\right\rangle\right]=-I_{10}e^{ik_{10}a_1}\int_0^h f_{10}(y)\,f_{2m}(y)\,dy, \tag{4.17}$$

where $k_{jm}=i\kappa_{jm}$ for $m=1,2,...$ and $\delta_{mn}=\begin{cases}1 & \text{for } m=n,\\ 0 & \text{for } m\neq n.\end{cases}$

Again, considering the mode-coupling relation as in Equation (4.15) on $\phi_{2x}(-a_1,y)$ along with the eigenfunction $f_{2m}(y)$ the relation leads to

$$\left\langle\phi_{2x}(-a_1,y),\,f_{2m}(y)\right\rangle=\int_0^h\phi_{2x}(-a_1,y)\,f_{2m}(y)dy-\frac{\alpha_1}{Q(k_{2n})}\left\{\phi_{2xy}(-a_1,0)\,f_{2m}'(0)\right\}+$$
$$\frac{\alpha_2}{Q(k_{2n})}\left\{\phi_{2xyyy}(-a_1,0)\,f_{2m}'(0)+\phi_{2xy}(-a_1,0)\,f_{2m}'''(0)\right\}+\frac{\beta_1}{P(k_{2n})}\phi_{2x}(-a_1,0)\,f_{2m}(0), \tag{4.18}$$

for $m=0,I,II,1,2...$ The orthogonality condition as in Equation (4.13) is applied for the eigenfunction $f_{2m}(y)$ and the continuity equation for velocity is applied across the vertical boundary at $x=-a_1,\ 0<y<h$ as in Equation (4.4) and the free edge condition $\partial_{xy^3}^4\phi_2(-a_1,0)=\wp\,\partial_{xy}^2\phi_2(-a_1,0)$ as in Equation (4.5) yields the simplified expression with unknowns $R_{1n},n=0,1,2,....$ A_{2n} and $B_{2n},n=0,I,II,1,2,....$ given by

$$ik_{10}e^{-ik_{10}a_1}R_{10}\int_0^h f_{10}(y)\,f_{2m}(y)dy-\sum_{n=1}^{M+2}\kappa_{1n}e^{\kappa_{1n}a_1}R_{1n}\int_0^h f_{1n}(y)\,f_{2m}(y)dy$$
$$-\left\{i\sum_{n=0,I}^{II}k_{2n}(A_{2n}e^{ik_{2n}a_1}-B_{2n}e^{-ik_{2n}a_1})\right.$$
$$\left.-\sum_{n=1}^{M}\kappa_{2n}(A_{2n}e^{-\kappa_{2n}a_1}-B_{2n}e^{\kappa_{2n}a_1})\right\}\left[\frac{\alpha_2}{Q(k_{2n})}\left\{\wp f_{2n}^{'}(0)\,f_{2m}^{'}(0)+f_{2n}^{'}(0)\,f_{2m}^{'''}(0)\right\}\right. \tag{4.19}$$
$$\left.-\frac{\alpha_1}{Q(k_{2n})}f_{2n}^{'}(0)\,f_{2m}^{'}(0)+\frac{\beta_1}{P(k_{2n})}f_{2n}(0)\,f_{2m}(0)-\delta_{mn}\left\langle f_{2n},f_{2m}\right\rangle\right]$$
$$=ik_{10}e^{ik_{10}a_1}I_{10}\int_0^h f_{10}(y)\,f_{2m}(y)\,dy,$$

for $k_{jm} = i\kappa_{jm}$ for $m = 1, 2, ...$ Next, considering the mode-coupling relation as in Equation (4.15) on $\phi_{j+1}(x, y)$ and $f_{(j+1)m}(y)$ at $x = -a_j$, $j = 2, 3, ..., (N+1)$ we have

$$\left\langle \phi_{j+1}(-a_j, y),\, f_{(j+1)m}(y) \right\rangle = \int_0^h \phi_{j+1}(-a_j, y)\, f_{(j+1)m}(y) dy - \frac{\alpha_1}{Q(k_{jn})} \left\{ \phi_{(j+1)y}(-a_j, 0)\, f'_{(j+1)m}(0) \right\}$$
$$+ \frac{\alpha_2}{Q(k_{jn})} \left\{ \phi_{(j+1)yyy}(-a_j, 0)\, f'_{(j+1)m}(0) + \phi_{(j+1)y}(-a_j, 0)\, f'''_{(j+1)m}(0) \right\}$$
$$+ \frac{\beta_1}{P(k_{jn})} \phi_{(j+1)}(-a_j, 0)\, f_{(j+1)m}(0). \tag{4.20}$$

Applying the continuity of pressure $\phi_j(-a_j, y) = \phi_{j+1}(-a_j, y)$ and articulation condition $\partial_y^3 \phi_{j+1}(-a_j, 0) = \frac{-k_{55}}{EI} \left\{ \phi_{jxy}^2(-a_j, 0) - \phi_{(j+1)xy}^2(-a_j, 0) \right\}$ along with the orthogonality condition, the simplified expression with the unknown coefficient A_{jn} and B_{jn}, $j = 2, 3, ..., (N+1)$, $n = 0, I, II, 1, 2, ...$ is obtained. Further, the mode coupling relation Equation (4.15) is applied to $\phi_{(j+1)x}(-a_j, y)$ and $f_{(j+1)m}(y)$ at $x = -a_j$, $j = 2, 3, ..., (N+1)$ we have

$$\left\langle \phi_{(j+1)x}(-a_j, y),\, f_{(j+1)m}(y) \right\rangle = \int_0^h \phi_{(j+1)x}(-a_j, y)\, f_{(j+1)m}(y) dy$$
$$- \frac{\alpha_1}{Q(k_{jn})} \left\{ \phi_{(j+1)xy}(-a_j, 0)\, f'_{(j+1)m}(0) \right\}$$
$$+ \frac{\alpha_2}{Q(k_{jn})} \left\{ \phi_{(j+1)xyyy}(-a_j, 0)\, f'_{(j+1)m}(0) + \phi_{(j+1)xy}(-a_j, 0)\, f'''_{(j+1)m}(0) \right\} \tag{4.21}$$
$$+ \frac{\beta_1}{P(k_{jn})} \phi_{(j+1)x}(-a_j, 0)\, f_{(j+1)m}(0).$$

Applying the continuity of velocity $\phi_{jx}(-a_j, y) = \phi_{(j+1)x}(-a_j, y)$ and the edge condition $\partial_{xy^3}^4 \phi_{(j+1)}(-a_j, 0) = \frac{k_{33}}{EI} \left\{ \phi_{jy}(-a_j, 0) - \phi_{(j+1)y}(-a_j, 0) \right\} + \wp \partial_{xy}^2 \phi_{(j+1)}(-a_j, 0)$ along with the orthogonality condition, the simplified expression with the unknown coefficient A_{jn} and B_{jn}, $j = 2, 3, ..., (N+1)$, $n = 0, I, II, 1, 2, ...$ is obtained.

Again, the mode coupling relation (4.15) is applied on $\phi_{N+2}(-a_{N+2}, y)$ and $f_{(N+2)m}(y)$ we have

$$\begin{aligned}\left\langle \phi_{(N+2)}(-a_{N+2}, y),\, f_{(N+2)m}(y) \right\rangle &= \int_0^h \phi_{(N+2)}(-a_{N+2}, y)\, f_{(N+2)m}(y)dy \\ &\quad - \frac{\alpha_1}{Q(k_{(N+2)n})}\left\{\phi_{(N+2)y}(-a_{N+2}, 0)\, f'_{(N+2)m}(0)\right\} \\ &\quad + \frac{\alpha_2}{Q(k_{(N+2)n})}\left\{\phi_{(N+2)yyy}(-a_{N+2}, 0)\, f'_{(N+2)m}(0) + \phi_{(N+2)y}(-a_{N+2}, 0)\, f'''_{(N+2)m}(0)\right\} \\ &\quad + \frac{\beta_1}{P(k_{(N+2)n})}\phi_{(N+2)}(-a_{N+2}, 0)\, f_{(N+2)m}(0),\end{aligned} \tag{4.22}$$

for $m = 0, I, II, 1, 2...$

Applying continuity for pressure $\phi_{(N+2)}(-a_{N+2}, y) = \phi_{(N+3)}(-a_{N+2}, y)$ and edge condition $\partial_y^3 \phi_{(N+2)}(-a_{N+2}, 0) = 0$ along with orthogonal property, the simplified expression with the unknown coefficient T_{1n}, $n = 0, 1, 2, \ldots.$, A_{jn} and B_{jn}, $j = 2, 3, ..., (N+1)$, $n = 0, I, II, 1, 2, \ldots.$ is obtained. Again the mode coupling relation as in Equation (15) is applied to $\phi_{(N+2)x}(-a_{N+2}, y)$ and $f_{(N+2)m}(y)$ we have

$$\begin{aligned}\left\langle \phi_{(N+2)x}(-a_{N+2}, y),\, f_{(N+2)m}(y) \right\rangle &= \int_0^h \phi_{(N+2)x}(-a_{N+2}, y)\, f_{(N+2)m}(y)dy \\ &\quad - \frac{\alpha_1}{Q\left(k_{(N+2)n}\right)}\left\{\phi_{(N+2)xy}(-a_{N+2}, 0)\, f'_{(N+2)m}(0)\right\} \\ &\quad + \frac{\alpha_2}{Q\left(k_{(N+2)n}\right)}\left\{\phi_{(N+2)xyyy}(-a_{N+2}, 0)\, f'_{(N+2)m}(0) + \phi_{(N+2)xy}(-a_{N+2}, 0)\, f'''_{(N+2)m}(0)\right\} \\ &\quad + \frac{\beta_1}{P\left(k_{(N+2)n}\right)}\phi_{(N+2)x}(-a_{N+2}, 0)\, f_{(N+2)m}(0),\end{aligned} \tag{4.23}$$

for $m = 0, I, II, 1, 2...$

Applying the continuity equation for velocity $\phi_{(N+2)x}(-a_{N+2}, y) = \phi_{(N+3)x}(-a_{N+2}, y)$ and the edge condition $\partial_{xy^3}^4 \phi_{(N+2)}(-a_{N+2}, 0) = \wp \partial_{xy}^2 \phi_{(N+2)}(-a_{N+2}, 0)$ along with orthogonality conditions, the simplified expression with the unknown coefficient T_{1n}, $n = 0, 1, 2, \ldots.$ A_{jn} and B_{jn}, $j = 2, 3, ..., (N+1)$, $n = 0, I, II, 1, 2, \ldots.$ is obtained.

On solving, an infinite series of the algebraic equations are obtained and the linear equations are truncated up to a finite number of 'M' terms to obtain a system of $(N+3)(M+2)$ equations for N articulation. The unknown constants $R_{1n}, T_{(N+3)n}$, $n=0,1,2...$ and $A_{jn}, B_{jn}, n=0,I,II,1,2...,\ j=2,3,...,(N+2)$ are obtained by solving the above system of linear equations. The wave reflection and transmission coefficient R_0 and T_0 are obtained as follows

$$K_r = |R_{10}| \text{ and } K_t = \left| \frac{\tanh k_{(N+3)0} h}{\tanh k_{10} h} T_{(N+3)0} \right|. \tag{4.24}$$

The reflection and transmission coefficients are observed to satisfy the energy balance relation as given by $K_r^2 + K_t^2 = 1.$

4.3.1.2 Shallow water approximation

The wave scattering due to a periodic array of finite floating elastic plate interconnected with articulation joints is analyzed considering shallow water theory. The velocity potentials for the open water region and the fluid domain covered with freely floating multiple articulated plate are of the form

$$\begin{aligned}
&\phi_1(x,y) = \left(I_{10} e^{-ik_{10}x} + R_{10} e^{ik_{10}x} \right), && x > -a_1, \\
&\phi_j(x,y) = A_{j0} e^{-ik_{j0}x} + \bar{A}_{j0} e^{ik_{j0}x} + \sum_{n=I}^{IV} A_{jn} e^{-ik_{jn}x}, && -a_{N+2} < x < -a_1, \\
& && j = 2,3,..,(N+2), \\
&\phi_{N+3}(x,y) = T_{(N+3)0} e^{-ik_{(N+3)0}x} && x < -a_{N+2},
\end{aligned} \tag{4.25}$$

where R_{10} and $T_{(N+3)0}$ are the unknown complex coefficient in the reflected and transmitted region with k_{j0} for $j=1,(N+3)$ are the roots for open water dispersion relation at shallow water depth. The coefficients A_{jn} are the unknowns with k_{jn} for $j=2,3..,(N+2),\ n=0,I,..,IV$ are the roots for dispersion relation in the fluid domain covered with a periodic array of the articulated floating elastic plate. The continuity of energy and mass flux at the interface $x=-a_j$ is given by

$$\phi_{jx} = \phi_{(j+1)x} \text{ and } \phi_j = \phi_{(j+1)} \text{ at } x=-a_j,\ j=2,3,...,(N+2). \tag{4.26}$$

The elastic plate is assumed to be freely floating and hence the bending moment and the shear force equation vanishes at the edge $x=-a_1$ and $x=-a_{N+2}$ as given by

$$\partial_x^4\phi_j=0 \text{ and } \partial_x^5\phi_j=\wp\partial_x^3\phi_j \text{ at } x=-a_1,-a_{N+2}, \text{ for } j=2,(N+2). \tag{4.27}$$

The bending moment and shear force at multiple articulated edges $x=-a_j,\ j=2,3,...,(N+1)$ are given as

$$EI\partial_x^4\phi_j(x+)=k_{55}\left\{\partial_x^3\phi_j(x+)-\partial_x^3\phi_{j+1}(x-)\right\}, \tag{428a}$$

$$EI\partial_x^4\phi_{j+1}(x-)=k_{55}\left\{\partial_x^3\phi_j(x+)-\partial_x^3\phi_{j+1}(x-)\right\}, \tag{4.28b}$$

$$EI\left[\partial_x^5\phi_j(x+)-\wp\partial_x^3\phi_j(x+)\right]=-k_{33}\left\{\partial_x^2\phi_j(x+)-\partial_x^2\phi_{j+1}(x-)\right\}, \tag{4.28c}$$

$$EI\left[\partial_x^5\phi_{j+1}(x-)-\wp\partial_x^3\phi_{j+1}(x-)\right]=-k_{33}\left\{\partial_x^2\phi_j(x+)-\partial_x^2\phi_{j+1}(x-)\right\}. \tag{4.28d}$$

The unknown coefficients are determined considering the continuity of energy and mass flux along with the free edge condition at $x=-a_1,-a_{N+2}$ and articulated edge conditions at $x=-a_j,\ j=2,3,...,(N+2)$ as in Equation (4.26) and Equations (4.28a-d) to solve the set of $(6N+8)$ algebraic linear equations. Once the unknown constants R_{10} and $T_{(N+3)0}$ are determined, the reflection and transmission coefficient are obtained as given by Equation (4.24).

4.3.1.3 Wide-spacing approximation method

The analysis of the periodic array of floating elastic plates interconnected with vertical and rotational spring stiffness using the wide spacing approximation (WSA) method is based on the distance between the consecutive plates. In order to reduce the complexity of the problem, it is assumed that the wavelength of the incident wave is less as compared to the distance between the consecutive multiple articulated floating elastic plate. The BVP is considered the same as defined in section 2 and the evanescent wave modes are considered to be negligible due to the presence of wide spacing between the plates. So, in the wide-spacing approximation only the progressive wave mode is considered in the formulation of the multiple articulated floating elastic plate (Karmakar et al., 2009) kept at periodic intervals. The incident wave interacting with

the multiple articulated elastic plates gets reflected and transmitted partially at the articulated joints, located at $x=-a_j,\ j=2,3,...,(N+1)$. Due to the absence of the evanescent wave mode, the local effects produced under the action of an incident wave on the connecting joints do not affect the subsequent interactions. Based on the assumptions of wide spacing between the articulated edges, the asymptotic form of the velocity potentials $\phi_j,\ j=1,2,...,(N+3)$ away from the connecting joints for the respective fluid domains are given by

$$\begin{aligned}
&\phi_1(x,y)\approx\left(I_{10}e^{-ik_{10}x}+R_{10}e^{ik_{10}x}\right)f_{10}(y) && \text{for } x>-a_1,\\
&\phi_j(x,y)\approx\left(A_{j0}e^{-ik_{j0}x}+B_{j0}e^{ik_{j0}x}\right)f_{j0}(y) && \text{for } -a_{N+2}<x<-a_1,\\
& && j=2,3,...,(N+2),\\
&\phi_{N+3}(x,y)\approx T_{(N+3)0}e^{-ik_{(N+3)0}x}\ f_{(N+3)0}(y) && \text{for } x<-a_{N+2},
\end{aligned} \tag{4.29}$$

where R_{10} and $T_{(N+3)0}$ are the unknown coefficient in the reflected and transmitted regions with k_{j0} at $j=1,(N+3)$ are the roots for the dispersion relation in the open water region. The unknown coefficients A_{jn} and B_{jn} and $k_{j0},\ j=2,3,...,(N+2)$ are the roots for dispersion relation in the fluid domain covered with an array of floating elastic plate with connecting joints. The wave scattering behaviour based on the wide-spacing approximation for the multiple articulated floating elastic plate involves components of the propagating waves travelling in the left and right direction at the articulated edges $x=-a_j,\ j=2,3,...,(N+1)$. The amplitudes for the reflected and transmitted waves in the respective regions generate a set of $2(N+2)$ unknowns given by $R_{10},\ T_{(N+3)0},$ $A_{j0},\ B_{j0},\ j=2,3,...,(N+2)$.

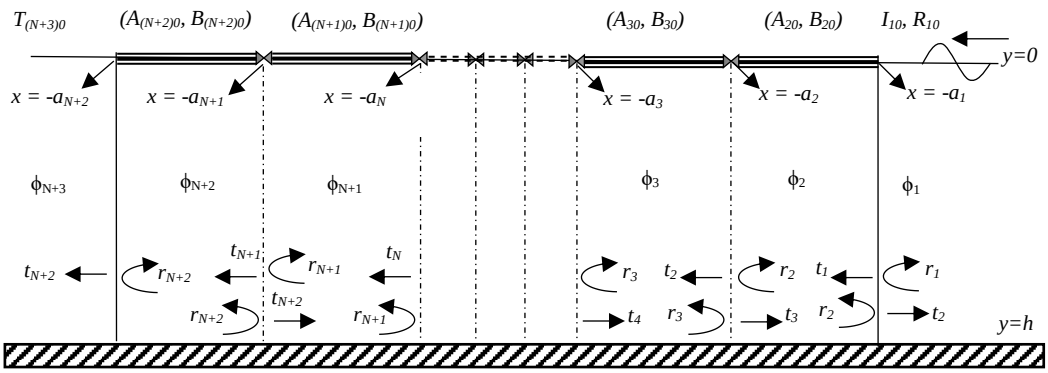

Figure 4.1(b): Wave scattering patterns in wide-spacing approximation

The numerical computation using the wide-spacing approximation requires the wave scattering patterns from a single articulated floating elastic plate. The fluid domain with respective scattering behaviour based on wide-spacing approximation is illustrated in Figure 4.1(b).

The plate covered region is an array of $(N+1)$ multiple articulated plate along with N articulation at $x=-a_j,\ j=2,3,...,(N+1)$. The plate edges at $x=-a_1$ and $x=-a_{N+2}$ is assumed to satisfy the free edge support condition. The wave amplitudes in the reflected and transmitted region from a single articulated plate acted upon by ocean wave are calculated as r_j and $t_j,\ j=1,2,...,(N+2)$. In order to determine $2(N+2)$ unknown complex coefficients, the matching conditions (Newman 1965, Karmakar et al. 2009) are applied at the articulated joint $x=-a_j,\ j=2,3,..,(N+1)$ and at the edge supports $x=-a_1$ and $x=-a_{N+2}$ for the amplitudes of the reflected and transmitted waves in the respective regions. Further, applying matching conditions, we get a set of $2(N+2)$ linear equations given by

$$
\begin{aligned}
&R_{10}e^{-ik_{10}a_1} = r_1e^{ik_{10}a_1} + t_2B_{20}e^{-ik_{20}a_1},\\
&A_{20}e^{ik_{20}a_1} = r_2B_{20}e^{-ik_{20}a_1} + t_1e^{ik_{10}a_1},\\
&B_{j0}e^{-ik_{j0}a_j} = r_jA_{j0}e^{ik_{j0}a_j} + t_{j+1}B_{(j+1)0}e^{-ik_{(j+1)0}a_j}, \qquad j=2,3,...,(N+1),\\
&A_{(j+1)0}e^{ik_{(j+1)0}a_j} = r_{j+1}B_{(j+1)0}e^{-ik_{(j+1)0}a_j} + t_jA_{j0}e^{ik_{j0}a_j}, \qquad j=2,3,...,(N+1),\\
&B_{(N+2)0}e^{-ik_{(N+2)0}a_{(N+2)}} = r_{N+2}A_{(N+2)0}e^{ik_{(N+2)0}a_{(N+2)}},\\
&T_{(N+3)0}e^{ik_{(N+3)0}a_{(N+2)}} = t_{N+2}A_{(N+2)0}e^{ik_{(N+2)0}a_{(N+2)}}.
\end{aligned}
\tag{4.30}
$$

The above set of equations are solved to obtain the unknown R_{10} and $T_{(N+3)0}$ which in turn gives the reflection and transmission coefficient for N number of articulations. The reflection and transmission coefficient follows the energy balance relation $K_r^2+K_t^2=1.$ Marchenko and Voliak (1996) presented a relation for the wave reflection and transmission coefficients R_N and T_N based on the coefficients of previous irregularities R_{N-1} and T_{N-1} for the periodic array of the floating structure. A simplified equation was obtained based on the geometric progressions for N number of plates having the same physical properties given by

$$R_N = R_{N-1} + \frac{\left(T_{N-1}\right)^2 e^{2ik_0 a_j} R_1}{1 - R_1 R_{N-1} e^{2ik_0 a_j}} \text{ and } T_N = \frac{T_{N-1} T_1 e^{ik_0 a_j} R_1}{1 - R_1 R_{N-1} e^{2ik_0 a_j}}, \tag{4.31}$$

where, R_1 and T_1 are the reflection and transmission coefficient for a single floating structure. Porter and Evans (2006) presented wide-spacing relation to calculate the reflection and transmission coefficient for a periodic array of N cracks of the form

$$R_N = \frac{R_1 \sigma_N}{\sigma_N - \lambda T_1 \sigma_{N-1}} \text{ and } T_N = \frac{T_1}{\lambda^{N-1}\left(\sigma_N - \lambda T_1 \sigma_{N-1}\right)}, \tag{4.32}$$

where $\sigma_N = \dfrac{\sin(N\alpha)}{\sin\alpha}$ and $\cos\alpha = \dfrac{\cos\left\{\arg\left(T_1\right) + k_0 a_j\right\}}{\left|T_1\right|}$ with R_1 and T_1 are the reflection and transmission coefficient for a single crack at $x = -a_1$ and for a wave incident from $x = \infty$, $\lambda = e^{ik_0 a_j}$. The numerical calculations performed based on the wide-spacing approximation method suggest that the pattern of the numerical results obtained by direct eigenfunction expansion method is similar to approximate formula as illustrated by Marchenko and Voliak (1996) and Porter and Evans (2006).

4.4 NUMERICAL RESULTS AND DISCUSSIONS

The scattering of waves due to the periodic arrays of multiple articulated floating elastic plate is analyzed for finite and shallow water depth using Timoshenko-Mindlin theory. The results obtained using the direct eigenfunction expansion method are compared with the wide-spacing approximation (WSA) method. The hydroelastic behaviour of plates in terms of reflection coefficient K_r, transmission coefficient K_t, deflection ζ_j, strain ε on the plate along with bending moment $M(x)$ and shear force $W(x)$ are analyzed. The following variables are considered to be fixed unless otherwise mentioned $E = 5\text{GPa}$, $\rho_p / \rho = 0.9$, $\nu = 0.3$ and $g = 9.8\text{ms}^{-2}$ for the comparison of numerical results in the case of multiple articulations. In order to check the accuracy of the numerical results, the wave reflection and transmission coefficients are observed to satisfy the energy relation $K_r^2 + K_t^2 = 1$.

The convergence of the evanescent mode for the determination of reflection and transmission coefficient in the case of single articulation considering $d / L = 0.05$,

$h/L=0.1$, $k_{33}=10^{10}$ Nm^{-1}, $k_{55}=10^{5}$ Nm/rad and $k_0h=10$ is presented in Table 4.3. The convergence in the wave reflection and transmission is observed to achieve for the evanescent mode $N\geq 20$. The non-dimensional bending moment along plate length for the articulated finite floating elastic plate is validated with the results obtained by Gao et. al. (2011) in Figure (4.2) considering the plate length $L=300\,\text{m}$, plate thickness $d=2\,\text{m}$, Young's modulus $E=11.9\,\text{GPa}$, density of plate $\rho_p=256.25\,\text{kg/m}^3$ and Poisson's ratio $\nu=0.13$.

Table 4.3: Convergence of evanescent modes.

No of evanescent modes (N)	Reflection Coefficient (Kr)	Transmission Coefficient (Kt)	Energy Relation
1	0.9945	0.1015	0.9993
5	0.9660	0.2540	0.9977
10	0.9848	0.1645	0.9969
15	0.9885	0.1405	0.9969
20	0.9883	0.1411	0.9966
25	0.9883	0.1409	0.9966
30	0.9883	0.1409	0.9966
35	0.9883	0.1409	0.9966
40	0.9883	0.1409	0.9966

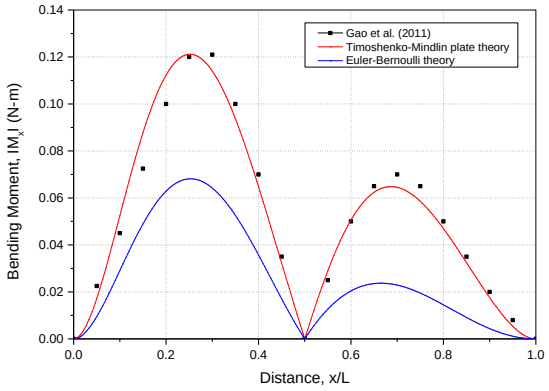

Figure 4.2: Non-dimensional bending moment along the plate length using Timoshenko-Mindlin plate theory, Euler- Bernoulli theory and Gao et. al. (2011).

The result obtained by Gao et al. (2011) for the articulated plate and the present approach using the orthogonal mode coupling relation based on Timoshenko Mindlin theory is observed to agree well. On the other hand, a significant variation in the non-dimensional bending moment using Euler-Bernoulli theory and Timoshenko Mindlin theory is observed which suggest that the rotary inertia and transverse shear deformation plays a significant role in the design and analysis of the very large floating structures of finite length.

4.4.1 Finite water depth

The scattering of waves due to the freely floating array of multiple articulated plates is analysed considering Timoshenko-Mindlin plate theory in the water of finite depth. The analysis for the wave reflection and transmission coefficient, deflection, strain in the floating elastic plate along with bending moment and shear force is performed using both direct eigenfunction expansion method and WSA method for the periodic array of multiple floating elastic plates to understand the scattering behaviour at varying water depth, plate thickness along with vertical and rotational spring stiffness.

4.4.1.1 Reflection and Transmission Coefficient

The relation for the wave reflection and transmission coefficients for the periodic arrays of multiple articulated floating elastic plate is the same as presented in Equation (4.24) for the direct eigenfunction expansion method. The wavenumber in the transmitted region is the same as the wave number in the incident region, so the relation for the K_r and K_t reduces to

$$K_r = \left|R_{10}\right| \text{ and } K_t = \left|T_{(N+3)0}\right|. \tag{4.33}$$

In Figure 4.3(a,b), the K_r and K_t are plotted varying $k_{10}h$ using both direct eigenfunction expansion method and WSA method. The wave reflection and transmission behaviour using the direct eigenfunction expansion method are compared with the WSA and also with the relation given by Marchenko and Voliak (1996) for two articulated floating elastic plates. The pattern of the reflection coefficient (Figure 4.3a) using direct method is observed to be similar with the WSA method. The variation of K_t versus the non-dimensional wave number as shown in Figure 4.3(b) is observed

to be of similar pattern for both the methods, implying the reliability of approximate methods for higher number of articulations in the periodic arrays of articulated floating plates. The slight variation in the wave reflection and transmission coefficient using the direct method and WSA method is observed, which is mainly due to neglecting the evanescent modes in the approximate methods. The reduction in wave transmission is observed for both the approximate methods as compared with the direct method, which is mainly due to the consideration of wide-spacing between the plates. The values of K_r and K_t are observed to be periodic in nature and the high wave transmission for certain higher values of the $k_{10}h$ is noted, which is due to the high wave oscillation in the articulated region. The reduction in the values of K_r is observed for the direct method as compared to wide-spacing approximation. The reduction in reflected waves is due to interference of waves due to periodic nature of the articulated joints in the floating elastic plate.

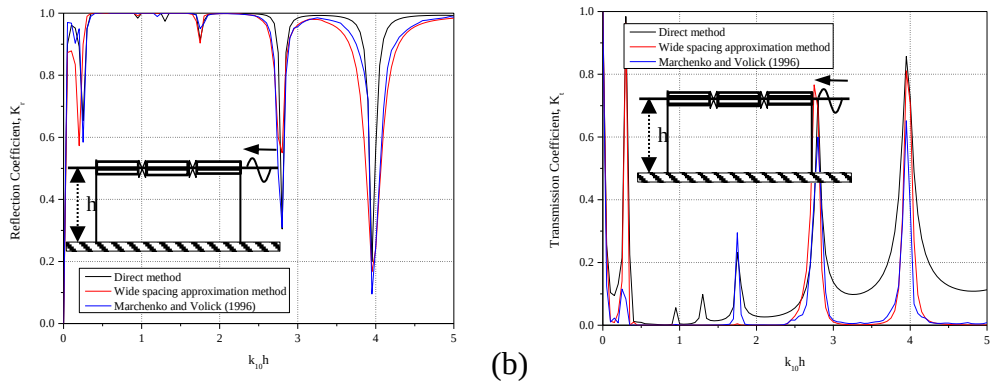

(a) (b)

Figure 4.3: (a) K_r and (b) K_t versus non-dimensional wavenumber using direct eigenfunction expansion method and WSA method for two articulated floating plates considering $h/L = 0.04$ and $d/L = 0.0047$.

In Figure 4.4(a,b), the variation in the K_r and K_t versus $k_{10}h$ is plotted for different number of articulation in the floating elastic plate. The minima in the wave reflection coefficient (Figure 4.4a) is observed with the increase in the values of the non-dimensional wavenumber $k_{10}h$. The minima in the reflection coefficient are higher for $4 < k_{10}h < 8$ and with the increase in the values of $k_{10}h$ the minima in the reflection coefficient increased for certain values of $k_{10}h$. The study suggests that for lower values of the wavelength the minima in the values of K_r is more as compared to longer

wavelengths. On the other hand, an opposite pattern is observed in the values of K_t as shown in Figure 4.4(b) and maxima in the transmission coefficient is higher for $4 < k_{10}h < 8$. The maxima in the transmission coefficient is termed as complete transmission of waves and the minima in the values of K_r indicates no-wave reflection. The complete reflection of waves is observed for lower values of $k_{10}h$ may be due to more waves of smaller wavelength getting trapped within the articulated region and as a result a maxima in K_r is noted. Further, with the increase in the number of articulations, the backward shift in the values of K_r is observed in Figure 4.4(a, b).

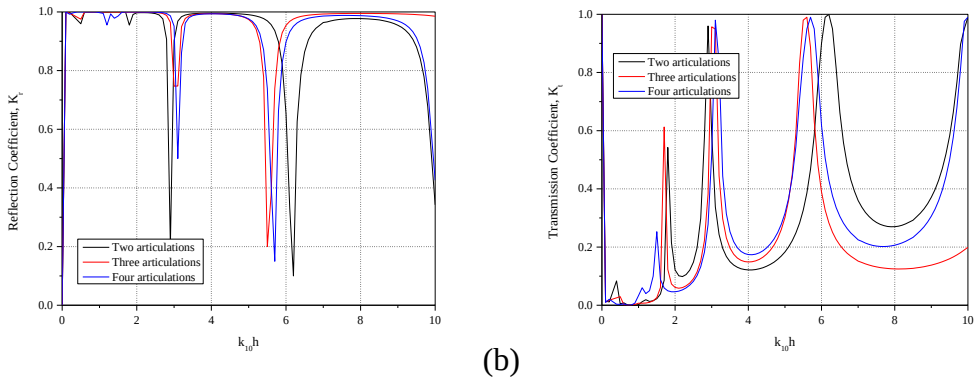

(a) (b)

Figure 4.4: (a) K_r and (b) K_t versus non-dimensional wavenumber for different number of articulations considering $h/L = 0.083$, $d/L = 0.0083$, $k_{33} = 10^5\,\text{Nm}^{-1}$ and $k_{55} = 10^5\,\text{Nm/rad}$.

In Figure 4.5(a,b), the variation in the K_r and K_t are plotted versus $k_{10}h$ for different values of k_{33} and k_{55}. In the case of the semi-rigid connection, the vertical linear and flexural rotational stiffness values $k_{33} < 10^5\,\text{Nm}^{-1}$ and $k_{55} < 10^5\,\text{Nm/rad}$, the variation in the K_r and K_t are observed to follow almost similar patterns and does not affect much on the wave transformation. On the other hand, the flexural rotational stiffness k_{55} is observed to be dominant as compared to vertical spring stiffness k_{33}. The higher values of k_{33} illustrate higher wave reflection as compared to the values of k_{55} whereas, an increase in the number of transmitted waves is observed for higher values of k_{33}. For very high values of both the spring stiffness k_{33} and k_{55}, the rigidity increases at the articulated joints and the array of multiple floating plates acts as a continuous plate.

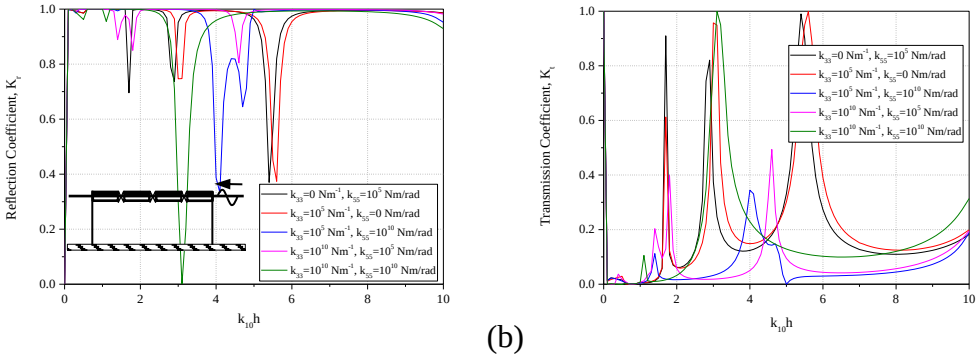

(a) (b)

Figure 4.5: (a) K_r and (b) K_t versus non-dimensional wavenumber $k_{10}h$ varying k_{33} and k_{55} in the case of three articulation considering $h/L = 0.083$ and $d/L = 0.0083$.

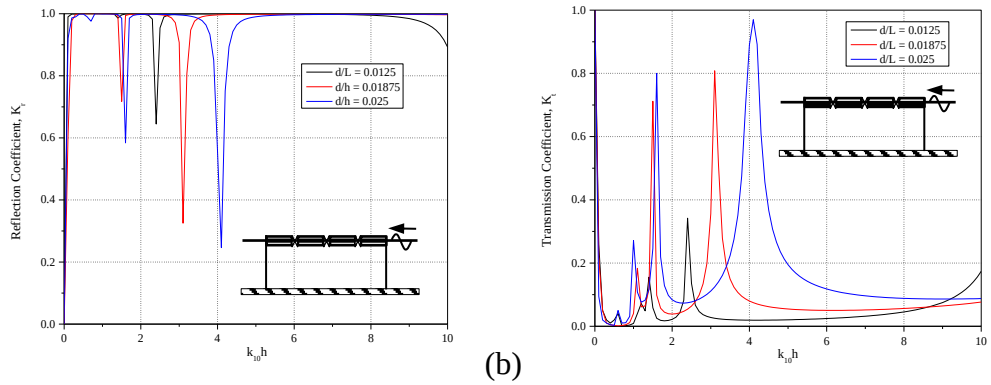

(a) (b)

Figure 4.6: (a) K_r and (b) K_t versus non-dimensional wavenumber $k_{10}h$ for varying plate thickness d/L in the case of three articulations considering $h/L = 0.125$, $k_{33} = 10^5$ Nm^{-1} and $k_{55} = 10^5$ Nm/rad.

In Figure 4.6(a,b), the variation of K_r and K_t are plotted versus $k_{10}h$ for different values of plate thickness d/L considering three articulation. The minima in the K_r is higher within $1 < k_{10}h < 3$ with the surge in the values of the plate thickness but with the increase in the values of $k_{10}h$, the complete reflection of waves and zero wave transmission is noted. The wave transmission reduces with the increase in the values of $k_{10}h$ as in Figure 4.6(b). The maxima in the transmission coefficient is higher for longer wavelength which may be due to the fact that more waves gets transmitted back for waves of longer wavelengths. Further, the wave reflection is observed to increase with the surge in plate thickness due to the surge in plate rigidity. The positive shift in the minima in K_r and maxima in K_t for higher values of $k_{10}h$ is noted with the surge in the

plate thickness which suggests that complete wave transmission for the articulated plate of higher thickness occurs for waves at shorter wavelengths.

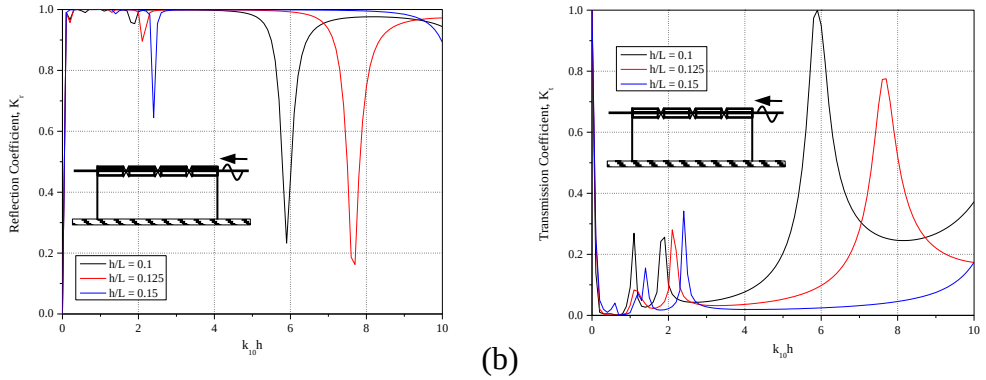

(a) (b)

Figure 4.7: (a) K_r and (b) K_t versus non-dimensional wavenumber $k_{10}h$ for varying water depth h/L in the case of three articulations considering $d/L = 0.0125$, $k_{33} = 10^5\,\text{Nm}^{-1}$ and $k_{55} = 10^5\,\text{Nm/rad}$.

The K_r and K_t are plotted versus $k_{10}h$ for different water depth h/L in Figure 4.7(a,b) in the case of three articulations. It is observed that with the surge in the water depth h/L the minima in the K_r is observed towards higher values of $k_{10}h$ which may be due to the increase in water depth h/L, more waves transmit for certain values of $k_{10}h$ and as a result minima in reflection is noted. The number of complete transmission of waves is observed for water depth $h/L = 0.1$ which may be due to the decrease in the oscillation of the wave for $h/L = 0.1$. The wave reflection is observed to decrease with the surge in the water depth h/L due to the surge in the oscillation of the waves as it propagates below the plate.

4.4.1.2 Plate deflection and strain in the floating plate

The deflection and wave-induced strain for an array of floating elastic plate with multiple articulation in the respective regions are given by

$$\zeta_j = \frac{i}{\omega}\phi_{jy} \quad \text{on} \quad y = 0, \quad j = 2,3,...,(N+2). \tag{4.34}$$

$$\varepsilon_j = \frac{d}{2}\partial_x^2\zeta_j = \frac{id}{2\omega}\partial_{x^2y}^3\phi_j \quad \text{at} \quad y = 0,\ j = 2,3,...,(N+2). \tag{4.35}$$

In Figure 4.8(a,b), the deflection for an array of multiple floating elastic plates connected with articulated joints are plotted for varying plate thickness d/L and water

depth h/L along the length of the floating elastic plate for a case of three articulations. The plate deflection is observed to reduce with the surge in plate thickness may be due to the surge in plate rigidity. A change in surface deflection is observed at the connecting joints due to the variation in the stiffness at the joints. The difference in surface deflection at the connecting joints are observed to increase with the surge in the values of plate thickness due to the higher stiffness in the corresponding plates. A surge in the values of plate deflection is also observed for the decrease in water depth, which is due to the increase in wave height for waves approaching shallower water depths.

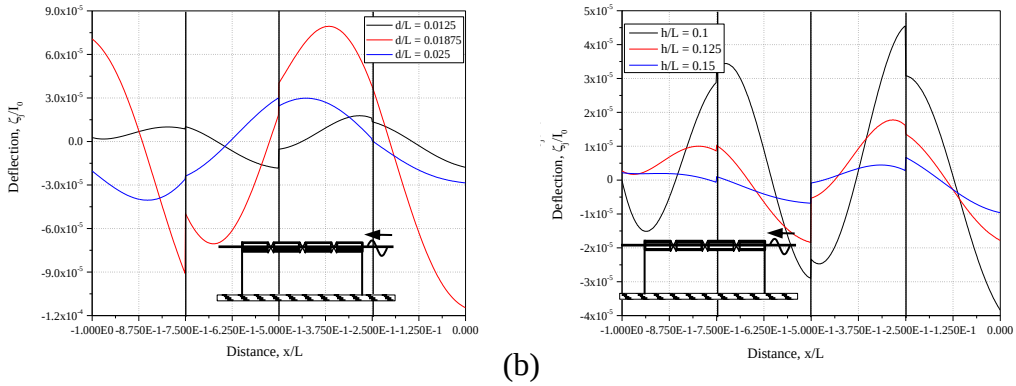

(a) (b)

Figure 4.8: Plate deflection along the length of the plate varying (a) non-dimensional plate thickness d/L and (b) non-dimensional water depth h/L in the case of three articulation considering $k_{33}=10^5\,\text{Nm}^{-1}$, $k_{55}=10^5\,\text{Nm/rad}$ and $k_{10}h=4.$

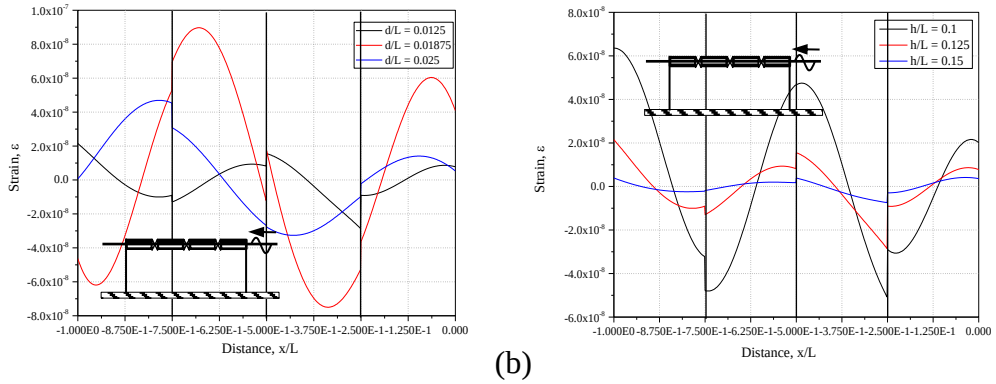

(a) (b)

Figure 4.9: Strain along the length of the plate varying (a) non-dimensional plate thickness d/L and (b) non-dimensional water depth h/L in the case of three articulation considering $k_{33}=10^5\,\text{Nm}^{-1}$, $k_{55}=10^5\,\text{Nm/rad}$ and $k_{10}h=4.$

In Figure 4.9(a,b), the strain along the array of the floating plate with three articulated joints is analyzed for varying plate thickness and water depth. The wave-induced strain is observed to decrease with the surge in the plate thickness, which is mainly due to the increase in restraints of the floating elastic plate for higher plate thickness. The strain

is observed to be negligible at the edges of the plate due to the considerations of free edge support condition. The increase in the values of the strain is observed for decreasing values of water depth, which is due to the surge in wave height as the wave approaches shallower water depths. It may be noted that, the strain at the plate edges increases with the surge in the water depth due to the free edge conditions. The difference in the strain at the connecting joints are observed to increase with the surge in the values of plate thickness due to the higher stiffness in the corresponding plates.

4.4.1.3 Bending moment and shear force

The bending moment and shear force for the articulated floating elastic plate due to the interaction of wave are given by the relation

$$M(x) = EI\partial_y^3\phi_j \quad \text{on} \quad y=0,\ j=2,3,...,(N+2). \tag{4.36}$$

$$W(x) = EI\left\{\partial_{xy^3}^4\phi_j - \wp\partial_{xy}^2\phi_j\right\} \quad \text{on} \quad y=0,\ j=2,3,...,(N+2). \tag{4.37}$$

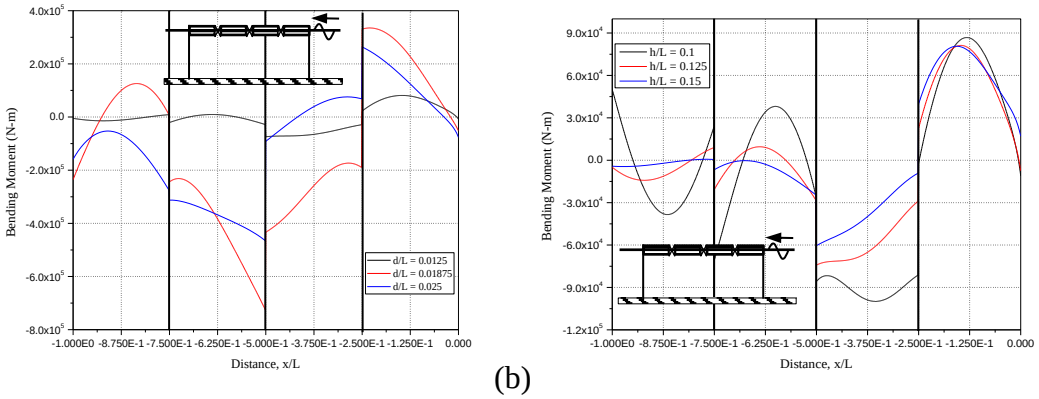

(a) (b)

Figure 4.10: Bending moment along the length of the plate varying (a) non-dimensional plate thickness d/L and (b) non-dimensional water depth h/L in the case of three articulation for $k_{33} = 10^5\,\text{Nm}^{-1}$, $k_{55} = 10^5\,\text{Nm/rad}$ and $k_{10}h = 4$.

In Figure 4.10(a,b), the bending moment for an array of floating elastic plate with three articulations is plotted along the length of the plate for varying plate thickness and water depth. The bending moment resultants are observed to be lower towards the transmission region due to the existence of articulated joints along the plate length. The bending moment along the plate length is observed to be within $-8\times10^5\,\text{Nm} < M(x) < 4\times10^5\,\text{Nm}$ and it is negligible at the plate edges due to free-free edge support condition. The bending moment resultants are observed to increase with the surge in plate thickness due to the surge in flexural rigidity. On the other hand, with

the decrease in the non-dimensional water depth, the bending moment along the floating elastic plate with articulated joints increases due to the increase in wave height in shallower water depth. The increase in bending moment of the floating plate at the connecting joints are due to the surge in the values of plate thickness due to the higher stiffness along the corresponding plates.

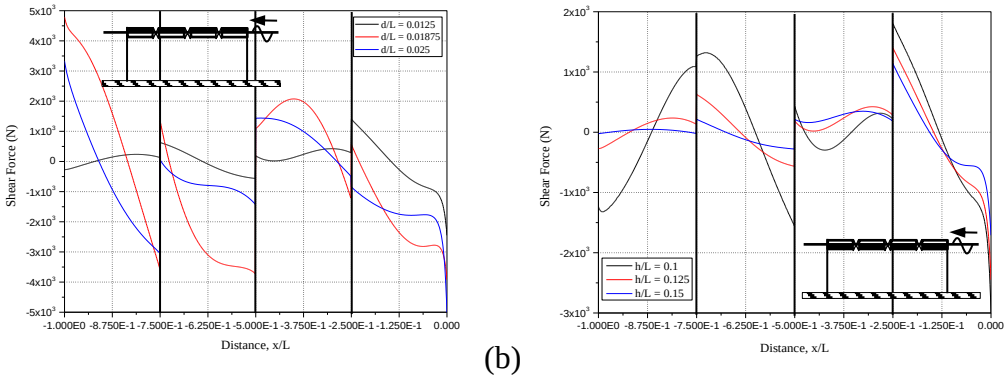

(a) (b)

Figure 4.11: Shear force along the length of the plate varying (a) non-dimensional plate thickness d/L and (b) non-dimensional water depth h/L in the case of three articulation considering $k_{33}=10^5\,\text{Nm}^{-1}$, $k_{55}=10^5\,\text{Nm/rad}$ and $k_{10}h=4$.

In Figure 4.11(a,b), the shear force for an array of an articulated floating elastic plate are plotted along the plate length with varying plate thickness and water depth for three articulations. An increase in the values of shear force resultants is observed with the surge in the plate thickness due to the surge in flexural rigidity. The shear force of the elastic plate is observed within $-5\times10^3\,\text{N}<W(x)<5\times10^3\,\text{N}$. The shear force resultants reduce as the waves progress along the plate length towards the transmitted region in the presence of the articulated joints along the plate. Further, the shear force for the array of floating elastic plate connected with spring stiffness decreases with the surge in the values of water depth due to the surge in wave height in shallower water depth. An increase in shear force at the connecting joints are observed with the surge in plate thickness due to the higher stiffness in the corresponding plates.

4.4.2 Shallow water approximation

In this subsection, the wave scattering due to the array of floating elastic plate with articulated joints is analyzed considering shallow water approximation. The hydroelastic behaviour is analyzed for different number of connecting joints to understand the effect of increase in the articulations in the floating elastic plate.

4.4.2.1 Reflection and transmission coefficient

The relation for the wave reflection and transmission coefficients for an array of floating elastic plate with connecting joints based on shallow water approximation are same as given by Equation (4.33). In Figure 4.12(a,b), the K_r and K_t are plotted varying $k_{10}h$ for different number of articulations of the floating elastic plate. The increase in the wave reflection is observed with the surge in number of articulations which is mainly due to the increase in the restraint from the connecting joints as shown in Figure 4.12(a). A regular pattern in the behaviour of reflected and transmitted waves are observed to increase indicating the complete transmission of waves with the increase in number of articulations. A sudden surge in wave transmission is observed at regular intervals, and the resonating patterns are observed to increase with the decrease in number of articulations. The transmission coefficient K_t with unity signifies complete wave transmission which is observed to reduce with the increase in the number of articulations as shown in Figure 4.12(b).

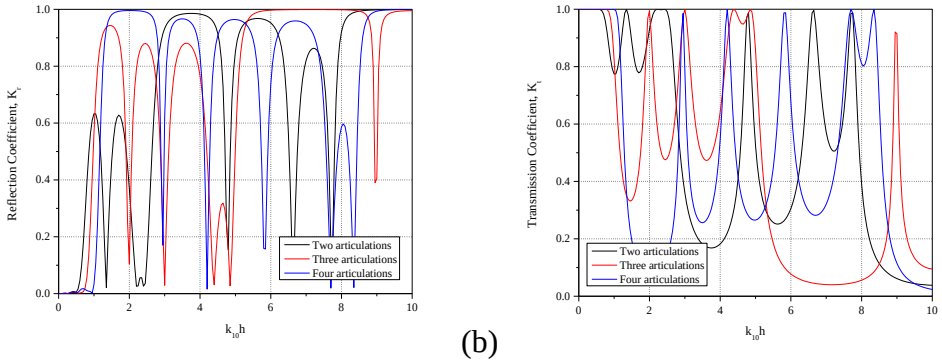

(a) (b)

Figure 4.12: (a) Reflection and (b) transmission coefficient versus non-dimensional wavenumber for different number of articulations considering $h/L = 0.083$, $d/L = 0.083$, $k_{33} = 10^5$ Nm^{-1} and $k_{55} = 10^5$ Nm/rad.

4.4.2.2 Plate deflection and wave-induced strain

The plate deflection and wave-induced strain for an array of floating elastic plate with connecting joints in shallow water depth are given by the relation

$$\zeta_j = \frac{ih}{\omega}\partial_x^2\phi_j \quad \text{for } j = 2,3,...,(N+2). \tag{4.38}$$

$$\varepsilon_j = \frac{d}{2}\partial_x^2\zeta_j = \frac{idh}{2\omega}\partial_x^4\phi_j, \text{ for } j = 2,3,...,(N+2). \tag{4.39}$$

The plate deflection and strain along the plate length are plotted for different number of articulations in shallow water depth as shown in Figure 4.13 (a,b). In Figure 4.13(a), the plate deflection for an array of floating elastic plate with articulated joints is plotted along the plate length. The plate deflection is observed to reduce with the surge in number of articulations due to the presence of additional connecting joints. A slight discontinuity is observed at the connecting joints due to lower stiffness as compared with the corresponding plates. It is also observed that the deflection is reduced as the wave progress towards the transmitted region, due to the restraints at the connecting joints. The surface deflection is high at the plate edge due to the consideration of free - free support condition. The plate deflection is observed within $-0.015 < \zeta_j(x) < 0.07$ and the plate deflection gets reduced at the plate edges with the surge in the number of articulations.

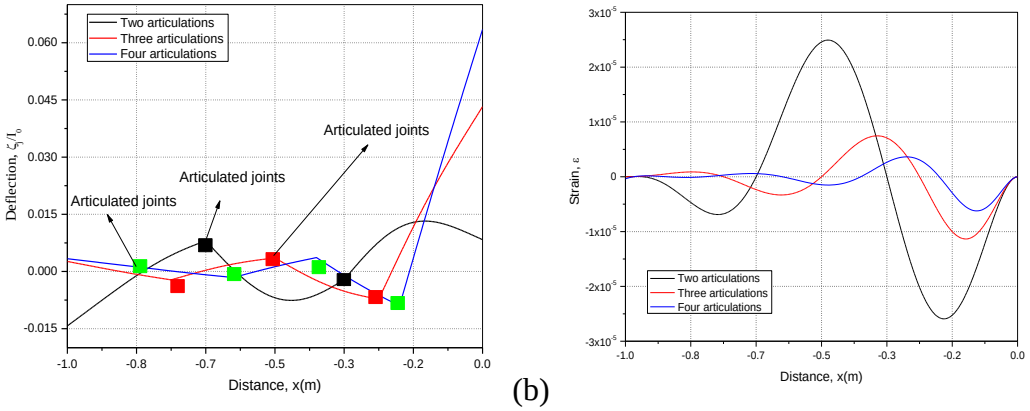

(a) (b)

Figure 4.13: (a) Plate deflection and (b) strain along the plate length for different number of articulations considering $k_{10}h = 5$, $h/L = 0.167$, $d/L = 0.0167$, $k_{33} = 10^5\,\text{Nm}^{-1}$ and $k_{55} = 10^5\,\text{Nm/rad}$.

In Figure 4.13(b), the strain-induced for an array of the floating plate with multiple articulations are analysed for different number of articulations. The wave-induced strain is observed to decrease with the surge in the number of articulations mainly due to the increase in restraints. The strain is observed to decrease as the wave progress along the plate length towards the transmitted region due to the restraints caused by the connecting joints. The strain is observed to be negligible at the connecting joints due to lower stiffness as compared with the corresponding plates. The strain is noted to be within $-3\times10^{-5} < \varepsilon < 3\times10^{-5}$ and is negligible at the edges due to the consideration of free-edge condition.

4.4.2.3 Bending moment and shear force

The bending moment and shear force of the articulated floating elastic plates are given by

$$M_j(x) = EI\partial_x^4\phi_j,\ j = 2,3,...,(N+2). \tag{4.40}$$

$$W_j(x) = EI\left\{\partial_x^5\phi_j - \wp\partial_x^3\phi_j\right\},\ j = 2,3,...,(N+2). \tag{4.41}$$

In Figure 4.14(a), the bending moment for an array of floating elastic plate connected by multiple articulations is plotted along the plate length for different articulations. The bending moment resultants are observed to reduce with the surge in number of articulations which may be due to the increase in number of restraints along the plate length. The bending moment is observed to approach closer to zero at the connecting joints due to lower stiffness as compared with the corresponding plates. The bending moment of the elastic plate observed to be within $-8\times10^4\,\text{Nm} < M(x) < 8\times10^4\,\text{Nm}$ and it is negligible at the plate edge due to free-free support condition. The bending moment resultants are observed to reduce with the progress of wave along the length towards the transmission end of the plate which may be due to the restraints at the connecting joints.

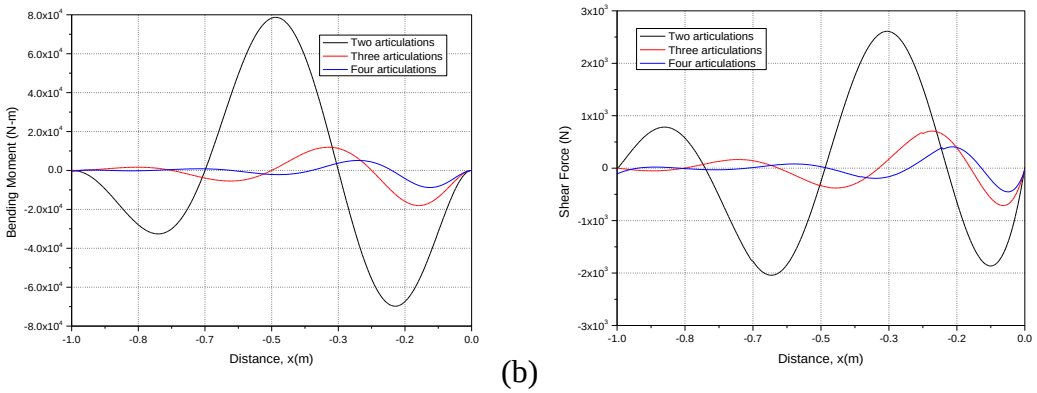

(a) (b)

Figure 4.14: (a) Bending moment and (b) shear force resultants along the plate length for different number of articulations in the floating elastic plate at $k_{10}h = 5$, $h/L = 0.167$, $d/L = 0.0167$, $k_{33} = 10^5\,\text{Nm}^{-1}$ and $k_{55} = 10^5\,\text{Nm/rad}$.

The shear force resultant is plotted along the plate as in Figure 4.14(b) for different articulations. The shear force resultants are observed to reduce with the surge in number of articulations due to the increase in the number of restraints along the plate length. The shear force approaches high values at the connecting joints due to lower stiffness

as compared with the corresponding plates. The shear force for an array of floating elastic plate is within $-3\times10^{3}\,\mathrm{N} < W(x) < 3\times10^{3}\,\mathrm{N}$ and it is negligible at the plate edge due to free-free support condition. The shear force resultants are observed to reduce with the progress of wave along the plate length towards the transmission region may be due to the presence of restraints at the connecting joints.

4.5 CONCLUSIONS

In this present study, the wave scattering from an array of multiple articulations in floating elastic plate considering Timoshenko-Mindlin's plate theory is analyzed in finite and shallow water depths. The hydroelastic behaviour of articulated floating elastic plates due to the action ocean waves is analyzed for different vertical linear and flexural rotational spring stiffness. The mathematical model for the floating thick elastic plate with articulated edge condition is presented and analyzed using the eigenfunction expansion approach and orthogonal mode-coupling relation. The direct method as used for the wave scattering due to the single articulated floating elastic plate is extended for multiple articulations in floating elastic plate and compared with the wide spacing approximation method. The following conclusions are drawn from the present study:

- The reflection coefficient does not show any significant variations using both direct eigenfunction expansion method and WSA method, whereas slight variations are observed for the case of transmission coefficient due to considerations of wide-spacing in between the plates and also neglecting the effect of evanescent wave modes in the approximate methods.
- The backward shift in the pattern of wave reflection and transmission coefficient is observed with the surge in the number of articulations. As the stiffness increases to a certain limit, the array of periodic multiple plates behaves as a continuous plate showing complete transmission of waves.
- The change in the hydroelastic behavior is observed at the connecting joints, which is found to increase with the surge in the values of plate thickness due to the higher stiffness in the corresponding plates at finite water depth.
- The shallow water depth showed an increase in the wave reflection with the increase in the number of articulations for the change in stiffness at the connecting joints.

- A sudden surge in wave transmission is noted at regular intervals, which increases with the decrease in number of articulations.
- The complete transmission of waves is observed to reduce with the increase in the number of articulations because the waves get trapped at the articulated joints.
- The hydroelastic behaviours in the form of plate deflection, strain, bending moment and shear force gets reduced with the increase in number of articulations along the length of the plate in shallow water depth.
- The hydroelastic behaviour is also observed to decrease along the plate length towards the transmitted region due to the interaction with the connecting joints, which restrain the propagation of waves.
- The wave reflection is observed to increase with the reduction of transmitted wave due to the existence of articulations in the floating plate, which has to be carefully studied for the design of floating structures and placement of spring stiffness along the plate.
- The plate thickness and plate rigidity constitute an important role in the mitigation of hydroelastic behaviour of the floating elastic plate.

CHAPTER 5

WAVE TRANSFORMATION DUE TO CHANGES IN BOTTOM TOPOGRAPHY

5.1 GENERAL INTRODUCTION

In the previous chapter, the wave scattering due to the array of multiple articulations in floating elastic plate is analysed based on Timoshenko-Mindlin's plate theory in finite water depth and shallow water approximations. The significance of connectors with linear and/or rotational spring stiffness in analysing the hydroelastic behaviour of articulated floating plates is also studied. Further, the application of wide-spacing approximation method in the hydroelastic analysis of periodic array of multiple articulated floating elastic plate is presented.

In this chapter, the wave transformation due to floating elastic plate over a varying sea bottom profile is studied based on Timoshenko-Mindlin plate theory. The analysis is carried out for different types of bottom topography below a floating elastic plate acted upon by ocean waves. The mathematical model is developed based on the eigenfunction expansion method to analyse the hydroelastic behaviour of a thick floating elastic plate varying water depths, step thickness and plate sizes acted upon by waves along the plate. The numerical computation is performed and the hydroelastic characteristics of the floating elastic plate is analysed in terms of plate deflection, wave induced strain, bending moment and shear force acted upon by ocean waves. Further, a detail comparison of the numerical results is performed for different types of bottom topography in the hydroelastic analysis of floating elastic plates. The present study will provide an insight into the effect of seabed profile for the waves interacting with large floating elastic plate in finite water depth.

5.2 MATHEMATICAL FORMULATION

The propagation of wave along the floating elastic platform based on Timoshenko-Mindlin theory over the varying sea bed profile is formulated considering linearized wave theory. A 2D plate along the x-y plane is modelled with the *y*-axis positive downward represents the water depth from the free surface and *x*-axis representing the

direction of the incident wave as illustrated in Figure 5.1. The fluid domain consists of finite floating elastic platform in the region $I_j \equiv \left(-a_j < x < -a_{j-1}\right)$ at $0 < y < h_j$ for $j = 2,3....,N$ with an upstream incident wave region of the fluid domain consisting of an open water region $I_1 \equiv \left(-a_1 < x < \infty\right)$ at $0 < y < h_1$, and the downstream transmission region of an open water region $I_{N+1} \equiv \left(-\infty < x < -a_N\right)$ at $0 < y < h_{N+1}$. The floating elastic platform is considered to be freely floating having the free edge support condition at the plate edges $x = -a_1$ and $x = -a_N$. The floating elastic platform is assumed to have significant thickness and modelled under the assumption of Timoshenko-Mindlin plate theory.

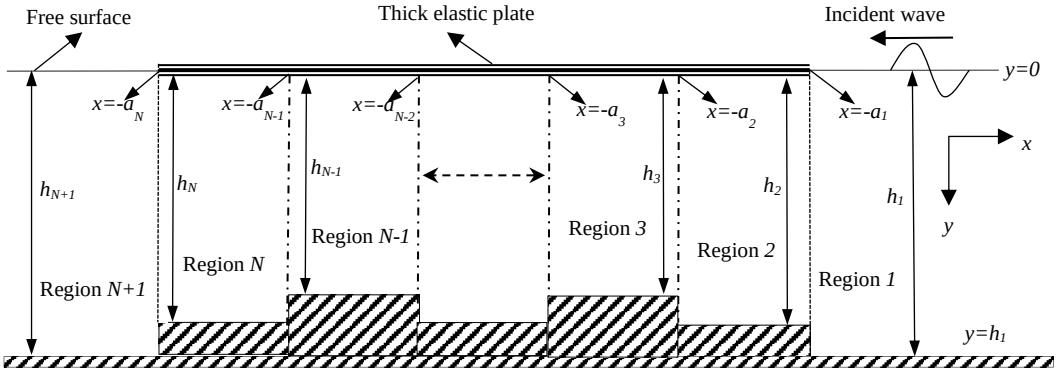

Figure 5.1: Schematic diagram for floating elastic platform over varying bottom topography.

The wave propagating over the ocean surface is assumed to be inviscid, incompressible and the motion is irrotational and simple harmonic in time with angular frequency. So, the assumption ensures that the velocity potential $\Phi_j\left(x,y,t\right)$ and the surface deflection $\zeta_j\left(x,t\right)$ are of the form $\Phi_j\left(x,y,t\right) = \mathrm{Re}\left\{\phi_j\left(x,y\right)\right\}e^{-i\omega t}$ and $\zeta_j\left(x,t\right) = \mathrm{Re}\left\{\zeta_j\left(x\right)\right\}e^{-i\omega t}$ where Re denotes the real part. Thus, the spatial velocity potential $\phi_j(x,y)$ satisfy the governing equation given by

$$\nabla^2\phi_j(x,y) = 0 \quad \text{at} \quad -\infty < x < \infty,\ 0 < y < h_j,\ j = 1,2,...,N+1. \tag{5.1}$$

The linearized free surface boundary condition in the open water region is of the form

$$\phi_{jy}\left(x,y\right) - \kappa\phi_j\left(x,y\right) = 0, \quad j = 1, N+1, \quad \text{for } x > -a_1 \text{ and } x < -a_N. \tag{5.2}$$

where $\kappa = \omega^2 / g.$

Combining the kinematic and dynamic free surface boundary condition along with the Timoshenko-Mindlin equation for thick plate, the plate covered boundary condition for $-a_N < x < -a_1$ is obtained as

$$\left\{\frac{EI}{\left(\rho g - m_s\omega^2\right)}\partial_x^4 + \left(\frac{m_s\omega^2 I}{\left(\rho g - m_s\omega^2\right)} - S\right)\partial_x^2 + \left(1 - \frac{m_s\omega^2 IS}{EI}\right)\right\}\partial_y\phi_j + \frac{\rho\omega^2}{\left(\rho g - m_s\omega^2\right)}\left\{1 - \frac{m_s\omega^2 IS}{EI} - S\partial_x^2\right\}\phi_j = 0,\ j = 2,3,...,N. \tag{5.4}$$

where $EI = Ed^3/12(1-\nu^2)$ is the plate rigidity, $G = E/2(1+\mu)$ is the shear modulus of the plate. $I = d^2/12$ is the rotary inertia, and $S = EI/\mu Gd$ is the shear deformation. The bottom boundary condition for the change in the bottom topography is given by

$$\frac{\partial\phi}{\partial n} = 0, \tag{5.4}$$

where n is the outward drawn normal at the bottom surface. The continuity equations for the velocity and pressure at the step edges and the free edge $x = -a_j,\ 0 < y < h_{j+1}$ for $j = 1,2,3...N$ is given by

$$\phi_{jx} = \phi_{(j+1)x} \text{ and } \phi_j = \phi_{(j+1)} \text{ at } x = -a_j,\ 0 < y < h_{j+1} \text{ for } j = 1,2,...,N. \tag{5.5}$$

In the case of a freely floating elastic plate, the bending moment and shear force at the edges $x = -a_1$ and $-a_N$ vanishes and are given by

$$\partial_y^3\phi_j(x,y) = 0 \text{ and } \partial_{xy^3}^4\phi_j(x,y) = \wp\partial_{xy}^2\phi_j(x,y),\ j = 2,N \text{ at } y = 0. \tag{5.6}$$

with $\wp = m\omega^2(S+I)/EI$. In addition, due to the presence of the step bottom topography, the continuity of deflection, slope, bending moment and shear force at the step interfaces $x = -a_j, 0 < y < h_{j+1}$ for $j = 2,3...,N-1$ (as in Karmakar et al., 2010) is of the form

$$\begin{aligned}
&\partial_y\phi_j(x,y) = \partial_y\phi_{(j+1)}(x,y), \quad \partial_{xy}^2\phi_j(x,y) = \partial_{xy}^2\phi_{(j+1)}(x,y),\\
&\partial_y^3\phi_j(x,y) = \partial_y^3\phi_{(j+1)}(x,y), \quad \left(\partial_{xy^3}^4 - \wp\partial_{xy}^2\right)\phi_j(x,y) = \left(\partial_{xy^3}^4 - \wp\partial_{xy}^2\right)\phi_{(j+1)}(x,y).
\end{aligned} \tag{5.7}$$

Finally, the far-field radiation condition is given by

$$\phi_j(x) = \begin{cases} \left(e^{-ik_{10}x} + R_{10}e^{ik_{10}x}\right) f_{10}(y) & \text{as} \quad x \to \infty, \\ T_{(N+1)0}e^{-ik_{(N+1)0}x} f_{(N+1)0}(y) & \text{as} \quad x \to -\infty, \end{cases} \tag{5.8}$$

with R_{10} and $T_{(N+1)0}$ are the complex wave amplitudes in the reflected and transmitted regions. The eigenfunctions $f_{j0}(y)$'s for $j = 1, N+1$ are of the form $f_{j0}(y) = \cosh k_{j0}(h-y)/\cosh k_{j0}h$ and k_{j0} for $j = 1, N+1$ are the positive real roots satisfies the dispersion relation in the case of finite water depth given by

$$k_{j0} \tanh k_{j0}h_j - \omega^2/g = 0. \tag{5.9}$$

The constant k_{j0} for $j = 1, N+1$ are the component of the wave numbers along the x-axis associated with the incident and transmitted waves. In the next subsection, the different types sea-bed bottom profile is discussed in detail to understand the behavior of the gravity wave transformation due to the floating thick elastic plate.

5.2.1 Different types of sea bottom profile

The wave transformation due to the waves interaction with the finite floating elastic thick platform over bottom topography with different sea bottom profiles are studied in detail. The multiple stepped type seabed profile is considered as the generalisation of the varying sea bottom profiles. In the present study, four different types of multiple step sea bottom profiles such as (a) single step-type, (b) sloping, (c) hump and (d) double hump is considered as shown in Figure 5.2(a-d).

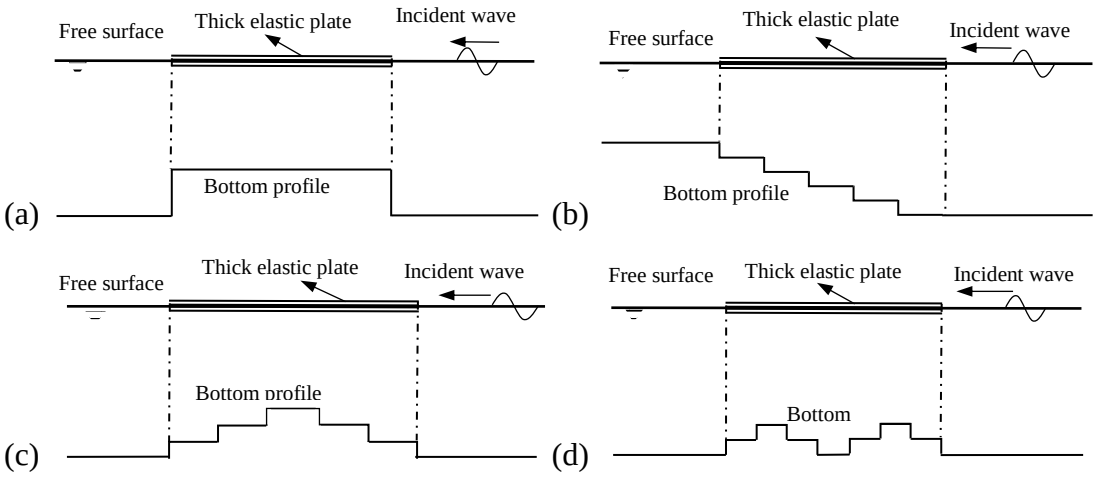

Figure 5.2. Schematic diagram for different types of sea bottom profile (a) Step-type, (b) Sloping, (c) Hump and (d) Double hump.

In the next section, the detail solution procedure for the wave scattering due to finite floating elastic platform over varying seabed profile is presented and discussed in detail.

5.3 METHOD OF SOLUTION

In this section, the solution procedure for the wave scattering due to varying seabed profile along the floating elastic plate acted upon by ocean waves are presented in the case of finite water depth. The bottom topography is divided into multiple steps to simplify the bottom profile. In the first case, the solution procedure for wave scattering due to single step bottom profile along the floating elastic plate is discussed and afterwards, the solution procedure is extended directly to multiple steps varying sea bottom profile. Finally, different patterns of multiple steps are analysed to understand different types of sea bottom profile.

5.3.1 Single step bottom topography

In this sub-section, the wave coefficient in the reflected and transmitted regions are calculated for the wave interaction with floating thick elastic platform over single step bottom profile in finite water depth. The boundary value problem (BVP) for the wave scattering due to finite floating elastic platform over single step bottom profile with free edge support condition is formulated. The velocity potentials $\phi_j(x,y)$ for $j=1,2,3$ satisfies the governing Equation (5.1) along with the boundary condition (5.2), (5.3), (5.4) and (5.8) as defined in section 2. The velocity potentials $\phi_j(x,y)$ for $j=1,2,3$ at the free surface and the plate covered regions are of the form

$$\phi_1(x,y)=\left(I_{10}e^{-ik_{10}x}+R_{10}e^{ik_{10}x}\right)f_{10}(y)+\sum_{n=1}^{\infty}R_{1n}e^{-\kappa_{1n}x}f_{1n}(y) \qquad \text{for } x>-a_1, 0<y<h_1,$$

$$\phi_2(x,y)=\sum_{n=0,I}^{II}\left(A_{2n}e^{-ik_{2n}x}+B_{2n}e^{ik_{2n}x}\right)f_{2n}(y)+\sum_{n=1}^{\infty}\left(A_{2n}e^{\kappa_{2n}x}+B_{2n}e^{-\kappa_{2n}x}\right)f_{2n}(y)$$
$$\text{for } -a_2<x<-a_1, 0<y<h_2,$$

$$\phi_3(x,y)=T_{30}e^{-ik_{30}x}\ f_{30}(y)+\sum_{n=1}^{\infty}T_{3n}e^{\kappa_{3n}x}f_{3n}(y) \qquad \text{for } x<-a_2, 0<y<h_3. \tag{5.10}$$

where $R_{1n}, n=0,1,2....$, $A_{2n}, B_{2n}, n=0,I,II,1,2....$ and $T_{3n}, n=0,1,2....$ are the unknown amplitudes in the respective regions to be determined.

The eigenfunction $f_{jn}(y)$'s as in Equation (5.10) is of the form

$$f_{jn}(y)=\frac{\cosh k_{jn}\left(h_j-y\right)}{\cosh k_{jn}h_j} \text{ for } n=0,I,II \text{ and } f_{jn}(y)=\frac{\cos k_{jn}\left(h_j-y\right)}{\cos k_{jn}h_j} \text{ for } n=1,2,..$$

(5.11)

where k_{jn} for $j=1,3$ and $n=0$ are the eigenvalues obtained based on the open water dispersion relation given by

$$k_{jn}\tanh k_{jn}h_j-\omega^2/g=0, \tag{5.12}$$

with $k_{jn}=i\kappa_{jn}$ for $j=1,3,\ n=1,2....$ Solving the relation as in Equation (5.12), we obtain one real root k_{j0} and an infinite number of purely imaginary roots κ_{jn} for $n=1,2....$ In the case of plate covered region the eigenvalues k_{jn} at $j=2$ are based on the plate covered dispersion relation given by

$$\left(\alpha_0-\alpha_1k_{jn}^2+\alpha_2k_{jn}^4\right)k_{jn}\tanh k_{jn}h_j-\left(\beta_0-\beta_1k_{jn}^2\right)=0, \tag{5.13}$$

where $\alpha_0=\left\{1-m_s\omega^2\left(\frac{IS}{EI}\right)\right\}$, $\alpha_1=\left\{\frac{m_s\omega^2I}{\left(\rho g-m_s\omega^2\right)}-S\right\}$, $\alpha_2=\frac{EI}{\left(\rho g-m_s\omega^2\right)}$,

$\beta_0=\frac{\rho\omega^2}{\left(\rho g-m_s\omega^2\right)}\left(1-m_s\omega^2\frac{IS}{EI}\right)$, $\beta_1=-\frac{\rho\omega^2S}{\left(\rho g-m_s\omega^2\right)}$, $m_s=\rho_p d$ is the mass per unit area. On solving the relation as in Equation (5.13), we obtain one real root k_{j0} and four complex roots k_{jn} for $n=I,II,III,IV$ of the form $\pm\alpha\pm i\beta$ along with an infinite numbers of purely imaginary roots $k_{jn}=i\kappa_{jn}$ for $n=1,2....$ The eigenfunctions $f_{jn}(y)$ satisfy the orthogonal mode-coupling relation in the open water and plate covered region given by

$$\left\langle f_{jm},f_{jn}\right\rangle_{j=1,3}=\begin{cases}0 & \text{for } m\neq n,\\ C_n' & \text{for } m=n,\end{cases} \text{ and } \left\langle f_{jm},f_{jn}\right\rangle_{j=2}=\begin{cases}0 & \text{for } m\neq n,\\ C_n'' & \text{for } m=n,\end{cases} \tag{5.14}$$

where $C_n'=\frac{2k_{jn}h_j+\sinh 2k_{jn}h_j}{4k_{jn}\cosh^2 k_{jn}h_j}$, $j=1,3.$

$$C_n''=\frac{(\alpha_0-\alpha_1k_{2n}^2+\alpha_2k_{2n}^4)2k_{2n}h_2+(\alpha_0-3\alpha_1k_{2n}^2+5\alpha_2k_{2n}^4)\sinh 2k_{2n}h_2+(4\beta_1k_{2n}\cosh^2 k_{2n}h_2)}{(4k_{2n}\cosh^2 k_{2n}h_2)(\alpha_0-\alpha_1k_{2n}^2+\alpha_2k_{2n}^4)},$$

which satisfies

$$\left\langle f_{jm},\, f_{jn}\right\rangle_{j=1,3} = \int_0^{h_j} f_{jm}(y)\, f_{jn}(y)dy, \tag{5.15}$$

$$\begin{aligned}\left\langle f_{2m},\, f_{2n}\right\rangle = \int_0^{h_2} f_{2m}(y)\, f_{2n}(y)dy - \frac{\alpha_1}{Q(k_{2n})}\left\{ f'_{2m}(0)\, f'_{2n}(0)\right\} \\ + \frac{\alpha_2}{Q(k_{2n})}\left\{ f'''_{2m}(0)\, f'_{2n}(0) + f'_{2m}(0)\, f'''_{2n}(0)\right\} + \frac{\beta_1}{P(k_{2n})}\, f_{2m}(0)\, f_{2n}(0),\end{aligned} \tag{5.16}$$

$P(k_{2n}) = \left(\alpha_0 - \alpha_1 k_{2n}^2 + \alpha_2 k_{2n}^4\right)$ and $Q(k_{2n}) = \left(\beta_0 - \beta_1 k_{2n}^2\right)$. The constant term C'_n, C''_n, $P(k_{2n})$ and $Q(k_{2n})$ for $n = 1, 2, \ldots$ are determined by replacing $k_{jn} = i\kappa_{jn}$ for $j = 1, 2, 3$.

In order to determine the unknown constants, the mode-coupling relation as in Equation (5.16) is applied on the velocity potential $\phi_2(x, y)$ at $x = -a_1$ and the eigenfunction $f_{2m}(y)$ given by

$$\begin{aligned}\left\langle \phi_2(-a_1, y),\, f_{2m}(y)\right\rangle = \int_0^{h_2} \phi_2(-a_1, y)\, f_{2m}(y)dy - \frac{\alpha_1}{Q(k_{2n})}\left\{\phi'_2(-a_1, y)\, f'_{2m}(0)\right\} \\ + \frac{\alpha_2}{Q(k_{2n})}\left\{\phi'''_2(-a_1, y)\, f'_{2m}(0) + \phi'_2(-a_1, y)\, f'''_{2m}(0)\right\} + \frac{\beta_1}{P(k_{2n})}\phi_2(-a_1, y)\, f_{2m}(0).\end{aligned} \tag{5.17}$$

The orthogonal property of the eigenfunction $f_{2m}(y)$ as in Equation (5.16) is used along with the expressions for velocity potentials as in Equation (5.10) and further applying the continuity equation for pressure as in Equation (5.5) across the interface $x = -a_1,\ 0 < y < h_2$ along with the edge condition as in Equation (5.6) to obtain

$$\begin{aligned}\left(R_{10}e^{-ik_{10}a_1}\right)\int_0^{h_2} f_{10}(y)\, f_{2m}(y)dy + \sum_{n=0}^{\infty} R_{1n}e^{\kappa_{1n}a_1}\int_0^{h_2} f_{1n}(y)\, f_{2m}(y)dy + \left\{\sum_{n=0,I}^{II}\left(A_{2n}e^{ik_{2n}a_1} + B_{2n}e^{-ik_{2n}a_1}\right)\right. \\ \left. + \sum_{n=1}^{\infty}\left(A_{2n}e^{-\kappa_{2n}a_1} + B_{2n}e^{\kappa_{2n}a_1}\right)\right\}\left\{\frac{\alpha_2}{Q(k_{2n})}\left\{ f'_{2n}(0)\, f'''_{2m}(0)\right\} - \frac{\alpha_1}{Q(k_{2n})}\left\{ f'_{2n}(0)\, f'_{2m}(0)\right\}\right. \\ \left. + \frac{\beta_1}{P(k_{2n})}\, f_{2n}(0)\, f_{2m}(0) - \left\langle f_{2n},\, f_{2m}\right\rangle\right\} = -\left(I_{10}e^{ik_{10}a_1}\right)\int_0^{h_2} f_{10}(y)\, f_{2m}(y)dy,\end{aligned} \tag{5.18}$$

for $m = 0, I, II, 1, 2, \ldots.$

Again the mode coupling relation (5.16) is applied on $\phi_{2x}(x,y)$ at $x=-a_1$ along with the eigenfunction $f_{2m}(y)$ is given by

$$\begin{aligned}\left\langle \phi_{2x}(-a_1,y),\, f_{2m}(y)\right\rangle &= \int_0^{h_2}\phi_{2x}(-a_1,y)\, f_{2m}(y)dy - \frac{\alpha_1}{Q(k_{2n})}\left\{\phi'_{2x}(-a_1,y)\, f'_{2m}(0)\right\}\\ &+\frac{\alpha_2}{Q(k_{2n})}\left\{\phi'''_{2x}(-a_1,y)\, f'_{2m}(0)+\phi'_{2x}(-a_1,y)\, f'''_{2m}(0)\right\}+\frac{\beta_1}{P(k_{2n})}\phi_{2x}(-a_1,y)\, f_{2m}(0).\end{aligned} \tag{5.19}$$

The orthogonal property of the eigenfunction $f_{2m}(y)$ as in Equation (5.16) is used along with the expression for velocity potential as in Equation (5.10) and further applying the continuity of velocity across the interface $x=-a_1,\ 0<y<h_2$ as in Equation (5.5) along with the edge condition as in Equation (5.6) to obtain

$$\begin{aligned}&ik_{10}R_{10}e^{-ik_{1n}a_1}\int_0^{h_2} f_{10}(y)\, f_{2m}(y)dy-\kappa_{1n}\sum_{n=1}^{\infty}R_{1n}e^{i\kappa_{1n}a_1}\int_0^{h_2} f_{1n}(y)\, f_{2m}(y)dy\\ &\qquad-\left\{ik_n\sum_{n=0,I}^{II}\left(A_{2n}e^{ik_{2n}a_1}-B_{2n}e^{-ik_{2n}a_1}\right)-\kappa_n\sum_{n=1}^{\infty}\left(A_{2n}e^{-\kappa_{2n}a_1}-B_{2n}e^{\kappa_{2n}a_1}\right)\right\}\\ &\left\{\frac{\alpha_2}{Q(k_{2n})}\left\{\wp f'_{2n}(0)\, f'_{2m}(0)+f'_{2n}(0)\, f'''_{2m}(0)\right\}-\frac{\alpha_1}{Q(k_{2n})}\left\{f'_{2n}(0)\, f'_{2m}(0)\right\}\right.\\ &\left.+\frac{\beta_1}{P(k_{2n})}f_{2n}(0)\, f_{2m}(0)-\delta_{mn}\left\langle f_{2n},\, f_{2m}\right\rangle\right\}=ik_{10}\left(I_{10}e^{ik_{10}a_1}\right)\int_0^{h_2} f_{10}(y)\, f_{2m}(y)dy,\end{aligned} \tag{5.20}$$

for $m=0,I,II,1,2,....$

Further, on applying the mode-coupling relation (5.16) for the velocity potential $\phi_2(x,y)$ at $x=-a_2$ along with the eigenfunction $f_{2m}(y)$ given by

$$\begin{aligned}\left\langle \phi_2(-a_2,y),\, f_{2m}(y)\right\rangle &= \int_0^{h_2}\phi_2(-a_2,y)\, f_{2m}(y)dy-\frac{\alpha_1}{Q(k_{2n})}\left\{\phi'_2(-a_2,y)\, f'_{2m}(0)\right\}\\ &+\frac{\alpha_2}{Q(k_{2n})}\left\{\phi'''_2(-a_2,y)\, f'_{2m}(0)+\phi'_2(-a_2,y)\, f'''_{2m}(0)\right\}+\frac{\beta_1}{P(k_{2n})}\phi_2(-a_2,y)\, f_{2m}(0),\end{aligned} \tag{5.21}$$

The orthogonal property of the eigenfunction $f_{2m}(y)$ as in Equation (5.16) is used along with the expressions for velocity potentials as in Equation (5.10) and further applying the continuity equation for pressure as in Equation (5.5) across the interface $x=-a_2$, $0<y<h_2$ along with the edge condition as in Equation (5.6) to obtain

$$T_{30}e^{ik_{30}a_2}\int_0^{h_2} f_{3n}(y)\,f_{2m}(y)dy+\sum_{n=0}^{\infty}T_{3n}e^{-\kappa_{3n}a_2}\int_0^{h_2} f_{3n}(y)\,f_{2m}(y)dy+\left\{\sum_{n=0,I}^{II}\left(A_{2n}e^{ik_{2n}a_2}+B_{2n}e^{-ik_{2n}a_2}\right)\right.$$
$$\left.+\sum_{n=1}^{\infty}\left(A_{2n}e^{-\kappa_{2n}a_2}+B_{2n}e^{\kappa_{2n}a_2}\right)\right\}\left\{\frac{\alpha_2}{Q(k_{2n})}\left\{f'_{2n}(0)\,f'''_{2m}(0)\right\}-\frac{\alpha_1}{Q(k_{2n})}\left\{f'_{2n}(0)\,f'_{2m}(0)\right\}\right.$$
$$\left.+\frac{\beta_1}{P(k_{2n})}f_{2n}(0)\,f_{2m}(0)-\delta_{mn}\left\langle f_{2n},\,f_{2m}\right\rangle\right\}=0, \tag{5.22}$$

for $m=0,I,II,1,2,....$ Finally, the mode coupling relation (5.16) is applied on $\phi_{2x}(x,y)$ at $x=-a_2$ along with the eigenfunction $f_{2m}(y)$ given by

$$\left\langle\phi_{2x}(-a_2,y),\,f_{2m}(y)\right\rangle=\int_0^{h_2}\phi_{2x}(-a_2,y)\,f_{2m}(y)dy-\frac{\alpha_1}{Q(k_{2n})}\left\{\phi'_{2x}(-a_2,y)\,f'_{2m}(0)\right\}$$
$$+\frac{\alpha_2}{Q(k_{2n})}\left\{\phi'''_{2x}(-a_2,y)\,f'_{2m}(0)+\phi'_{2x}(-a_2,y)\,f'''_{2m}(0)\right\}+\frac{\beta_1}{P(k_{2n})}\phi_{2x}(-a_2,y)\,f_{2m}(0). \tag{5.23}$$

The orthogonal property of the eigenfunction $f_{2m}(y)$ as in Equation (5.16) is used along with the expression for velocity potential as in Equation (5.10) and further applying the continuity of velocity across the interface $x=-a_2,\,0<y<h_2$ as in Equation (5.5) along with the edge condition as in Equation (5.6) to obtain

$$-ik_{3n}\sum_{n=0}^{\infty}T_{3n}e^{ik_{3n}a_2}\int_0^{h_2} f_{3n}(y)\,f_{2m}(y)dy+\kappa_n\sum_{n=1}^{\infty}T_{3n}e^{-\kappa_{3n}a_2}\int_0^{h_2} f_{3n}(y)\,f_{2m}(y)dy+$$
$$-\left\{ik_{2n}\sum_{n=0,I}^{II}(A_{2n}e^{ik_{2n}a_2}-B_{2n}e^{-ik_{2n}a_2})-\kappa_n\sum_{n=1}^{\infty}(A_{2n}e^{-\kappa_{2n}a_2}-B_{2n}e^{\kappa_{2n}a_2})\right\}\left\{\frac{\alpha_2}{Q(k_{2n})}\left\{\omega f'_{2n}(0)\,f'_{2m}(0)\right.\right.$$
$$\left.\left.+\,f'_{2n}(0)\,f'''_{2m}(0)\right\}-\frac{\alpha_1}{Q(k_{2n})}\left\{f'_{2n}(0)\,f'_{2m}(0)\right\}+\frac{\beta_1}{P(k_{2n})}f_{2n}(0)\,f_{2m}(0)-\delta_{mn}\left\langle f_{2n},\,f_{2m}\right\rangle\right\}=0, \tag{5.24}$$

for $m=0,I,II,1,2,....$ and $\delta_{mn}=\begin{cases}1 & \text{for } m=n,\\ 0 & \text{for } m\neq n.\end{cases}$.

From the above solution procedure, an infinite series of sum of the algebraic expressions as in (5.18), (5.20), (5.22) and (5.24) are obtained. These linear equations are limited up to a finite number of M terms to solve a set of $(4M+12)$ algebraic equations.

The $(4M+12)$ unknown coefficients such as $R_{1n}, T_{3n},\ n=0,1,2,...M, M+1, M+2,$ $A_{2n}, B_{2n}, n=0, I, II, 1, 2, ..., M$ in the set of $(4M+12)$ algebraic equation are solved to obtain the complex amplitudes in the respective regions. The amplitudes of the reflection and transmission coefficient are obtained as

$$K_r = |R_0| \text{ and } K_t = \left| \frac{k_{30} \tanh k_{30} h_3}{k_{10} \tanh k_{10} h_1} T_0 \right|. \tag{5.25}$$

The wave coefficients in the reflected and transmitted region are observed to satisfy the energy balance relation $K_r^2 + \chi K_t^2 = 1.$

where $\chi = \dfrac{k_{30} k_{10}^2 \sinh 2k_{10} h_1}{k_{10} k_{30}^2 \sinh 2k_{30} h_3} \left\{ \dfrac{2k_{30} h_3 + \sinh 2k_{30} h_3}{2k_{10} h_1 + \sinh 2k_{10} h_1} \right\}.$ (5.26)

5.3.2 Multiple step bottom topography

In this subsection, the wave scattering due to the finite floating thick elastic plate in the presence of multiple step bottom topography is analysed considering Timoshenko-Mindlin plate theory. The BVP is formulated considering free edge support condition. The velocity potentials $\phi_j(x,y),\ j=1,2...,N+1$ satisfies Equation (5.1) in the fluid domain and boundary condition (5.2), (5.3), (5.4) and (5.8) as explained in the previous section. The velocity potentials $\phi_j(x,y),\ j=1,2,3,...,N+1,$ in the respective regions are given by

$$\begin{aligned}
\phi_1(x,y) &= \left(I_{10} e^{-ik_{10}x} + R_{10} e^{ik_{10}x} \right) f_{10}(y) + \sum_{n=1}^{\infty} R_{1n} e^{-\kappa_{1n}x} f_{1n}(y) \text{ for } x > -a_1, 0 < y < h_1, \\
\phi_j(x,y) &= \sum_{n=0,I}^{II} \left(A_{jn} e^{-ik_{jn}x} + B_{jn} e^{ik_{jn}x} \right) f_{jn}(y) + \sum_{n=1}^{\infty} \left(A_{jn} e^{\kappa_{jn}x} + B_{jn} e^{-\kappa_{jn}x} \right) f_{jn}(y), \\
&\qquad \text{for } -a_1 < x < -a_N, 0 < y < h_j,\ j = 2,3,...,N, \\
\phi_{N+1}(x,y) &= T_{(N+1)0} e^{-ik_{(N+1)0}x} f_{(N+1)0}(y) + \sum_{n=1}^{\infty} T_{(N+1)n} e^{\kappa_{(N+1)n}x} f_{(N+1)n}(y) \\
&\qquad \text{for } x < -a_N, 0 < y < h_{N+1}.
\end{aligned} \tag{5.27}$$

The eigenfunctions $f_{jn}(y)$'s are same as defined in Equation (5.11), where k_{j0} for $j=1, N+1$ are the eigenvalues in the open water region. The eigenvalues correspond to the roots for the open water dispersion relation as given by Equation

(5.12) with $k_{jn} = i\kappa_{jn}$ for $n = 1, 2....$ The coefficients $R_{1n}, T_{(N+1)n}$ at $n = 0, 1, 2...$, A_{jn} and B_{jn}, $j = 2, 3, ..., N$ for $n = 0, I, II, 1, 2...$ are the unknown wave constants to be determined. The eigenvalues k_{jn} for $j = 2, 3, ..N$ are the roots for the plate covered dispersion relation as defined in Equation (5.13). The eigenfunction $f_{jn}(y)$'s in the open water and plate covered region satisfy the orthogonality relation as defined by

$$\left\langle f_{jm}, f_{jn} \right\rangle_{j=1,N+1} = \begin{cases} 0 & \text{for } m \neq n, \\ C'_n & \text{for } m = n, \end{cases} \quad \text{and} \quad \left\langle f_{jm}, f_{jn} \right\rangle_{j=2,3,...,N} = \begin{cases} 0 & \text{for } m \neq n, \\ C''_{jn} & \text{for } m = n, \end{cases} . \tag{5.28}$$

$$\left\langle f_{jm}, f_{jn} \right\rangle_{j=1,N+1} = \int_0^{h_1 \text{ or } h_{N+1}} f_{jm}(y) f_{jn}(y) dy, \tag{5.29}$$

$$\begin{aligned} \left\langle f_{jm}, f_{jn} \right\rangle_j = {} & \int_0^{h_j} f_{jm}(y) f_{jn}(y) dy - \frac{c_1}{Q(k_n)} \left\{ f'_{jm}(0) f'_{jn}(0) \right\} \\ & + \frac{c_2}{Q(k_n)} \left\{ f'''_{jm}(0) f'_{jn}(0) + f'_{jm}(0) f'''_{jn}(0) \right\} + \frac{d_1}{P(k_n)} f_{jm}(0) f_{jn}(0), \end{aligned} \quad \text{for } j = 2, 3, ..., N, \tag{5.30}$$

where $P(k_{jn}) = (\alpha_0 - \alpha_1 k_{jn}^2 + \alpha_2 k_{jn}^4)$, $Q(k_{jn}) = (\beta_0 - \beta_1 k_{jn}^2)$,

$$C'_n = \frac{2k_{jn}h_j + \sinh 2k_{jn}h_j}{4k_{jn} \cosh^2 k_{jn}h_j}, \; j = 1, N+1,$$

$$C''_n = \frac{(\alpha_0 - \alpha_1 k_{jn}^2 + \alpha_2 k_{jn}^4) 2k_{jn}h_j + (\alpha_0 - 3\alpha_1 k_{jn}^2 + 5\alpha_2 k_{jn}^4) \sinh 2k_{jn}h_j + (4\beta_1 k_{jn} \cosh^2 k_{jn}h_j)}{(4k_{jn} \cosh^2 k_{jn}h_j)(\alpha_0 - \alpha_1 k_{jn}^2 + \alpha_2 k_{jn}^4)},$$

for $j = 2, 3, ..., N$. The constant term $C'_n, C''_n, P(k_{jn})$ and $Q(k_{jn})$, $j = 2, 3...N$ for $n = 1, 2, ...$ are determined on replacing $k_{jn} = i\kappa_{jn}$ for $j = 1, 2, ...N+1$.

Applying the mode coupling relation to $\phi_2(-a_1, y)$ along with the eigenfunction $f_{2m}(y)$ at $0 < y < h_2$ we have

$$\begin{aligned} \left\langle \phi_2(-a_1, y), f_{2m}(y) \right\rangle = {} & \int_0^{h_2} \phi_2(-a_1, y) f_{2m}(y) dy - \frac{\alpha_1}{Q(k_{2n})} \left\{ \phi'_2(-a_1, y) f'_{2m}(0) \right\} \\ & + \frac{\alpha_2}{Q(k_{2n})} \left\{ \phi'''_2(-a_1, y) f'_{2m}(0) + \phi'_2(-a_1, y) f'''_{2m}(0) \right\} + \frac{\beta_1}{P(k_{2n})} \phi_2(-a_1, y) f_{2m}(0). \end{aligned} \tag{5.31}$$

The orthogonality relation of the eigenfunction $f_{2m}(y)$ as in Equation (5.30) is used along with the expression for velocity potentials as in Equation (5.27) and further continuity of pressure as in Equation (5.5) across the interface $x=-a_1,-a_N,\ 0<y<h_j$ along with the edge condition as in Equation (5.6) to obtain

$$R_{10}e^{-ik_{10}a_1}\int_0^{h_2} f_{10}(y)\,f_{2m}(y)dy+\sum_{n=0}^{\infty}R_{1n}e^{\kappa_{1n}a_1}\int_0^{h_2} f_{1n}(y)\,f_{2m}(y)dy+\left\{\sum_{n=0,I}^{II}\left(A_{2n}e^{ik_{2n}a_1}+B_{2n}e^{-ik_{2n}a_1}\right)\right.$$
$$\left.+\sum_{n=1}^{\infty}\left(A_{2n}e^{-\kappa_{2n}a_1}+B_{2n}e^{\kappa_{2n}a_1}\right)\right\}\left\{\frac{\alpha_2}{Q(k_{2n})}\left\{f'_{2n}(0)\,f'''_{2m}(0)\right\}-\frac{\alpha_1}{Q(k_{2n})}\left\{f'_{2n}(0)\,f'_{2m}(0)\right\}\right.$$
$$\left.+\frac{\beta_1}{P(k_{2n})}f_{2n}(0)\,f_{2m}(0)-\langle f_{2n},\,f_{2m}\rangle\right\}=-I_0e^{ik_{10}a_1}\int_0^{h_2} f_{10}(y)\,f_{2m}(y)dy, \tag{5.32}$$

for $m=0,I,II,1,2...$ Again, the mode coupling relation is applied on $\phi_{2x}(-a_1,y)$ along with the eigenfunction $f_{2m}(y)$ at $0<y<h_2$ we have

$$\left\langle\phi_{2x}(-a_1,y),\,f_{2m}(y)\right\rangle=\int_0^{h_2}\phi_{2x}(-a_1,y)\,f_{2m}(y)dy-\frac{\alpha_1}{Q(k_{2n})}\left\{\phi'_{2x}(-a_1,y)\,f'_{2m}(0)\right\}$$
$$+\frac{\alpha_2}{Q(k_{2n})}\left\{\phi'''_{2x}(-a_1,y)\,f'_{2m}(0)+\phi'_{2x}(-a_1,y)\,f'''_{2m}(0)\right\}+\frac{\beta_1}{P(k_{2n})}\phi_{2x}(-a_1,y)\,f_{2m}(0). \tag{5.33}$$

The orthogonal relation for the eigenfunction $f_{2m}(y)$ as in Equation (5.30) is used along with the expressions of velocity potentials as in Equation (5.27) and the continuity of velocity across the interface $x=-a_1,\ 0<y<h_2$ as in Equation (5.5) along with the edge condition as in Equation (5.6) to obtain

$$ik_{10}R_{10}e^{-ik_{1n}a_1}\int_0^{h_2} f_{10}(y)\,f_{2m}(y)dy-\kappa_{1n}\sum_{n=1}^{\infty}R_{1n}e^{i\kappa_{1n}a_1}\int_0^{h_2} f_{1n}(y)\,f_{2m}(y)dy$$
$$-\left\{ik_{2n}\sum_{n=0,I}^{II}\left(A_{2n}e^{ik_{2n}a_1}-B_{2n}e^{-ik_{2n}a_1}\right)-\kappa_{2n}\sum_{n=1}^{\infty}\left(A_{2n}e^{-\kappa_{2n}a_1}-B_{2n}e^{\kappa_{2n}a_1}\right)\right\}$$
$$\left\{\frac{\alpha_2}{Q(k_{2n})}\left\{\wp f'_{2n}(0)\,f'_{2m}(0)+f'_{2n}(0)\,f'''_{2m}(0)\right\}-\frac{\alpha_1}{Q(k_{2n})}\left\{f'_{2n}(0)\,f'_{2m}(0)\right\}\right.$$
$$\left.+\frac{\beta_1}{P(k_{2n})}f_{2n}(0)\,f_{2m}(0)-\delta_{mn}\langle f_{2n},\,f_{2m}\rangle\right\}=ik_{10}I_{10}e^{ik_{10}a_1}\int_0^{h_2} f_{10}(y)\,f_{2m}(y)dy, \tag{5.34}$$

for $m=0,I,II,1,2...$

Again, the mode coupling relation is applied to $\phi_j\left(-a_j, y\right)$ along with the eigenfunctions $f_{jm}(y),\ 0 < y < h_j\ \ j = 2,3,...,(N-1)$ we have

$$\begin{aligned}\left\langle \phi_j(-a_j, y),\, f_{jm}(y)\right\rangle &= \int_0^{h_j} \phi_j(-a_j, y)\, f_{jm}(y)dy - \frac{\alpha_1}{Q\left(k_{jn}\right)}\left\{\phi_j'\left(-a_j, y\right) f_{jm}'(0)\right\} \\ &+ \frac{\alpha_2}{Q\left(k_{jn}\right)}\left\{\phi_j'''\left(-a_j, y\right) f_{jm}'(0) + \phi_j'\left(-a_j, y\right) f_{jm}'''(0)\right\} + \frac{\beta_1}{P\left(k_{jn}\right)}\phi_j\left(-a_j, y\right) f_{jm}(0),\end{aligned} \tag{5.35}$$

where h_j is the water depth in the regions based on the bottom topography. The orthogonal relation for the eigenfunction $f_{jm}(y)$ as in Equation (5.30) is used along with the expression of velocity potentials as in Equation (5.27) and further the continuity equation of pressure as in Equation (5.5) across the interface $x = -a_j, 0 < y < h_j$ along with the continuity equations for bending moment $\partial_y^3\phi_j\left(-a_j, 0\right) = \partial_y^3\phi_{(j+1)}\left(-a_j, 0\right)$ and deflection $\partial_y\phi_j\left(-a_j, 0\right) = \partial_y\phi_{(j+1)}\left(-a_j, 0\right)$ as in Equation (5.7) to obtain

$$\begin{aligned}&\left\{\sum_{n=0,I}^{II}\left(A_{(j+1)n}e^{ik_{(j+1)n}a_j} + B_{(j+1)n}e^{-ik_{(j+1)n}a_j}\right) + \sum_{n=1}^{\infty}\left(A_{(j+1)n}e^{-\kappa_{(j+1)n}a_j} + B_{(j+1)n}e^{\kappa_{(j+1)n}a_j}\right)\right\} \\ &\left\{\int_0^{h_j} f_{(j+1)n}\left(y\right) f_{jm}(y)dy + \frac{\alpha_2}{Q(k_{jn})}\left\{f_{(j+1)n}'''\left(0\right) f_{jm}'(0) + f_{(j+1)n}'\left(0\right) f_{jm}'''(0)\right\}\right. \\ &\left. - \frac{\alpha_1}{Q(k_{jn})}\left\{f_{(j+1)n}'\left(0\right) f_{jm}'(0)\right\}\right\} + \left\{\sum_{n=0,I}^{II}\left(A_{jn}e^{ik_{jn}a_j} + B_{jn}e^{-ik_{jn}a_j}\right) + \sum_{n=1}^{\infty}\left(A_{jn}e^{-\kappa_{jn}a_j} + B_{jn}e^{\kappa_{jn}a_j}\right)\right\} \\ &\left\{\frac{\beta_1}{P(k_{jn})} f_{jn}\left(0\right) f_{2m}(0) - \delta_{mn}\left\langle f_{jn}\left(y\right), f_{jm}(y)\right\rangle\right\} = 0,\end{aligned} \tag{5.36}$$

for $m = 0, I, II, 1, 2...$, $j = 2,3,...,(N-1)$. Again, the mode coupling relation is applied to $\phi_{jx}\left(-a_j, y\right)$ along with the eigenfunctions $f_{jm}(y),\ 0 < y < h_j\ \ j = 2,3,...,(N-1)$ we have

$$\begin{aligned}\left\langle \phi_{jx}(-a_j, y),\, f_{jm}(y)\right\rangle &= \int_0^{h_j} \phi_{jx}(-a_j, y)\, f_{jm}(y)dy - \frac{\alpha_1}{Q\left(k_{jn}\right)}\left\{\phi_{jx}'\left(-a_j, y\right) f_{jm}'(0)\right\} \\ &+ \frac{\alpha_2}{Q\left(k_{jn}\right)}\left\{\phi_{jx}'''\left(-a_j, y\right) f_{jm}'(0) + \phi_{jx}'\left(-a_j, y\right) f_{jm}'''(0)\right\} + \frac{\beta_1}{P\left(k_{jn}\right)}\phi_{jx}\left(-a_j, y\right) f_{jm}(0),\end{aligned} \tag{5.37}$$

Using the orthogonal property of the eigenfunction $f_{jm}(y)$ as in Equation (5.30) and the expressions of velocity potentials as in Equation (5.27) along with the continuity of velocity as in Equation (5.5) across the interface $x=-a_j, 0<y<h_j,\ j=2,3,...,(N-1)$ and applying the continuity of slope of the deflection and shear force we have

$$-\left\{ik_{(j+1)n}\sum_{n=0,I}^{II}\left(A_{(j+1)n}e^{ik_{(j+1)n}a_j}-B_{(j+1)n}e^{-ik_{(j+1)n}a_j}\right)-\kappa_{(j+1)n}\sum_{n=1}^{\infty}\left(A_{(j+1)n}e^{-\kappa_{(j+1)n}a_j}-B_{(j+1)n}e^{\kappa_{(j+1)n}a_j}\right)\right\}$$
$$\left\{\int_0^{h_j} f_{(j+1)n}(y)\,f_{jm}(y)dy+\frac{\alpha_2}{Q(k_{jn})}\left\{f'''_{(j+1)n}(0)\,f'_{jm}(0)-\wp f'_{(j+1)n}(0)\,f'_{jm}(0)+f'_{(j+1)n}(0)\,f'''_{jm}(0)\right\}-\right.$$
$$\left.\frac{\alpha_1}{Q(k_{jn})}\left\{f'_{(j+1)n}(0)\,f'_{jm}(0)\right\}\right\}-\left\{ik_{jn}\sum_{n=0,I}^{II}\left(A_{jn}e^{ik_{jn}a_j}-B_{jn}e^{-ik_{jn}a_j}\right)-\kappa_{jn}\sum_{n=1}^{\infty}\left(A_{jn}e^{-\kappa_{jn}a_j}-B_{jn}e^{\kappa_{jn}a_j}\right)\right\}$$
$$\left(\frac{\alpha_2}{Q(k_{jn})}\left\{\wp f'_{jn}(0)\,f'_{jm}(0)\right\}+\frac{\beta_1}{P(k_{jn})}f_{jn}(0)\,f_{jm}(0)-\delta_{mn}\left\langle f_{jn},f_{jm}\right\rangle\right)=0,$$

(5.38)

for $m=0,I,II,1,2...,\quad j=2,3,...,(N-1)$. Applying the mode coupling relation to $\phi_N(-a_N,y)$ along with the eigenfunction $f_{Nm}(y)$ at $0<y<h_N$ we have

$$\left\langle\phi_N(-a_N,y),f_{Nm}(y)\right\rangle=\int_0^{h_N}\phi_N(-a_N,y)\,f_{Nm}(y)dy-\frac{\alpha_1}{Q(k_{Nn})}\left\{\phi'_N(-a_N,y)\,f'_{Nm}(0)\right\}$$
$$+\frac{\alpha_2}{Q(k_{Nn})}\left\{\phi'''_N(-a_N,y)\,f'_{Nm}(0)+\phi'_N(-a_N,y)\,f'''_{Nm}(0)\right\}+\frac{\beta_1}{P(k_{Nn})}\phi_N(-a_N,y)\,f_{Nm}(0).\tag{5.39}$$

The orthogonality relation of the eigenfunction $f_{(N-1)m}(y)$ as in Equation (5.30) is used along with the expression for velocity potentials as in Equation (5.27) and further continuity of pressure as in Equation (5.5) across the interface $x=-a_N,\ 0<y<h_N$ along with the edge condition as in Equation (5.6) to obtain

$$T_{(N+1)0}e^{ik_{(N+1)0}a_N}\int_0^{h_N}f_{(N+1)n}(y)\,f_{Nm}(y)dy+\sum_{n=0}^{\infty}T_{(N+1)n}e^{-\kappa_{(N+1)n}a_N}\int_0^{h_N}f_{(N+1)n}(y)\,f_{Nm}(y)dy+$$
$$\left\{\sum_{n=0,I}^{II}\left(A_{Nn}e^{ik_{Nn}a_N}+B_{Nn}e^{-ik_{Nn}a_N}\right)+\sum_{n=1}^{\infty}\left(A_{Nn}e^{-\kappa_{Nn}a_N}+B_{Nn}e^{\kappa_{Nn}a_N}\right)\right\}\left\{\frac{\alpha_2}{Q(k_{Nn})}\left\{f'_{Nn}(0)\,f'''_{Nm}(0)\right\}\right.$$
$$\left.-\frac{\alpha_1}{Q(k_{Nn})}\left\{f'_{Nn}(0)\,f'_{Nm}(0)\right\}+\frac{\beta_1}{P(k_{Nn})}f_{Nn}(0)\,f_{Nm}(0)-\delta_{mn}\left\langle f_{Nn},f_{Nm}\right\rangle\right\}=0,$$

(5.40)

for $m = 0, I, II, 1, 2...$ Again, the mode coupling relation is applied on $\phi_{Nx}(-a_N, y)$ along with the eigenfunction $f_{Nm}(y)$ at $0 < y < h_N$ we have

$$\left\langle \phi_{Nx}(-a_N, y),\, f_{Nm}(y) \right\rangle = \int_0^{h_N} \phi_{Nx}(-a_N, y)\, f_{Nm}(y) dy - \frac{\alpha_1}{Q(k_{Nn})} \left\{ \phi'_{Nx}(-a_N, y)\, f'_{Nm}(0) \right\} + \frac{\alpha_2}{Q(k_{Nn})} \left\{ \phi'''_{Nx}(-a_N, y)\, f'_{Nm}(0) + \phi'_{Nx}(-a_N, y)\, f'''_{Nm}(0) \right\} + \frac{\beta_1}{P(k_{Nn})} \phi_{Nx}(-a_N, y)\, f_{Nm}(0). \tag{5.41}$$

The orthogonal relation for eigenfunction $f_{Nm}(y)$ as in Equation (5.30) is used along with the expressions of velocity potentials as in Equation (5.27) and further the continuity of velocity across the interface $x = -a_N$, $0 < y < h_N$ as in Equation (5.5) along with the edge condition as in Equation (5.6) to obtain

$$-ik_{(N+1)n} T_{(N+1)n} e^{ik_{(N+1)n} a_N} \int_0^{h_N} f_{(N+1)n}(y)\, f_{Nm}(y) dy + \kappa_{(N+1)n} \sum_{n=1}^{\infty} T_{(N+1)n} e^{-\kappa_{(N+1)n} a_N} \int_0^{h_N} f_{(N+1)n}(y)\, f_{Nm}(y) dy - \left\{ ik_{Nn} \sum_{n=0,I}^{II} (A_{Nn} e^{-ik_{Nn} a_N} - B_{Nn} e^{ik_{Nn} a_N}) - \kappa_n \sum_{n=1}^{\infty} (A_{Nn} e^{\kappa_{Nn} a_N} - B_{Nn} e^{-\kappa_{Nn} a_N}) \right\}$$

$$\left\{ \frac{\alpha_2}{Q(k_{Nn})} \left\{ \wp f'_{Nn}(0)\, f'_{Nm}(0) + f'_{Nn}(0)\, f'''_{Nm}(0) \right\} - \frac{\alpha_1}{Q(k_{Nn})} \left\{ f'_{Nn}(0)\, f'_{Nm}(0) \right\} + \frac{\beta_1}{P(k_{Nn})} f_{Nn}(0)\, f_{Nm}(0) - \delta_{mn} \left\langle f_{Nn},\, f_{Nm} \right\rangle \right\} = 0. \tag{5.42}$$

The algebraic sum of linear equations is obtained by using the continuity equations across the vertical interface and the edge support conditions. The infinite series of a sum of the numerical equations is truncated upto a finite number of M terms to obtain $2N(M+3)$ equations for N number of multiple stepped bottom topography. Solving the above equations, the unknown constants $R_{1n}, T_{(N+1)n}, n = 0, 1, 2, ..., M, M+1, M+2$ and A_{jn}, B_{jn}, $n = 0, I, II, 1, 2, ..., M$, $j = 2, 3, ..., N$ are obtained and the reflection and transmission coefficient satisfying the energy balance relation $K_r^2 + \chi K_t^2 = 1$ are obtained as

$$K_r = |R_0| \text{ and } K_t = \left| \frac{k_{(N+1)0} \tanh k_{(N+1)0} h_{(N+1)}}{k_{10} \tanh k_{10} h_1} T_0 \right|, \tag{5.43}$$

where $\chi = \dfrac{k_{(N+1)0} k_{10}^2 \sinh 2k_{10}h_1}{k_{10} k_{(N+1)0}^2 \sinh 2k_{(N+1)0}h_{(N+1)}} \left\{ \dfrac{2k_{(N+1)0}h_{(N+1)} + \sinh 2k_{(N+1)0}h_{(N+1)}}{2k_{10}h_1 + \sinh 2k_{10}h_1} \right\}$.

5.4 NUMERICAL RESULTS AND DISCUSSIONS

The hydroelastic characteristics of floating elastic platform over a varying sea bed profile is studied considering Timoshenko-Mindlin theory. The plate deflection ζ_j / I_0, the wave induced strain on the plate ε, bending moment $M(x)$ and shear force $W(x)$ along plate length with varying sea bottom profile are analysed. In the present study, the numerical values of the parameters $E = 5\text{GPa}$, $\nu = 0.3$, $\rho_p / \rho_w = 0.9$ and $g = 9.81\text{ms}^{-2}$ are fixed. In the numerical computation water depth in the incident and transmitted region is denoted as h_r and h_t whereas the water depths below the floating elastic plate is denoted as h_j, $j = 1, 2, ...$ The parameters that are kept fixed throughout the computation are $d / h_r = 0.1$ and $L / h_r = 10$. A comparative study is carried out for varying number of steps to understand the significance of slope and number of step interfaces. The numerical results are checked to satisfy the energy balance relation given by $K_r^2 + \chi K_t^2 = 1$.

5.4.1 Single step bottom topography

The wave interaction with thick floating elastic platform over sloping sea bottom, hump-type sea bottom topography is analysed to understand the hydroelastic characteristics for the two cases of sea bottom profile. The different types of seabed configurations are examined using the step approximation. The wave characteristics due to the effect of hump type and sloping type sea bottom profiles are illustrated and the hydroelastic performance of a floating elastic platform are also discussed.

5.4.1.1 Reflection and transmission coefficient

In Figure 5.3(a,b) the K_r and K_t are plotted versus non-dimensional wave number $k_{10}h_r$ for the ocean waves interacting with a floating elastic platform over a single step hump type sea bottom profile for different water depth h_1 / h_r along the plate covered region. The minimum values of K_r (Figure 5.3a) indicate higher wave transmission

through the plate. In the case of lower values of $k_{10}h_r < 1.5$, higher wave reflection is observed due to the obstruction caused by the step height at the interfaces. The resonating pattern in the K_r is observed for higher values of $k_{10}h_r$ which shows that for the waves with shorter wavelength, the complete wave transmission reduces. A sudden increase in the wave transmission is visualized at particular points, where there is a resonating trough occurs in the K_r which may be due to wave interference overcoming the step height hindrance along with the reducing wavelength. Further, the wave transmission (Figure 5.3b) reduces due to the combined effect of sea bottom profile and floating plate. In the case of $k_{10}h_r < 6.5$, the reflection of waves is observed to increase with the surge in the step height due to the trapping of waves at the step interface. Further, for higher value of $k_{10}h_r > 6.5$, the wave transmission is noticed to increase with the reduction in the step height due to the reduction of wavelength.

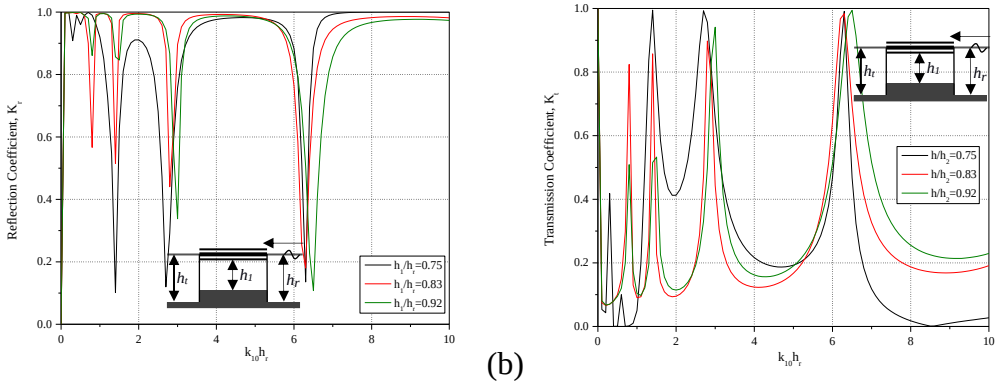

(a) (b)

Figure 5.3: (a) K_r and (b) K_t versus $k_{10}h_r$ for varying water depth h_1 / h_r in the case of single step bottom profile considering $h_t / h_r = 1.0$.

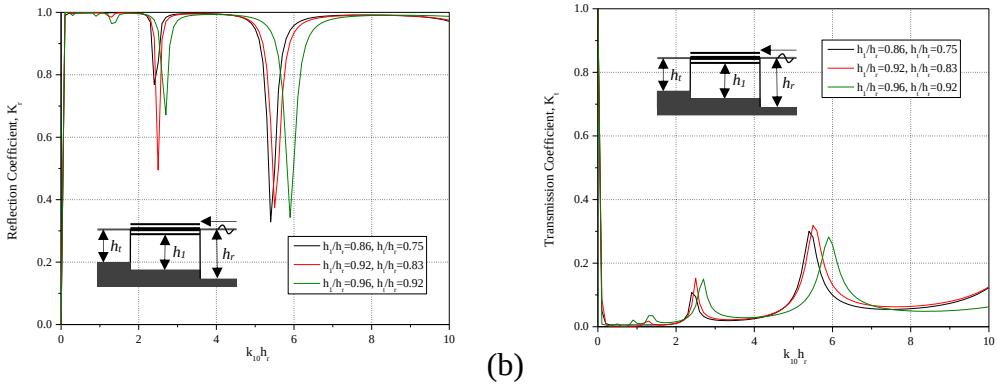

(a) (b)

Figure 5.4: (a) K_r and (b) K_t versus $k_{10}h_r$ for varying water depth h_1 / h_r and h_t / h_r in the case of stepped sloping bottom profile.

In Figure 5.4(a,b) the K_r and K_t are plotted versus $k_{10}h_r$ due to the floating elastic platform over a two stepped sloping type sea bottom profile for different water depth h_1/h_r and h_t/h_r. In the case of lower values of $k_{10}h_r$, almost uniform estimation in the K_r and K_t are observed due to varying step heights. The increase in the slope of step height reduces the number of completely transmitted waves mainly due to the interaction of waves with the increased step height. A forward shift in the wave reflection coefficient (Figure 5.4a) and transmission coefficient (Figure 5.4b) is noticed with the increasing slope of step height due to the increment in wavenumber for the interaction of waves at the step interface. The zeros in the wave reflection for lower values of $k_{10}h_r$ is not observed for the case of two-stepped sloping type sea bottom profile. The wave transmission K_t increases with the increase in the values of $k_{10}h_r$ which suggest more waves gets transmitted for shorter wavelength. It is also observed that the waves get trapped at the step in the bottom profile along the plate covered region reducing the transmission of waves.

5.4.1.2 Deflection and strain in the floating elastic plate

The response of the floating elastic plate in terms of ζ_j / I_0 and ε is noticed to reduce with the increase in step height as illustrated in Figure 5.5(a,b) due to the trapping of waves below the floating elastic plate with the increase in the step height. The plate deflection ζ_j / I_0 is noticed to reduce immensely at the incident end following a slight reduction as the waves progressed towards the transmitted region as in Figure 5.5(a) due to the wave trapping at the step interface. The reduction in the plate deflection with the increase in the step height h_1/h_r is found to be within $-2\times10^{-4} < \zeta_j / I_0 < 1.5\times10^{-4}$ but for higher step height h_1/h_r the plate deflection ζ_j / I_0 is within $-5\times10^{-5} < \zeta_j / I_0 < 5\times10^{-5}$. On the other hand, the values of ε in Figure 5.5(b) is noticed to surge slightly and is observed to be within $-1.5\times10^{-7} < \varepsilon < 1.5\times10^{-7}$ which may be due to the increase in stress at the step interfaces as the waves progressed towards the transmitted region. The oscillating peaks and troughs are noticed in periodic intervals, however, around 71.5% and 79% reduction in the plate deflection is observed for $h_1/h_r = 0.75$ and $h_1/h_r = 0.83$ as compared with $h_1/h_r = 0.92$ with the

enhancement in the wave reflection due to change in rigid step height which causes the significant change in the wave transformation. A gradual change in the wave induced strain ε (Figure 5.5b) is noticed for $h_1/h_r = 0.92$ at each of the oscillating peak and variation in the trend in strain ε with variation in the step height is almost similar as in Figure 5.5(a).

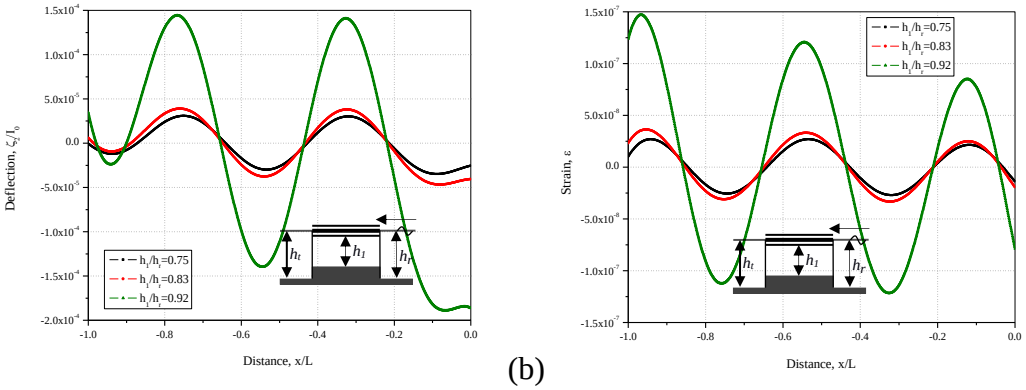

(a) (b)

Figure 5.5: (a) Deflection ζ_j / I_0 and (b) stain ε along the plate length x/L for varying water depth h_1/h_r in the case of single step bottom profile considering $k_{10}h_r = 3$ and $h_t/h_r = 1.0$.

The deflection ζ_j / I_0 and stain ε along the plate length x/L over a two stepped sloping type sea bottom profile for different water depth h_1/h_r and h_t/h_r is presented in Figure 5.6(a,b). The response in terms of ζ_j / I_0 and ε is noticed to reduce with the increase in the step height as illustrated in Figure 6(a, b) due to the trapping of waves with the increase in the step height. The plate deflection ζ_j / I_0 is noticed to reduce gradually as the wave progress towards the transmitted region as in Figure 5.6(a) which may be due to the wave trapping at the step interfaces for a sloping type step bottom profile. The plate deflection ζ_j / I_0 is noticed to be within $-4\times10^{-5} < \zeta_j / I_0 < 4\times10^{-5}$ and with the reduction in the step height the plate deflection further reduces and is observed to be within $-1\times10^{-5} < \zeta_j / I_0 < 1\times10^{-5}$. However, the variation in the plate deflection ζ_j / I_0 (Figure 6a) and stain ε (Figure 5.6b) is observed to be oscillatory nature with variation in the plate length x/L. Around 65% for $h_1/h_r = 0.75$ and 77% for $h_1/h_r = 0.83$ reduction in the deflection ζ_j / I_0 is observed as compared with the $h_1/h_r = 0.92$ at each of the local minima and local maxima. As a comparison between

the single step and double step bottom, the plate deflection is observed minimum for the case of two stepped sloping type sea bottom profile as compared with single step bottom profile. The reduction in the plate deflection in the case of two stepped sloping type sea bottom profile may be due to the change in the phase of the incident and transmitted wave. Further, the values of ε in Figure 5.6(b) is noticed to reduce with the increase in the step height and is observed to be within $-3\times10^{-8} < \varepsilon < 4\times10^{-8}$. The strain ε in the floating elastic plate for the case of sloping type step bottom profile is less as compared with single step bottom profile, which may be due to the increase in the stress at the step interfaces for a sloping type stepped bottom topography as the wave progress towards the transmitted region.

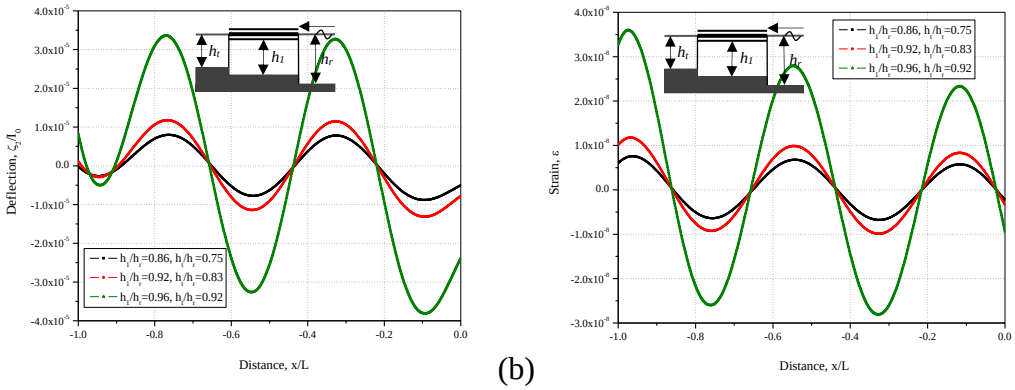

(a) (b)

Figure 5.6: (a) Deflection ζ_j / I_0 and (b) stain ε along the plate length x/L for varying water depth h_1 / h_r and h_t / h_r in the case of stepped sloping bottom profile considering $k_{10}h_r = 3.$

5.4.1.3 Bending moment and shear force

The hydroelastic response in terms of bending moment and shear force resultants along the plate length x/L due to the interaction of ocean waves with floating elastic plate over a single hump type sea bottom profile for different water depth h_1 / h_r is presented in Figure 5.7(a,b). The bending moment $M(x)$ (Figure 5.7a) and shear force $W(x)$ (Figure 5.7b) is noticed to reduce with the increase in step height due to the enhancement in the wave reflection due to the presence of the rigid step. The bending moment $M(x)$ and shear force $W(x)$ are noticed to be minimum due to the consideration of free edge support condition for the floating elastic plate. The bending moment $M(x)$ is also observed to reduce towards the supporting edges with higher

reduction at the incident end as in Figure 5.7(a) due to the combined effect of support condition and wave trapping at the step interface. The bending moment $M(x)$ of the floating elastic plate is observed to be within $-1.5\times10^{5}\,\text{Nm} < M(x) < 1.5\times10^{5}\,\text{Nm}$ and the values of $M(x)$ reduces with the increase in the step height and is observed to be within $-5\times10^{4}\,\text{Nm} < M(x) < 5\times10^{4}\,\text{Nm}$. Further, the shear force $W(x)$ as in Figure 5.7(b) is noticed to increase throughout the length of the plate and is observed to be within $-2\times10^{3}\,\text{N} < W(x) < 1.5\times10^{3}\,\text{N}$, which may be due to the increase in the stress at the step interfaces. However, the local minima and local maxima in the bending moment $M(x)$ and shear force $W(x)$ is observed for variable plate length x/L and, around 78% and 85% reduction in the bending moment $M(x)$ is observed for $h_1/h_r = 0.75$, $h_1/h_r = 0.83$ as compared with the $h_1/h_r = 0.92$ at each of the oscillating crests and troughs.

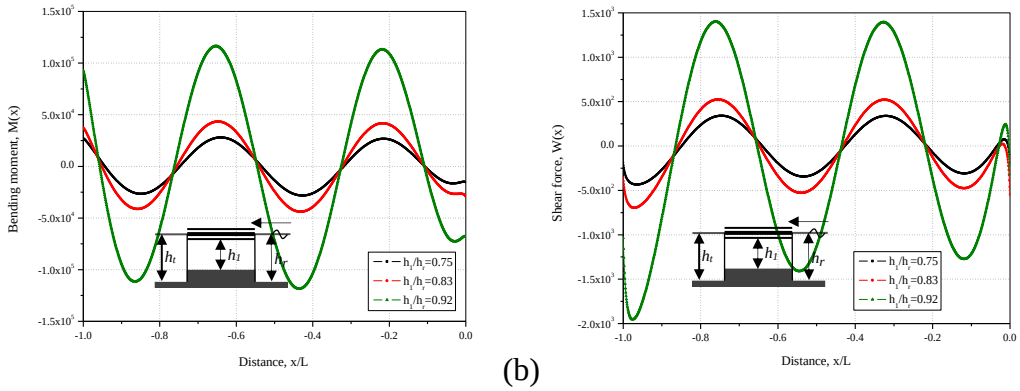

(a) (b)

Figure 5.7: (a) Bending moment and (b) shear force along the plate length x/L for varying water depth h_1/h_r in the case of single step bottom profile considering $k_{10}h_r = 3$ and $h_t/h_r = 1.0$.

The bending moment and shear force resultants along the plate length x/L over a two stepped sloping type sea bottom profile for different water depth h_1/h_r and h_t/h_r is presented in Figure 5.8(a,b). The bending moment $M(x)$ (Figure 5.8a) and shear force $W(x)$ (Figure 5.8b) resultants are noticed to reduce with the increase in step height, which may be due to the change in the wave reflection due to the presence of sloping bottom (approximated into multiple rigid steps). The bending moment $M(x)$ and shear

force $W(x)$ are noticed to be minimal at the plate edges due to the consideration of free edge support condition for the floating elastic platform. The $M(x)$ is noticed to reduce towards the supporting edges and high reduction at the incident end as in Figure 5.8(a) due to the combined effect of support condition and wave trapping at the sloping type step interface. The bending moment for the case of the sloping type sea bottom is less as compared to the single step bottom profile and is observed to be within $-6.5\times10^{4}\,\text{Nm} < M(x) < 6.5\times10^{4}\,\text{Nm}$. On the other hand, shear force $W(x)$ resultant as in Figure 5.8(b) is noticed to increase throughout the length of the plate, with the increase in the water depth below the plate and reduction in the step height. The shear force $W(x)$ for the case of double-step seabed profile is observed to be within $-1.5\times10^{3}\,\text{N} < W(x) < 1\times10^{3}\,\text{N}$ and minimal variation is observed as compared to the single step bottom profile. The reduction in the shear force $W(x)$ with the increase in the step height may be due to the increase in the stress at the step interfaces along the sloping type stepped sea bottom profile.

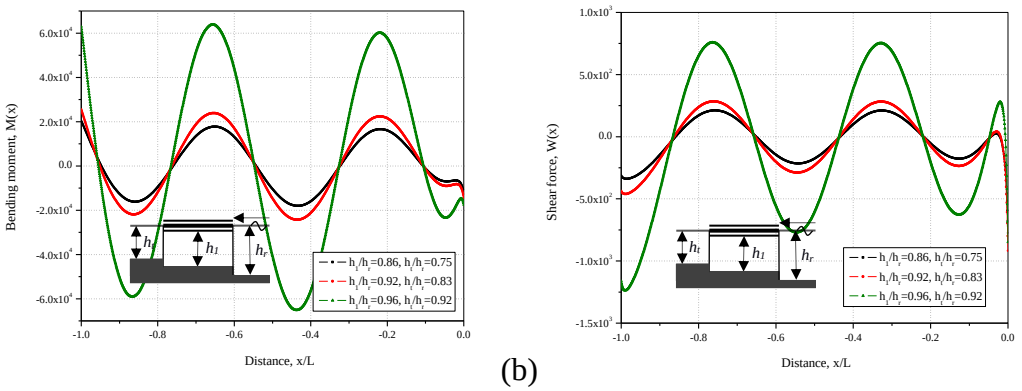

(a) (b)

Figure 5.8: (a) Bending moment and (b) shear force along the plate length x/L for varying water depth h_1/h_r and h_t/h_r in the case of stepped sloping bottom profile considering $k_{10}h_r = 3$.

5.4.2 Two-step bottom topography

The wave propagation over two step bottom topography is analysed to understand the hydroelastic characteristics for the two cases of sea bottom profile. The two profiles considered for bottom topography are a two-step hump type and three step sloping type. The wave characteristics due to the effect of hump type and sloping type sea bottom

profiles are illustrated and the hydroelastic performance of a floating elastic plate are discussed in detail.

5.4.2.1 Reflection and transmission coefficient

In Figure 5.9(a,b) the K_r and K_t are plotted versus $k_{10}h_r$ for the wave interaction with a floating elastic platform over a two-step hump type sea bottom profile for different water depth h_1/h_r and h_2/h_r. The minimum values in the K_r indicate high wave transmission through the plate but at lower values of $k_{10}h_r<1$, higher reflection of wave is observed due to the obstruction caused by the step height at the interfaces.

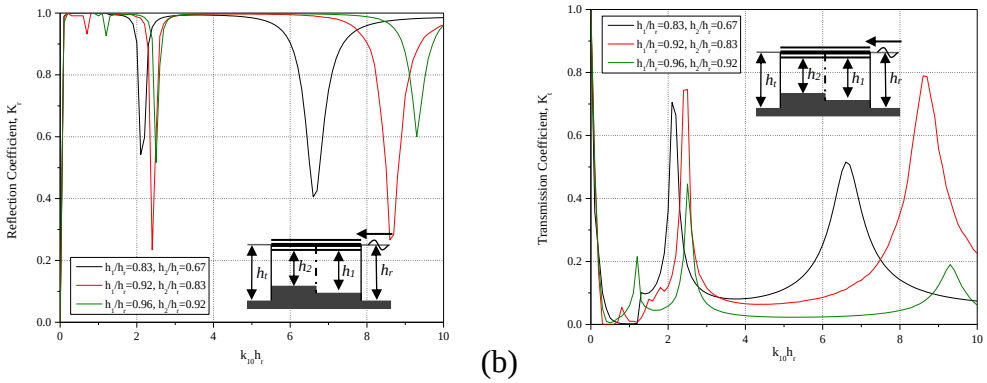

(a) (b)

Figure 5.9: (a) K_r and (b) K_t versus $k_{10}h_r$ varying water depth h_1/h_r and h_2/h_r in the case of two-stepped hump type bottom profile considering $h_t/h_r=1.0$.

The wave reflection is observed higher within $2.5<k_{10}h_r<6$ and minimum K_t is noted due to the trapping of the waves with the increase in the step height. The forward shift in the K_r for higher values of $k_{10}h_r$ is observed with the increase in the step height. A sudden increase in the wave transmission (Figure 5.9b) is visualized at $1.5<k_{10}h_r<2.5$ due to the wave interference at the step height along with the reducing wavelength. Further, the transmission of waves reduces and forward shift in K_t for higher values of $k_{10}h_r$ is noted due to the combined effect of sea bottom profile and floating plate. However, the resonating peaks and troughs are observed high in the K_r and K_t due to the sea bottom discontinuity which causes multiple interaction with the incident wave. The transmission of wave K_t is observed to increase with the surge in the slope of the step height and the wave height increases at the shallow water depth. The forward shift in the wave reflection and transmission coefficients with the increasing slope of step

height may be due to the increment in the wavenumber at the step interface. The wave transmission is noticed to increase with the surge in the value of the step height due to the surge in wave height at shallower water depth. The comparative study with the single step topography as in Figure 5.4(a,b) shows that the wave transmission is higher with the increase in the number of steps and the resonating pattern in the K_r and K_t also increases due to the change in step height.

In Figure 5.10(a,b) the K_r and K_t are plotted versus $k_{10}h_r$ over a three stepped sloping type sea bottom profile for different water depth h_1/h_r, h_2/h_r and h_t/h_r. The variation in the rigid step height shows the minimal impact on the wave transformation in the form of the resonating minor troughs in K_r (Figure5.10a) and resonating minor crests in K_t (Figure 5.10b) at similar intervals within $4 < k_{10}h_r < 8$ due to the higher incident wave amplitude. The number of completely transmitted waves gets reduced with the increase in water depth due to the propagation of waves at shallow water depths. A forward shift in the wave reflection and transmission coefficients is noticed with the increasing slope of step height within $4 < k_{10}h_r < 8$ due to the increment in wavenumber for the interacting waves at the step interface. It is also observed that the waves get trapped at the step interface along the bottom profile below the plate covered region reducing the transmission of waves. The comparative study between the three stepped sloping bottom profile and two-stepped hump type bottom profile suggest that the wave transmission is less for the three stepped sloping bottom profile causing formation of standing waves due to the abrupt changes in the water depth.

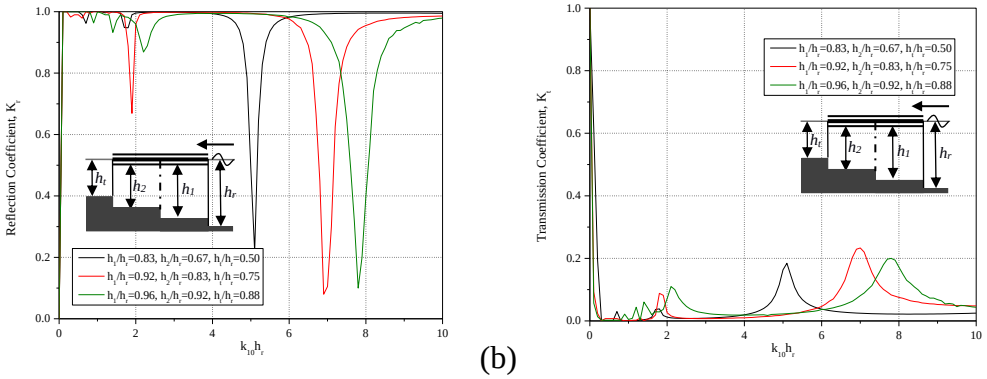

(a) (b)

Figure 5.10: (a) K_r and (b) K_t versus $k_{10}h_r$ varying water depth h_1/h_r, h_2/h_r and h_t/h_r in the case of stepped sloping bottom profile.

5.4.2.2 Deflection and strain of the floating elastic plate

In Figure 5.11(a,b), the plate deflection ζ_j / I_0 and stain ε are plotted along the plate length x/L over two step hump type sea bottom profile for varying water depth h_1/h_r and h_2/h_r. The response in terms of ζ_j / I_0 and ε are observed to reduce with the surge in step height as illustrated in Figure 5.11(a,b) due to the trapping of waves with the increasing step height. The plate deflection ζ_j / I_0 and strain ε in the floating elastic plate is noticed to reduce as the wave progress towards the transmitted region as in Figure 5.11(a) due to the trapping of waves and increase in the stress at the step interface. The higher hydroelastic response is noticed along the initial step, which is mainly due to the wave interference caused by the reflected wave with incident wave at the step interface.

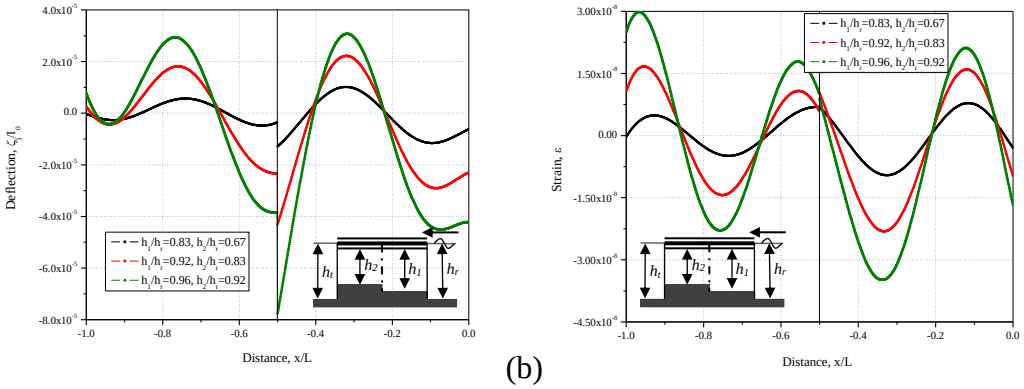

(a) (b)

Figure 5.11: (a) Deflection ζ_j / I_0 and (b) stain ε along the plate length x/L for varying water depth h_1/h_r and h_2/h_r in the case of two step bottom profile considering $k_{10}h_r = 3$ and $h_t/h_r = 1.0$.

The plate deflection is observed to be within $-8\times10^{-5} < \zeta_j / I_0 < 4\times10^{-5}$ but a sharp change in the hydroelastic response is observed due to the interference of wave with the increase in the step height. Further, the strain ε (Figure 5.11b) in the floating elastic plate at the edges of the incident plate edge is less as compared to the transmitted plate edge and is observed to be within $-4.5\times10^{-8} < \varepsilon < 3\times10^{-8}$. The variations in the hydroelastic behaviour at regular intervals of step length are observed due to the obstruction caused at the step edge. However, the local minima and local maxima is observed at particular intervals and, around 40% and 83% reduction in the plate deflection ζ_j / I_0 for $h_2/h_r = 0.83$ and $h_2/h_r = 0.67$ is observed at each of the

oscillating peak due to the change in the step height. Similarly, 44% and 83% reduction in the strain for $h_2 / h_r = 0.83$ and $h_2 / h_r = 0.67$ at $x / L = 0.95$ is achieved at the point where the oscillating peak is developed.

The hydroelastic response of floating elastic platform due to the interaction of ocean wave in terms of deflection ζ_j / I_0 and stain ε along the plate length x / L over a three steeped slope bottom profile for varying water depth h_1 / h_r, h_2 / h_r and h_t / h_r is presented in Figure 5.12(a,b). The response in terms of plate deflection ζ_j / I_0 (Figure 5.12a) and strain ε (Figure 5.12b) is noticed to reduce with the surge in step height due to the considerable variation in the wave reflection by each of the rigid step. The plate deflection ζ_j / I_0 is noticed to reduce gradually throughout the elastic plate as the wave progress towards the transmitted region as shown in Figure 5.12(a), which may be due to the wave trapping and increase in the stress at the step interface for a sloping type step bottom profile. The higher hydroelastic response is noticed along the initial step, which is mainly due to the wave interference caused by reflected wave with incident wave at the step interface. The variations in the hydroelastic behaviour at regular intervals of step length are observed due to the obstruction caused at the step edge. The significant reduction in the plate deflection ζ_j / I_0 and the strain ε in the floating elastic plate is observed for the stepped slope bottom profile towards the transmitted end as compared to the two stepped hump bottom profile as in Figure 5.11(a,b).

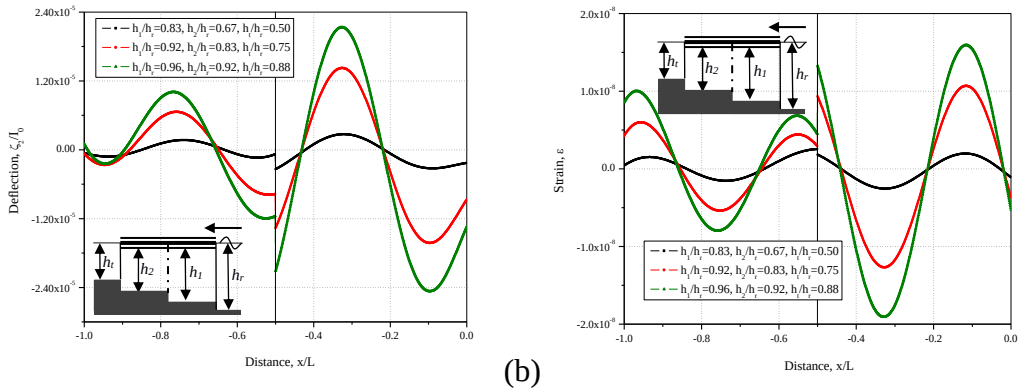

(a) (b)

Figure 5.12: Deflection ζ_j / I_0 and (b) stain ε along the plate length x / L for varying water depth h_1 / h_r, h_2 / h_r and h_t / h_r in the case of three stepped bottom profile considering $k_{10} h_r = 3$.

As a comparison with two-step bottom as in Figure 5.11(a,b), the 29% for $h_2 / h_r = 0.92$, 36% for $h_2 / h_r = 0.83$ and 70% for $h_2 / h_r = 0.67$ reduction in the plate deflection ζ_j / I_0 at primary oscillating peak $x / L = -0.325$ along with the 66% for $h_2 / h_r = 0.92$, 60% for $h_2 / h_r = 0.83$ and 50% for $h_2 / h_r = 0.67$ reduction in the plate deflection ζ_j / I_0 at secondary oscillating peak $x / L = -0.775$ is achieved due to the presence of the third step in the leeward free water region as compared with double-step bottom. On the other hand, the 26% for $h_2 / h_r = 0.92$, 31% for $h_2 / h_r = 0.83$ and 73% for $h_2 / h_r = 0.67$ decrease in the strain ε is achieved due to the presence of three-step sloping bottom as compared with double step sloping bottom. As study stated, the variation in the wave transformation and wave trapping due to the presence of the multiple rigid steps plays a major role in reducing the hydroelastic response.

5.4.3 Three step bottom topography

The wave interaction on a thick floating elastic platform over three step bottom topography is analysed to understand the hydroelastic characteristics for the two cases of sea bottom profile. The two profiles considered for bottom topography are a three-step hump and sloping type sea bottom profile. The wave characteristics due to the effect of hump type and sloping type sea bottom profiles are illustrated and the hydroelastic performance of a floating elastic plate are discussed in detail.

5.4.3.1 Reflection and transmission coefficient

In Figure 5.13(a,b) the K_r and K_t are plotted versus $k_{10}h_r$ for the wave interacting with the floating elastic platform over a three-step hump type sea bottom profile for different water depth h_1 / h_r, h_2 / h_r and h_3 / h_r. The occurrence of maxima in the values of K_r (Figure 5.13a) or minima in the wave transmission through the plate is observed for lower values of $k_{10}h_r < 1.5$. The higher reflection of wave is observed due to the obstruction caused by the step height at the interfaces in the case of longer wavelengths. A sudden increase in wave transmission and decrease in wave reflection is visualized at $1.5 < k_{10}h_r < 4$ due to the reduction in wavelength. In the case of higher values of $k_{10}h_r > 6$ the forward shift in the K_r and K_t is noted for higher values of water depth

ratios which suggest that as the step height reduces more shorter wave gets trapped below the plate. Further, similar pattern in the transmission of waves is observed due to the combined effect of sea bottom profile and floating plate. At higher values of $k_{10}h_r$, the reflection of waves is observed to increase with the surge in the step height due to the presence of zero velocity near the rigid step, which enhances the wave reflection at the step interface. The comparative study with the single and two step-type hump profile as in Figure 5.3(a,b) and 5.9(a,b) shows that the resonating pattern or the increase in the transmission coefficient for certain values of $k_{10}h_r$ increases as the number of steps increases. However, the resonating troughs in the K_r (Figure 5.13a) and resonating crests in the K_t (Figure 5.13b) influences the design and placement of the VLFS in the presence of abrupt changes in the seabed for better performance and life period.

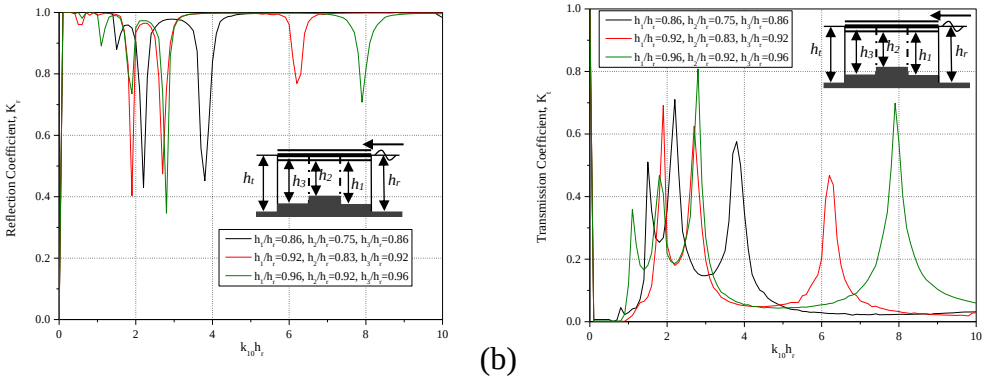

(a) (b)

Figure 5.13: (a) K_r and (b) K_t versus $k_{10}h_r$ for varying water depth h_1/h_r, h_2/h_r and h_3/h_r in the case of three step hump type bottom profile considering $h_t/h_r = 1.0$.

In Figure 5.14(a,b), the K_r and K_t are plotted versus $k_{10}h_r$ for the waves interacting with the floating elastic platform over a three stepped sloping seabed profile for different water depth h_1/h_r, h_2/h_r and h_3/h_r. The occurrence of the higher values of the wave transmission for certain values of $k_{10}h_r$ is noted for $0 < k_{10}h_r < 4$, which suggests that for the waves with longer wavelengths, the wave transmission is higher. Further with the increase in the water depth ratio the forward shift in the K_r and K_t is noted. The increment in the slope of step height reduces the number of completely transmitted waves mainly due to the waves interacting with increased step height as in Figure 5.14(b). The transmission of wave is observed to increase with the surge in the

slope of the step height and hence increasing the wave height at the shallower water depth. It is noticed that the waves get trapped at the step interface along the seabed profile in the plate covered region reducing the transmission of waves.

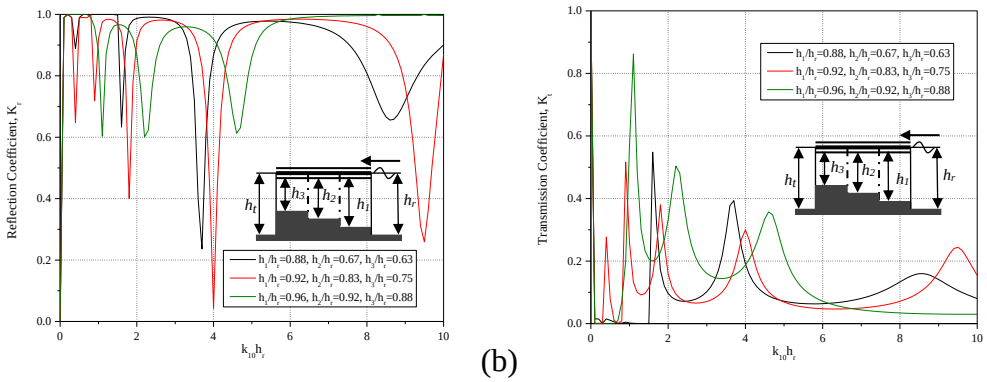

(a) (b)

Figure 5.14: (a) K_r and (b) K_t versus $k_{10}h_r$ for varying water depth h_1/h_r, h_2/h_r and h_3/h_r in the case of three stepped sloping type bottom profile considering $h_t/h_r = 1.0$.

5.4.3.2 Deflection and strain of the floating elastic plate

In Figure 5.15(a,b), the deflection ζ_j / I_0 and stain ε along the plate length x/L over a varying three hump type step bottom profile for different water depth h_1/h_r, h_2/h_r and h_3/h_r is presented. The response in terms of ζ_j / I_0 and ε is noticed to reduce as the wave progress towards the transmitted region as in Figure 5.15(a,b) due to the trapping of waves and increase in stress at the step interface. The higher deflection ζ_j / I_0 (Figure 5.15a) is noticed along the initial step mainly due to the wave interference caused by reflected wave with incident wave at the step interface. The variations in the hydroelastic behaviour at regular intervals of step length are observed due to the obstruction caused at the step edge. The strain ε in the floating elastic plate near to the change in step height shows a sharp discontinuity due to the interference of the waves with the change in the step height. The strain in the floating plate is observed to be within $-2\times10^{-7} < \varepsilon < 1.5\times10^{-7}$ and is higher as compared with the two-step hump bottom profile as in Figure 5.11(b). It is also noted that the oscillatory peaks show a significant variation in the strain ε (Figure 5.15b) for variable step height. Around 45% reduction in the secondary resonating peak at x/L=-0.55 and 30% reduction in the third resonating peak at x/L=-0.975 as compared with the primary resonating peak at x/L=-0.125 for $h_3/h_r = 0.96$, which suggest that the increase in the step heights shows

the significant impact on the hydroelastic response and maximum impact on the wave transformation. However, the sharp rise and fall in the hydroelastic response is evident in the design of VLFS placed on the three-step hump type seabed for better outcomes.

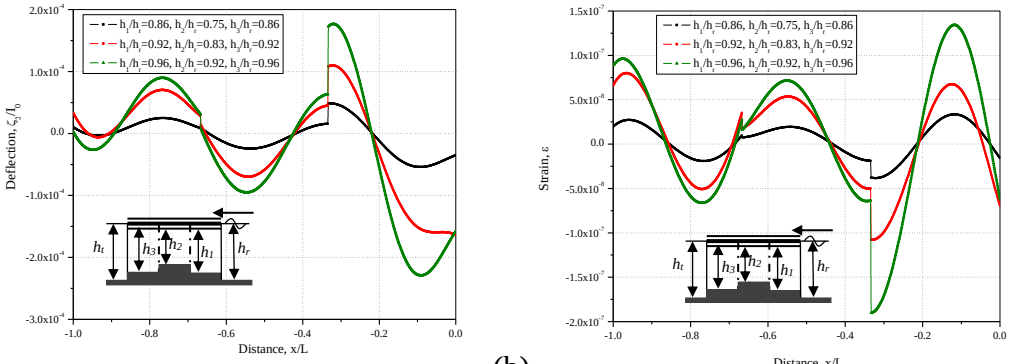

(a) (b)

Figure 5.15: (a) Deflection ζ_j / I_0 and (b) stain ε along the plate length x/L for varying water depth h_1/h_r, h_2/h_r and h_3/h_r in the case of three step hump type sea bottom profile considering $k_{10}h_r = 3$ and $h_t/h_r = 1.0$.

In Figure 5.16(a,b), the deflection ζ_j / I_0 and stain ε along the plate length x/L over a varying three stepped sloping type bottom profile for different water depth h_3/h_r is presented. The response in terms of ζ_j / I_0 and ε is noticed to reduce gradually throughout the elastic plate as the waves progress towards the transmission region as shown in Figure 5.16(a), which may be due to the fact that the incident wave interacts with multiple rigid steps and reflected back towards the seaside open water region or trapped under the plate covered region.

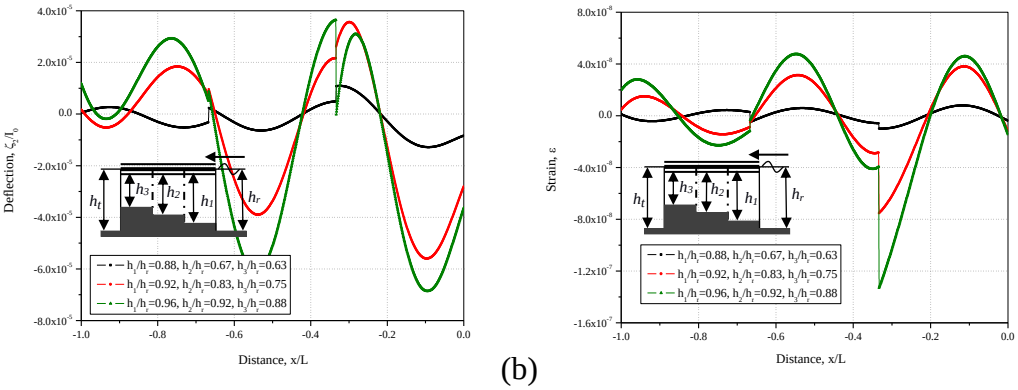

(a) (b)

Figure 5.16: (a) Deflection ζ_j / I_0 and (b) stain ε along the plate length x/L for varying water depth h_1/h_r, h_2/h_r and h_3/h_r in the case of three stepped sloping sea bottom profile considering $k_{10}h_r = 3$ and $h_t/h_r = 1.0$.

It is also noted that, the reduction in the deflection ζ_j / I_0 and stain ε in the floating elastic plate is observed as the wave progressed towards the transmitted region. The plate deflection is observed to be within $-8\times10^{-5} < \zeta_j / I_0 < 4\times10^{-5}$ and the strain in the floating plate is within $-1.6\times10^{-7} < \varepsilon < 8\times10^{-8}$ as in Figure 5.16(a,b). The variations in the hydroelastic behaviour at regular intervals of step length are observed due to the obstruction caused at the step edge. However, around 15% reduction in the secondary resonating peak at x/L=-0.55 and 60% reduction in the third resonating peak at x/L=-0.925 is noted as compared with the primary resonating peak at x/L=-0.125 for $h_3/h_r = 0.75$. The study suggest that the increase in the third step height h_3/h_r shows an immense variation in the stain ε (Figure 5.16b) and successful in reducing the oscillatory peaks and troughs. As a comparison with the three step hump sea bed profile (Figure 5.15b), the third step height h_3/h_r shows the critical role in reducing the oscillating peak and it is proved that, if the third step height is lower as compared with the second step height, the local maxima reaches to the higher estimation. Similarly, if the third step height is higher as compared with the primary and secondary step heights, there exists a significant reduction in the local maxima as compared with the other oscillating peaks due to the enhancement in the wave reflection by each of the rigid step which causes minimum impact on the floating plate.

5.4.4 Comparative study for different number of steps

The wave interaction with thick floating elastic platform over varying bottom topography using step approximation (single and multi-step seabed) is analysed in the case of finite water depth considering $h_t/h_r = 0.83$. The slope of the steps are varied to incorporate the varying number of steps along the seabed profile. The wave characteristics due to varying number of steps in sloping type bottom profile is compared and the hydroelastic performance of a floating elastic platform are also compared and discussed.

5.4.4.1 Reflection and transmission coefficient

In Figure 5.17(a,b) the K_r and K_t are plotted versus $k_{10}h_r$ for waves interacting with floating elastic platform over a varying number of steps in sloping type bottom profile at finite water depth $h_t/h_r = 0.83$. Significant variation in the K_r (Figure 5.17a) is

observed between the one, two and three-step impermeable sea bottom at primary resonating troughs within $1 < k_{10}h_r < 3$. Thereafter, the secondary resonating troughs are obtained within $6 < k_{10}h_r < 8$ due to the presence of one, two and three impermeable steps. However, the higher estimation and minimum oscillation is obtained in the K_r for three-step bottom at secondary resonating trough. The 36% (two-step bottom) and 53% (single-step bottom) reduction in the K_r is achieved as compared with the three-step seabed at each of the secondary resonating troughs within $6 < k_{10}h_r < 8$ due to the addition of the reflection by third impermeable step. Similarly, the number of transmitted wave is observed increasing and tend to shift towards lower values of $k_{10}h_r$ with the increasing number of steps along the plate covered region due to the reduction in the slope for the step height. On the other hand, the transmission of wave is noticed to reduce with the increasing number of steps mainly due to the interaction of waves at the interfaces and subsequently gets reflected as the steps increased. The higher resonating peak is observed for single-step impermeable bottom and there is an effective reduction in the K_t (Figure 5.17b) with increase in the steps at each of the secondary resonating peaks within $6 < k_{10}h_r < 8$. As a comparison with single-step seabed, the 35% and 69% reduction in the K_t is obtained for two-step seabed and tree-step seabed at each of the resonating crests. The changes caused in the wave transmission is due to the enhancement in the wave reflection by the three-step seabed. However, the sloping bottom (approximated into three-steps) shows a significant role in balancing the K_r and K_t due to the wave trapping. A significant increase in the transmission of waves is observed for the case of no step in the bottom topography.

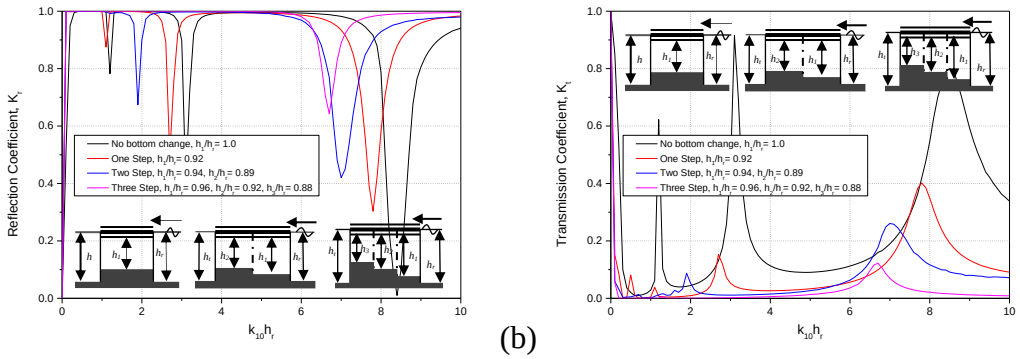

(a) (b)

Figure 5.17: (a) K_r and (b) K_t versus $k_{10}h_r$ for varying number of steps along the plate covered region.

5.4.4.2 Deflection and strain of the floating elastic plate

In Figure 5.18(a,b), the plate deflection ζ_j / I_0 and stain ε along the plate length x/L over a stepped type sloping seabed profile is presented for varying number of steps. The plate deflection ζ_j / I_0 and stain ε along the floating plate is observed to be varying with the change in the number of steps.

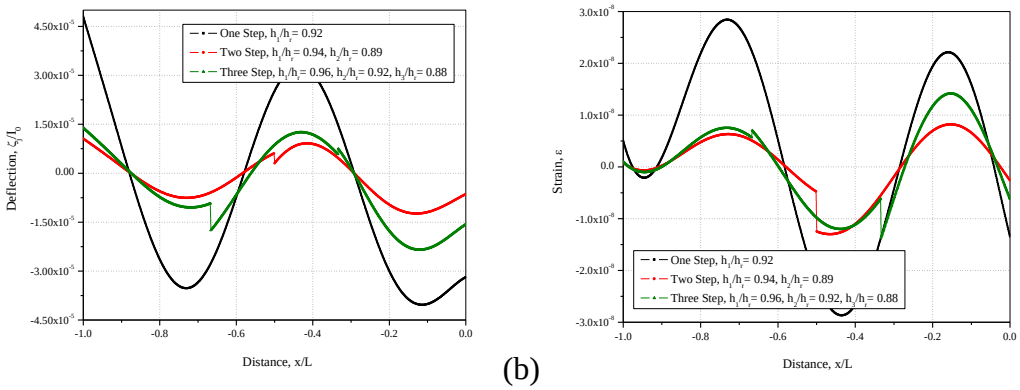

(a) (b)

Figure 5.18: (a) Deflection ζ_j / I_0 and (b) stain ε along the plate length x/L for varying number of steps considering $k_{10}h_r = 3$.

The oscillating peaks reaches to the maximum values for single step and gradually deceasing with increase in the number of steps. The response is noticed to decrease significantly due to the presence of steps along the plate covered region, which is mainly due to the wave trapping along the step interfaces. Further, the increase in number of steps along the plate covered region are noticed to increase the responses due to the reduction in the slope of step heights. The responses are also noticed to reduce along the length of the plate due to the wave trapping at step interfaces. The discontinuity in the hydroelastic response at regular intervals of step length are noticed due to the sudden change in the step height caused at the step interfaces.

5.5 CONCLUSIONS

The wave scattering due to the floating elastic platform over a varying seabed profile is analysed based on Timoshenko-Mindlin plate theory in water of finite depth. The mathematical model is based on eigenfunction expansion method along with orthogonal mode coupling relation. The seabed profile is modelled considering multiple steps to signify a generalized sea bottom profile. The edges of the floating elastic plate are considered to satisfy free edge support conditions along with continuity conditions at

the step interfaces. The wave characteristics are analysed and are observed to follow the energy balance relation. The hydroelastic characteristics of floating elastic plate are compared over varying bottom topography acted upon by ocean waves. In addition, a brief comparison of the numerical results is carried out for varying number of steps along the plate covered region. The following conclusions drawn from the present study are as follows:

- The wave transmission is noticed to increase with the reduction in the step height due to the reduction of wavelength for both the case of single step seabed profile. An initial increase in transmission coefficient with increase in slope of step height is noticed for a hump type single stepped sea bed profile as compared to sloping type stepped seabed profile, which remained similar at higher wavenumbers.
- The hydroelastic response is noticed to reduce with the increase in step height due to the trapping of waves. The plate deflection for both the cases of single stepped seabed profile is noticed to reduce at the incident end following a reduction thereafter as the waves progressed towards the transmission region due to the wave trapping at the step interface.
- The hydroelastic response in terms of strain, bending moment and shear force for both the cases of single stepped seabed profile is noticed to slightly surge, which may be due to the increase in stress at the step interfaces as the waves progressed towards the transmitted region.
- The hydroelastic response is noticed to reduce gradually throughout the elastic plate along with discontinuity at the step interfaces as the wave progress towards the transmitted region may be due to the wave trapping at the step interfaces for varying number of steps below floating elastic platform.
- A sudden increase in wave transmission is visualized at lower values of wave numbers due to the interference of waves at the step height along with the reduction of wavelength for varying number of multiple steps below floating elastic platform.
- The higher transmission of wave is noticed at lower values of wavenumbers with the increase in slope of step height for a hump type stepped sea bed profile as compared to sloping type stepped seabed profile, which remained similar at higher wavenumbers.

- At higher values of wavenumber, the reflection of waves is observed to increase with the surge in the step height due to trapping of waves at the step interface for multiple stepped seabed profile below a floating elastic platform.
- The wave transmission is noticed to reduce with the increasing number of steps mainly due to the interaction of waves at the step interfaces. The 35% and 69% reduction in the K_t is obtained for two-step seabed and tree-step seabed as compared with the single-step seabed at each of the resonating crests.
- The increment in number of steps along the plate covered region are noticed to increase the responses due to the reduction in slope of step heights as compared to very high response for single-step. The variations in the hydroelastic response at regular interval of step length are observed due to the obstruction caused at the step interfaces.

CHAPTER 6

WAVE ATTENUATION DUE TO THE PRESENCE OF SUBMERGED STRUCTURES

6.1 GENERAL INTRODUCTION

In the previous chapter, the wave transformation due to floating elastic plate based on Timoshenko-Mindlin's plate theory over varying sea bottom profile is discussed and provided an insight into the effect of seabed profile over waves interacting with large floating elastic plate in finite water depth. Further, a detail comparison of the numerical results was performed for different step type bottom topography in the hydroelastic analysis of floating elastic plates.

In this chapter, the wave attenuation due the interaction with vertical barriers in front of the large floating structures is analysed based on Timoshenko-Mindlin plate theory in finite water depth. In addition, the mitigation in hydroelastic response due to the wave interaction with articulated floating elastic plate in combination with either a bottom standing or surface piercing vertical barrier is performed. The eigenfunction expansion method along with the orthogonal mode coupling relation is used in the mathematical formulation and solution of the problem for the case of finite water depth. The influence of different edge support conditions in mitigating the hydroelastic behaviour of articulated floating elastic plate in the presence of vertical barrier is also studied. The numerical study is performed to analyse the wave reflection, transmission and dissipation characteristics from the floating plate due to the presence of vertical porous barriers. The wave energy dissipation is evaluated by calculating the values of wave dissipation coefficients and checked to satisfy the energy balance relation.

6.2 MATHEMATICAL FORMULATION

The wave interaction with the very large floating structures for different support conditions in the presence of bottom standing, surface piercing and fully extended, vertical barriers is formulated based on the linearized wave theory. The boundary value problem (BVP) is modelled as a two-dimensional coordinate system for the wave interaction with floating plate as shown in Figure 6.1(a,b). The monochromatic wave is

incident along the positive x-axis horizontally and the y-axis is considered positive vertically downward. The floating elastic plate is considered to be articulated and floating at the free surface of the fluid $-a_3 < x < -a_1, y = 0$ and termed as plate covered region due to the presence of articulation at $x = -a_2$. The free surface in the upstream open water domain $-a_1 < x < \infty, 0 < y < h$ is divided into two regions due to the presence of the vertical barriers at $x = 0$. The downstream open water domain $-\infty < x < -a_3$, $0 < y < h$ is termed as transmitted region. The two edges of the floating thick elastic plate at $x = -a_1$ and $x = -a_3$ are considered to satisfy the applicable edge support boundary conditions.

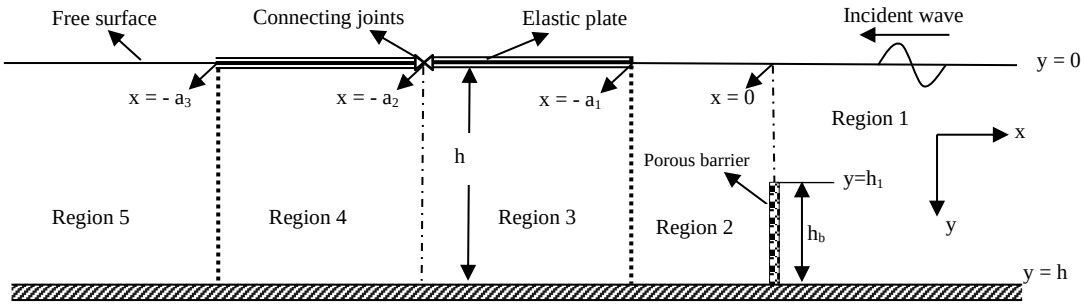

Figure 6.1(a): Schematic diagram for articulated floating elastic plate with bottom standing barrier.

The velocity potential ϕ_j, $j = 1, 2, .., 5$ in the fluid domain satisfies the Laplace equation given by

$$\nabla^2 \phi_j = 0 \text{ at } -\infty < x < \infty, 0 < y < h. \tag{6.1}$$

The linearized plate covered boundary condition on the free surface is obtained by combining the linearized kinematic and dynamic boundary condition with the Timoshenko-Mindlin equation of the form

$$\begin{aligned} &\left\{ \frac{EI}{\left(\rho g - m_s \omega^2\right)} \partial_x^4 + \left(\frac{m_s \omega^2 I}{\left(\rho g - m_s \omega^2\right)} - S \right) \partial_x^2 + \left(1 - \frac{m_s \omega^2 IS}{EI} \right) \right\} \phi_{jy}(x, y) \\ &+ \frac{\rho \omega^2}{\left(\rho g - m_s \omega^2\right)} \left\{ 1 - \frac{m_s \omega^2 IS}{EI} - S \partial_x^2 \right\} \phi_j(x, y) = 0, \qquad \text{for } -a_3 < x < -a_1, \end{aligned} \tag{6.2}$$

where, d is the plate thickness, ρ_p is the plate density, $EI = Ed^3/12(1-\nu^2)$ is the plate rigidity, E is the Young's Modulus, ν is the Poisson's ratio, $G = E/2(1+\mu)$ is the shear

modulus of the plate, and $\mu = \pi^2/12$ is the transverse shear coefficient of the plate, ρ is the density of water, g is the acceleration due to gravity, $m_s = \rho_p d$ is the mass of the plate, $I = d^2/12$ is the rotary inertia, and $S = EI/\mu Gd$ is the shear deformation. In the fluid domain $j = 1, 2, 5$ the linearized free surface boundary condition is given by

$$\frac{\partial \phi_j}{\partial y} - \frac{\omega^2}{g}\phi_j = 0, \quad \text{for} \quad x > -a_1 \text{ and } x < -a_3. \tag{6.3}$$

The continuity of velocity and pressure at the interface $x = 0, -a_1, -a_2$ and $-a_3$, $0 < y < h$ is given by

$$\phi_{jx}(x,y) = \phi_{(j+1)x}(x,y) \text{ and } \phi_j(x,y) = \phi_{(j+1)}(x,y) \text{ for } j = 1, 2, 3, 4. \tag{6.4}$$

The two plates are assumed to be connected at $x = -a_2$ by a vertical linear spring with stiffness k_{33} and flexural rotational spring with stiffness k_{55}. The shear force and the bending moment at the articulated edge as in Praveen et al. (2018, 2019) in terms of velocity potential for $j = 3$ satisfy the condition

$$-EI\partial^3_{yyy}\phi_j(x,y) = k_{55}\left\{\partial^2_{xy}\phi_j(x,y) - \partial^2_{xy}\phi_{j+1}(x,y)\right\}, \tag{6.5a}$$

$$-EI\partial^3_{yyy}\phi_{j+1}(x,y) = k_{55}\left\{\partial^2_{xy}\phi_j(x,y) - \partial^2_{xy}\phi_{j+1}(x,y)\right\}, \tag{6.5b}$$

$$EI\left[\partial^4_{xyyy}\phi_j(x,y) - \wp\partial_x\phi_j(x,y)\right] = k_{33}\left\{\partial_y\phi_j(x,y) - \partial_y\phi_{j+1}(x,y)\right\}, \tag{6.5c}$$

$$EI\left[\partial^4_{xyyy}\phi_{j+1}(x,y) - \wp\partial_x\phi_{j+1}(x,y)\right] = k_{33}\left\{\partial_y\phi_j(x,y) - \partial_y\phi_{j+1}(x,y)\right\}. \tag{6.5d}$$

Depending upon the nature of the vertical linear spring stiffness and/or a flexural rotational spring stiffness, the articulated joints are described. The articulated joints are termed as free-free edge, if both the vertical linear spring stiffness and flexural rotational spring stiffness are absent, i.e. $k_{33} = 0$ and $k_{55} = 0$. The interconnected floating elastic plate is termed as hinged connection, if either of the vertical linear spring stiffness and flexural rotational spring stiffness is having higher values, i.e. $k_{33} = 0$ and $k_{55} \to \infty$ or $k_{33} \to \infty$ and $k_{55} = 0$. Further, the articulated edge is termed as rigid connection, if both the vertical linear spring stiffness and flexural rotational spring stiffness is having higher values, i.e. $k_{33} \to \infty$ and $k_{55} \to \infty$. The interconnected edge

is termed as semi-rigid connection if both the vertical linear spring stiffness and flexural rotational spring stiffness is having intermediate values, i.e. k_{33} and k_{55} intermediate value.

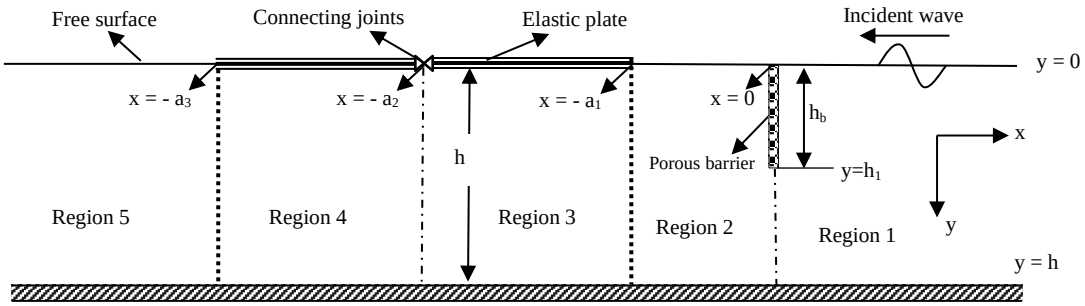

Figure 6.1(b): Schematic diagram for articulated floating elastic plate with surface piercing barrier.

Due to the presence of vertical porous barrier with height h_b at $x = 0$ in front of the floating elastic plate, the boundary condition considering Darcy's law is given by

$$\partial\phi_{jx} = -ik_{10}G_0(\phi_2 - \phi_1),\ j = 1, 2, \tag{6.6}$$

where $G_0 = G_r + iG_i$ is the complex porous effect parameter with the real part G_r represents the resistance effect of the porous material against the seepage flow while the imaginary part G_i denotes the inertia effect of the fluid inside the porous material. The complex porous effect parameter is defined by Yu and Chwang (1994) as given by

$$G_0 = \frac{\varepsilon\left(f + iS_i\right)}{k_{10}d\left(f^2 + S_i^{\,2}\right)}, \tag{6.7}$$

where ε is the porosity constant, f is the resistance force coefficient, S_i is the inertial force coefficient, d is the thickness of the porous medium and k_{10} is the wavenumber of the incident wave. On combining the boundary condition at the vertical porous barrier as in Equation (6.6) and the equation of continuity at the $x = 0$, the boundary condition for the porous vertical barrier and the open gap for $j = 1, 2$ is given by

$$-ik_{10}G_0(\phi_2 - \phi_1) = \begin{cases} 0, & \text{for open gap,} \\ \dfrac{\partial\phi_j}{\partial x}, & \text{for vertical barrier.} \end{cases} \tag{6.8}$$

Further, the floating elastic plate is considered to satisfy one of the following edge support conditions as defined in Timoshenko and Krieger (1959), Rao (2007). The free edge support conditions for floating elastic plate represents zero bending moment and zero shear force at the plate edge. In the case of finite water depth, the shear force and bending moment at the plate edge $x=-a_1$ and $x=-a_3$ for $j=3,4$ satisfies the relation given by

$$\partial_y^3\phi_j(x,y)=0 \text{ and } \partial_{xy^3}^4\phi_j(x,y)=\wp\partial_{xy}^2\phi_j(x,y) \text{ for } x=-a_1,-a_3 \text{ at } y=0. \quad (6.9a)$$

where $\wp=m\omega^2(S+I)/EI$. In the case of simply supported edge, the edge condition represents the bending moment and deflection to vanish at the support. The deflection/displacement and bending moment at the plate edge $x=-a_1$ and $x=-a_3$ for $j=3,4$ satisfies the relation given by

$$\partial_y\phi_j(x,y)=0 \text{ and } \partial_y^3\phi_j(x,y)=0 \text{ for } x=0,-a_3 \text{ at } y=0. \quad (6.9b)$$

In the case of fixed edge condition, the deflection and slope vanish at the edge. The slope and deflection/displacement at the plate edge $x=-a_1$ and $x=-a_3$ for $j=3,4$ satisfies the relation given by

$$\partial_y\phi_j(x,y)=0 \text{ and } \partial_{xy}^2\phi_j(x,y)=0 \text{ for } x=0,-a_3 \text{ at } y=0. \quad (6.9c)$$

The far-field radiation condition is given by

$$\phi_j(x)=\begin{cases}\left(e^{-ik_{10}x}+R_{10}e^{ik_{10}x}\right)f_{10}(y) & \text{as } x\to\infty,\\ \left(T_{50}e^{-ik_{50}x}\right)f_{50}(y) & \text{as } x\to-\infty,\end{cases} \quad (6.10)$$

with R_{10} and T_{50} are the complex wave amplitudes in reflection and transmission. The eigenfunction $f_{j0}(y)$'s for $j=1,5$ are of the form $f_{j0}(y)=\cosh k_{j0}(h-y)/\cosh k_{j0}h$ with k_{j0} for $j=1,5$ are the positive real roots satisfying the open water dispersion relation at finite water depth given by

$$k_{j0}\tanh k_{j0}h-\omega^2/g=0. \quad (6.11)$$

In the subsequent section, the solution procedure for the wave attenuation in the presence of vertical porous barrier is presented and discussed in detail.

6.3 METHOD OF SOLUTION

In this section, the solution procedure for the wave attenuation due to the presence of vertical barriers in front of an articulated large floating structures based on Timoshenko-Mindlin plate theory is presented. The boundary value problem for the wave scattering from a finite articulated floating elastic plate along with vertical barriers is formulated in finite water depth. The velocity potentials $\phi_j(x,y)$ for $j=1,2,..5$ satisfying the governing Equation (6.1) along with the boundary condition (6.4), (6.6), (6.7) and (6.9) are of the form

$$\begin{aligned}
\phi_1(x,y) &= \left(I_{10}e^{-ik_{10}x}+R_{10}e^{ik_{10}x}\right)f_{10}(y)+\sum_{n=1}^{\infty}R_{1n}e^{-\kappa_{1n}x}f_{1n}(y), && \text{for } x>0,\\
\phi_2(x,y) &= \left(A_{20}e^{-ik_{20}x}+B_{20}e^{ik_{20}x}\right)f_{20}(y)+\sum_{n=1}^{\infty}\left(A_{2n}e^{\kappa_{2n}x}+B_{2n}e^{-\kappa_{2n}x}\right)f_{2n}(y), && \\
& && \text{for } -a_1<x<0,\\
\phi_3(x,y) &= \sum_{n=0,I}^{II}\left(A_{3n}e^{-ik_{3n}x}+B_{3n}e^{ik_{3n}x}\right)f_{3n}(y)+\sum_{n=1}^{\infty}\left(A_{3n}e^{\kappa_{3n}x}+B_{3n}e^{-\kappa_{3n}x}\right)f_{3n}(y), && \\
& && \text{for } -a_2<x<-a_1,\\
\phi_4(x,y) &= \sum_{n=0,I}^{II}\left(A_{4n}e^{-ik_{4n}x}+B_{4n}e^{ik_{4n}x}\right)f_{4n}(y)+\sum_{n=1}^{\infty}\left(A_{4n}e^{\kappa_{4n}x}+B_{4n}e^{-\kappa_{4n}x}\right)f_{4n}(y), && \\
& && \text{for } -a_3<x<-a_2,\\
\phi_5(x,y) &= T_{50}e^{-ik_{50}x}f_{50}(y)+\sum_{n=1}^{\infty}T_{5n}e^{\kappa_{5n}x}f_{5n}(y), && \text{for } x<-a_3,
\end{aligned} \tag{6.12}$$

where $R_{1n}, A_{jn}, B_{jn}, T_{5n}$, $j=2$ and $n=0,1,2...$ and A_{jn}, B_{jn}, $j=3,4$, $n=0,I,II,1,2....$ are the unknown constants to be determined. The eigenfunctions $f_{jn}(y)$'s are given by

$$f_{jn}(y)=\frac{\cosh k_{jn}(h-y)}{\cosh k_{jn}h} \text{ for } n=0,I,II \quad \text{and} \quad f_{jn}(y)=\frac{\cos \kappa_{jn}(h-y)}{\cos \kappa_{jn}h} \text{ for } n=1,2,.... \tag{6.13}$$

where k_{jn} for $j=1,2,3,4,5$ are the eigenvalues.

These eigenvalues satisfy the dispersion relation in the open water region for $j=1,2,5$ is given by

$$k_{j0}\tanh k_{j0}h-\omega^2/g=0. \tag{6.14}$$

with $k_{jn} = i\kappa_{jn}$ for $n = 1, 2....$ and the dispersion relation has one real root k_{j0} and an infinite number of purely imaginary roots κ_{jn} for $n = 1, 2...$ In the plate covered region, the k_{jn} for $j = 3, 4$ satisfies the dispersion relation given by

$$\left(\alpha_0 - \alpha_1 k_{jn}^2 + \alpha_2 k_{jn}^4\right) k_{jn} \tanh k_{jn} h - \left(\beta_0 - \beta_1 k_{jn}^2\right) = 0. \tag{6.15}$$

where $\alpha_0 = \left\{1 - m_s \omega^2 \left(\frac{IS}{EI}\right)\right\}$, $\alpha_1 = \left\{\frac{m_s \omega^2 I}{\left(\rho g - m_s \omega^2\right)} - S\right\}$, $\alpha_2 = \frac{EI}{\left(\rho g - m_s \omega^2\right)}$,

$\beta_0 = \frac{\rho \omega^2}{\left(\rho g - m_s \omega^2\right)}\left(1 - m_s \omega^2 \frac{IS}{EI}\right)$, $\beta_1 = -\frac{\rho \omega^2 S}{\left(\rho g - m_s \omega^2\right)}$. The dispersion relation as in Equation (6.15) has two real root k_{j0} and four complex roots k_{jn} for $n = I, II, III, IV$ of the form $\pm\alpha \pm i\beta$. In addition, there is infinite numbers of purely imaginary roots $k_{jn} = i\kappa_{jn}$ for $n = 1, 2....$ It may be noted that the eigenfunctions $f_{jn}(y)$'s in the open water and plate covered region satisfy the orthogonality relation as given by

$$\left\langle f_{jm}, f_{jn} \right\rangle_{j=1,2,5} = \begin{cases} 0 & \text{for } m \neq n, \\ C_n' & \text{for } m = n, \end{cases} \text{ and } \left\langle f_{jm}, f_{jn} \right\rangle_{j=3,4} = \begin{cases} 0 & \text{for } m \neq n, \\ C_n''' & \text{for } m = n, \end{cases} \tag{6.16}$$

with respect to the orthogonal mode-coupling relation defined by

$$\left\langle f_{jm}, f_{jn} \right\rangle_{j=1,2,5} = \int_0^h f_{jm}(y) f_{jn}(y) dy, \tag{6.17}$$

$$\begin{aligned} \left\langle f_{jm}, f_{jn} \right\rangle_{j=3,4} = & \int_0^h f_{jm}(y) f_{jn}(y) dy - \frac{\alpha_1}{Q\left(k_{jn}\right)} \left\{ f_{jm}'(0) f_{jn}'(0) \right\} \\ & + \frac{\alpha_2}{Q\left(k_{jn}\right)} \left\{ f_{jm}'''(0) f_{jn}'(0) + f_{jm}'(0) f_{jn}'''(0) \right\} + \frac{\beta_1}{P\left(k_{jn}\right)} f_{jm}(0) f_{jn}(0), \end{aligned} \tag{6.18}$$

where $C_n' = \frac{2k_{jn}h + \sinh 2k_{jn}h}{4k_{jn} \cosh^2 k_{jn}h}$ for $j = 1, 2, 5,\ m = n = 0,$

$$C_n''' = \frac{(\alpha_0 - \alpha_1 k_{jn}^2 + \alpha_2 k_{jn}^4) 2k_{jn}h + (\alpha_0 - 3\alpha_1 k_{jn}^2 + 5\alpha_2 k_{jn}^4) \sinh 2k_{jn}h + (4\beta_1 k_{jn} \cosh^2 k_{jn}h)}{(4k_{jn} \cosh^2 k_{jn}h)(\alpha_0 - \alpha_1 k_{jn}^2 + \alpha_2 k_{jn}^4)}$$

for $j = 3, 4,\ m = n = 0, I, II,$

with $P\left(k_{jn}\right) = \left(\alpha_0 - \alpha_1 k_{jn}^2 + \alpha_2 k_{jn}^4\right)$ and $Q\left(k_{2n}\right) = \left(\beta_0 - \beta_1 k_{jn}^2\right)$.

The constant term C_n', C_n'', $P\left(k_{jn}\right)$ and $Q\left(k_{jn}\right)$ for $n=1,2,...$ are obtained by substituting $k_{jn}=i\kappa_{jn}$ for $j=1,2,3,4,5.$ In order to determine the unknown coefficients, the mode-coupling relation is applied on the velocity potential along with the respective eigenfunction and the edge conditions to obtain the system of linear equation. The mode-coupling relation as in Equation (6.18) is applied on the velocity potential $\phi_1\left(x,y\right)$ along with the eigenfunction $f_{1m}(y)$ at $x=0$ to obtain the equations given by

$$\left\langle \phi_1\left(0,y\right),\, f_{1m}(y)\right\rangle = \int_0^{h_1} \phi_1\left(0,y\right) f_{1m}(y)dy + \int_{h_1}^{h} \phi_1\left(0,y\right) f_{1m}(y)dy. \tag{6.19}$$

Further the orthogonality condition as in Equation (6.17) is applied for the eigenfunction $f_{1m}(y)$ and the expression of velocity potentials as in Equation (6.12) along with the boundary condition of the vertical porous barrier as in Equation (6.8) applied across the vertical boundary at $x=0, 0<y<h$ yields the simplified expression of unknowns $R_{1n}, n=0,1,2,...A_{2n}, B_{2n}, n=0,I,II,1,2,...$ for the cases of surface piercing and bottom standing barrier given by

$$\begin{aligned}
&-\left\{R_{10}+\sum_{n=1}^{\infty}R_{1n}\right\}\delta_{mn}\left\langle f_{1n},\, f_{1m}\right\rangle+\left\{\left(A_{20}+B_{20}\right)+\sum_{n=1}^{\infty}\left(A_{2n}+B_{2n}\right)\right\}\int_0^h f_{2n}(y)\, f_{1m}(y)dy \\
&-\left(\frac{1}{ik_{10}G}\right)\left\{ik_{20}\left(A_{20}-B_{20}\right)-\sum_{n=1}^{\infty}\kappa_{2n}\left(A_{2n}-B_{2n}\right)\right\}\int_0^{h_1} f_{2n}(y)\, f_{1m}(y)dy = I_{10}\delta_{mn}\left\langle f_{1n},\, f_{1m}\right\rangle,
\end{aligned} \tag{6.20a}$$

and in the case of bottom standing barrier for $m=0,1,2,....$

$$\begin{aligned}
&-\left\{R_{10}+\sum_{n=1}^{\infty}R_{1n}\right\}\delta_{mn}\left\langle f_{1n},\, f_{1m}\right\rangle+\left\{\left(A_{20}+B_{20}\right)+\sum_{n=1}^{\infty}\left(A_{2n}+B_{2n}\right)\right\}\int_0^h f_{2n}(y)\, f_{1m}(y)dy \\
&-\left(\frac{1}{ik_{10}G}\right)\left\{ik_{20}\left(A_{20}-B_{20}\right)-\sum_{n=1}^{\infty}\kappa_{2n}\left(A_{2n}-B_{2n}\right)\right\}\int_{h_1}^h f_{2n}(y)\, f_{1m}(y)dy = I_{10}\delta_{mn}\left\langle f_{1n},\, f_{1m}\right\rangle.
\end{aligned} \tag{6.20b}$$

The mode-coupling relation as in Equation (6.18) is applied on the velocity potential $\phi_{1x}\left(x,y\right)$ along with the eigenfunction $f_{1m}(y)$ at $x=0$ to obtain the equations given by

$$\left\langle \phi_{1x}\left(0,y\right),\, f_{1m}(y)\right\rangle = \int_0^{h_1} \phi_{1x}\left(0,y\right) f_{1m}(y)dy + \int_{h_1}^{h} \phi_{1x}\left(0,y\right) f_{1m}(y)dy. \tag{6.21}$$

The orthogonality condition as in Equation (6.17) is applied for the eigenfunction $f_{1m}(y)$ and the expression of velocity potentials as in Equation (6.12) along with the boundary condition of the vertical porous barrier as in Equation (6.8) applied across the vertical boundary at $x=0, 0<y<h$ yields the simplified expression of unknowns $R_{1n}, n=0,1,2,...A_{2n}, B_{2n}, n=0, I, II, 1, 2,...$ for the cases of surface piercing and bottom standing barrier given by

$$\begin{aligned}\left\{ik_{20}\left(A_{20}-B_{20}\right)-\sum_{n=1}^{\infty}\kappa_{2n}\left(A_{2n}-B_{2n}\right)\right\}\int_{0}^{h} f_{2n}\left(y\right) f_{1m}(y)dy \\ +\left\{ik_{20}R_{10}-\sum_{n=1}^{\infty}\kappa_{2n}R_{1n}\right\}\left\langle f_{1n},\, f_{1m}\right\rangle = ik_{10}I_{10}\delta_{mn}\left\langle f_{1n},\, f_{1m}\right\rangle,\end{aligned} \tag{6.22}$$

for $m=0,1,2,....$

Applying the mode-coupling relation as in Equation (6.18) on the velocity potential $\phi_3\left(x,y\right)$ at $x=-a_j,\ j=1,2$ along with the eigenfunction $f_{3m}(y)$ to obtain the equations given by

$$\begin{aligned}\left\langle \phi_3\left(-a_j,y\right),\, f_{3m}(y)\right\rangle = \int_{0}^{h}\phi_3\left(-a_j,y\right) f_{3m}(y)dy-\frac{\alpha_1}{Q\left(k_n\right)}\left\{\phi_3'\left(-a_j,y\right) f_{3m}'(0)\right\} \\ +\frac{\alpha_2}{Q\left(k_n\right)}\left\{\phi_3'''\left(-a_j,y\right) f_{3m}'(0)+\phi_3'\left(-a_j,y\right) f_{3m}'''(0)\right\}+\frac{\beta_1}{P\left(k_n\right)}\phi_3\left(-a_j,y\right) f_{3m}(0).\end{aligned} \tag{6.23}$$

The orthogonality condition as in Equation (6.18) is applied for the eigenfunction $f_{1m}(y)$ and the expression of velocity potentials as in Equation (6.12) along with the edge boundary condition of floating elastic plate as in Equation (6.9a-c) applied across the vertical boundary at $x=0, 0<y<h$ yields the simplified expression of unknowns $A_{jn}, B_{jn},\ j=2,3, n=0, I, II, 1, 2,...$ given by

$$\begin{aligned}&\left\{\left(A_{20}e^{ik_{20}a_1}+B_{20}e^{-ik_{20}a_1}\right)+\sum_{n=1}^{\infty}\left(A_{2n}e^{-\kappa_{2n}a_1}+B_{2n}e^{\kappa_{2n}a_1}\right)\right\}\int_{0}^{h} f_{2n}\left(y\right) f_{3m}(y)dy \\ &+\left\{\sum_{n=0,I}^{II}\left(A_{3n}e^{ik_{3n}a_1}+B_{3n}e^{-ik_{3n}a_1}\right)+\sum_{n=1}^{\infty}\left(A_{3n}e^{-\kappa_{3n}a_1}+B_{3n}e^{\kappa_{3n}a_1}\right)\right\}\left\{\frac{\alpha_2}{Q\left(k_{3n}\right)}\left\{f_{3n}'(0)\, f_{3m}'''(0)\right\}\right. \\ &\left.-\frac{\alpha_1}{Q\left(k_{3n}\right)}\left\{f_{3n}'(0)\, f_{3m}'(0)\right\}+\frac{\beta_1}{P\left(k_{3n}\right)}\left\{f_{3n}(0)\, f_{3m}(0)\right\}-\delta_{mn}\left\langle f_{3n},\, f_{3m}\right\rangle\right\}=0.\end{aligned} \tag{6.24}$$

The orthogonality condition as in Equation (6.18) is applied for the eigenfunction $f_{4m}(y)$ and the expression of velocity potentials as in Equation (6.12) along with the articulated boundary condition of floating elastic plate as in Equation (6.5a-d) applied across the vertical boundary at $x=0, 0<y<h$ yields the simplified expression of unknowns $A_{jn}, B_{jn}, j=3,4, n=0, I, II, 1, 2, ...$

$$\begin{aligned}
&\left\{\sum_{n=0,I}^{II}\left(A_{4n}e^{ik_{4n}a_2}+B_{4n}e^{-ik_{4n}a_2}\right)+\sum_{n=1}^{\infty}\left(A_{4n}e^{-\kappa_{4n}a_2}+B_{4n}e^{\kappa_{4n}a_2}\right)\right\}\int_0^h f_{4n}(y)\,f_{3m}(y)dy \\
&+\left\{\sum_{n=0,I}^{II}\left(A_{3n}e^{ik_{3n}a_2}+B_{3n}e^{-ik_{3n}a_2}\right)+\sum_{n=1}^{\infty}\left(A_{3n}e^{-\kappa_{3n}a_2}+B_{3n}e^{\kappa_{3n}a_2}\right)\right\}\left\{\frac{\alpha_2}{Q(k_{3n})}\left\{f'_{3n}(0)\,f'''_{3m}(0)\right\}\right. \\
&\left.-\frac{\alpha_1}{Q(k_{3n})}\left\{f'_{3n}(0)\,f'_{3m}(0)\right\}+\frac{\beta_1}{P(k_{3n})}\left\{f_{3n}(0)\,f_{3m}(0)\right\}-\delta_{mn}\left\langle f_{3n},\,f_{3m}\right\rangle\right\} \qquad (6.25)\\
&\qquad-\left\{\frac{k_{55}}{EI}\sum_{n=0,I}^{II,1,\ldots,\infty}ik_{4n}\left(A_{4n}e^{ik_{4n}a_2}-B_{4n}e^{-ik_{4n}a_2}\right)\frac{\alpha_2}{Q(k_{3n})}\,f'_{4n}(0)\,f'_{3m}(0)\right\} \\
&\qquad+\left\{\frac{k_{55}}{EI}\sum_{n=0,I}^{II,1,\ldots,\infty}ik_{3n}\left(A_{3n}e^{ik_{3n}a_2}-B_{3n}e^{-ik_{3n}a_2}\right)\frac{\alpha_2}{Q(k_{3n})}\left\{f'_{3n}(0)\,f'_{3m}(0)\right\}\right\}=0,
\end{aligned}$$

for $m=0, I, II, 1, 2, ...$

Applying the mode-coupling relation as in Equation (6.18) on the velocity potential $\phi_{3x}(x,y)$ at $x=-a_j, j=1,2$ along with the eigenfunction $f_{3m}(y)$ to obtain the equations given by

$$\begin{aligned}
&\left\langle\phi_{3x}(-a_j,y),\,f_{3m}(y)\right\rangle=\int_0^h\phi_{3x}(-a_j,y)\,f_{3m}(y)dy-\frac{\alpha_1}{Q(k_n)}\left\{\phi'_{3x}(-a_j,y)\,f'_{3m}(0)\right\} \\
&+\frac{\alpha_2}{Q(k_n)}\left\{\phi'''_{3x}(-a_j,y)\,f'_{3m}(0)+\phi'_{3x}(-a_j,y)\,f'''_{3m}(0)\right\}+\frac{\beta_1}{P(k_n)}\phi_{3x}(-a_j,y)\,f_{3m}(0).
\end{aligned} \qquad (6.26)$$

The orthogonality condition as in Equation (6.18) is applied for the eigenfunction $f_{1m}(y)$ and the expression of velocity potentials as in Equation (6.12) along with the edge boundary condition of floating elastic plate as in Equation (6.9a-c) applied across the vertical boundary at $x=0, 0<y<h$ yields the simplified expression of unknowns $A_{jn}, B_{jn}, j=2,3, n=0, I, II, 1, 2, ...$ given by

$$\left\{ik_{20}\left(A_{20}e^{ik_{20}a_1}-B_{20}e^{-ik_{20}a_1}\right)-\sum_{n=1}^{\infty}\kappa_{2n}\left(A_{2n}e^{-\kappa_{2n}a_1}-B_{2n}e^{\kappa_{2n}a_1}\right)\right\}\int_0^h f_{2n}(y)\,f_{3m}(y)dy$$
$$+\left\{\sum_{n=0,I}^{II}ik_{3n}\left(A_{3n}e^{ik_{3n}a_1}-B_{3n}e^{-ik_{3n}a_1}\right)-\sum_{n=1}^{\infty}\kappa_{3n}\left(A_{3n}e^{-\kappa_{3n}a_1}-B_{3n}e^{\kappa_{3n}a_1}\right)\right\}\left\{\frac{\alpha_2}{Q(k_{3n})}\{\wp f'_{3n}(0)\,f'_{3m}(0)\right.$$
$$\left.+f'_{3n}(0)\,f'''_{3m}(0)\}-\frac{\alpha_1}{Q(k_{3n})}\{f'_{3n}(0)\,f'_{3m}(0)\}+\frac{\beta_1}{P(k_{3n})}\{f_{3n}(0)\,f_{3m}(0)\}-\delta_{mn}\langle f_{3n},\,f_{3m}\rangle\right\}=0. \tag{6.27}$$

The orthogonality condition as in Equation (6.18) is applied for the eigenfunction $f_{4m}(y)$ and the expression of velocity potentials as in Equation (6.12) along with the articulated boundary condition of floating elastic plate as in Equation (6.5a-d) applied across the vertical boundary at $x=0, 0<y<h$ yields the simplified expression of unknowns $A_{jn}, B_{jn}, j=3,4, n=0,I,II,1,2,...$

$$\left(\sum_{n=0,I}^{II}ik_{4n}\left(A_{4n}e^{ik_{4n}a_2}-B_{4n}e^{-ik_{4n}a_2}\right)-\sum_{n=1}^{\infty}\kappa_{4n}\left(A_{4n}e^{-\kappa_{4n}a_2}-B_{4n}e^{\kappa_{4n}a_2}\right)\right)\int_0^h f_{4n}(y)\,f_{3m}(y)dy$$
$$+\frac{k_{33}}{EI}\left\{\sum_{n=0,I}^{II}\left(A_{4n}e^{ik_{4n}a_2}+B_{4n}e^{-ik_{4n}a_2}\right)+\sum_{n=1}^{\infty}\left(A_{4n}e^{-\kappa_{4n}a_2}+B_{4n}e^{\kappa_{4n}a_2}\right)\right\}\left\{\frac{\alpha_2}{Q(k_{3n})}\left(f'_{4n}(0)\,f'_{3m}(0)\right)\right\}$$
$$-\frac{k_{33}}{EI}\left\{\sum_{n=0,I}^{II}\left(A_{3n}e^{ik_{3n}a_2}+B_{3n}e^{-ik_{3n}a_2}\right)+\sum_{n=1}^{\infty}\left(A_{3n}e^{-\kappa_{3n}a_2}+B_{3n}e^{\kappa_{3n}a_2}\right)\right\}\left\{\frac{\alpha_2}{Q(k_{3n})}\left(f'_{3n}(0)\,f'_{3m}(0)\right)\right\}$$
$$+\left(\sum_{n=0,I}^{II}ik_{3n}\left(A_{3n}e^{ik_{3n}a_2}-B_{3n}e^{-ik_{3n}a_2}\right)-\sum_{n=1}^{\infty}\kappa_{3n}\left(A_{3n}e^{-\kappa_{3n}a_2}-B_{3n}e^{\kappa_{3n}a_2}\right)\right)\left\{\frac{\alpha_2}{Q(k_{3n})}\{f'_{3n}(0)\,f'''_{3m}(0)\right.$$
$$\left.-\wp f'_{3n}(0)\,f'_{3m}(0)\}-\frac{\alpha_1}{Q(k_{3n})}\{f'_{3n}(0)\,f'_{3m}(0)\}+\frac{\beta_1}{P(k_{3n})}\,f_{3n}(0)\,f_{3m}(0)-\delta_{mn}\langle f_{3n},\,f_{3m}\rangle\right\}=0, \tag{6.28}$$

for $m=0,I,II,1,2,....$ The mode-coupling relation as in Equation (6.18) is applied on the velocity potential $\phi_4(x,y)$ at $x=-a_3$ along with the eigenfunction $f_{4m}(y)$ to obtain the equations given by

$$\langle\phi_4(-a_3,y),\,f_{4m}(y)\rangle=\int_0^h\phi_4(-a_3,y)\,f_{4m}(y)dy-\frac{\alpha_1}{Q(k_n)}\{\phi'_4(-a_3,y)\,f'_{4m}(0)\}$$
$$+\frac{\alpha_2}{Q(k_n)}\{\phi'''_4(-a_3,y)\,f'_{4m}(0)+\phi'_4(-a_3,y)\,f'''_{4m}(0)\}+\frac{\beta_1}{P(k_n)}\phi_4(-a_3,y)\,f_{4m}(0). \tag{6.29}$$

Further, the orthogonality condition as in Equation (6.18) is applied for the eigenfunction $f_{4m}(y)$ in Equation (6.27-6.28) and the expression of velocity potentials as in Equation (6.12) along with the edge boundary conditions of floating elastic plate as in Equation (6.9a-c) applied across the vertical boundary at $x=0, 0<y<h$ yields the simplified expression of unknowns $A_{4n}, B_{4n}, n=0, I, II, 1, 2, ..., T_{5n}, n=0, 1, 2, ...$ of the form

$$\left\{T_{50}e^{ik_{50}a_3}+\sum_{n=1}^{\infty}T_{5n}e^{-\kappa_{5n}a_3}\right\}\int_0^h f_{5n}(y)\,f_{4m}(y)dy+\left\{\sum_{n=0,I}^{II,1,...,\infty}\left(A_{4n}e^{ik_{4n}a_3}+B_{4n}e^{-ik_{4n}a_3}\right)\right\}$$
$$\left\{\frac{\alpha_2}{Q(k_{4n})}f'_{4n}(0)\,f'''_{4m}(0)-\frac{\alpha_1}{Q(k_{4n})}f'_{4n}(0)\,f'_{4m}(0)+\frac{\beta_1}{P(k_{4n})}f_{4n}(0)\,f_{4m}(0)-\delta_{mn}\langle f_{4n},\,f_{4m}\rangle\right\}=0, \tag{6.30}$$

for $m=0, I, II, 1, 2, ...$ The mode-coupling relation as in Equation (6.18) is applied on the velocity potential $\phi_{4x}(x,y)$ at $x=-a_3$ along with the eigenfunction $f_{4m}(y)$ to obtain the equations given by

$$\begin{aligned}\langle\phi_{4x}(-a_3,y),\,f_{4m}(y)\rangle&=\int_0^h\phi_{4x}(-a_3,y)\,f_{4m}(y)dy-\frac{\alpha_1}{Q(k_n)}\{\phi'_{4x}(-a_3,y)\,f'_{4m}(0)\}\\&+\frac{\alpha_2}{Q(k_n)}\{\phi'''_{4x}(-a_3,y)\,f'_{4m}(0)+\phi'_{4x}(-a_3,y)\,f'''_{4m}(0)\}+\frac{\beta_1}{P(k_n)}\phi_{4x}(-a_3,y)\,f_{4m}(0).\end{aligned} \tag{6.31}$$

Further, the orthogonality condition as in Equation (6.18) is applied for the eigenfunction $f_{4m}(y)$ in Equation (6.27-6.28) and the expression of velocity potentials as in Equation (6.12) along with the edge boundary conditions of floating elastic plate as in Equation (6.9a-c) applied across the vertical boundary at $x=0, 0<y<h$ yields the simplified expression of unknowns $A_{4n}, B_{4n}, n=0, I, II, 1, 2, ..., T_{5n}, n=0, 1, 2, ...$ of the form

$$\left\{ik_{50}T_{50}e^{ik_{50}a_3}-\sum_{n=1}^{\infty}\kappa_{5n}T_{5n}e^{-\kappa_{5n}a_3}\right\}\int_0^h f_{5n}(y)\,f_{4m}(y)dy+$$
$$\left(\sum_{n=0,I}^{II}ik_{4n}\left(A_{4n}e^{ik_{4n}a_3}-B_{4n}e^{-ik_{4n}a_3}\right)-\sum_{n=1}^{\infty}\kappa_{4n}\left(A_{4n}e^{-\kappa_{4n}a_3}-B_{4n}e^{\kappa_{4n}a_3}\right)\right)\left\{\frac{\alpha_2}{Q(k_{4n})}\{f'_{4n}(0)\,f'_{4m}(0)\right.$$
$$\left.+f'_{4n}(0)\,f'''_{4m}(0)\}-\frac{\alpha_1}{Q(k_{4n})}f'_{4n}(0)\,f'_{4m}(0)+\frac{\beta_1}{P(k_{4n})}f_{4n}(0)\,f_{4m}(0)-\delta_{mn}\langle f_{4n},\,f_{4m}\rangle\right\}=0, \tag{6.32}$$

for $m = 0, I, II, 1, 2, \ldots$. On solving the infinite series sum of algebraic equations truncated up to a finite number of M terms in order to solve the system of $(8M + 20)$ linear equations having the unknown coefficients such as $R_{1n}, A_{jn}, B_{jn}, T_{5n}$, $j = 2$, $n = 0, 1, 2..., M$ and A_{jn}, B_{jn}, $j = 3, 4$, $n = 0, I, II, 1, 2...., M$. The wave reflection and transmission coefficients are obtained as

$$K_r = |R_0| \text{ and } K_t = \left| \frac{k_{50} \tanh k_{50} h}{k_{10} \tanh k_{10} h} T_0 \right|. \tag{6.33}$$

Due to the presence of vertical porous barriers a part of wave energy is dissipated, so the energy dissipation coefficient K_d (Chwang and Chan, 1998) is obtained as

$$K_d = 1 - K_r^2 + K_t^2. \tag{6.34}$$

6.4 NUMERICAL RESULTS AND DISCUSSIONS

The hydroelastic behaviour of the floating elastic plate in the presence of vertical bottom standing and surface piercing barriers for different support conditions under the action of the incident wave is analysed based on Timoshenko-Mindlin theory in finite water depth. The study is performed to analyze the reflection coefficient K_r, transmission coefficient K_t, dissipation coefficient K_d, plate deflection ζ_j / I_0, bending moment $M(x)$, shear force $W(x)$ and strain on the plate ε. The analysis is carried out for varying values of porosity, barrier heights and spacing between the barrier and floating elastic plate. The study also considers the various articulation conditions in the floating elastic plate. Three different cases of edge support condition i.e. free-free edge, simply supported edge and fixed edge conditions are considered and compared in detail. The evanescent wave mode is truncated upto $M = 20$ throughout the numerical computation and the convergence in the numerical result is achieved for $M \geq 15$. The numerical computations are carried out considering Young's Modulus $E = 5\text{GPa}$, $\rho_p / \rho_w = 0.9$, $\nu = 0.3$, $g = 9.8\text{ms}^{-2}$, complex porous effect parameter $G_0 = 0.5 + 0.5i$, barrier height $h_1 / h = 0.5$, spacing between the barrier and plate edge $L_1 / L = 0.1$, vertical linear spring stiffness $k_{33} = 10^5\,\text{Nm}^{-1}$ and flexural rotational spring stiffness $k_{55} = 10^5\,\text{Nm/rad}$ unless otherwise mentioned. The accuracy of the computed numerical results is checked with the energy balance relation as in Equation (6.34).

6.4.1 Bottom standing vertical porous barrier

The mitigation of hydroelastic behaviour due to the wave interaction with bottom standing vertical barrier in front of an articulated floating thick elastic plate is analysed in finite water depth for varying porosity, barrier height and spacing between a barrier and floating elastic plate.

6.4.1.1 Wave reflection, transmission and dissipation coefficients

The wave reflection, transmission and dissipation coefficients are plotted versus non-dimensional wavenumber $k_{10}h$ for varying porous effect parameter, depth of the barrier and spacing between the articulated floating plate and bottom standing vertical barrier. The resonating phenomenon is observed for various combinations of porous effect parameter G_0 within $0.1 < k_{10}h < 6$ in the wave reflection coefficient (Figure 6.2a), transmission coefficient (Figure 6.2b) and wave dissipation coefficient (Figure 6.2c). The increase in the $k_{10}h$ shows the higher estimation in the wave reflection coefficient (Figure 2a), minor values in the wave transmission coefficient (Figure 6.2b) and an opposite trend is observed in the wave dissipation coefficient (Figure 6.2c) as compared with the wave reflection coefficient. It is also noted that the energy dissipation is increasing with reduction in the porous effect parameter G_0 within $0.1 < k_{10}h < 6$, mainly due to the increasing porosity of the vertical bottom standing porous barrier. In general, the higher G_0 indicates that the higher friction factor and porosity of the vertical barrier. The increase in the porosity shows significant enhancement in the wave damping but the higher values in the friction factor shows the considerable impact on wave reflection coefficient. A moderate friction factor shows the applicable estimation in the wave reflection and energy damping. In the case of $k_{10}h > 6$, it is observed that there is no significant variation in wave reflection, transmission and dissipation coefficients for varying values of porous effect parameter G_0, due to reduction in wavelength of the incident waves. The variation in K_t for varying values of G_0 is not significant, which implies that the dissipated energy is mainly contributed by the dispersion of reflected waves and the present study shows that $G_0 = 0.5 + 0.5i$ is suitable to achieve high energy damping in the case of bottom standing barrier away from the articulated floating elastic plate.

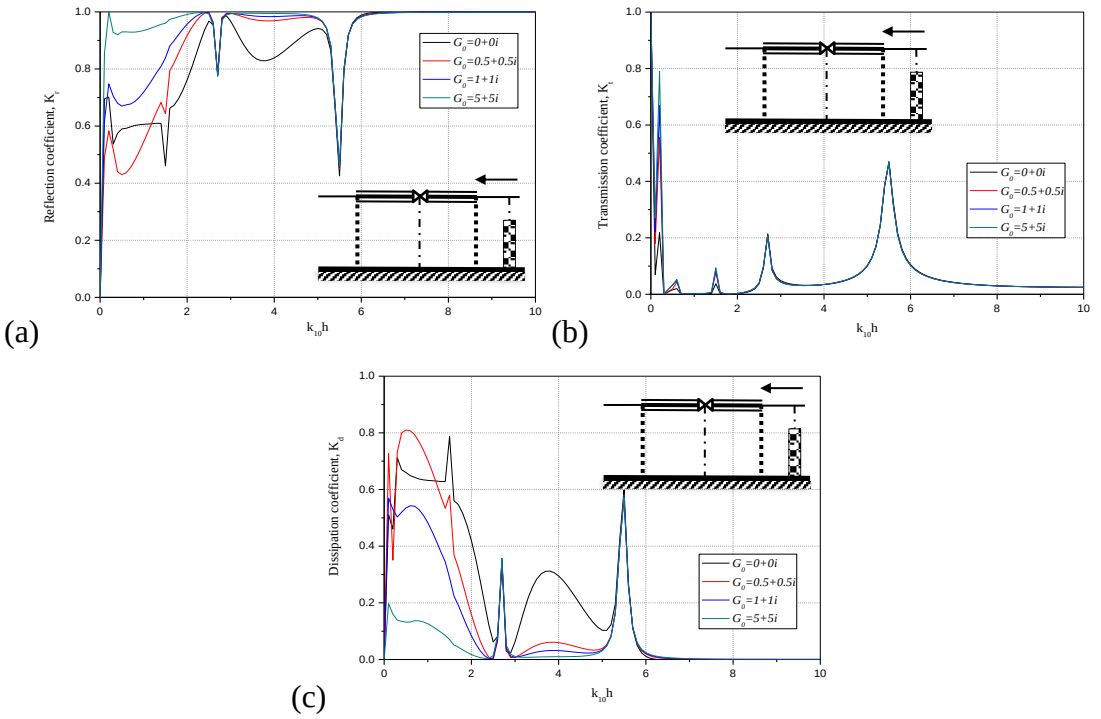

Figure 6.2: (a) Reflection, (b) transmission and (c) dissipation coefficient versus non-dimensional wavenumber for varying porosity effect parameter G_0 considering $h_1/h = 0.5$ and $L_1/L = 0.1$.

In the Figure 6.3(a-c), the wave reflection coefficient (Figure 6.3a), transmission coefficient (Figure 3b) and dissipation coefficient (Figure 6.3c) is presented for variable barrier height. In the case of bottom standing barrier, $h_1/h = 0$ implies the barrier height reaches to the free surface and $h_1/h = 1$ shows the vertical barrier is absent. The rapid rise and fall in the K_r is obtained with increase in the $k_{10}h$ and the change in barrier height shows the significant impact on reducing the resonating troughs at particular intervals. However, the resonating pattern in the wave transformation is due to the wave transmission in the presence of barrier and wave reflection by the articulated plate. The wave transmission (Figure 3b) reaches to minor values for all the combinations of barrier height due to the trapping of the incident waves in the spacing existing between the vertical barrier and articulated plate. The energy dissipation (Figure 6.3c) reduces with surge in the values of the height of the barrier h_1/h, which is mainly due to the decrease in the height of bottom standing porous barrier. However, if the barrier height reaches to the free surface, the energy damping reaches to the maximum values $K_d = 1$ for particular intervals and the reduction in the barrier height shows the minor

oscillations in the K_d and wave dissipation approaches to zero. At $k_{10}h = 4.0$, there is a 56%, 93% and 98% reduction in the K_d as observed for $h_1/h = 0.25$, $h_1/h = 0.5$, and $h_1/h = 0.75$ respectively as compared with $h_1/h = 0$. The reduction in the K_d suggests that, the performance of the bottom standing barrier solely depends upon the barrier height and better energy damping is possible in the presence of fully extended barrier.

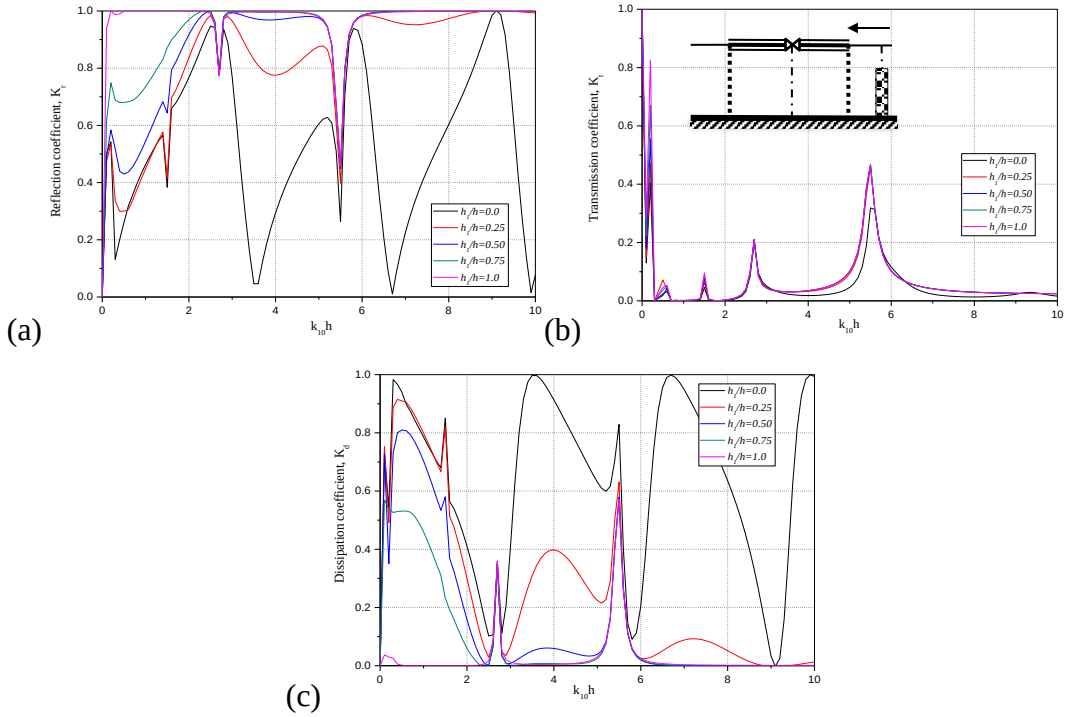

Figure 6.3: (a) Reflection, (b) transmission and (c) dissipation coefficient versus non-dimensional wavenumber for varying barrier heights considering $G_0 = 0.5 + 0.5i$ and $L_1 / L = 0.1$.

The spacing between the barrier and articulated plate is one of the influencing phenomena in trapping of the incident waves. In the Figure 6.4(a-c), the K_r (Figure 6.4a), K_t (Figure 6.4b) and K_d (Figure 6.4c) is presented for various combinations of spacing within $0.05 < L_1/L < 0.2$. It is observed that with the increase in the L_1/L, the oscillations in the wave reflection gets broadens and influences the energy damping and the K_d is observed increasing with reduction in the values of L_1/L mainly due to the change in the spacing between the barrier and floating elastic plate. In the case of non-dimensional wavenumber $k_{10}h > 6$, it is observed that there is no significant variation in transmission coefficient for varying spacing between the barrier and floating plate,

due to the reduction in wavelength, which implies the dissipated energy is mainly contributed by the dispersion of reflected waves. However, the enhance in the energy damping K_d is possible for high spacing within $0.1 \le k_{10}h \le 1$ and K_d reduces with increase in the $k_{10}h$ within $1 \le k_{10}h \le 4$. Thereafter, the uniform values of energy damping is obtained within $4 \le k_{10}h \le 10$ for all the combinations of L_1/L due to the porous barrier by achieving the full reflection and zero transmission coefficients.

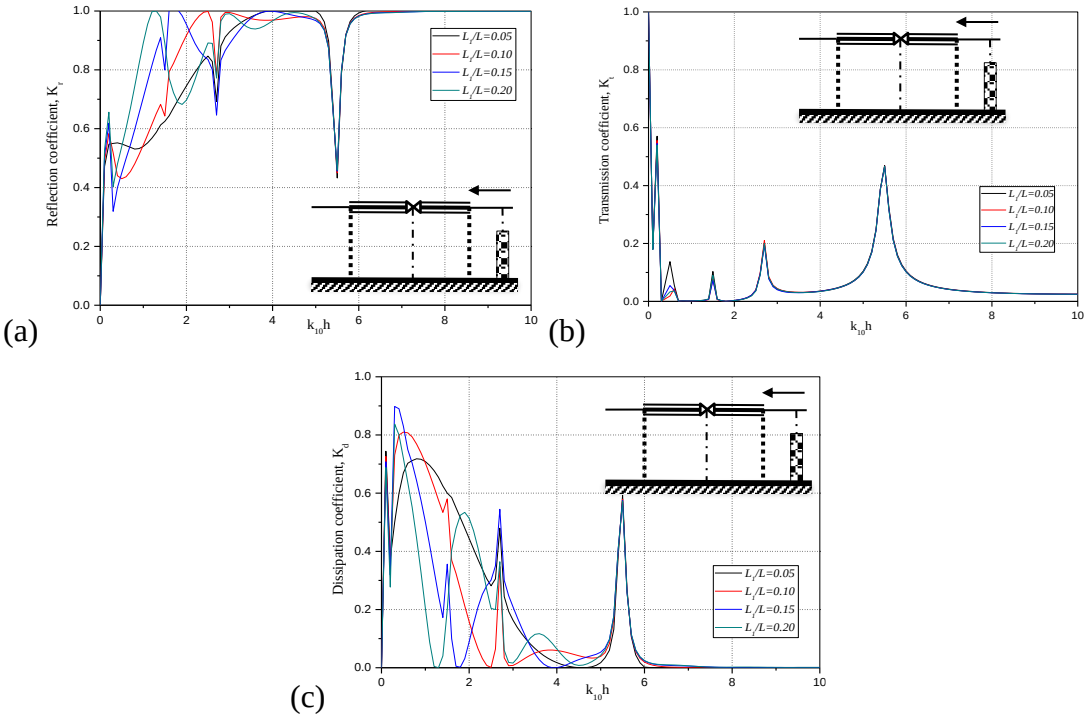

Figure 6.4: (a) Reflection, (b) transmission and (c) dissipation coefficient versus non-dimensional wavenumber for varying spacing between the barrier considering $G_0 = 0.5 + 0.5i$ and $h_1 / h = 0.5$.

6.4.1.2 Hydroelastic responses of the articulated floating plate

The hydroelastic response of articulated floating elastic plate under the action of ocean waves in terms of plate deflection ζ_j / I_0, stain in the floating plate ε, bending moment $M(x)$ and shear force $W(x)$ resultants along the plate length x/L for varying porous effect parameter, barrier height and spacing between the bottom standing barrier and the articulated floating elastic plate is presented. The hydroelastic responses are noticed to reduce due to the presence of articulated joint in the floating elastic plate as illustrated in Figure 6.5(a-d).

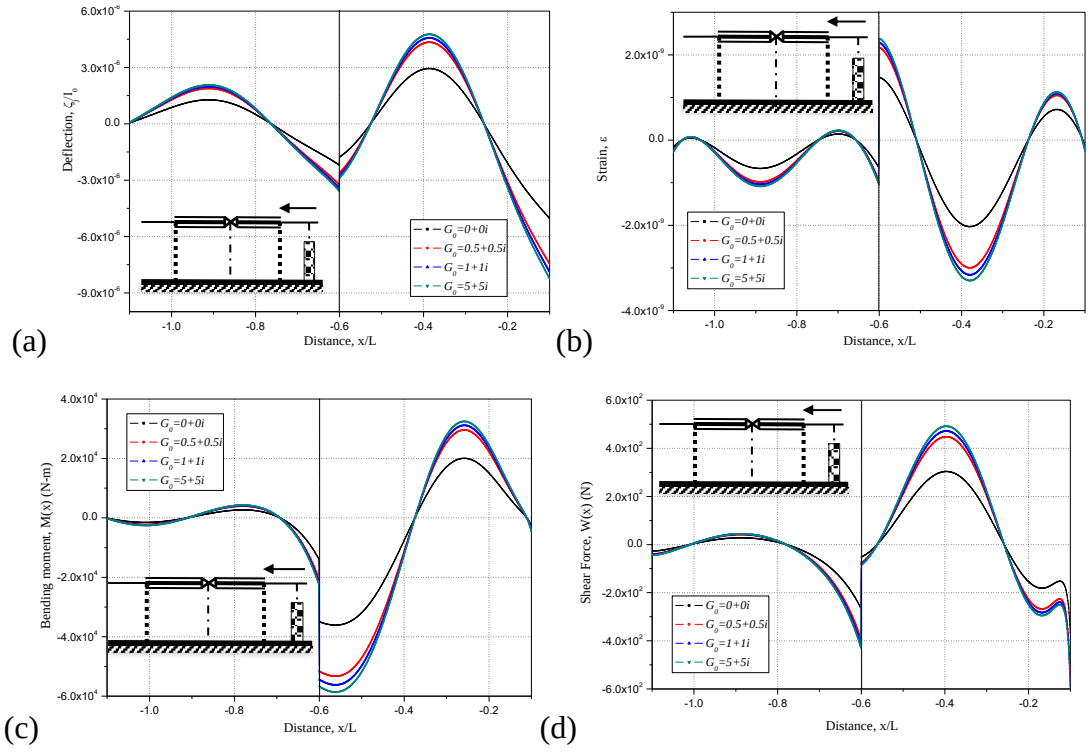

Figure 6.5: (a) Plate deflection (b) wave induced strain (c) bending moment and (d) shear force resultants along the plate length x/L for different porosity of the bottom standing barrier considering $k_{10}h = 2.0,\quad h_1/h = 0.5$ and $L_1/L = 0.1$.

The 58% (Figure 6.5a), 81% (Figure 6.5b), 84% (Figure 6.5c) and 92 % (Figure 6.5d) reduction in the plate deflection ζ_j/I_0, stain of the floating plate ε, bending moment $M(x)$ and shear force $W(x)$ is obtained due to the presence of the articulation at the oscillatory peak for $G_0 = 5+5i$ and similar trend is noticed for various combinations of porous effect parameter G_0 in the form of oscillatory peaks and troughs. The difference in the plate deflection and strain is also observed at the articulated joint due to change in rigidity at the connecting joints. The responses are observed to increase with the surge in porous effect parameter G_0, due to increase in energy dissipation along with the reduction in the barrier porosity. The pattern of responses is observed to remain similar for varying porous effect parameter. However, 30%, 11% and 4% increase in the ζ_j/I_0 is obtained for $0.5+0.5i \le G \le 5+5i$ as compared with the $G_0 = 0+0i$ due to the increase in the permeability of the barrier at oscillatory peak, but an opposite trend is obtained in the strain ε (Figure 5b) with increase in the porous effect parameter G_0.

Similar trend in bending moment $M(x)$ and shear force $W(x)$ in the articulated floating elastic plate is observed for the case of varying porous effect parameter in the presence of bottom standing barrier.

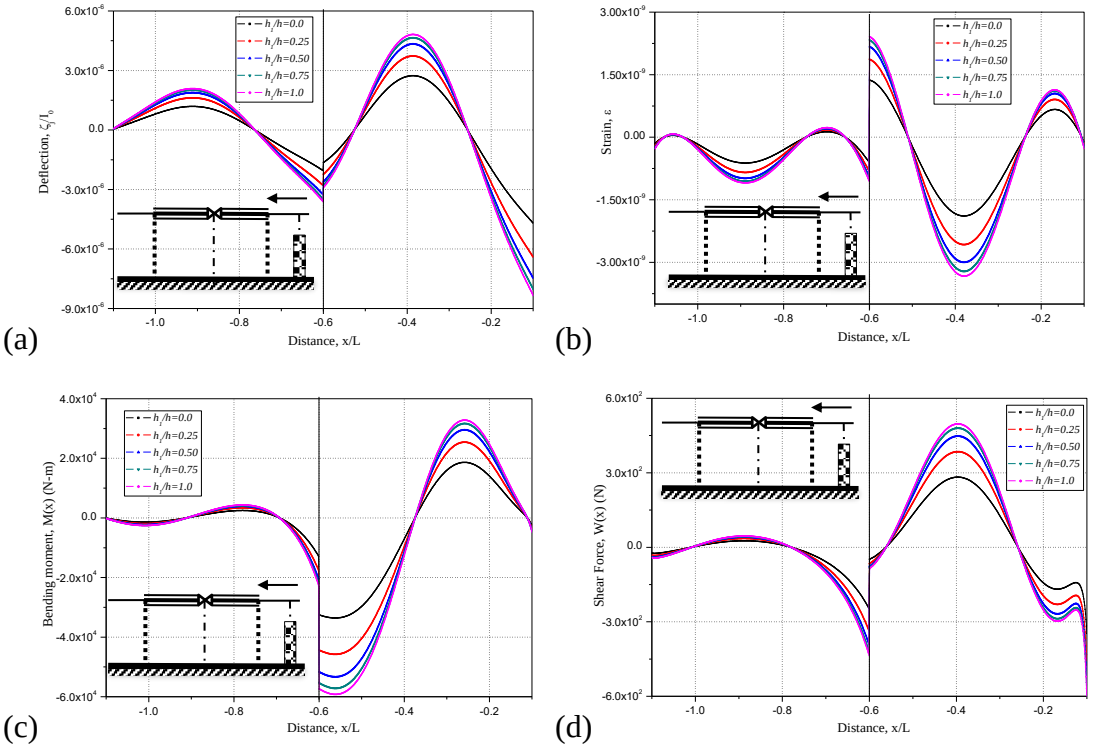

Figure 6.6: (a) Plate deflection (b) wave induced strain (c) bending moment and (d) shear force resultants along the plate length x/L for varying barrier heights considering $k_{10}h=2.0,\ G_0=0.5+0.5i$ and $L_1/L=0.1$.

The hydroelastic responses are noticed to increase with the surge in the values of h_1/h due to the reduction in the barrier height, signifying lesser energy dissipation as illustrated in Figure 6.6(a-d). The presence of the articulated joint in the floating elastic plate shows difference in response and further reduction in the hydroelastic response due to the change in the rigidity at the connecting joints. The pattern of the hydroelastic responses is observed to remain same for varying porous effect parameter. The 57% (Figure 6.6a), 83% (Figure 6.6b), 85% (Figure 6.6c) and 91 % (Figure 6.6d) reduction in the plate deflection ζ_j/I_0, stain ε, bending moment $M(x)$ and shear force $W(x)$ is noted due to the presence of the articulation at each of the peak point for $h_1/h=1$. A similar reduction in the hydroelastic response in achieved for all the combinations of height of the porous barrier h_1/h.

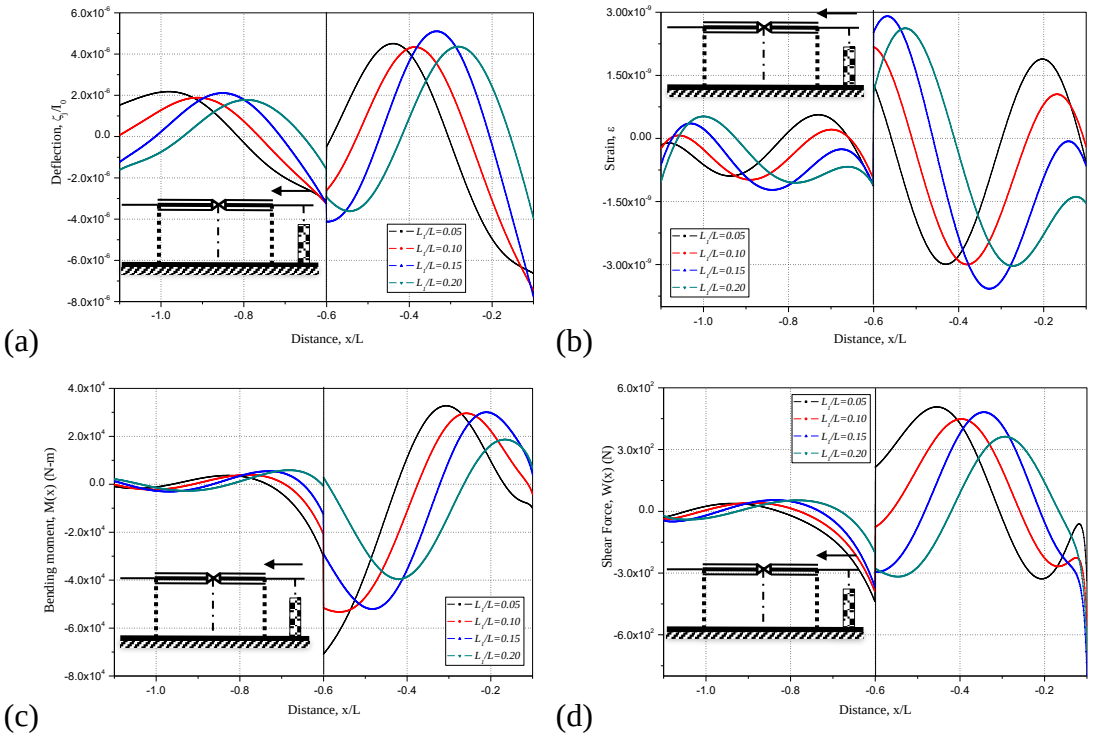

Figure 6.7: (a) Plate deflection (b) wave induced strain (c) bending moment and (d) shear force resultants along the plate length x/L for finite spacing L_1/L considering $k_{10}h = 2.0,\ G_0 = 0.5 + 0.5i$ and $h_1/h = 0.5$.

6.4.2 Surface piercing vertical porous barrier

The significance of surface piercing barrier away from the articulated floating elastic plate on the wave scattering is analysed for finite water depth varying porosity, barrier height and spacing between a barrier and floating elastic plate.

6.4.2.1 Wave reflection and transmission coefficients

The reflection, transmission and dissipation coefficients are plotted versus non-dimensional wavenumber $k_{10}h$ for the surface piercing vertical barrier in front of the articulated floating elastic plate. The wave reflection coefficient (Figure 6.8a), transmission coefficient (Figure 6.88b) and dissipation coefficient (Figure 6.8c) are examined for various values of the porous effect parameter G_0. The increase in the G_0 means increase in the porosity, friction factor and inertia effect. The increase in the friction factor enhances the wave reflection and the increase in the porosity enhances the energy damping. However, the barrier is thin and porosity of the barrier performs minor role as compared with the friction factor offered by the vertical barrier. In the

present case the variation in the G_0 shows the resonating peaks and troughs in the K_r for various combinations of G_0 and the resonating troughs are obtained, which may be due to the formation of standing waves. However, the resonating crests and troughs broaden with increase in the $k_{10}h$ and influence the wave scattering. The wave transmission K_t (Figure 6.8b) is observed to reduce with the decrease in the values of G_0 mainly due to the dissipation of waves from barriers. The energy dissipation (Figure 6.8c) is observed increasing with the reduction in the values of G_0, which is mainly due to the increase in the porosity and friction factor offered by the vertical porous barrier. On the other hand, at very low values of G_0, high reflection and dissipation of wave is observed which is mainly due to the blocking of waves by the barrier. The energy damping due to the presence of surface piercing barrier is observed high as compared with the bottom standing barrier due to the fact that the wave energy is concentrated on the free surface.

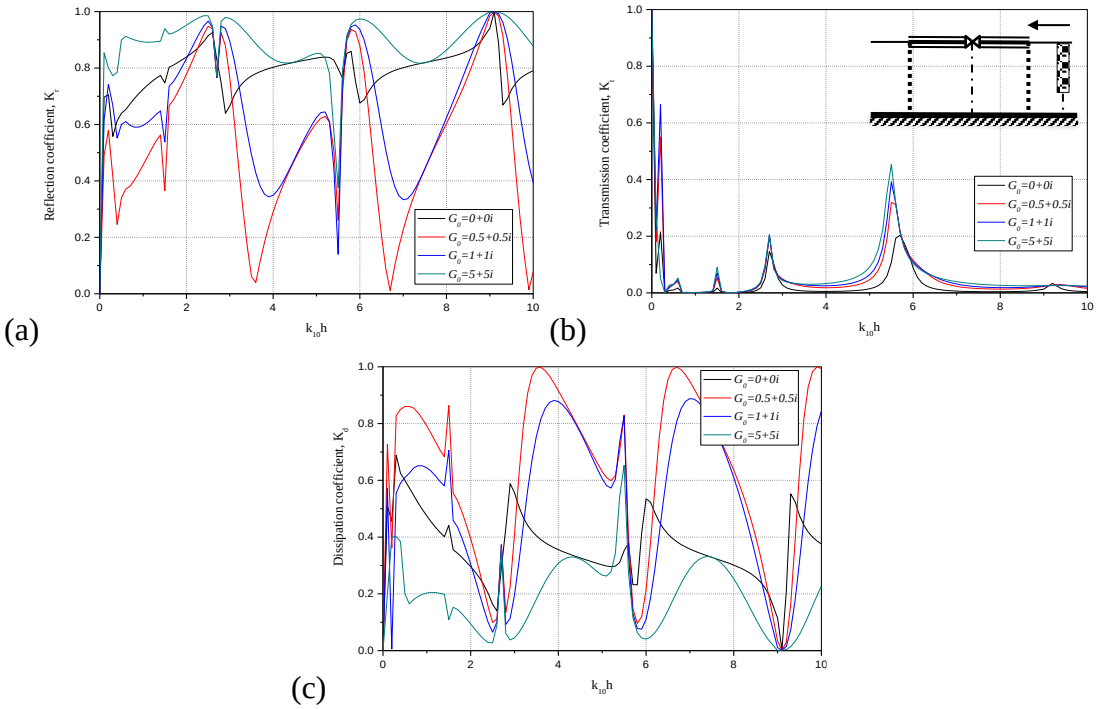

Figure 6.8: (a) Reflection, (b) transmission and (c) dissipation coefficient versus non-dimensional wavenumber for varying porosity of vertical barrier considering $L_1 / L = 0.1$ and $h_1 / h = 0.5$.

In the Figure 6.9(a-c), the wave reflection (Figure 6.9a), transmission (Figure 6.9b) and wave energy dissipation (Figure 6.9c) are presented varying the barrier depth h_1/h

within $0 \le h_1/h \le 1$. In the case of surface piercing barrier, the value $h_1/h = 0$ corresponds to the no barrier case suggesting direct incident of wave on to the articulated floating elastic plate, signifying zero energy dissipation and higher transmission of incident waves and $h_1/h = 1$ corresponds to the fully extended barrier. In the absence of the barrier $h_1/h = 0$, the wave reflection reaches to the unity and wave transmission shows the minimum value. On the other hand, for $0.25 \le h_1/h \le 1$ shows almost uniform estimation in the wave transformation, and resonating peaks and troughs are evident in the design of the surface piercing barrier. The variation in the K_r and K_d is minimum for dimensionless wave number within $1.8 \le k_{10}h \le 10$ for various combinations of $0.25 \le h_1/h \le 1$ and it is mainly due to the barrier position. In the present case, the barrier is placed near to the free surface and depth of the barrier is increased. In general, the wave energy potential is concentrated on the free surface and it is trapped by the spacing available between the barrier and articulated plate. However, the depth of the barrier shows minor role in enhancing the wave damping in the case of the surface piercing barrier and the height of the bottom standing barrier shows a significant role in enhancing the energy damping.

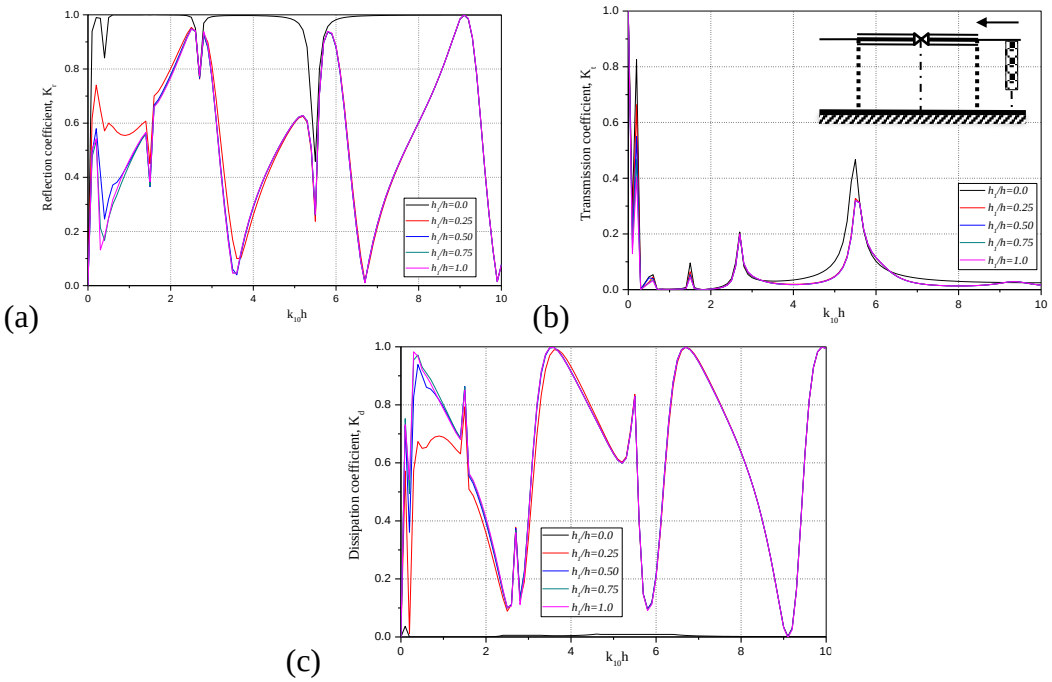

Figure 6.9: (a) Reflection, (b) transmission and (c) dissipation coefficient versus non-dimensional wavenumber for varying barrier heights considering $G_0 = 0.5 + 0.5i$, and $L_1 / L = 0.1$

In Figure 6.10(a-c), the wave reflection (Figure 6.10a) is observed varying in the oscillatory manner and broadens with increase in the L_1/L. The resonating peaks and troughs influences the wave reflection in the periodic intervals and it is evident that the resonating peaks and troughs may be due to the constructive and destructive interferences. The wave transmission (Figure 6.10b) reaches to the minor values for all the combinations of L_1/L with increases in the $k_{10}h$. It is also observed that the energy dissipation peaks are increasing with increasing values of L_1/L, which is mainly due to the increase in the spacing between the barrier and floating elastic plate further causing resonance in that region. Slight surge in the values of K_t is observed for increasing spacing between the barrier and floating elastic plate, which implies the dissipated energy is mainly contributed from the dispersion of reflected waves. However, the resonating troughs in the K_r and dissipating peaks in the K_d are helpful in the actual design of the spacing between the vertical barrier away from the articulated floating plate.

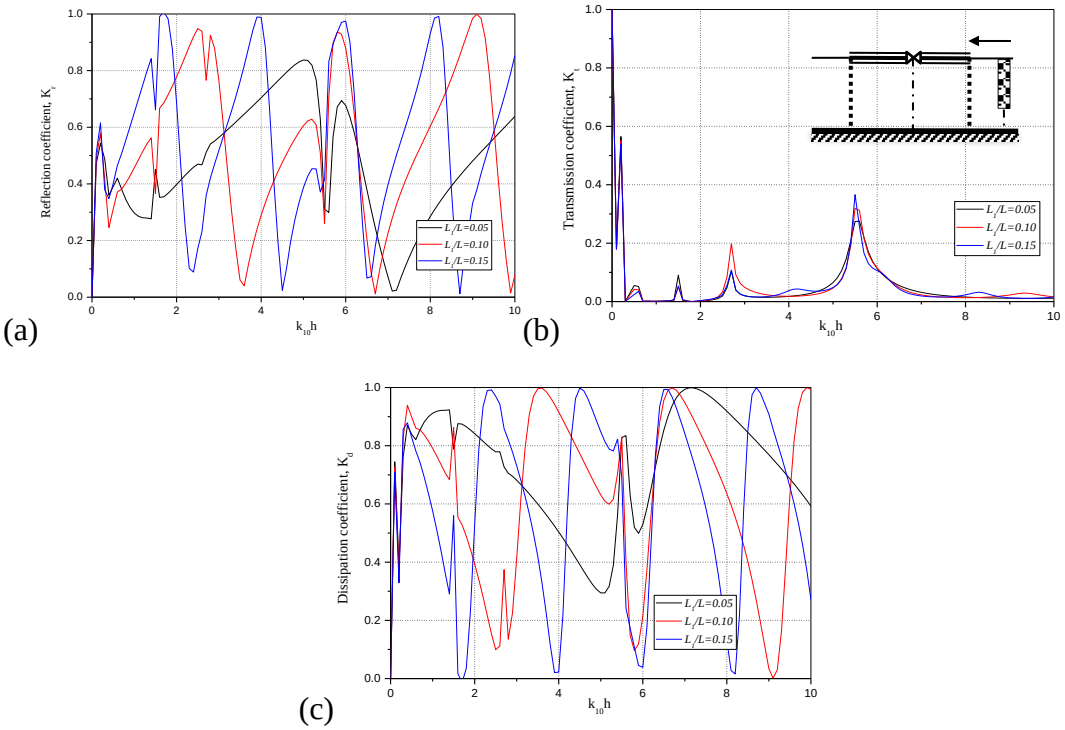

Figure 6.10: (a) Reflection, (b) transmission and (c) dissipation coefficient versus non-dimensional wavenumber for varying spacing between the barrier and floating elastic plate considering $G_0 = 0.5 + 0.5i$ and $h_1 / h = 0.5$.

6.4.2.2 Hydroelastic responses of floating plate

The hydroelastic responses of articulated floating elastic plate under the action of ocean waves along the plate length x/L for varying the parameters of surface piercing vertical barrier in front of the articulated floating elastic plate is presented. The hydroelastic responses are noticed to reduce due to the presence of articulated joint in the floating elastic plate as illustrated in Figure 6.11(a-d). The difference in the response is also observed at the articulated joint due to change in rigidity at the connecting joints.

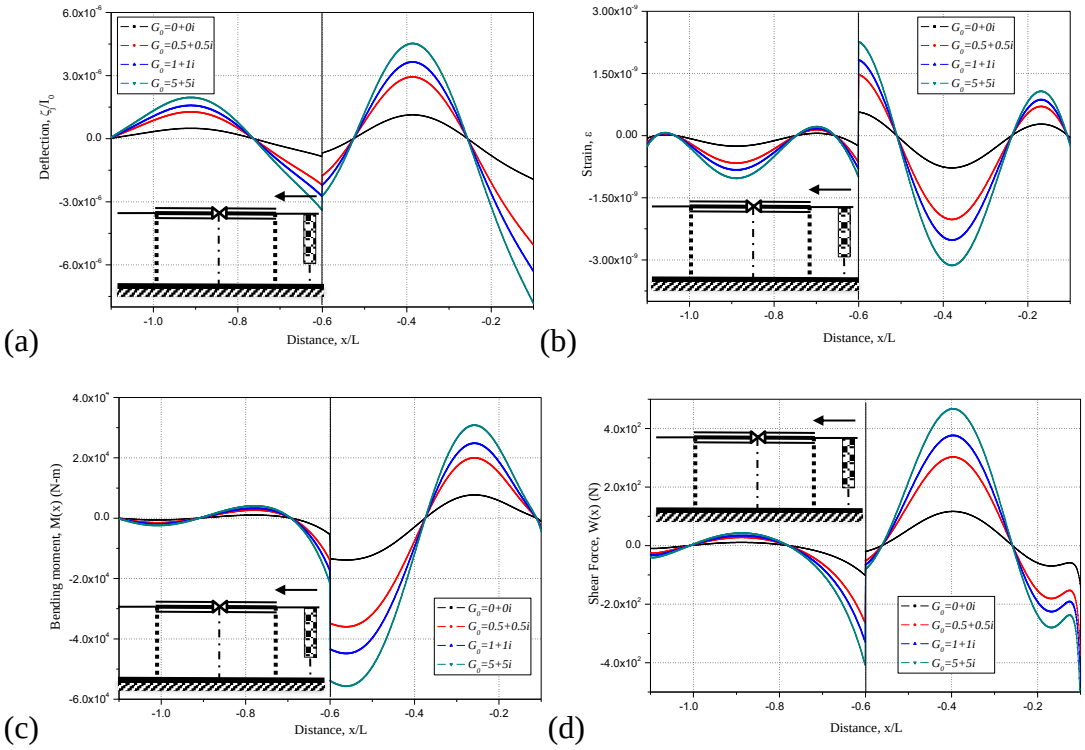

Figure 6.11: (a) Plate deflection (b) wave induced strain (c) bending moment and (d) shear force resultants along the plate length x/L for varying porosity considering $k_{10}h = 2,\ L_1/L = 0.1$ and $h_1/h = 0.5$.

The responses are observed to increase with the surge in porous effect parameter G_0, due to increase in energy dissipation along with the reduction in the barrier porosity. The pattern of responses is observed to remain similar for varying values of porous effect parameter. The increase in the porous effect parameter G_0 shows significant changes in the hydroelastic response and each of the oscillatory peak and trough attains maximum value due to the high porosity and friction factor, which allows more incident waves through the barrier for higher values of G_0. The comparative study is performed

to show the articulation impact on the hydroelastic response. The 55% (Figure 6.11a), 82% (Figure 6.11b), 87% (Figure 6.11c) and 89 % (Figure 6.11d) decrease in the plate deflection ζ_j/I_0, wave induced stain ε, bending moment $M(x)$ and shear force $W(x)$ is noted at each of the peak point due to the presence of the articulation for porous effect parameter $G_0 = 5+5i$. Thereafter, a gradual reduction in the hydroelastic responses is achieved with the reduction in the G_0 and the variation is evident at the point where oscillatory peaks and troughs are dominant.

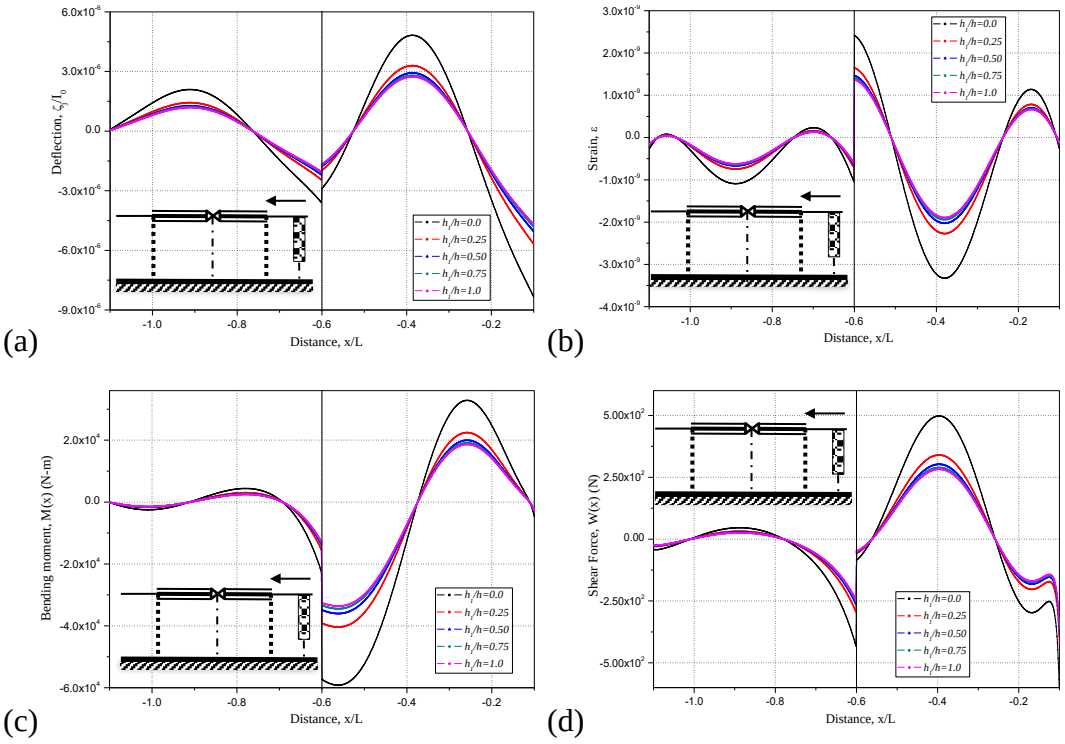

Figure 6.12: (a) plate deflection (b) wave induced strain (c) bending moment and (d) shear force resultants along the plate length x/L for varying heights of the surface piercing barrier considering $k_{10}h = 2$, $G_0 = 0.5+0.5i$, and $L_1/L = 0.1$.

In Figure 6.12(a-d), the hydroelastic responses are noticed to decrease with the surge in the values of h_1/h due to increase in the barrier height which signifies higher energy dissipation. The presence of articulated joint in the floating elastic plate shows difference in response and further reduction in the hydroelastic response due to the change in rigidity at the connecting joints. However, the increase in the barrier depth shows the significant changes in the hydroelastic response at the each of the peaks and troughs. The 59% (Figure 6.12a), 79% (Figure 6.12b), 85% (Figure 6.12c) and 90%

(Figure 6.12d) decrease in the plate deflection ζ_j / I_0, wave induced stain ε, bending moment $M(x)$ and shear force $W(x)$ is achieved due to the presence of the articulation for no barrier condition $h_1/h = 0.$ Thereafter, a gradual reduction in the hydroelastic responses is observed due to the change in the barrier depth and it shows very little variation in the hydroelastic response due to the barrier position which is placed near to the free surface. On comparing in the case of the bottom standing barrier as in Figure 6.6(a-d), the barrier height shows significant impact on the wave transformation and hydroelastic response as compared with the barrier placed near to the surface. However, the surface piercing barrier shows significant impact on the hydroelastic response for minimum depth of the barrier $h_1/h = 0.25.$

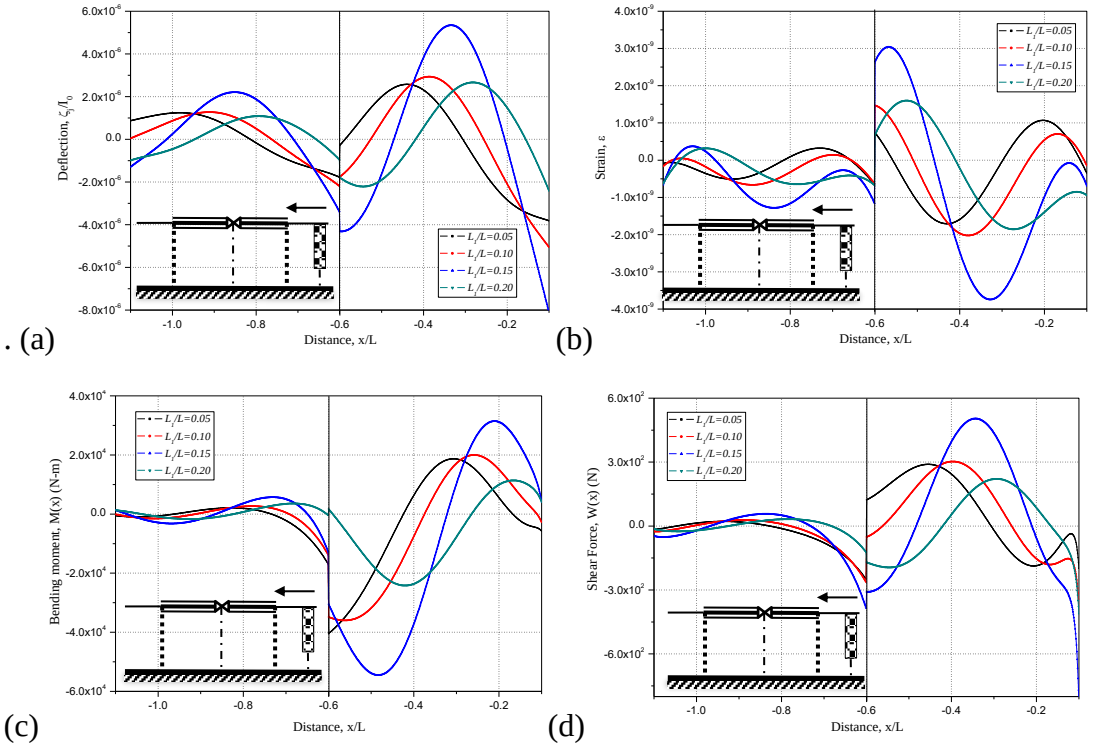

Figure 6.13: (a) Plate deflection (b) wave induced strain (a) bending moment and (b) shear force resultants along the plate length x/L for finite spacing L_1/L considering $k_{10}h = 2,\ G_0 = 0.5 + 0.5i,$ and $h_1/h = 0.5.$

In Figure 6.13(a-d), the hydroelastic response are noticed to shift backwards due to the reduction in the spacing between the barrier and the floating elastic plate L_1/L. The oscillatory peaks and troughs are noticed to vary with the change in the spacing between

the barrier and the floating elastic plate L_1/L and the oscillating peaks may be due to the high penetration of waves by the barrier and oscillating troughs are observed may be due to the standing wave formation which is evident in the design of the spacing L_1/L. However, the presence of articulated joint in the floating elastic plate shows difference in response and further reduction in the hydroelastic response due to the change in rigidity at the connecting joints.

6.4.3 Effect of articulation on floating plate

The mitigation of hydroelastic behaviour due to the wave interaction with vertical barriers in front of the articulated floating elastic thick plate is analysed in finite water depth for varying vertical linear spring stiffness and flexural rotational spring stiffness to understand the effect of articulation in the presence of vertical barriers.

6.4.3.1 Wave reflection and transmission coefficients

In Figure 6.14(a-c), the reflection coefficient (Figure 6.14a), transmission coefficient (Figure 6.14b) and dissipation coefficient (Figure 6.14c) are plotted versus non-dimensional wave number for different vertical linear spring stiffness and flexural rotational spring stiffness k_{33} and k_{55} at the connecting joints along the floating elastic plate with bottom standing vertical barrier. Minimal variation in the wave reflection coefficient is observed for the spring stiffness $k_{33} < 10^5\,\text{Nm}^{-1}$ and $k_{55} < 10^5\,\text{N/rad}$. The wave transmission is observed to shift towards lower values of non-dimensional wave number for lower values of spring stiffness. However, the resonating peaks and troughs are widely developed in the case of wave transmission for various values of k_{33} and k_{55}. On the other hand, the vertical linear spring stiffness is observed to be dominant as compared to flexural rotational spring stiffness, signifying lower transmission of waves. The variation between the outcomes in the K_d is observed to be very minimum within $0.1 \le k_{10}h \le 2.5$ thereafter, an oscillating phenomenon is noted with increase in the $k_{10}h$ Minimum values of k_{33} and k_{55} shows the higher estimation in the energy damping and increase in the k_{33} and k_{55} presents the reduction in the oscillations along with energy damping. The presence of bottom standing vertical barrier in combination with varying articulation contributes in dissipation of wave energy from reflected waves.

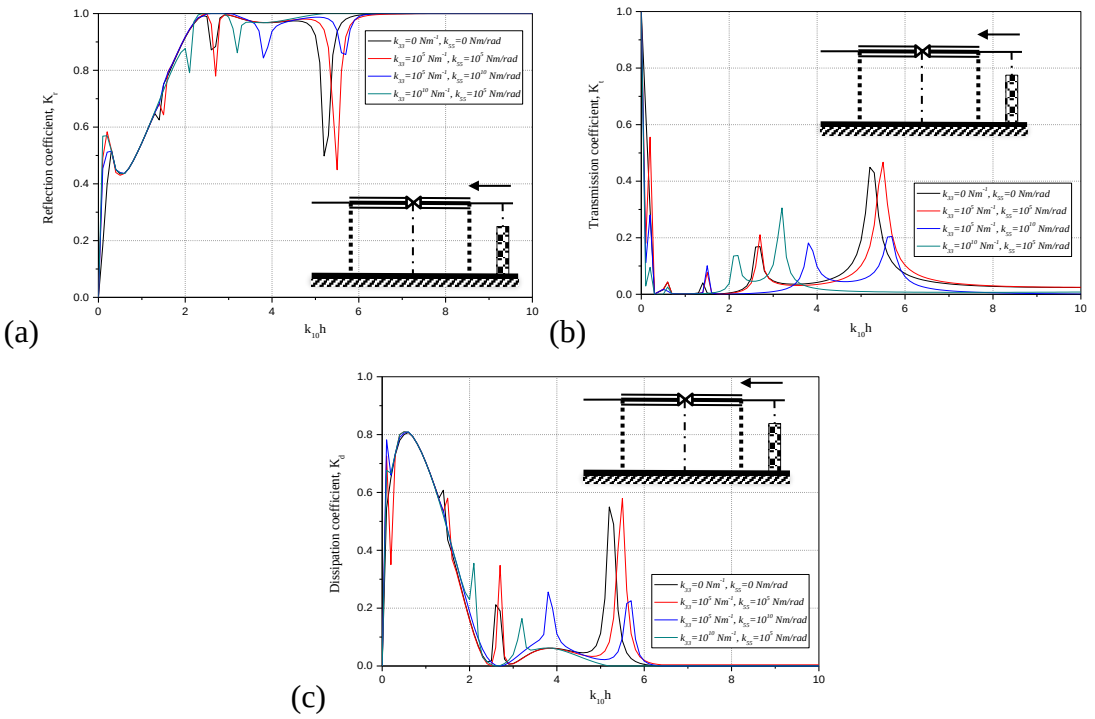

Figure 6.14: (a) Reflection, (b) transmission and (c) dissipation coefficient versus non-dimensional wavenumber for varying k_{33} and k_{55} considering $G_0 = 0.5 + 0.5i$, $L_1 / L = 0.1$ and $h_1 / h = 0.5$ in the case of bottom standing porous barrier.

In the Figure 6.15(a-c), the wave reflection coefficient (Figure 6.15a), transmission coefficient (Figure 6.15b) and dissipation coefficient (Figure 6.15c) are plotted versus non dimensional wave number $k_{10}h$ for different vertical linear spring stiffness k_{33} and flexural rotational spring stiffness k_{55} at the connecting joints along the floating elastic plate with surface piercing vertical barrier. Almost uniform estimation is obtained in the wave reflection coefficient in the behaviour of waves for the spring stiffness $k_{33} < 10^5\,\text{Nm}^{-1}$ and $k_{55} < 10^5\,\text{N/rad}$ as observed similar in the case of bottom standing barrier as in Figure 14a. A continuous pattern of peaks in wave refection and dissipation is observed due to the resonance caused in between the barrier and floating elastic plate. However, for all the combinations of k_{33} and k_{55} an oscillating pattern is obtained in the wave reflection coefficient and almost negligible transmission coefficient along with resonating pattern in the energy damping is achieved. It is also observed that, the optimum points in the wave reflection coefficient is significant to achieve the resonating crests in the energy damping. However, k_{33} and k_{55} influences the wave scattering for particular intervals but high energy damping can be achieved due to the presence of

surface piercing barrier. As a comparison with the bottom standing barrier, the surface piercing barrier shows the significant role in reducing the wave transmission coefficient and enhances the energy damping, which also influences the design of surface piercing barrier in order to reduce the wave impact on the articulated floating structure. However, the resonating crests in the energy damping is evident in order to reduce the wave impact on the articulated floating plate for better life period.

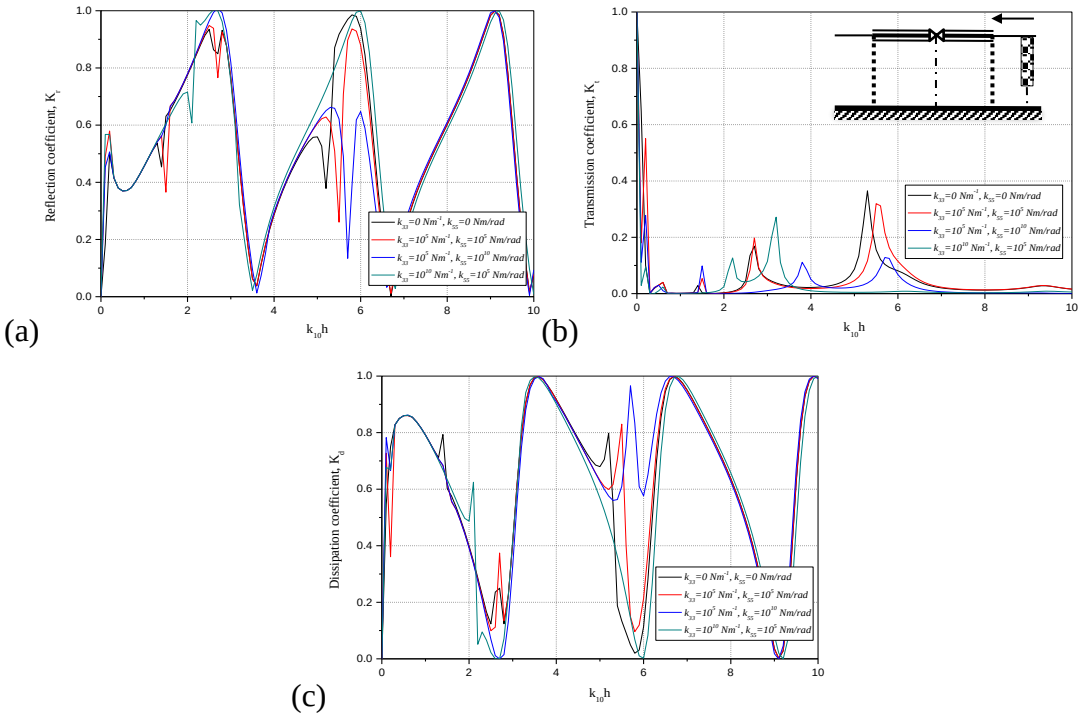

Figure 6.15: (a) Reflection, (b) transmission and (c) dissipation coefficient versus non-dimensional wavenumber for varying k_{33} and k_{55} considering $G_0 = 0.5 + 0.5i$, $L_1 / L = 0.1$ and $h_1 / h = 0.5$ in the case of surface piercing porous barrier.

6.4.3.2 Hydroelastic responses of floating plate

The hydroelastic response of the floating elastic plate are presented for varying spring stiffness at the connecting joint of articulated floating elastic plate along with a bottom standing vertical barrier as illustrated in Figure 6.16(a-d). The difference in the response is observed at the articulated joint due to change in rigidity at the connecting joints. The responses are observed to reduce with the surge in the values of spring stiffness k_{33} and k_{55} at the connecting joints due to increase in rigidity. The oscillating crests and troughs are observed in the hydroelastic response of the floating plate with increase in the k_{33} and k_{55} which is similar as in the previous sections. Particularly, rigid connection shows

higher estimation in the hydroelastic response as compared with the other type of articulations. A comparative study is performed for rigid connection between the crest values before and after articulation. The 46% (Figure 6.16a), 24% (Figure 6.16b), 80% (Figure 6.16c) and 86% (Figure 6.16d) decrease in the plate deflection ζ_j / I_0 at oscillating crest, wave induced stain ε at oscillating trough, bending moment $M(x)$ and shear force $W(x)$ at oscillating crests is achieved due to the presence of the articulated floating elastic plate combined with bottom standing barrier.

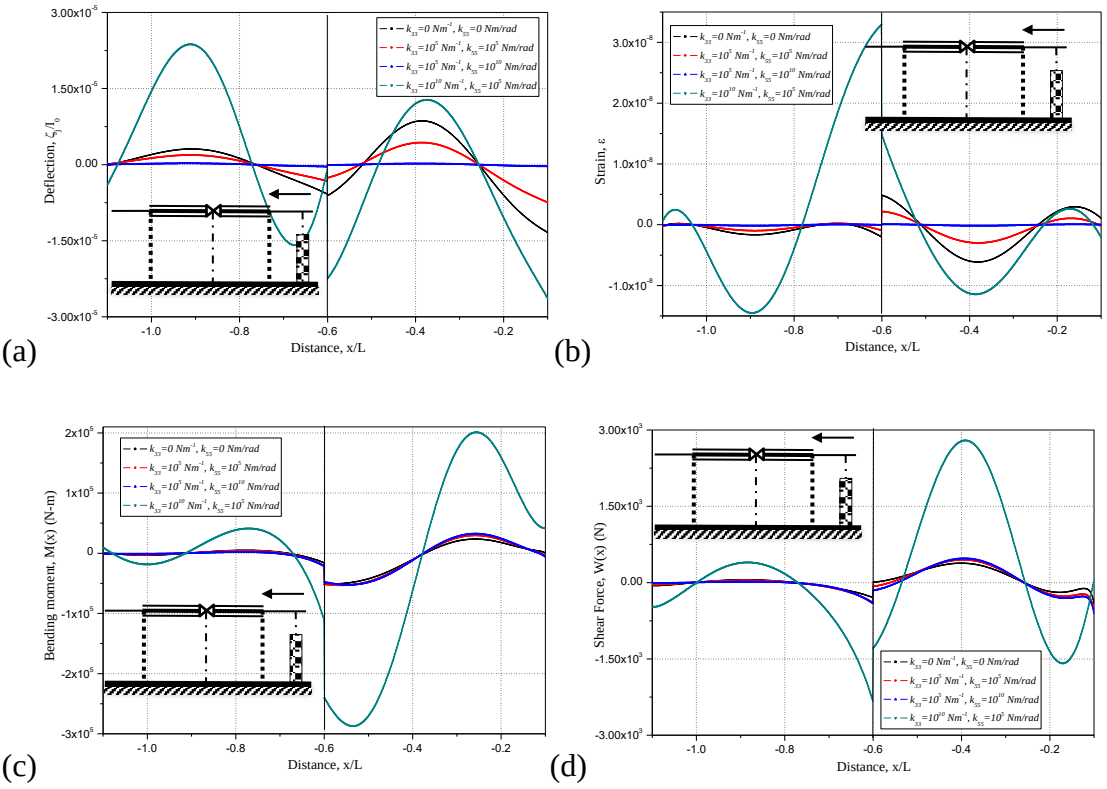

Figure 6.16: (a) Plate deflection (b) wave induced strain (c) bending moment and (d) shear force resultants along the plate length x/L for varying k_{33} and k_{55} considering $k_{10}h = 2$, $G_0 = 0.5 + 0.5i$, $L_1/L = 0.1$ and $h_1/h = 0.5$ in the case of bottom standing barrier.

In Figure 6.17(a-d), the plate deflection ζ_j / I_0, wave induced stain ε, bending moment $M(x)$ and shear force $W(x)$ are plotted varying spring stiffness at a connecting joint in an articulated floating elastic plate along with surface piercing vertical barrier. The responses in the presence of surface piercing vertical barrier are observed to reduce as

compared with bottom standing vertical barrier due to higher values of wave dissipation. The 47% (Figure 6.17a) increase in the in the plate deflection ζ_j/I_0 at oscillating crest, 22% (Figure 6.17b) decrease in the stain ε at oscillating trough, 79% (Figure 6.17c) and 85% (Figure 6.17d) reduction in the bending moment $M(x)$ and shear force $W(x)$ at oscillating crest is observed due to the presence of the rigid articulation. A gradual variation in plate deflection ζ_j/I_0, wave induced stain ε, bending moment $M(x)$ and shear force $W(x)$ is noted at each of the oscillating crest and trough with variation in the k_{33} and k_{55}. However, an almost uniform estimation or minor variation in the hydroelastic responses is noticed for $k_{33}=10^5\,\text{Nm}^{-1}$ and $k_{55}=10^{10}\,\text{Nm/rad}$.

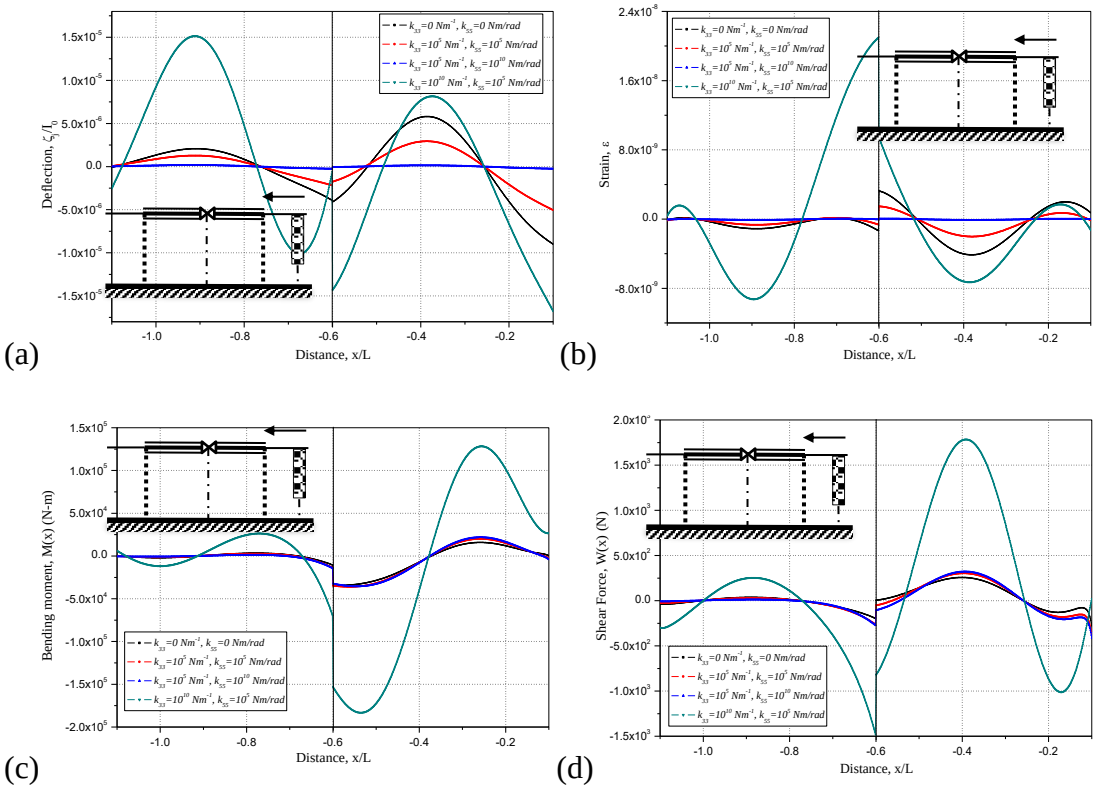

Figure 6.17: (a) Plate deflection (b) wave induced strain (c) bending moment and (d) shear force resultants along the plate length x/L for varying k_{33} and k_{55} considering $k_{10}h=2$, $G_0=0.5+0.5i$, $L_1/L=0.1$ and $h_1/h=0.5$ in the case of surface piercing barrier.

6.4.4 Effect of different support conditions

The mitigation of hydroelastic behaviour due to the wave interaction with vertical barriers in front of the articulated floating elastic thick plate is analysed in finite water depth for different edge support conditions of floating elastic plate.

6.4.4.1 Wave reflection, transmission and dissipation coefficients

The wave reflection coefficient (Figure 18a), transmission coefficient (Figure 18b) and dissipation coefficient (Figure 18c) are plotted versus non-dimensional wave number for different support condition along the edges of articulated floating elastic plate with bottom standing vertical barrier.

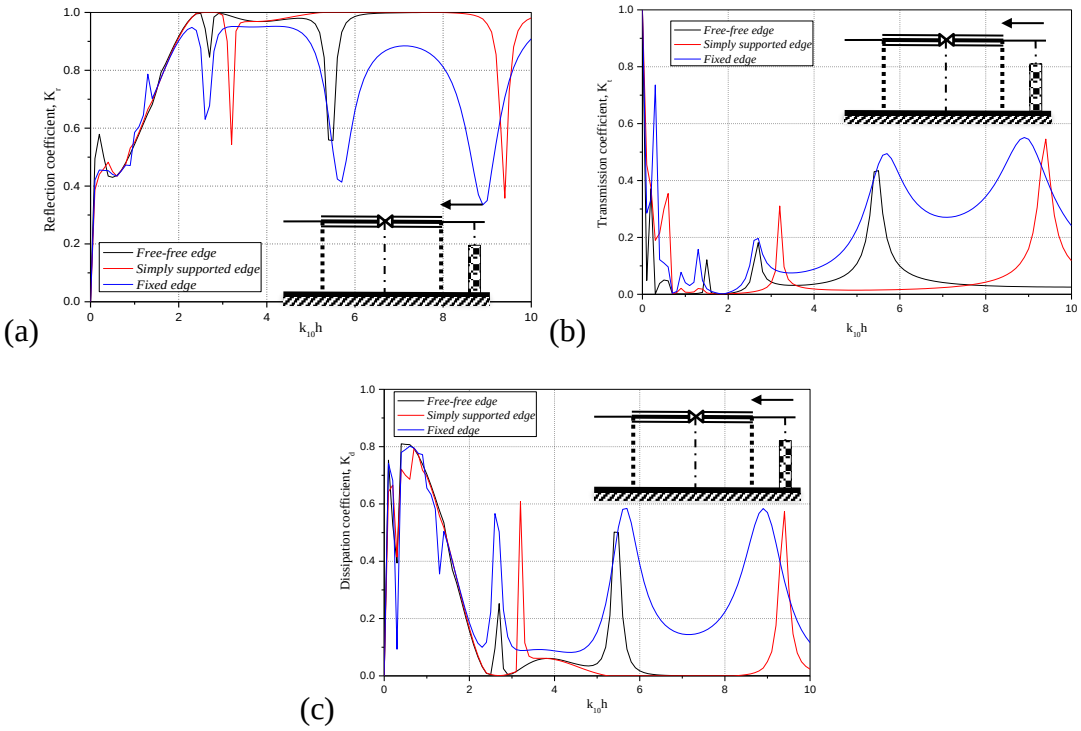

Figure 6.18: (a) Reflection, (b) transmission and (c) dissipation coefficient versus non-dimensional wavenumber for different support condition considering $G_0 = 0.5 + 0.5i$, $L_1 / L = 0.1$ and $h_1 / h = 0.5$ in the case of bottom standing barrier.

From Figure 6.18: (a,b), the resonating peaks and troughs are obtained in the wave transformation for particular $k_{10}h$ values for free-free edge, simply-supported edge and fixed edge conditions. A higher wave dissipation is observed for wavenumber within $0 < k_{10}h < 2$, which is mainly contributed by wave reflection from the vertical barrier for

all the support conditions. The maximum estimation in the K_r and minimum estimation in the K_t is obtained for simply supported edge condition as compared with the free-free edge and fixed edge conditions. The fixed edge support shows significantly low wave reflection coefficient as compared with free-free edge and simply supported edge condition, which is mainly due to the zero bending moment at the edges. The number of completely transmitted wave is minimal for fixed edge condition of floating elastic plate, due to zero slope at the edges.

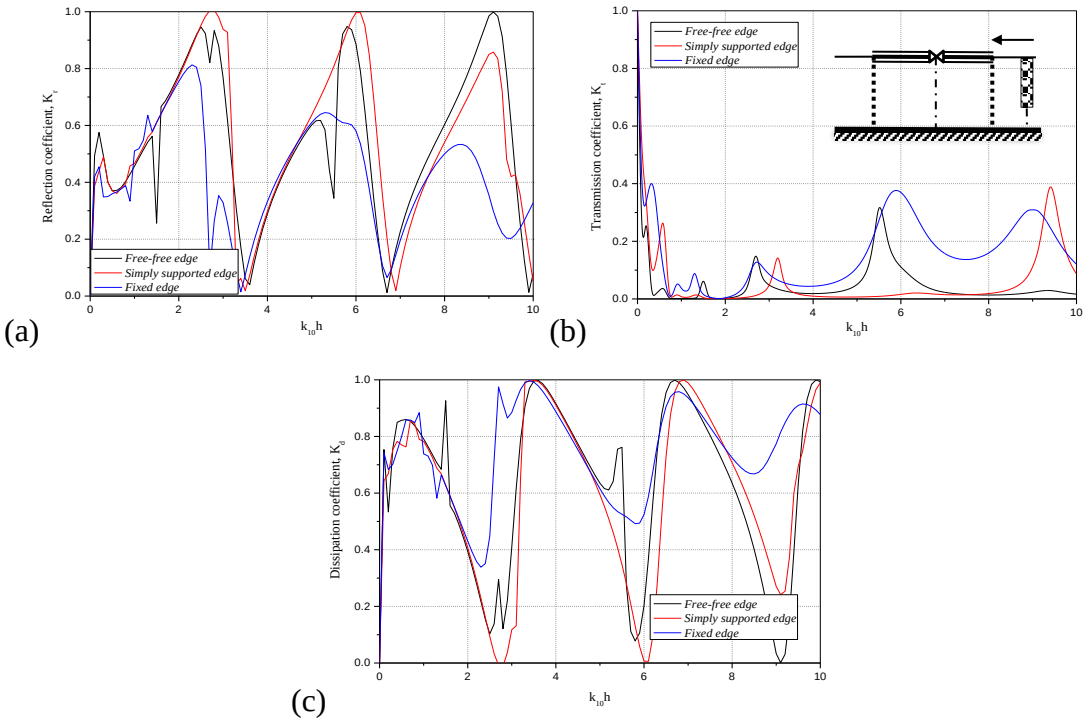

Figure 6.19: (a) Reflection, (b) transmission and (c) dissipation coefficient versus non-dimensional wavenumber for different support conditions considering $G_0 = 0.5 + 0.5i$, $L_1 / L = 0.1$ and $h_1 / h = 0.5$ in the case of surface piercing barrier.

In the Figure 6.19(a-c), the wave reflection coefficient (Figure 6.19a), transmission coefficient (Figure 6.19b) and energy damping coefficient (Figure 6.19c) are plotted versus non-dimensional wave number for different support conditions along the edges of articulated floating elastic plate with surface piercing vertical barrier. A higher wave dissipation is observed in the resonating phenomenon which is mainly contributed by wave reflection from the vertical barrier for all the support conditions. A regular pattern in the energy dissipation is observed in the case of surface piercing barrier as compared to bottom standing barrier. Further, the transmission of wave is observed to be low as

compared to bottom standing vertical barrier, mainly due to the interaction of wave with the surface piercing vertical barrier. In order to achieve the high energy damping the resonating peaks in the K_d is evident to achieve the minimum wave impact on the floating elastic plate and it is helpful in the design and construction of articulated floating plate with surface piercing barrier.

6.4.4.2 Hydroelastic response of floating plate

In Figure 20(a-d), the hydroelastic response of the floating elastic plate is plotted for different support condition along the edges of articulated floating elastic plate with bottom standing vertical barrier. The difference in the response is observed at the articulated joint due to change in rigidity at the connecting joints. The oscillating peaks and troughs are observed in each of the free-free edge, simply supported edge and fixed edge conditions.

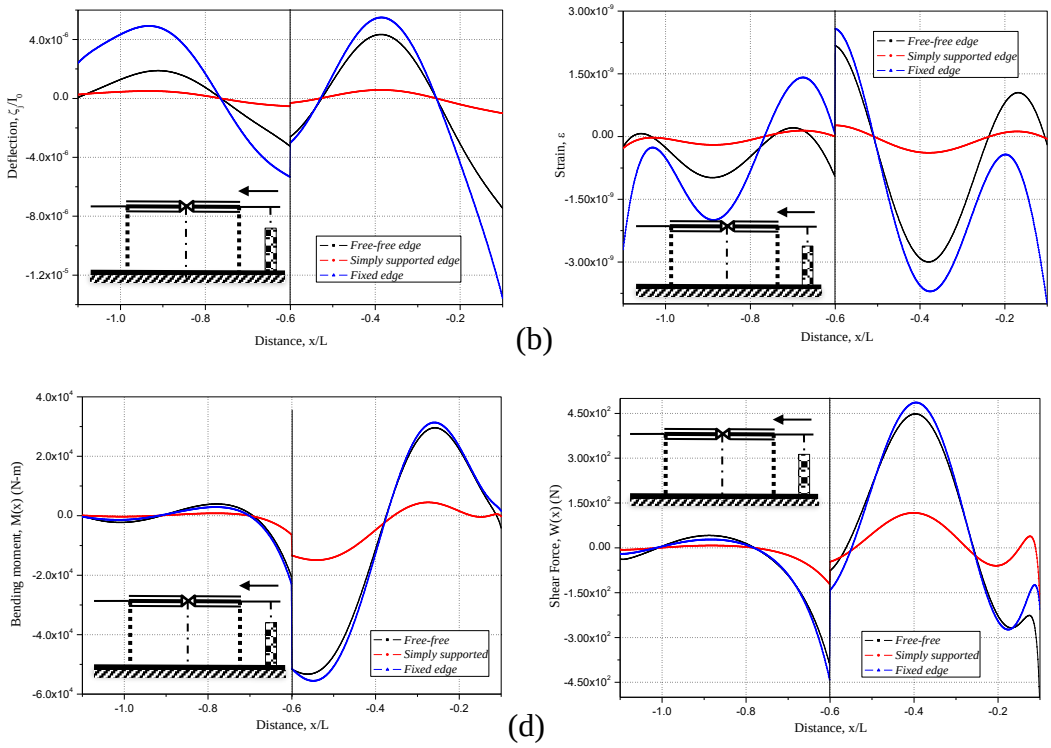

Figure 6.20: (a) Plate deflection (b) wave induced strain (c) bending moment and (d) shear force resultants along the articulated plate length x/L for different edge support conditions considering $k_{10}h = 2,\ G_0 = 0.5 + 0.5i,\ L_1/L = 0.1$ and $h_1/h = 0.5$ in the case of bottom standing barrier.

In all the combinations the fixed edge condition shows the high peak value and trough value in the plate deflection (Figure 20a), strain (Figure 6.20b), bending moment (Figure 6.20c) and shear force (Figure 6.20d). Thereafter, simply supported edge conditions shows the minor variation in the hydroelastic behaviour as compared with the free-free edge and fixed edge conditions mainly due to the combination of zero deflection and bending moment at the edges. Around 9% reduction in the plate deflection (Figure 6.20a) at peak point, 47% reduction in the strain (Figure 20b) at oscillatory trough, 90% and 95% reduction in the bending moment (Figure 20c) and shear force (Figure 20d) are obtained for the fixed edge condition.

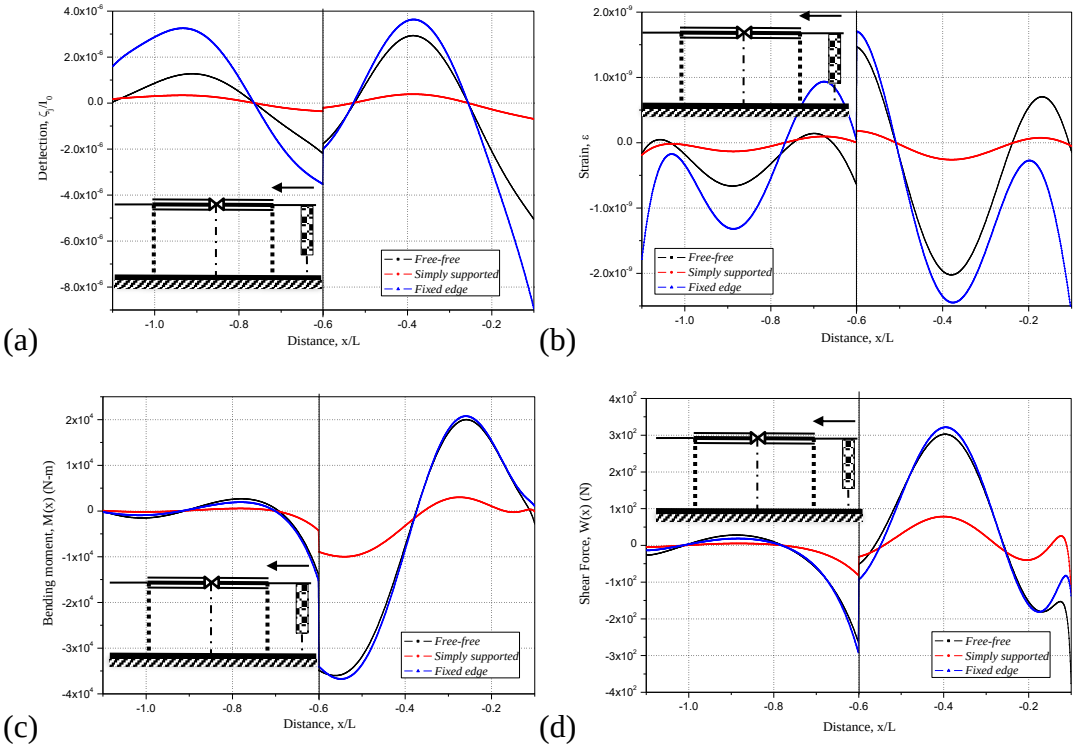

Figure 6.21: (a) Plate deflection (b) wave induced strain (c) bending moment and (d) shear force resultants along the articulated plate length x/L for different edge support conditions considering $k_{10}h=2,\ G_0=0.5+0.5i,\ L_1/L=0.1$ and $h_1/h=0.5$ in the case of surface piercing barrier.

The hydroelastic responses for different support condition along the edges of articulated floating elastic plate with surface piercing vertical barrier is illustrated in Figure 6.21(a-d). The pattern in the plate deflection ζ_j/I_0, wave induced stain ε, bending moment $M(x)$ and shear force $W(x)$ is observes similar as in Figure 6.20 (a-d). The responses

are observed to be low for surface piercing barrier as compared to the bottom standing vertical barriers due to the wave damping by surface piercing vertical barrier. A comparative study is performed for the hydroelastic response due to the presence of articulated plate away from the bottom standing barrier (Figure 6.20a-d) and surface piercing barrier Figure (6.21a-d) for fixed edge condition. A 31% reduction in the plate deflection, 35% reduction in the wave induced strain, 33% reduction in the bending moment and 35% reduction in the shear force is achieved at each of the peak point due to the surface piercing barrier as compared with the bottom standing barrier.

6.5 CONCLUSIONS

The wave attenuation due to the interaction of vertical porous barrier in front of the articulated floating plate is analysed based on Timoshenko-Mindlin plate theory in finite water depth. The mathematical model is developed based on eigenfunction expansion method along with orthogonal mode-coupling relation for linearized wave theory. The numerical computations are performed to analyse the wave reflection coefficient, wave transmission coefficient, dissipation coefficient and hydroelastic behaviour of the elastic plate under the action of an incident wave. The wave energy dissipation due to the presence of vertical barrier either bottom standing or surface piercing is computed and checked to satisfy the energy balance relation. In addition, a brief comparison of the numerical results for different types of support conditions is discussed in detail. The conclusions drawn from the present study are as follows:

- The increase in the porosity, height of the barrier and change in the spacing between the vertical barrier and articulated floating elastic plate has suggested an increase in the wave energy dissipation for both the bottom standing and surface piercing vertical barrier.
- A regular pattern in wave reflection and dissipation is observed for barriers up to free surface due to the resonance phenomena. The surface piercing vertical barrier shows higher reduction in wave transmission and significant increase in the wave energy damping as compared to bottom standing vertical barrier.
- The hydroelastic responses are observed to increase with the reduction in the barrier porosity and barrier height due to the increase in wave energy dissipation. On the

other hand, the backward shift in the responses are observed due to the reduction in the spacing between the barrier and floating elastic plate.

- Higher hydroelastic response is observed for a bottom standing barrier in comparison with surface piercing vertical barriers in front of large floating elastic plate due to higher wave energy dissipation from a surface piercing vertical barrier.
- The variation in articulation condition contributes in the wave energy dissipation in combination with vertical barrier which allows the designers to design the structure as per the required functionality and safety.
- The responses are observed to reduce with the surge in the values of spring stiffness k_{33} and k_{55} at the connecting joints due to increase in rigidity.
- The fixed edge support shows significantly low wave reflection as compared to free-free edge and simply supported edge condition, which is mainly due to the zero bending moment at the edges.
- The simply supported edges show lower responses as compared to other edge conditions, which is mainly due to the combination of zero deflection and bending moment at the edges.
- The comparative study between the bottom standing and surface piercing barriers with floating elastic plate suggests that the 31% reduction in the plate deflection, 35% reduction in the wave induced strain, 33% reduction in the bending moment and 35% reduction in the shear force is achieved at each of the peak point.

CHAPTER 7

CONCLUSIONS AND FUTURE WORK

7.1 SUMMARY OF RESEARCH WORK

The study focused on the hydroelastic behaviour of large floating flexible structures based on Timoshenko-Mindlin plate theory. The significance and importance of rotary inertia and shear deformation in analysing the hydroelastic behaviour large floating structures are studied. The eigenfunction expansion method along with mode coupling relation is applied to analyse the hydroelastic behaviour of the large floating elastic plate in finite water depth. The work also aimed at studying the influence of different types of edge support conditions on the hydroelastic behaviour of the large floating elastic plate. The study involved the effect of articulation with varying stiffness in the hydroelastic behaviour of articulated large floating structures in finite and shallow water depth. Further, the wide spacing approximation is applied to reduce the complexity due to the periodic array of multiple articulated floating elastic plate. The wave attenuation due to the interaction with submerged vertical porous barriers in front of the large floating structures is studied to understand the significance of wave trapping due to varying bottom topography for the waves interacting with floating elastic plate. The primary purpose of the study is to reduce the hydroelastic response of large floating flexible structures under the action of ocean waves. The use of articulated joints, varying bottom topography and submerged structures are observed in the wave attenuation and reduction of the hydroelastic response of VLFS. The study forms a basis for scientists and engineers in the detail design and analysis of the VLFS for future megastructures. A brief summary of research work pursed are as follows:

- A boundary value problem was developed based on linearized boundary condition in open and plate covered regions along with required edge boundary for the case of finite and shallow water depth. The plate covered boundary condition is based on Timoshenko-Mindlin plate theory (Fox and Squire, 1991) which includes the effect of rotary inertia and transverse shear deformation.

- The generalized eigenfunction expansion method along with the orthogonal mode coupling relation is applied to solve the higher-order boundary value problem for the case of finite water depth. Further, the continuity of energy and mass flux was applied in the solution method at shallow water depth. The far-field boundary condition is applied along the open water regions.
- The contour plot for the roots of plate covered dispersion relation is plotted to show the distribution and complexity in the higher-order boundary value problem.
- The set of algebraic equations are solved up to a finite number of evanescent modes to obtain the unknown wave amplitudes. Using the wave amplitudes along the open water region, the wave reflection and transmission coefficients were computed and observed to satisfy the energy balance relation for both the cases of water depths.
- The computed wave amplitudes along the plate covered region are utilized to obtain the hydroelastic behaviour along the floating elastic plate based on Timoshenko-Mindlin plate theory. The variation in hydroelastic behaviour of floating elastic plate for different plate properties and water depth are studied in detail.
- The numerical computation is carried out to analyse the hydroelastic behaviour of floating elastic plate at different cases of edge support conditions. Further, a comparative study for the case of free-free edge, simply supported edge and fixed edge condition was done to analyse the hydroelastic behaviour of the floating elastic plate.
- The mathematical model and the hydroelastic analysis are carried out for the articulated floating elastic plate along with edge boundary conditions and varying spring stiffness along the articulated joints for the case of finite and shallow water depth.
- The hydroelastic analysis of articulated floating elastic plate is analysed and compared for three cases of articulated joints i.e. open gap, hinged connection and continuous plate.
- The direct eigenfunction expansion method is used in the hydroelastic analysis of single and multiple articulated floating elastic plate. The complexity with an increasing number of periodic arrays of multiple articulations along the floating elastic plate is simplified with the application of wide spacing approximation.

- The hydroelastic analysis is carried out for the floating elastic plate acted upon by ocean waves over varying bottom topography. The orthogonal mode-coupling relation is employed along with the continuity equations for pressure, velocity, deflection, bending moment, slope and shear force for waves over variable bottom topography.
- The wave trapping and transformation due to single and multiple stepped bottom topography are analysed. Detail comparison of the wave scattering and hydroelastic behaviour of the floating elastic plate is performed for different types of step bottom topography.
- The mathematical model is developed to analyse the wave attenuation due to the presence of submerged vertical porous barriers in front of the articulated floating elastic plate. The boundary condition for the vertical porous barrier is defined based on Darcy's law.
- The wave attenuation due to the presence of submerged vertical barriers in front of the articulated floating elastic plate is demonstrated for bottom standing and surface piercing vertical barriers.
- The mitigation in hydroelastic response along the floating elastic plate due to the combination of different support conditions and the articulated joint is also studied. The wave energy dissipation due to the presence of vertical barrier either bottom standing, or surface piercing is computed and checked to satisfy the energy balance relation.

7.2 SIGNIFICANT CONTRIBUTION OF THE THESIS

The work presented in this thesis has been aimed towards developing analytical tools for wave structure interaction problems and to analyse physical problems which are of recent interest in Ocean Engineering and Offshore Structures. The main contributions from the work done in the thesis are as follows:

- The expansion formulae modified based on Timoshenko Mindlin plate theory associated with the governing equation satisfy higher-order boundary condition to obtain the solution for the wave interaction with the finite floating elastic plate.

- The rotary inertia and transverse shear deformation are observed to play an important role in the hydroelastic analysis of the floating flexible structures and hence the consideration of Timoshenko Mindlin plate theory are significant in the analysis. The contour plots for the roots in the plate covered dispersion relation are presented to illustrate the distribution and complexity in the roots for the plate covered dispersion relation.
- The shallow water approximations showed higher unity in the wave reflection as compared to the finite water depth which is due to the high wavelength for the incident waves. In shallower water depths, the wave transmission is observed to increase due to the increase in wave heights. The increase in the plate rigidity significantly reduces the wave transmission and at certain wavenumbers, complete transmission or wave reflection is observed due to the resonance phenomenon in all water depths. The free-free edge support condition shows higher transmission of waves whereas, lower wave transmission for fixed edge support is observed at finite and shallow water depth.
- The plate thickness and plate rigidity are significant in the reduction of the hydroelastic response of the floating elastic plate, which is explained in detail for varying plate properties. The influence of the different type of edge support conditions on the hydroelastic behaviour of the floating elastic plate is also studied. The hydroelastic behaviour is found to be higher for free-free edge support conditions and least for fixed edge due to restraints from the boundary conditions in the case of finite water depth. On the other hand, the bending moment and shear force resultants are found to be highest for fixed edge support and least for simply supported edge condition in the case of shallow water depth.
- The complete transmission of waves is observed to reduce with the increase in the number of articulations because the waves get trapped at the articulated joints. The wave reflection increased with the reduction of the transmitted wave due to the existence of articulations in the floating plate, must be carefully studied for the design of floating structures and placement of spring stiffness along the plate.
- A significant reduction in hydroelastic behaviour of floating elastic thick plate is achieved due to the presence of articulation with varying vertical linear and flexural rotational spring stiffness. In the case of finite water depth, the reduction in the plate

deflection and strain for the articulated floating elastic plate is achieved with the application of rotational spring stiffness in the hinged connection. Whereas, a considerable reduction in bending moment and shear force is observed with the application of hinge connection having either of the spring stiffness at the connecting joint. The hydroelastic behaviour is also observed to decrease along the plate length towards the transmitted region due to the interaction with the connecting joints, which restrained the propagation of waves.

- For an array of multiple articulations in floating elastic plate, the reflection coefficient does not show any significant variations using both direct method and wide spacing approximations method, whereas slight variations are observed for the case of transmission coefficient due to the considerations of wide-spacing in between the plates and also neglecting the effect of evanescent wave modes in the approximate methods.
- The wave transmission is noticed to increase with the reduction in the step height due to the reduction of wavelength for both the case of single-step seabed profile along the plate covered region. The wave transmission is noticed to reduce with the increasing number of steps mainly due to the interaction of waves at the step interfaces.
- The increase in the step height has contributed to the reduction of the hydroelastic response of floating elastic plate due to the wave trapping by the increasing step height. The hydroelastic response is noticed to reduce gradually throughout the elastic plate along with discontinuity at the step interfaces as the waves progressed towards the transmission region may be due to the wave trapping at the step interfaces for the varying number of steps below floating elastic platform. Further, the increment in the number of steps along the plate covered region is noticed to increase the responses due to the reduction in the slope of step heights as compared to very high response for single step along the region.
- A regular pattern in wave reflection and dissipation is observed for barriers up to water surface due to the resonance phenomena. The surface piercing vertical barrier shows a higher reduction in wave transmission as compared to bottom standing vertical barriers.

- The hydroelastic responses are observed to increase with the reduction in the barrier porosity and height due to the increase in wave energy dissipation. In comparison, a higher hydroelastic response is observed for a bottom standing than with surface piercing vertical barriers in front of the large floating elastic plate due to higher wave energy dissipation from a surface piercing vertical barrier.
- The increase in porosity, height and decrease in between the vertical barrier and articulated floating elastic plate has suggested an increase in the wave energy dissipation for both the bottom standing and surface piercing vertical barrier.

7.3 FUTURE SCOPE OF RESEARCH

In this section the possible extensions of the present investigation are presented below:

- The present study can be extended for the wave interaction with floating structures considering porous bottom boundary condition in both single and two-layer fluid.
- The efforts will be made to study the wave interaction with finite floating rectangular plates in three dimensions.
- The study will be extended to analyse the wave transformation due to the floating elastic plate of different material properties.
- The findings on the variations in bottom topography can be extended from stepped type to any shape of seabed profile using mild slope approximations.
- The study on the wave interaction with the floating structure in time domain using spectral method can be performed.
- The condition of articulation can be extended for both the longitudinal and lateral direction along the floating elastic plate to contribute to the development of VLFS.
- The variation in the shape of VLFS can be studied as per the requirement and purpose of the structure.
- The attempt will be made to extend the study for non-linear wave structure interaction.

REFERENCES

Agarwal, N., and Nair, E.S. (2014). "Structural response of a floating runway excited by the taking off of an airplane." *Journal of Naval Architecture and Marine Engineering*, *11*(2), 131-138.

Amabili, M. and Kwak, M. K. (1999). "Vibration of circular plates on a free fluid surface: effect of surface waves." *Journal of Sound and Vibration*, *226*(3), 407-424.

Andrianov, A.I. (2005). "Hydroelastic analysis of Very Large Floating Structures." PhD Thesis, p 1-157.

Andrianov, A.I., and Hermans, A.J. (2003). "The influence of water depth on the hydroelastic response of a very large floating platform." *Marine Structures*, *16*(5), 355-371.

Andrianov, A.I., and Hermans, A.J. (2005). "Hydroelasticity of a circular plate on water of finite or infinite depth." *Journal of Fluids and Structures*, *20*(5), 719-733.

Andrianov, A.I. and Hermans, A.J. (2006a). "Hydroelastic analysis of floating plate of finite draft." *Applied Ocean Research*. 28, 313–325.

Andrianov A.I and Hermans A.J. (2006b) "Hydroelastic behaviour of a floating ring shaped plate." *Journal of Engineering Mathematics*, 54(1), 31–48.

Athanassoulis, G.A. and Belibassakis, K.A. (1999). "A consistent coupled-mode theory for the propagation of small-amplitude water waves over variable bathymetry regions." *Journal of Fluid Mechanics, 389,* 275–301.

Athanassoulis, M.A. and Belibassakis, K. (2009). "A novel coupled-mode theory with application to hydroelastic analysis of thick, non-uniform floating bodies over general bathymetry." *Journal of Engineering for the Maritime Environment*, 223, 419-438.

Bai, W., Zhang, T., and McGovern, D. J. (2017). "Response of small sea ice floes in regular waves: A comparison of numerical and experimental results." *Ocean Engineering*, 129, 495-506.

Balmforth, N.J. and Craster, R.V. (1999). "Ocean waves and ice sheets." *Journal of Fluid Mechanics*, 395, 89-124.

Barrett, M.D. and Squire, V.A. (1996). "Ice-coupled wave propagation across an abrupt change in ice rigidity density or thickness." *Journal of Geophysical Research*. 101, 20,825-20,832.

Bates, H.F. and Shapiro, L.H. (1980) "Long-period gravity waves in ice-covered sea." *Journal of Geophysical Research*, 85(C2), 1095-1100.

Behera, H., Kaligatla, R.B., and Sahoo, T. (2015). "Wave trapping by porous barrier in the presence of step type bottom." *Wave Motion*, 57, 219–230.

Behera, H., Koley, S., and Sahoo, T. (2015). "Wave transmission by partial porous structures in two-layer fluid." *Engineering Analysis with Boundary Elements*, *58*, 58–78.

Belibassakis, K.A. and Athanassoulis, G.A. (2004). "Hydroelastic responses of Very Large Floating Structures lying over variable bathymetry regions." *The Fourteenth International Offshore and Polar Engineering Conference 2004 Jan 1. International Society of Offshore and Polar Engineers*, 584–591.

Belibassakis, K.A. and Athanassoulis, G.A. (2005). "A coupled-mode model for the hydroelastic analysis of large floating bodies over variable bathymetry regions" *J of Fluid Mechanics* 531, 221–249.

Belibassakis K.A. and Athanassoulis, G.A. (2006). "A coupled-mode model for weakly nonlinear wave interaction with large floating structures lying over variable bathymetry regions." *Applied Ocean Research,* 28, 59-76.

Belibassakis, K.A. and Athanassoulis, G.A. (2011). "A coupled-mode system with application to nonlinear water waves propagating in finite water depth and in variable bathymetry regions." *Coastal Engineering*, 58(4), 337–350.

Belibassakis, K.A., Athanassoulis G.A. and Gerostathis, T.P. (2013). "Hydroelastic analysis of very large floating bodies over variable bathymetry regions." *10th HSTAM International Congress on Mechanics,* Chania, Crete, Greece, 25 – 27 May, 2013

Bennetts, L.G. and Squire, V.A. (2012). "On the calculation of an attenuation coefficient for transects of ice-covered ocean." *Proceeding of Royal Society, London. A,* 468(2137), 136-162.

Bhattacharjee, J, and Guedes Soares, C. (2011). "Oblique wave interaction with a floating structure near a wall with stepped bottom." *Ocean Engineering*, 38(13), 1528–1544.

Bhattacharjee, J. and Guedes Soares, C. (2012) "Flexural gravity wave over a floating ice sheet near a vertical wall." *Journal of Engineering Mathematics,* 75, 29-48.

Bhattacharjee, J, Karmakar, D. and Sahoo, T. (2008) "Transformation of flexural gravity waves by heterogeneous boundaries.", *Journal of Engineering Mathematics,* 62, 173-188.

Bird, H.W.K. and Shepherd, R. (1984). "On the interactions of surface waves with immersed structures." *International Journal for Numerical Methods in Fluids*, *4*(8), 765–780.

Brocklehurst, P., Korobkin, A. and Părău, E.I. (2011) "Hydroelastic wave diffraction by a vertical cylinder." *Philosophical transactions. Series A, Mathematical, Physical, and Engineering Sciences,* 369, 2832-2851.

Chakrabarti, A. (2000). "On the solution of the problem of scattering of surface-water waves by the edge of an ice cover." *Proceeding of the Royal Society*, London, 1087-1099.

Chen, X.J., Jensen, J.J., Cui, W.C. and Fu, S.X. (2003). "Hydroelasticity of a floating plate in multidirectional waves." *Ocean Engineering*, 30, 1997–2017.

Chen, X.J, Moan, T., Fu, S. and Cui, W. (2006a). "Second-order hydroelastic analysis of a floating plate in multidirectional Irregular waves." International *Journal of Non-Linear Mechanics*, 41, 1206 – 1218.

Chen, X.J., Wu, Y., Cui, W.C and Jensen, J.J, (2006b). "Review of hydroelasticity theories for global response of marine structures." *Ocean Engineering*, 33, 439-457.

Chen, X.J., Wu, Y., Cui, W.C and Tang, X. (2006c). "Nonlinear hydroelastic analysis of a moored floating body." *Ocean engineering*, 30, 965-1003.

Cheng, Y., Zhai, G.J., and Ou, J. (2014). "Time-domain numerical and experimental analysis of hydroelastic response of a very large floating structure edged with a pair of submerged horizontal plates." *Marine Structures*, 39, 198-224.

Cho, I.H., and Kim, M.H. (1999). "Wave deformation by a submerged flexible circular disk." *Applied Ocean Research*, 21(5), 263–280.

Chung, H. and Linton, C.M. (2003). "Interaction between water waves and elastic plates: using the residue calculus technique." *Proceedings of the 18th International Workshop on Water Waves and Floating Bodies*, France, 37-40.

Chung, H. and Fox, C. (2005). "Transition conditions at the interface between floating plates." *Proceedings of the 20th International Workshop on Water Waves and Floating Bodies* (IWWWFB); May 29–Jun 1; Longyearbyen, Norway.

Chung, H. and Fox, C. (2009). "A direct relationship between bending waves and transition conditions of floating plate." *Wave Motion*, 46, 468-479.

Chwang, A.T. and Chan, A.T. (1998). "Interaction between porous media and wave motion." *Annual Review of Fluid Mechanics*, 30(1), 53-84.

Dai, J., Wang, C.M., Utsunomiya, T. and Duan, W. (2018). "Review of recent research and developments on floating breakwaters." *Ocean Engineering*, 158, 132-151.

Dhillon, H., Banerjea, S. and Mandal, B.N. (2013). "Oblique wave scattering by a semi-infinite rigid dock in the presence of bottom undulations." *Indian Journal of Pure and Applied Mathematics*, *44*(2), 167-184.

Dhillon, H., Banerjea, S., and Mandal, B.N. (2016). "Water wave scattering by a finite dock over a step-type bottom topography." *Ocean Engineering*, 113, 1-10.

Evans, D.V. and Davies, T.V. (1968). "Wave-ice interaction." Stevens Institute of Technology: Report, 1313. New Jersey.

Evans, D.V. and Linton, C.M. (1994). "On step approximations for water-wave problems." *Journal of Fluid Mechanics*, 278(1), 229–249.

Evans, D.V and Porter, R. (2003). "Wave scattering by narrow cracks in ice sheets floating on water of finite depth." *Journal of Fluid Mechanics*, 484, 143–165.

Ertekin, R.C., Kim, J.W. and Xia, D. (1998). "Hydroelastic response of a mat-type, floating runway near a breakwater in irregular seas." *IEEE*, 839-847.

Ertekin, R.C., Riggs, H.R., Che, X.L. and Du, S.X. (1993). "Efficient methods for hydroelastic analysis of very large floating structures." *Journal of Ship Research*, 37(1): 58–76.

Ertekin, R.C., and Xia, D. (2014). "Hydroelastic response of a floating runway to cnoidal waves." *Physics of Fluids*, *26*(2), 1–16.

Fitzgerald, C.J. and Meylan, M.H. (2011). "Generalized eigenfunction method for floating bodies." *Journal of Fluid Mechanics*, 667, 544-554.

Fox, C. and Squire, V.A. (1991). "Coupling between the ocean and an ice shelf." *Annals of Glaciology*. 101-108.

Fu, S., Moan, T., Chen, X.J., and Cui, W. (2007). "Hydroelastic analysis of flexible floating interconnected structures." *Ocean Engineering*, 34: 1516-1531.

Fujikubo, M. and Yao, T. (2001). "Structural modeling for global response analysis of VLFS." *Marine Structures*, 14, 295-310.

Fujikubo, M. (2005). "Structural analysis for the design of VLFS." *Marine Structures*, 18, 201–226.

Gao, R.P, Tay, Z.Y, Wang, C.M. and Koh, C.G. (2011). "Hydroelastic response of very large floating structure with a flexible line connection." *Ocean Engineering*, 38, 1957–1966.

Gao, R.P., Wang, C.M. and Koh, C.G. (2013). "Reducing hydroelastic response of pontoon-type very large floating structures using flexible connector and gill cells." *Engineering Structures*, 52, 372–383.

Garrison, C.J. and Rao, V.S. (1971). "Interaction of waves with submerged objects." *Journal of the Waterways*, Harbors and Coastal Engineering Division, 97(2), 259-277.

Garrison, C.l. and Chow, P. (1972). "Wave forces on submerged bodies." Journal of Waterways, Harbors and Coast Engineering, 98.WW3.

Gerostathis, T.P., Belibassakis, K.A., and Athanassoulis, G.A. (2016). "3D hydroelastic analysis of very large floating bodies over variable bathymetry regions." *Journal of Ocean Engineering and Marine Energy*, *2*(2), 159–175.

Girard, A., Empey, D., Borges de Sousa, J., Spry, S. and Hedrick, J. (2001). "An Experimental test bed for mobile offshore base control concepts." University of California at Berkeley, Berkeley.

Goo, J.S. and Yoshida, K. (1990). "A numerical method for huge semisubmersible responses in waves." *SNAME Transactions,* 98, 365–387.

Gran, S., (1973). "Wave forces on submerged cylinders." In Offshore Technology Conference. *Offshore Technology Conference*.

Grue, J. (1992). "Nonlinear water waves at a submerged obstacle or bottom topography." *Journal of Fluid Mechanics, 244,* 455-476.

Guo, Y., Liu, Y. and Meng, X., (2016). Oblique wave scattering by a semi-infinite elastic plate with finite draft floating on a step topography. *Acta Oceanologica Sinica*, 35(7), 113-121.

Hang, L.T.T., Wang, C.M. and Wu, T.Y. (2005). "Exact vibration results for stepped circular plates with free edges." *International Journal of Mechanical Sciences,* 47, 1224-1248.

Havelock, T.H. (1929), "Forced surface waves on water", *Philosophical Magazine*, 8, 569–576.

Hermans, A.J. (2000). "A boundary element method for the interaction of free-surface waves with a very large floating flexible platform." *Journal of Fluids and Structures*, 14(7), 943-956.

Hermans, A.J. (2001). "A geometrical-optics approach for the deflection of a floating flexible platform." *Applied Ocean Research*; 23(5), 269–76.

Hermans, A.J. (2003a). "The ray method for the deflection of a floating flexible platform in short waves." *Journal of Fluids and Structures*, 17(4), 593–602

Hermans, A.J, (2003b) "Interaction of free-surface waves with a floating dock." *Journal of Engineering Mathematics*, 45, 39–53.

Hermans, A.J. (2004). "Interaction of free-surface waves with floating flexible strips." *Journal of Engineering Mathematics*. 49, 133-147.

Hermans, A.J. (2007). "Free-surface wave interaction with a thick flexible dock or very large floating platform." *Journal of Engineering Mathematics*. 58, 77-90.

Holdsworth, G. (1969). "Flexure of a floating ice tongue." *Journal of Glaciology*, 8, 385-397.

Hong, S. and Lee, J.S. (2016). "Hydroelastic response analysis of pneumatically supported floating structures using a BEM-FEM coupling method." KSCE *Journal of Civil Engineering*, 20(7), 2875–2884.

Inoue, K., Nagata, S. and Niizato, H. (2002). "Stress analysis for detailed mega float structures subject to wave loads." *International Society of Offshore and Polar Engineers*, ISOPE-I-02-043.

Jeong, K.H. and Kim, K.J. (2005). "Hydroelastic vibration of a circular plate submerged in a bounded compressible fluid." *Journal of Sound and Vibration*, 283(1–2), 153–172.

Kara, F. (2015). "Time domain prediction of hydroelasticity of floating bodies." *Applied Ocean Research, 51,* 1–13.

Karmakar, D. (2009). "Fourier analysis and allied methods in the hydroelastic analysis of floating structures." PhD Thesis, Indian Institute of Technology, Kharagpur.

Karmakar, D., Bhattacharjee, J., and Guedes Soares, C. (2013). "Scattering of Gravity Waves by Multiple Surface-piercing Floating Membrane." *Applied Ocean Research*, 39, 40–52.

Karmakar, D., Bhattacharjee, J. and Sahoo, T. (2007). "Expansion formulae for wave structure interaction problems with applications in hydroelasticity." *International Journal of Engineering Science,* 45, 807–828.

Karmakar, D., Bhattacharjee, J. and Sahoo, T. (2009). "Wave interaction with multiple articulated floating elastic plates." *Journal of Fluids and Structures,* 25(6), 1065– 1078.

Karmakar, D. Bhattacharjee, J. and Sahoo, T. (2010). "Oblique flexural gravity-wave scattering due to changes in bottom topography." *Journal of Engineering Mathematics,* 66, 325-341.

Karmakar, D., Bhattacharjee, J. and Sahoo, T. (2011), "Contemporary approaches in the hydroelastic analysis of floating and submerged structures." *Marine Technology and Engineering,* C. Guedes Soares et al., (Eds), London, UK: Taylor & Francis Group, Vol - 1, pp 461-478.

Karmakar, D. and Guedes Soares, C. (2012). "Oblique scattering of gravity waves by moored floating membrane with changes in bottom topography." *Ocean Engineering*, 54, 87-100.

Karmakar, D., and Guedes Soares, C. (2015). "Propagation of gravity waves past multiple bottom-standing barriers." *Journal of Offshore Mechanics and Arctic Engineering*, 137(1), 011101-1-10.

Karmakar, D. and Sahoo, T. (2005). "Scattering of waves by articulated floating elastic plates in water of infinite depth." *Marine Structures,* 18(5–6), 451–471.

Karmakar, D. and Sahoo, T. (2006). "Flexural gravity wavemaker problem-revisited." *Proceedings of International Conference on Application of Fluid Mechanics in Industry and Environment, ISI, Kolkata, India,* Fluid Mechanics in Industry and Environment, B.S Dandapat & B.S Majumder (Eds.), Research Publishing Services, Singapore, pp 285-291.

Karmakar, D. and Sahoo, T. (2008). "Gravity wave interaction with floating membrane due to abrupt change in water depth." *Ocean Engineering,* 35(7), 598-615.

Karmakar, D., and Sahoo, T. (2012a). "Scattering of gravity waves by a moored finite floating elastic plate." *Applied Ocean Research*, 34, 135-149.

Karmakar, D., and Sahoo, T. (2012b). "Oblique scattering of gravity waves by moored floating membrane with changes in bottom topography." *Ocean Engineering*, 54, 87-100.

Karperaki, A. E., Belibassakis, K. A., and Papathanasiou, T. K. (2016). "Time-domain, shallow-water hydroelastic analysis of VLFS elastically connected to the seabed." *Marine Structures,* 48, 33-51.

Keller, J.B. (1998). "Gravity waves on ice-covered water." *Journal of Geophysics*. 103, 7663-7669.

Khabakhpasheva, T.I. and Korobkin, A.A. (2001). "Reduction of hydroelastic response of floating platform in waves." *Proceedings of the 16th International Workshop on Water Waves and Floating Bodies*, Hiroshima, Japan,73-76.

Khabakhpasheva, T.I. and Korobkin, A.A. (2002a). "Hydroelastic behaviour of compound floating plate in waves." *Journal of Engineering Mathematics*, 44(1), 21–40.

Khabakhpasheva T.I. and Korobkin, A.A. (2002b). "Exact solutions of floating elastic plate problem." *Proceedings of the 17th International Workshop on Water Waves and Floating Bodies*, Cambridge, UK, p.81-84.

Kirby, J. T. (1986). "A general wave equation for waves over rippled beds." *Journal of Fluid Mechanics, 162,* 171-186

Kim, J.W. and Ertekin, R.C. (1998). "An eigenfunction expansion method for predicting hydroelastic behavior of a shallow-draft VLFS." *Proceedings of the 2nd International Conference on Hydroelasticity in Marine Technology*, Fukuoka, 47-59.

Kim B.W., Hong, S.Y., Kyoung, J.H. and Cho, S.K. (2007). "Evaluation of bending moments and shear forces at unit connections of very large floating structures using hydroelastic and rigid body analyses." *Ocean Engineering*, 34, 1668–1679.

Kim, K.H., Bang, J.S., Kim, J.H., Kim, Y., Kim, S.J. and Kim, Y. (2013). "Fully coupled BEM-FEM analysis for ship hydroelasticity in waves." *Marine Structures, 33,* 71–99.

Kagemoto, H Fujino, M and Murai, M (1998). "Theoretical and experimental predictions of the hydroelastic response of a very large floating structure in waves." *Applied Ocean Research*, 20, 135-144.

Kagemoto, H. and Yue, D.K.P. (1993). "Hydrodynamic interaction analyses of very large floating structures." *Marine Structures*, 6, 295-322.

Kaligatla, R.B. and Sahoo, T. (2017). Wave trapping by dual porous barriers near a wall in the presence of bottom undulation. *Journal of Marine Science and Application*, 16(3), 286-297.

Kashiwagi, M. (1998). "A B-spline Galerkin scheme for calculating hydroelastic response of a very large floating structure in waves." *Journal of Marine Science and Technology*, 3(1), 37–49.

Kashiwagi, M. (2000). "Research on hydroelastic responses of VLFS: Recent progress and future work." *International Journal of Offshore and Polar Engineering*, 81–90.

Kyoung, J.H., Hong, S.Y., Kim, B.W. and Cho, S.K. (2005). "Hydroelastic response of a very large floating structure over a variable bottom topography." *Ocean Engineering,* 32, 2040–2052.

Korobkin, A. A. (2000). "Numerical and asymptotic study of the two-dimensional problem on hydroelastic behavior of a floating plate in waves." *Journal of Applied Mechanics and Technological Physics*, 41: 286-293.

Kohout, A.L. and Meylan, M.H. (2009). "Wave scattering by multiple floating elastic plates with spring or hinged boundary conditions." Marine Structures, 22(4), 712-729.

Kohout, A.L., Meylan, M.H., and Plew, D.R. (2011). "Wave attenuation in a marginal ice zone due to the bottom roughness of ice floes." *Annals of Glaciology, 52*(57), 118-122.

Konig, M., González, D.F., Maksoud, M.A. and Duster, A. (2014). "Hydrodynamic behaviour of Very Large Floating Structures (VLFS) in Waves" *PAMM*, 14(1), 531-32.

Koley, S. and Sahoo, T. (2017). "Scattering of oblique waves by permeable vertical flexible membrane wave barriers." *Applied Ocean Research*, 62, 156-168.

Koley, S., Kaligatla, R.B. and Sahoo, T. (2015). "Oblique wave scattering by a vertical flexible porous plate." *Studies in Applied Mathematics*, 135(1), 1-34.

Koley, S., Mondal, R., and Sahoo, T. (2018). "Fredholm integral equation technique for hydroelastic analysis of a floating flexible porous plate." *European Journal of Mechanics / B Fluids*, 67, 291–305.

Lawrie, J. B. and Abrahams, I. D., (1999), "An orthogonality relation for a class of problems with high-order boundary conditions; applications in sound structure interaction." *Q. J. Mech. Appl. Math.*, 52(2):161–181.

Liao, C.Y., and Ma, C.C. (2016). "Vibration characteristics of rectangular plate in compressible inviscid fluid." *Journal of Sound and Vibration, 362*, 228–251.

Linton, C.M. and Chung, H. (2003). "Reflection and transmission at the ocean/sea-ice boundary." *Wave Motion*, 38, 43-52.

Loukogeorgaki, E., Lentsiou, E. N., Aksel, M., & Yagci, O. (2017). Experimental investigation of the hydroelastic and the structural response of a moored pontoon-type

modular floating breakwater with flexible connectors. Coastal Engineering, 121, 240-254.

Loukogeorgaki, E., Vasileiou, M. and Rapanta, E. (2015). "3D Experimental and Numerical Investigation of the Performance of a Modular Floating Structure. Twenty-fifth International Offshore and Polar Engineering Conference." *International Society of Offshore and Polar Engineers.*

Loukogeorgaki, E., Yagci, O. and Kabdasli, M.S. (2014). "3D Experimental investigation of the structural response and the effectiveness of a moored floating breakwater with flexibly connected modules." *Coastal Engineering, 91*, 164-180.

Lu, D., Fu, S., Zhang, X., Guo, F. and Gao, Y. (2016). "A method to estimate the hydroelastic behaviour of VLFS based on multi-rigid-body dynamics and beam bending." *Ships and Offshore Structures, 5302*, 1–9.

Manam, S. R., Bhattacharjee, J. and Sahoo, T., (2006), "Expansion formulae in wave structure interaction problems." *Proc. Roy. Soc. Lond. Ser. A*, 462(2065):263–287.

Manam, S. R., and Sahoo, T. (2005). "Waves past porous structures in a two-layer fluid." *Journal of Engineering Mathematics*, 52(4), 355-377.

Marchenko, A.V. and Voliak, K.I. (1996). "Surface wave propagation in shallow water beneath an inhomogeneous ice cover." *Journal of Physical Oceanography*, 27, 1602-1613.

Mei, C.C. and Black, J.L. (1969). "Scattering of surface waves by rectangular obstacles in waters of finite depth." *Journal of Fluid Mechanics*, 38, 499- 511.

Meylan, M.H. (2001). "A variational equation for the wave forcing of floating thin plates." *Applied Ocean Research*; 23(4), 195-206.

Meylan, M.H., (2002). "Wave response of an ice floe of arbitrary geometry." *Journal of Geophysical Research*, 107, 5-1–5-11.

Meylan, M.H. and Squire, V.A. (1994). "The response of ice floes to ocean waves." *Journal of Geophysics*, 99, 891-900.

Meylan M.H. and Squire, V.A. (1996). "Response of a circular ice floe to ocean waves." *Journal of Geophysical Research*, 101(C4), 8869-8884.

Michailides, C., Loukogeorgaki, E., and Angelides, D.C. (2013). "Response analysis and optimum configuration of a modular floating structure with flexible connectors." *Applied Ocean Research, 43*, 112-130.

Mindlin, R.D. (1951). "Influence of rotary inertia and shear on flexural motion of isotropic elastic plates." *Journal of Applied Mechanics (ASME)*, 18: 31-38.

Mohapatra, S.C., and Sahoo, T. (2014a). "Wave interaction with a floating and submerged elastic plate system." *Journal of Engineering Mathematics*, 87(1), 47–71.

Mohapatra, S.C., and Sahoo, T. (2014b). "Oblique wave diffraction by a flexible floating structure in the presence of a submerged flexible structure." *Geophysical and Astrophysical Fluid Dynamics, 108*(6), 615–638.

Mohapatra, S.C., and Soares, C. G. (2016). "Effect of submerged horizontal flexible membrane on a moored floating elastic plate." *Maritime Technology and Engineering*, 3, 1181–1188.

Mondal, A. and Gayen, R. (2015). "Wave interaction with dual circular porous plates." *Journal of Marine Science and Application, 14*(4), 366–375.

Namba, Y. and Ohkusu, M. (1999). "Hydroelastic behaviour of floating artificial islands in waves." *International Journal of Offshore and Polar Engineering*, 9(1), 239-247.

Newman, J.N. (1965). "Propagation of water waves past long two-dimensional obstacles." *Journal of Fluid Mechanics*, 23, 23-29.

Newman, J.N. (2005). "Efficient hydrodynamic analysis of very large floating structures." *Marine Structures* 18, 169–180.

O'Hare, T. J., and Davies, A. G. (1992). "A new model for surface wave propagation over undulating topography." *Coastal Engineering, 18*(3-4), 251-266.

O'Hare, T. J., and Davies, A. G. (1993). "A comparison of two models for surface-wave propagation over rapidly varying topography." *Applied Ocean Research, 15*(1), 1-11.

Ohkusu, M. and Namba, Y. (2004). "Hydroelastic analysis of a large floating structure." *Journal of Fluids and Structures*, 19, 543–555

Ohmatsu, S. (1998). "Numerical calculation of hydroelastic behavior of pontoon type VLFS in waves." *Proceedings of 17th International Conference of Offshore Mechanics and Artic Engineering (ASME)*, 98-4333.

Ohmatsu, S. (2000). "Numerical calculation method for the hydroelastic response of a pontoon-type very large floating structure close to a breakwater." *Journal of marine science and technology*, 5(4), 147-160.

Ohmatsu, S. (2005). "Overview: Research on wave loading and responses of VLFS." *Marine Structures*, 18(2), 149–168.

Pardo, M.L., Iglesias, G. and Carral, L, (2015). "A review of Very Large Floating Structures (VLFS) for coastal and offshore uses." *Ocean Engineering*, 109, 677–690.

Panda, S., and Martha, S.C. (2014). "Oblique wave scattering by undulating porous bottom in a two-layer fluid: Fourier transform approach." *Geophysical and Astrophysical Fluid Dynamics,* 108(6), 587–614.

Papaioannou, I., Gao, R.P., Rank, E. and Wang, C.M. (2013). "Stochastic hydroelastic analysis of pontoon-type very large floating structures considering directional wave spectrum." *Probabilistic Engineering Mechanics,* 33, 26–37.

Papathanasiou, T.K. and Belibassakis, K.A. (2014). "Hydroelastic analysis of very large floating structures based on modal expansions and FEM." *Recent Advances in Mechanical Engineering and Mechanics*, 17-24.

Papathanasiou, T., Karperaki, A., Theotokoglou, E.E., and Belibassakis, K. (2014). "A higher order FEM for time-domain hydroelastic analysis of large floating bodies in an inhomogeneous shallow water environment." *Proceedings of the Royal Society A: Mathematical, Physical and Engineering Sciences*, *471*(2173), 20140643–20140643.

Peter, M.A. and Meylan, M.H. (2004) **"**Infinite-depth interaction theory for arbitrary floating bodies applied to wave forcing of ice floes**."** *Journal of Fluid Mechanics*, 500, 145-167.

Peter, M, Meylan, M. and Linton, C. (2006) **"**Water-wave scattering by a periodic array of arbitrary bodies**."** *Journal of Fluid Mechanics*, 548, 237-256.

Pham, D.C., Wang, C.M., and Utsunomiya, T. (2008). "Hydroelastic analysis of pontoon-type circular VLFS with an attached submerged plate." *Applied Ocean Research*, 30(4), 287–296.

Peter M.A., Meylan M.H. and Chung, H. (2003). "Wave scattering by a circular plate in water of finite depth: a closed form solution." *Proceedings of the 13th International Offshore and Polar Engineering Conference*, Honolulu, USA, vol. I, pp.180- 185.

Porter, D. and Porter, R. (2003). **"**Approximations to wave scattering by an ice sheet of variable thickness over undulating topography**."** *Journal of Fluid Mechanics*, 509, 145-179.

Porter, R., and Evans, D. V. (2006). "Scattering of flexural waves by multiple narrow cracks in ice sheets floating on water." *Wave Motion*, 43(5), 425-443.

Press, F. and Ewing, M. (1951). **"**Propagation of elastic waves in a floating ice sheet**."** *American Geophysical Union*. 32, 673-678.

Rao, S.S. (2007). "Vibration of Continuous Systems." John Wileys. ISBN-13, 978-0.

Remseth, S., Leira, B. J., Okstad, K. M., and Mathisen, K.M. (1999). "Dynamic response and fluid/structure interaction of submerged floating tunnels." *Computers and Structures* 72, 659 – 685.

Rezanejad, K., Bhattacharjee, J. and Guedes Soares, C. (2015). "Analytical and numerical study of dual-chamber oscillating water columns on stepped bottom." *Renewable Energy*, 75, 272–282.

Rhodes-Robinson, P. F. (1971). "On the forced surface waves due to a vertical wave-maker in the presence of surface tension." *In Mathematical Proceedings of the Cambridge Philosophical Society*, 70(2), 323-337.

Riyansyah, M, Wang, C.M., Choo, Y.S. (2010). "Connection design for two floating beam system for minimum hydroelastic response." *Marine Structure*. 23, 67–87.

Sahoo, T., Yip, T.L. and Chwang, A.T. (2001) "Scattering of surface waves by a semi-infinite floating elastic plate." *Physics of Fluids*. 11, 3215.

Seto, H., Ohta, M., Ochi, M. and Kawakado, S. (2005). "Integrated hydrodynamic-structural analysis of very large floating structures (VLFS) ." *Marine Structures*, 181-200.

Singla, S., Martha, S. C. and Sahoo, T. (2018). "Mitigation of structural responses of a very large floating structure in the presence of vertical porous barrier." *Ocean Engineering*, 165, 505-527.

Sim, I.H. and Choi, H.S. (1998). "An analysis of the hydroelastic behavior of large floating structures in oblique waves." *Proceeding 2nd Hydroelasticity Marine Technology*, Japan. 195.

Sturova, I.V. (2009). "Unsteady behavior of an elastic articulated beam floating on shallow water." *Journal of Applied Mechanics and Technical Phys*ics, 50(4):589–598.

Squire, V.A. (2007). "Review of ocean waves and sea-ice revisited." *Cold Regions Science and Technology*, 49, 110–133.

Squire, V.A. (2011). "Past, present and impendent hydroelastic challenges in the polar and subpolar areas." *Philosophical Transactions of Royal Society* A, 369, 2813-2831.

Squire, V.A and Dixon, T.W. (2001). "On modelling an iceberg embedded in shore-fast sea ice." *Journal of Engineering Mathematics*, 40, 211–226.

Stoker J.J. (1958). "Water waves." New York: Interscience

Suzuki, H. (2005) "Overview of Megafloat: Concept, design criteria, analysis, and design." *Marine Structures*, 18, 111-132.

Takagi, K. (1999). "Hydroelastic behavior of a very large floating structure." *Proceedings of the 14th International Workshop on Water Waves and Floating Bodies*, 137-140.

Takagi, K. (2002). "Hydroelastic response of a very large floating structure in waves-a simple representation by the parabolic approximation." *Applied Ocean Research*, 24, 175-183.

Tavana, H and Khanjani, M.J. (2013). "Reducing hydroelastic response of very large floating structure: A literature review." Int*ernational Journal of Computer Applications*, 71, 13-17.

Takagi, K. and Nagayasu, M. (2001). "Hydroelastic behavior of a mat-type very large floating structure of arbitrary geometry." *Annual Conference of the Marine-Technology-Society*, Honolulu, HI, pp.1923–1929.

Takagi, K. and Nagayasu, M. (2007). "Ray theory for predicting hydroelastic behavior of a very large floating structure in waves." *Ocean Engineering*, 34, pp. 362–370.

Takagi K, Shimada, K. and Ikebuchi, Y. (2000). "An anti-motion device for a very large floating structure." *Marine Structures,* 13, 421–36.

Tay, Z.Y. and Wang, C.M. (2012). "Reducing hydroelastic response of very large floating structures by altering their plan shapes." *Ocean Systems Engineering,* 69-81.

Taylor, R.E. (2007). "Hydroelastic analysis of plates and some approximations." *Journal of Engineering Mathematics,* 58(1-4), 267-278.

Taylor, R.E. and Ohkusu, M. (2000). "Green functions for hydroelastic analysis of vibrating free-free beams and plates." *Applied Ocean Research,* 22, 295-314.

Teng, B., Cheng, L., Liu, S.X. and Li, F.J., (2001). "Modified eigenfunction expansion methods for interaction of water waves with a semi-infinite elastic plate." *Applied Ocean Research,* 23(6), 357-368.

Timoshenko, S.P. and Krieger, S.W. (1959). "Theory of plates and shells." McGraw-hill.

Tkacheva, L.A. (2001). "Hydroelastic behaviour of a floating plate in water." *Journal of Applied Mechanics and Technical Physics,* 42, 991-996.

Utsunomiya, T. and Okafuji, T. (2007). "Wave response analysis of a VLFS by accelerated Green's function method in infinite water depth." *International Journal of Offshore and Polar Engineering,* 17(1), 30-38.

Utsunomiya, T. and Watanabe, E. (2002). "Accelerated higher order boundary element method for wave diffraction/radiation problems and its applications." *Twelfth International Offshore and Polar Engineering Conference,* 26-31 May, Kitakyushu, Japan.

Utsunomiya, T., Watanabe, E., Wu, C., Hayashi, N., Nakai, K. and Sekita, K. (1995). "Wave response analysis of a flexible floating structure by BE-FE combination method." *Fifth International Offshore and Polar Engineering Conference,* The Hague, The Netherlands.

Wang, C. D. and Meylan, M. H.,(2002) "The linear wave response of a floating thin plate on water of variable depth." *Appl. Ocean Res*., 24(3):163–174.

Wang, C.M., Gao, R.P., Koh, C.G., and Kitipornchai, S. (2012). "Novel hybrid system for reducing hydroelastic response of very large floating structures." *31st International Conference on Ocean, Offshore and Arctic Engineerin,* pp. 7-14.

Wang, C. M., and Tay, Z. Y. (2011). "Very large floating structures: applications, research and development." *Procedia Engineering*, 14, 62-72.

Wang, C.M. and Tay, Z.Y. (2011). "Very large floating structures: Applications, Research and Development." *Twelfth East Asia-Pacific Conference on Structural Engineering and Construction*, Procedia Engineering 14, 62–72.

Wang, C.M., Watanabe, E. and Utsunomiya, T. (2007). "Very Large Floating Structures." *Taylor and Francis*, 270 Madison Ave, New York, NY 10016.

Wang, S, Ertekin, R.C and Riggs, H.R. (1997). "Computationally efficient techniques in the Hydroelasticity analysis of very large Floating structures." *Computers and Structures*, 62(4). 603-610.

Wang, S., Karmakar, D. and Guedes Soares, C. (2016). "Hydroelastic impact of a horizontal floating plate with forward speed." *Journal of Fluids and Structures*, 60, 97-113.

Wang, P., and Cheng, Z. (2013). "Nonlinear hydroelastic waves beneath a floating ice sheet in a fluid of finite depth." *Abstract and Applied Analysis*, (1).

Wang, P., and Lu, D. (2013). "Analytic approximation to nonlinear hydroelastic waves traveling in a thin elastic plate floating on a fluid." *Science China Physics, Mechanics and Astronomy*, *56*(11), 2170-2177.

Watanabe, E., Utsunomiya, T., Kuramoto, M., Ohta, H., Torii, T., and Hayashi, N. (2003). "Wave response analysis of VLFS with an attached submerged plate." *International Journal of Offshore and Polar Engineering*, 13(03).

Watanabe, E., Utsunomiya, T. and Wang, C.M. (2004). "Hydroelastic analysis of pontoon-type VLFS: a literature Survey." *Engineering Structures*, 26(2), 245-256.

Watanabe, E., Utsunomiya, T., Wang, C.M., and Hang, L.T. (2006). "Benchmark hydroelastic responses of a Circular VLFS under wave action." *Engineering Structures*, 28, 423-430.

Watanabe, E., Utsunomiya, T., Wang, C.M. and Xiang, Y. (2003). "Hydroelastic analysis of pontoon-type circular VLFS." *Proceedings of the 13th International Offshore and Polar Engineering Conference*, Honolulu, USA, 93-99

Weitz, M. and Keller, J.B. (1950). "Reflection of water waves from floating Ice in water of finite depth." *Communications on Pure and Applied Mathematics*, 3(3), 305–318.

Williams, T. D., Bennetts, L. G., Squire, V. A., Dumont, D., & Bertino, L. (2013a). Wave–ice interactions in the marginal ice zone. Part 1: Theoretical foundations. Ocean Modelling, 71, 81-91.

Williams, T. D., Bennetts, L. G., Squire, V. A., Dumont, D., & Bertino, L. (2013b). Wave–ice interactions in the marginal ice zone. Part 2: Numerical implementation and sensitivity studies along 1D transects of the ocean surface. Ocean Modelling, 71, 92-101.

Williams, T.D and Squire, V.A. (2004). "Oblique scattering of plane flexural gravity waves by heterogeneities in sea-ice." *Proceeding of the Royal Society*, London. 1087-1099.

Wu, C., Watanabe, E. and Utsunomiya, T. (1995). "An eigenfuntion expansion-matching method for analyzing the wave induced responses of an elastic floating plate." *Applied Ocean Research*, 15, 301-310.

Xia, D.W., Kim, J.W. and Ertekin, R.C., (2000). "On the hydroelastic behavior of two dimensional articulated plates." *Marine Structures*. 13(4–5), 261–278.

Xu, F., and Lu, D. Q. (2009). "An optimization of eigenfunction expansion method for the interaction of water waves with an elastic plate." *Journal of Hydrodynamics*, 21(4), 526-530.

Xu, F. and Lu, D. (2011). "Hydroelastic interaction between water waves and a thin elastic plate of arbitrary geometry." *Science China Physics Mechanical Astronomy*, 54, 59-66.

Yu, X., and Chwang, A.T. (1993). "Analysis of wave scattering by submerged circular disk." *Journal of Engineering Mechanics*, 119(9), 1804-1817.

Yu, X. and Chwang, A.T (1994). "Wave motion through porous structures.*" Journal of Engineering Mechanics*, 120(5), 989-1008.

Zhao, C., Hao, X., Liang, R. and Lu, J. (2015). "Influence of hinged conditions on the hydroelastic response of compound floating structures." *Ocean Engineering*, *101*, 12-24.

Zilman, G. and Miloh, T. (2000). "Hydroelastic buoyant circular plate in shallow water: A closed form solution." *Applied Ocean Research*, 22(4), 191–198.

AUTHOR'S RESUME

Name: **Praveen K.M.**

Address: # 274-4, Near Sangam circle, M.G.Koppal,
Vijayanagar 2nd stage post,
Mysuru – 570017, Karnataka, INDIA

Email: praveen.kodalingana@gmail.com

ORCID: 0000-0001-9696-0695

ResearchGate: www.researchgate.net/profile/Praveen_K_M2

The author was born on 6th May, 1987 in Kodagu, Karnataka, India. Having passed secondary examination from Jnanodaya Bethani English Medium High School, Mangalore in 2003 and higher secondary examination from Maharajas PU College, Mysore in 2005, he graduated with Bachelor in Civil Engineering from National Institute of Engineering, Mysore in 2009. Thereafter, he obtained the Post Graduate degree in Infrastructure Development and Management, NICMAR-SODE, Pune in 2011 and Masters in Naval architecture and Ocean engineering from Indian Maritime University, Vishakhapatnam in the year 2014. After completing his master's degree he joined the doctoral research programme in the Department of Applied Mechanics and Hydraulics, National Institute of Technology, Karnataka, Surathkal in the year 2015. The author's interest lies in the field of hydroelasticity and wave structure interaction. During the period of his research, he communicated and published his work in various reputed international journals and conference proceedings. The detail list of publication are presented below:

(a) List of publication in Journals:

1. Praveen, K.M., Karmakar, D. & Guedes Soares, C. (2020), "Wave interaction with floating elastic plate based on Timoshenko-Mindlin plate theory." *Journal of Offshore Mechanics and Arctic Engineering (ASME),* vol 142(1), pp. 011601-1-15.
2. Praveen, K.M., Karmakar, D. & C. Guedes Soares (2019), "Hydroelastic analysis of periodic arrays of multiple articulated floating elastic." *Ships and Offshore Structures,* DOI: 10.1080/17445302.2019.1615167, (In Press).
3. Praveen, K.M., Karmakar, D. & Guedes Soares, C. (2019), "Influence of support conditions on the hydroelastic behaviour of floating thick elastic plate." *Journal of Marine Science and Applications,* vol. 18(3), pp. 295-313.
4. Praveen, K.M., Karmakar, D. & Guedes Soares, C. (2018), "Hydroelastic analysis of articulated floating elastic plate based on Timoshenko–Mindlin plate theory." *Ships and Offshore Structures,* 13(S1), pp. 287-301.

5. Praveen, K.M., Venkateswarlu, V. & Karmakar, D. (2020). "Wave transformation due to finite floating elastic plate with abrupt change in bottom topography." (Submitted).
6. Praveen, K.M., Venkateswarlu, V. & Karmakar, D. (2020). "Hydroelastic response of floating elastic plate in the presence of vertical porous barriers." (Submitted).

(b) List of publication in Book Chapters:

1. Praveen, K.M., Karmakar, D., & Nasar, T. (2016), "Hydroelastic analysis of floating elastic thick plate in shallow water depth." *Perspectives in Science*, Vol *8*, pp 770-772. (*International Conference on Recent Trends in Engineering and Materials Science* (ICEMS-2016), 17th -19th March 2016, Jaipur National University, Jaipur).
2. Praveen, K.M., Karmakar, D. (2019), "Wave Transformation Due to Floating Elastic Thick Plate over Changing Bottom Topography." *Lecture Notes in Civil Engineering, book series*, vol 23, pp 417-430, Springer, Singapore (*4th International Conference in Ocean Engineering* (ICOE 2018), 18th - 21st February 2018, IIT Madras, Chennai, India).
3. Praveen, K.M. and Karmakar, D. (2019). "Wave transformation due to floating elastic thick plate over multiple stepped bottom topography." *IOP: Journal of Physics Conference Series*, vol. 1276(1), pp. 012-18, IOP Publishing. (*International Conference on Recent Advances in Fluid and Thermal Sciences* (iCRAFT 2018), 5th – 8th December 2018, BITS Pilani, Dubai Campus, Dubai, UAE.)

(c) List of publication in Conference Proceedings:

1. Praveen K.M. and Karmakar, D. (2016). "Hydroelastic analysis of floating elastic plate in finite water depth based on Timoshenko-Mindlin Theory." *21st Conference on Hydraulics, Water resources & Environmental Engineering* (HYDRO 2016), 8th - 10th December 2016, Central Water & Power Research Station, Pune, India.
2. Praveen, K.M., Karmakar, D & Guedes Soares, C. (2018), "Hydroelastic analysis of articulated floating elastic plate based on Timoshenko–Mindlin plate theory." *2nd International Conference on Ships and Offshore Structures* (ICSOS 2017), 11th - 13th September 2017, Shenzhen, China.
3. Praveen K.M. and Karmakar, D. (2018). "Wave interaction with multiple articulated floating elastic plates based on Timoshenko Mindlin Plate Theory." *6th Indian National Conference on Coastal, Harbour and Ocean Engineering* (INCHOE 2018), 26th – 28th September 2018, CWPRS, Pune, India.
4. Praveen K M, Venkateswarlu, V and Karmakar, D. (2019). "Wave attenuation due to the presence of submerged barrier along with floating VLFS." *24th Conference on Hydraulics, Water Resources & Environmental Engineering* (HYDRO 2019), 18th – 20th December 2019, Osmania University, Hyderabad, India.